HUNGARIAN UNIVERSITY OF AGRICULTURE AND LIFE SCIENCES

(SZENT ISTVÁN UNIVERSITY formerly)

Incorporation of phase change material into building envelope under hot location

DOI: 10.54598/003590

PhD Dissertation

by

Qudama M. Q. Al-Yasiri

Gödöllő

2023

Doctoral school

Denomination: Doctoral School of Mechanical Engineering

Science: Mechanical Engineering

Leader: Prof. Dr. Gábor Kalácska, DSc

Institute of Technology

Hungarian University of Agriculture and Life Sciences,
Szent István Campus, Gödöllő, Hungary

Supervisor: Associate Prof. Dr. Márta Szabó, PhD

Institute of Technology

Hungarian University of Agriculture and Life Sciences,
Szent István Campus, Gödöllő, Hungary

……...…… ….....……

Affirmation of supervisor Affirmation of head of school

CONTENTS

NOMENCLATURE AND ABBREVIATIONS

Abbreviations

AHGR	Average heat gain reduction [%]
AITR	Average indoor temperature reduction [°C]
ASHRAE	American Society of Heating, Refrigeration and Air-conditioning Engineers
ATFR	Average temperature fluctuation reduction [°C]
CondFD	Conduction finite difference
CO_2ES	CO_2 emission saving [kg CO_2/day]
DF	Decrement factor
DSC	Differential scanning calorimeter
ECS	Energy cost saving [IQD/day]
EPS	Expanded polystyrene
EPW	EnergyPlus weather file
HG	Heat gain [W]
HGR	Heat gain reduction [%]
HHGR	Hourly heat gain reduction [%]
HTD	Hourly temperature difference [°C]
HTF	Heat transfer fluid
HTR	Hourly temperature reduction [%]
HVAC	Heating, ventilation and air-conditioning systems
IDF	Information data file
IEA	International Energy Agency
IQD	Iraqi dinar
MITR	Maximum indoor temperature reduction [°C]
MTR	Maximum temperature reduction [°C]
NNV	Natural night ventilation
OT	Operative temperature [°C]
$OT_{av.,modified}$	Average operative temperature of a modified room with PCM/PCM-EPS [°C]
$OT_{av.,reference}$	Average operative temperature of reference room [°C]
OTR	Operative temperature reduction [%]
PCM	Phase change material
RMTR	Room maximum temperature reduction [%]
SR	Solar radiation [W/m^2]
TL	Time lag [min, h]
TLL	Thermal load levelling index
TTLR	Thermal load levelling reduction
WWR	Window-to-wall-ratio [%]
X	Average decrease of indoor temperature during day hours [°C]
Y	Average increase of indoor temperature during night hours [°C]

Symbols

A	Area [m^2]
C_p	Specific heat capacity [kJ/kg.K]
h	Specific enthalpy of PCM [kJ/kg]
h_i	Combined convective and radiative heat transfer coefficient for the interior element surface and interior room temperature [W/m^2.K]
h_o	Combined convective and radiative heat transfer coefficient for the outer element surface [W/m^2.K]
H_f	Enthalpy content [kJ/kg]
I_{inc}	Inclined solar radiation intensity on elements [W/m^2]

k	Thermal conductivity [W/m.K]
k_E	Thermal conductivity for the interface between *i* node and *i-1* node [W/m.K]
k_W	Thermal conductivity for the interface between *i* node and *i+1* node [W/m.K]
m	Mass [kg]
n	Number of cycles [cycle/day]
T	Node temperature [K]
T_i	Indoor air temperature (model/room temperature) [°C]
$T_{i(av.)modified}$	Average indoor temperature of a modified room with PCM/PCM-EPS [°C]
$T_{i(av.)reference}$	Average indoor temperature of reference room [°C]
$T_{in,max}$	Maximum inner surface temperature of the element [°C]
$T_{in,min}$	Minimum inner surface temperature of the element [°C]
T_l	PCM temperature at liquid state [K]
$\bar{T}_{mr}$	Mean radiant temperature [°C]
T_o	Outdoor air temperature (ambient dry-bulb temperature) [°C]
$T_{out,max}$	Maximum outer surface temperature of the element [°C]
$T_{out,min}$	Minimum outer surface temperature of the element [°C]
T_{PCM}	PCM layer temperature [°C]
T_s	PCM temperature at the solid state [K]
$T_{sol\text{-}air}$	Solar-air temperature [K]
V_{PCM}	Volume of PCM [m^3]
ΔT	Temperature difference between the interior element surface and indoor air [K]
Δt	Time step [s]
Δx	Layer thickness [m]

Greek symbols

α	Absorptivity coefficient
ρ	Density [kg/m^3]
$\tau_{i,max}$	Time at maximum inner surface temperature of element [min]
$\tau_{out,max}$	Time at maximum outer surface temperature of element [min]

Subscripts/superscripts

i	The modelled node
i+1	Adjacent node towards the indoor zone
i-1	Adjacent node towards the outdoor environment
j	Previous time step of *i* [s]
j+1	Instant time step of *i* [s]

1. INTRODUCTION, OBJECTIVES

This chapter describes the background and objectives of the current research.

1.1. Introduction

Energy consumption in buildings has become an urgent issue in most countries worldwide. Globally, the energy consumed for space heating and cooling is as high as 40% and 61% out of the total energy demand in commercial and residential buildings, respectively (Ürge-Vorsatz et al., 2015). According to the International Energy Agency (IEA), the building sector is most responsible for the highest share of the total energy consumption worldwide. Furthermore, this trend will continue, where the energy consumed for space heating and cooling is predicted to be high by up to 12% and 37%, respectively, in 2050 (IEA (International Energy Agency), 2018).

Building envelope plays a predominant role in controlling building energy by adjusting the heating/cooling loads between the indoor and outdoor environments to satisfy the building's thermal requirements. A latest report of IEA stated that most investments and expenditures in the building sector had been spent on the renovation and construction of building envelopes (IEA (International Energy Agency) and UN Environment Programme, 2019). The report further revealed that building construction and operations accounted for 36% of the final global energy used in buildings and 39% of the energy-related CO_2 emissions in 2018. Therefore, a good opportunity to increase building energy efficiency could be achieved through building envelope.

Different solutions have been introduced to minimise the heating and cooling loads through building envelopes towards energy-efficient buildings (Gan et al., 2020). Amongst other successful strategies, incorporating phase change materials (PCMs) into building envelopes has proven to have the desired impact of controlling the thermal load, thereby resulting in a remarkable energy saving (Kishore et al., 2020; Ye et al., 2020). PCMs are implemented to minimise the cooling and heating loads through the building envelope due to their massive energy storage potential during melting and solidification, thereby maintaining acceptable thermal comfort (Ortega Del Rosario et al., 2020). The research in this area is still ongoing, considering new types of PCM and applying different techniques to reach optimal thermal behaviour and the highest performance.

PCMs are typically applied passively or actively into the building envelope. Although the passive technique has economic and technical benefits, it still suffers from thermal control issues such as unrestrained heat flow (De Gracia, 2019) and inefficient heat charging/discharging concerns (Kośny, 2015). Therefore, adopting a proper PCM integration procedure is essential, considering the suitable PCM type, effective PCM position and quantity, and the efficient incorporation method. Researchers rarely consider all the above influential aspects which influence the thermal performance of PCM during the service period (Mazzeo et al., 2017).

Literature studies have verified different applications of PCMs in building elements, including walls (Yan et al., 2020), floors (Lu et al., 2020), windows (Li et al., 2018), roofs (Hu and Yu, 2020), cladding (Frigione et al., 2019) and plastering (Ramakrishnan et al., 2019). For instance, Kishore et al. (Kishore et al., 2021) numerically investigated different PCM types using a dynamic wall system under various locations. The main outcomes indicated that PCM-integrated walls could reduce heat gain by 15%–72% annually, influenced by the building location. Al-Rashed et al. (Al-Rashed et al., 2021a) numerically studied the heat gain obtained from incorporating a 20 mm PCM layer in a building envelope (roof and walls) considering three different PCMs (RT-31, RT-35 and RT-42) under Kuwait climate conditions. The study found that the higher the PCM Tm, the better the thermal performance of the building envelope. Therefore, incorporating RT-42 has reduced the heat gain of the roof by 15.37% and that of walls by 13.78%, respectively, compared with the reference case. Moreover, the findings showed that RT-31 could minimise CO_2 emissions

by 98.65-481 kWh/m^2.year in worst cases. Li and Shi (Li and shi, 2021) studied the energy-saving of mortar-based composite paraffin/expanded vermiculite-diatomite for wall application. The results showed temperature reduction and energy-saving of wall-based composite PCM by respectively 2.68 °C and 17.03% compared with the pristine mortar. Saxena et al. (Saxena et al., 2020) conducted experimental work under Delhi (India) climate conditions to investigate the PCM thermal performance when incorporated into bricks by single and dual capsules. The results indicated a temperature reduction of 4 °C and 9.5 °C with single and dual PCM capsules, along with a heat transfer reduction of 40%-60% across bricks during peak hours.

1.2. Objectives

PCM application in the building envelope has been investigated in different regions worldwide, showing considerable advancements (Arıcı et al., 2022; Syath Abuthakeer et al., 2023). However, there is still a lack of studies dealing with experimentation and long-term evaluation under severe hot climate conditions (Saffari et al., 2017). Besides, most experimental studies did not consider all of the PCM incorporation's influential aspects, such as the optimal PCM position, optimal thickness and the proper encapsulation method, mostly conducted numerically (Costanzo et al., 2018; Köse Murathan and Manioğlu, 2020). The negative behaviour of PCM during the night period represented a challenging task in the PCM-buildings studies and got little attention in the literature studies. Therefore, this research aims to consider all these aspects to study the PCM thermal performance incorporated in typical residential construction materials. A detailed energetic and thermal comfort assessment will be conducted experimentally and numerically under severe hot climate conditions of Al Amarah city, southern Iraq, where ambient temperatures often reach 50 °C during summer days. The thermal evaluation of PCM incorporated full room will consider the best cases attained during follow-up experiments. Furthermore, numerical studies will extend the evaluation and show the role of thermal insulation and night ventilation in enhancing PCM effectiveness during the night. According to the authors' best knowledge, no similar research has been done under the conditions of this city to date. The results of this work are believed to afford a clear vision of the PCM-enhanced envelope thermal behaviour and contribution to building energy under severe hot climates for further modifications and PCM performance optimisation.

The main objectives of the present work are summarised as follows:

a) To specify the optimal passive PCM layer position in composite roof construction compared to bare roof construction.

b) To investigate the optimal passive PCM layer thickness within the composite roof construction at the optimal PCM position obtained in (a).

c) To examine the optimal integration of passive PCM capsules into constructive bricks.

d) To quantify the thermal comfort and energy-saving of a scaled PCM room under no-ventilation on an hourly, daily, and monthly basis.

e) To study the role of thermal insulation when combined with a PCM room considering the optimal position and thickness of insulation concerning the PCM incorporated.

f) To explore the effect of natural night ventilation through a single-side opening (window) on the PCM room thermal performance.

2. LITERATURE REVIEW

This chapter seeks to provide a thorough overview of PCMs, their main characteristics and possible applications in different thermal sectors. Besides, the main incorporation methods into the building envelope and influential aspects are also presented and discussed. In addition, identifying the main incorporation techniques presented in the literature studies are also highlighted in detail.

2.1. General overview of PCMs

2.1.1. Concept of PCMs

PCM incorporation is a fast-growing and promising technology in the building industry, where thermal energy management and energy saving are required in buildings. They have been mainly investigated to bridge the thermal energy source with energy consumption (building loads). PCMs are used in buildings for different purposes, including thermal load shaving and shifting, cooling/heating load reduction, thermal comfort, control of building material temperature, and increase in building durability, efficiency and energy saving. According to IEA/SHC Task 42 (ECES Annex 29) Compact Thermal Energy Storage, PCMs have an essential role in improving building efficiency and thermal comfort. They should be used in building products to offer better temperature control, especially those that suffer from overheating during summer (Rommel et al., 2015). PCMs can absorb and release heat during phase transition (mainly from the solid to liquid state and vice versa) under a relatively constant temperature, as shown in Fig. 2.1. These materials have the potential to store and release vast amounts by about 4-16 times more than traditional materials in a latent form. PCMs can efficiently manage the energy in different applications by storing the heat during the melting/charging phase and releasing it during the solidification/discharging phase, thereby controlling the need for energy. Moreover, PCMs are applied to shift the peak load to the off-peak time, positively affecting the efficiency of buildings (Tyagi et al., 2016; Al-Absi et al., 2018).

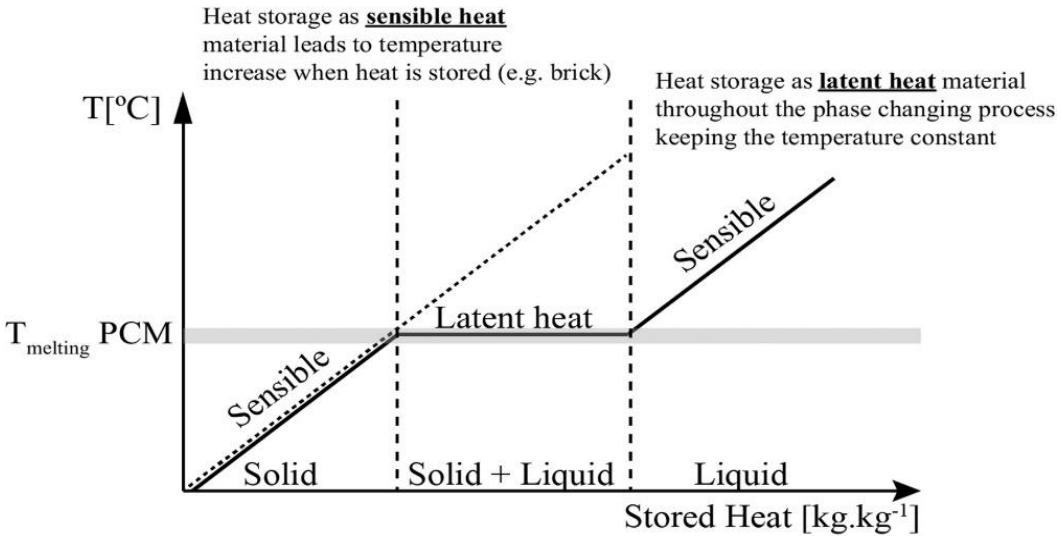

Fig. 2.1. Heat transition regions of PCM (Amaral et al., 2017)

2.1.2. Classification and characteristics of PCMs

Based on their chemical composition, PCMs are mainly classified as organic, inorganic and eutectic materials (Fig. 2.2). Each category has a range of working temperatures (Fig. 2.3) and thermo-physical properties; thus, they are more suitable for a specific application than others.

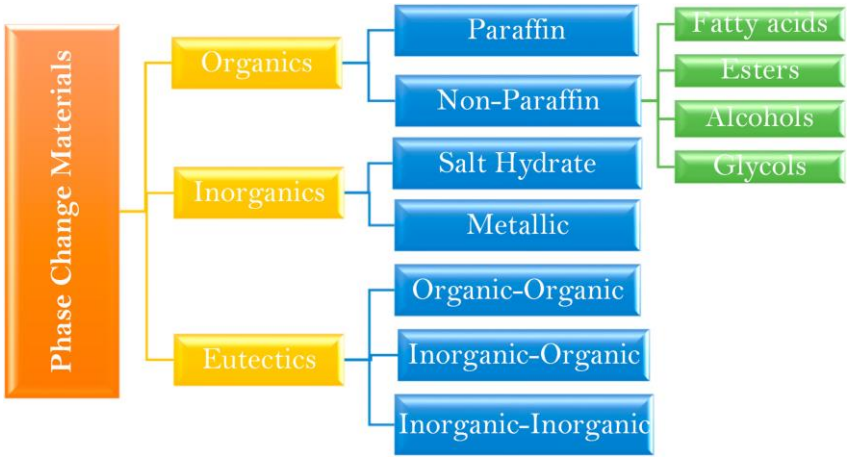

Fig. 2.2. Classification of PCMs (Faraj et al., 2020)

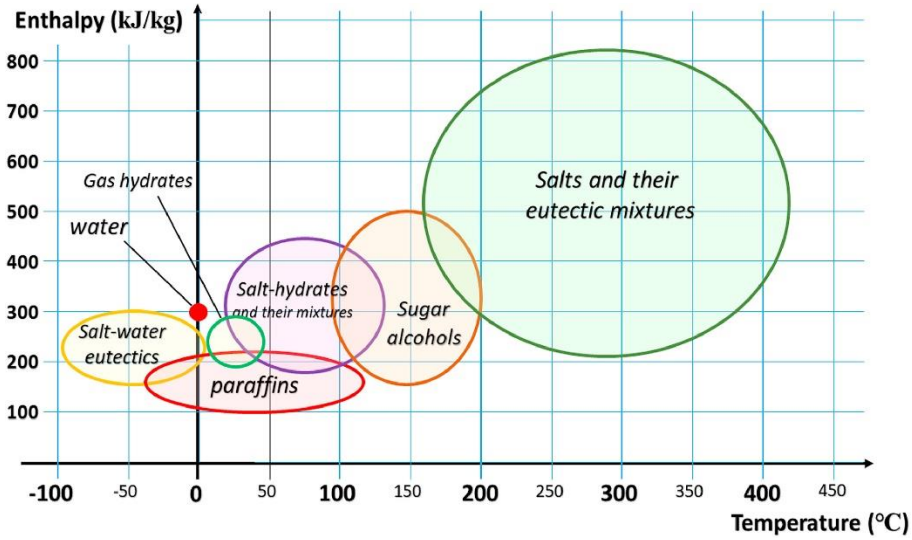

Fig. 2.3. Working range of various PCMs (Baetens et al., 2010)

The common characteristics of the three categories are listed in Table 2.1, indicating their main advantages and drawbacks. The appropriate selection of PCM depends highly on the operating temperature range of the application and melting temperature of the selected PCM, in addition to the other desired characteristics.

Table 2.1. Characteristics of PCMs (Pasupathy et al., 2008; Chandel and Agarwal, 2017)

PCM Type	Advantages	Disadvantages
Organics (Paraffin wax, fatty acids and vegetable oils)	• Availability in a wide temperature range • High heat of fusion • No subcooling • No segregation • Stable after many cycles • Chemically and physically stable • Compatibility with a wide range of containers • Corrosiveness materials • Environmentally safe, nonreactive • Recyclable	• Low thermal conductivity • Large volume change during phase transition except for some fatty acids. • Unstable at high temperatures • No sharp phase transition • Non compatible with the plastic containers • Costly in pure form • Low enthalpy • Flammable • Different toxicity levels
Inorganic (Salt hydrates)	• High thermal storage capacity • Good thermal conductivity • Low cost • Available easily	• Show subcooling • Considerable change in volume • Show phase segregation

	• Sharp melting points • Low vapour pressure • Non flammable	• Incompatible with metallic containers
Eutectic	• Sharp melting and boiling points • Higher volumetric storage density than the organic PCM	• Costly • Limited data available for thermo-physical properties

2.1.3. Applications of PCMs

PCMs have been proven to have remarkable potential in different heat transfer and energy storage applications. The recent work on PCMs focuses on their potential in many solar applications because they show high performance in many heat transfer systems (Javadi et al., 2020). Other studies have investigated the potential of PCMs as thermal storage media in refrigeration and air-conditioning systems (Bista et al., 2018; Nada et al., 2020), heat storage tanks (Mendecka et al., 2019; Hirmiz et al., 2020; Koukou et al., 2020), solar distillers (Mevada et al., 2020) and solar cookers (Bhave and Kale, 2020). They are often used as heat sink media in electronic devices (Ren et al., 2020) and photovoltaic modules (Elsheniti et al., 2020). Furthermore, PCMs are utilised as insulation materials in shipping containers (Byron Craig Owens ; Jeffrey Neal Cox ; Peter Franz Horwath ; Reyad I, 2018), for heat dissipation in electrical distribution transformers (Hasan and Abduladheem, 2019) and efficiently incorporated with building envelope as heat barriers or suppliers. Other applications are illustrated in Fig. 2.4.

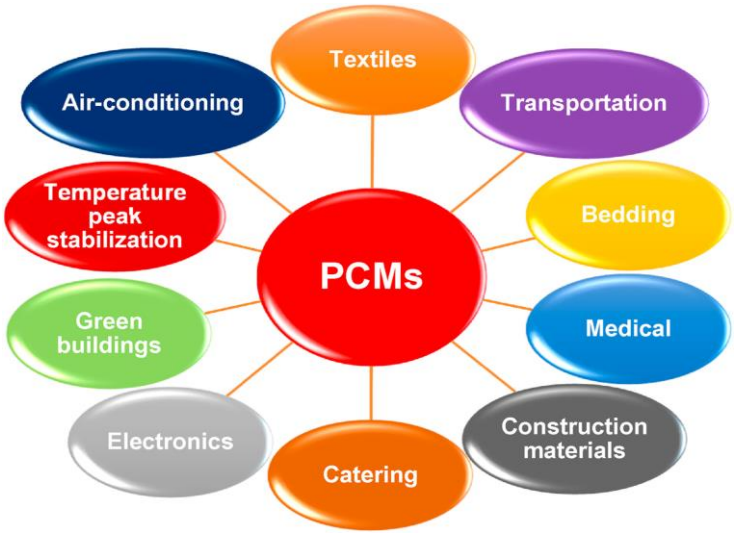

Fig. 2.4. Applications of PCM (Nicholas et al., 2018)

2.2. PCM-incorporated building envelope

Building envelope represents the shield that wraps the building and separates the internal atmosphere from the outside by its elements, such as the roof, floor, external walls and windows. Therefore, it regulates the thermal loads, impacts the need for heating and cooling and manages human comfort. The application of PCM is a revolutionary approach to enhance the thermal mass of the building structure and, as a result, the performance of the building. PCMs are applied to a building envelope in numerous techniques and configurations to be part of the construction materials and ensure maximum utilisation of its heat storage potential. The properties of PCM and the incorporation process provide a complex range of parameters to be considered in this research area.

2.2.1. Selection criteria of PCM

The PCM type should be adequately selected, considering the desired properties for effective use in a particular application. These properties can be grouped as follows:

- *Thermo-physical properties*: Melting temperature in the range of mean temperature of application, high heat storage capacity (latent heat), high specific heat and thermal conductivity, no subcooling, high density, low vapour pressure, small volumetric change during phase changes and completed cycles (melting/solidification) over a long term of service. Table 2.2 shows the main properties of PCMs used in different studies.
- *Chemical properties*: Nontoxic, irradiative, non-flammable, non-corrosive, nonexplosive, no segregation, no interaction with the encapsulation material and stable phase transition cycles over a long service life.
- *Other*: Available easily, low cost, environmentally friendly and recyclable.

Table 2.2. Thermo-physical properties of PCM reported in different literature studies

PCM type	**Melting temperature [°C]**	**H_f [kJ/kg]**	**k [W/(m.K)] (Liquid/Solid)**	**ρ [kg/m^3] (Liquid/Solid)**	**C_p [kJ/(kg.K)] (Liquid/Solid)**	**Ref.**
Paraffin	27–29	245	0.2 (Liquid)	770/880	2 (Liquid)	(Sun Jovanovic et al., 2019)
BioPCM OM32	28.85 31.85	219 200	0.2/0.2 0.145/0.219	860/860 870/928	1.97/1.97 2.3/1.95	(Saikia et al., 2018)
PureTemp 23	22.23–24.17	170.71	0.15/0.25	830/910	2.06/1.56	(Navarro et al., 2019)
OM35 Eicosane	35 36–38	160 202	0.16/0.2 0.15/0.39	870/900 780/815	2.71/2.31 2.46/1.92	(Saxena et al., 2020)
Paraffin wax	44	174.12	0.13 (Liquid)	783/830	2.53/2.44	(Hasan et al., 2018)
Paraffin RT27	28	147	0.2 (Liquid)	750/870	---------	(Sun et al., 2018)
OM37	35–40	218	o.13 (Liquid)	860	---------	(Rathore and Shukla, 2020)
HS29	26–29	190	0.55/1.05	1530/1681	2.62 (Liquid)	(Kumar et al., 2019)

The thermophysical properties of PCM are usually tested to ensure its suitability in the building application under study. The PCM is tested using different methods, and the differential scanning calorimeter (DSC) is the most adapted method. DSC is widely used to analyse the thermo-physical properties of PCMs. This method can specify the melting temperature, solidification temperature, enthalpies, heat storage capacity and specific heat of the PCM. However, researchers report some limitations of DSC, mostly owing to the small size of the tested PCM sample (in millilitres), thereby influencing the thermal characteristics of the tested PCM and resulting in inaccuracies (Kośny, 2015). Generally, the manufacturers and suppliers of PCM provide a technical data sheet of their products, indicating all necessary thermo-physical properties over a certain number of heat transition cycles.

Weather conditions should be considered and appropriately studied when selecting the PCM type, especially for changeable climate locations. Similarly, the design and implementation should be cautiously performed to prevent segregation and subcooling, representing significant issues restricting the applicability of PCM technology (Bao et al., 2020). In practice, satisfying all desired properties in one PCM candidate is difficult or even impossible. Instead, a trade-off may be made to select the excellent PCM. Thus, some studies recommend multiple attribute decision-making methods for this purpose (Liu et al., 2018).

2.2.2. Methods of incorporation

Practically, PCMs are incorporated into building envelope elements by one of the following methods:

a) Direct incorporation

b) Immersion

c) Encapsulation (micro or macro encapsulation)

d) Shape-stabilised PCMs

e) Form-stable PCM composites.

In the direct incorporation method, the PCM in powder or liquid state is added directly to the construction material, such as gypsum mortar, cement mortar and concrete mixture. This method is the easiest and most economical because it does not require experience and is easy to incorporate (Lu et al., 2017). On the contrary, the major drawback of this method is the leakage of PCM during the melting phase. This leakage causes incompatibility of mixed materials and increases the risk of fire (for flammable PCMs). In addition, this method weakens the mechanical properties of constructed elements during high temperatures, given that the PCM is added to the mixture in a liquid state, thereby decreasing the water content ratio (Pereira da Cunha and Eames, 2016).

In the immersion method, a porous construction material immerses into the liquid PCM; it is absorbed due to capillarity. The main drawbacks of this method are leakage, construction incompatibility and the corrosion of reinforced steel when incorporated with concrete elements, thereby affecting its service life (Cellat et al., 2017).

Encapsulation is a suitable method to avoid PCM leakage issues and enhance its compatibility with the building structure. Encapsulation is performed by covering the PCM with a shell to protect it from the outside environment and prevent leakage. This method is also essential to increase the heat transfer area and, hence, the thermal conductivity of PCM to ensure effective utilisation of its storage capacity (Chandel and Agarwal, 2017). The PCM can be macroencapsulated using shells, tubes, channels and thin plates or microencapsulated when the microsized PCM is covered by unique polymeric material (Fig. 2.5) (Giro-Paloma et al., 2015; Milián et al., 2017)

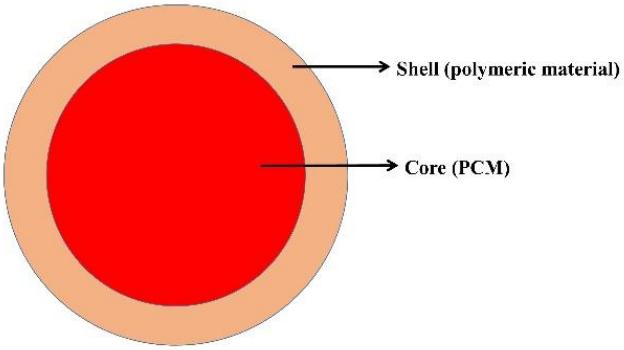

Fig. 2.5. Microencapsulation concept

In both methods, the encapsulation material should have unique characteristics, such as preventing leakage, retaining all thermal characteristics of PCM, not reacting with PCM, compatible with PCM and its application, providing structural stability and securing handling (Bland et al., 2017). Furthermore, it should control any volumetric change of PCM during phase changes and provide appropriate protection for the PCM against environmental degradation and good thermal conductivity and mechanical strength over PCM life cycles (Singh Rathore et al., 2020). Pipes, panels and foils made from aluminium, copper and stainless steel are commonly used for

macroencapsulation because they offer excellent thermal conductivity, compatibility and support to the mechanical strength of building materials (Rathore and Shukla, 2019). More macroencapsulation forms are shown in Fig. 2.6.

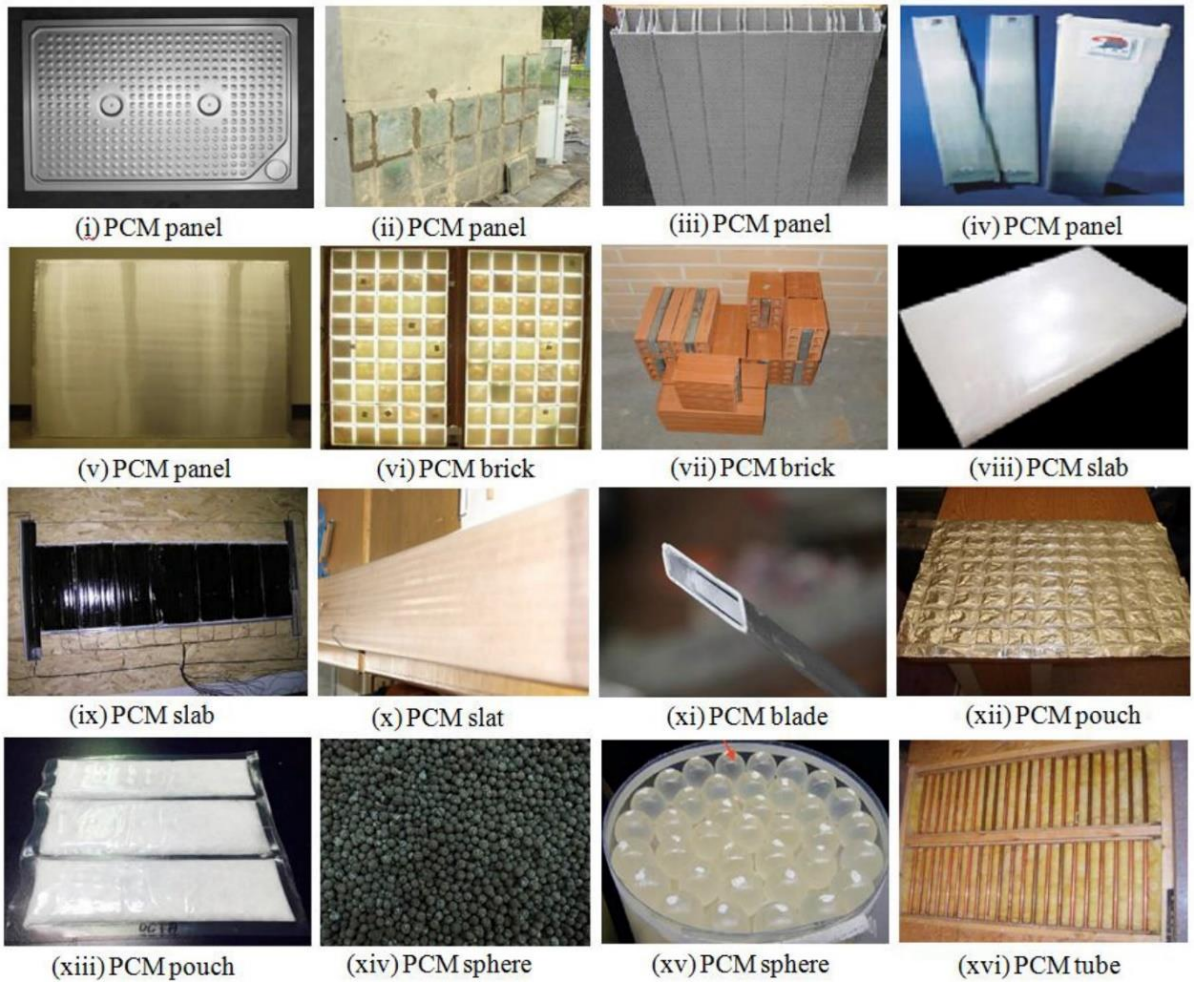

Fig. 2.6. Different macroencapsulation forms used with building structure (Liu et al., 2018)

The shape-stabilised method contains the PCM inside a carrier matrix. This method is promising because it provides better thermal conductivity and large specific heat and maintains the shape over many phase transition cycles. More information regarding its configurations and preparation techniques has been described by (Cheng et al., 2015; Frigione et al., 2019).

The form-stabilised PCM is also an advanced method of incorporation. It is a specific definition of composite material, retaining the maximum amount of one or more types of PCM and showing no leakage at melting temperatures. Although the two latter methods are expensive to implement, they are the most reliable among others. Reliability indicates that the PCM cycles (melting/solidification) are repeated in high performance without degradation, and this feature is crucial for applications that require high performance for a long term, such as buildings (Fallahi et al., 2017).

2.2.3. Influential parameters on PCM performance in the building envelope

Incorporating PCM within the building envelope can reduce the peak temperature by up to 4 °C, thereby maintaining stable thermal comfort conditions during summer daytime (N. Beemkumar et al., 2020). The thermal performance of PCM is affected by several parameters, which influence its activity; sometimes, it performs negatively. Dealing with such parameters is highly recommended to ensure the best performance of PCM and exploit its potential efficiently. The most influencing parameters are discussed in the following section.

2.2.3.1.Melting temperature

The melting temperature of PCM is the most determining parameter of its performance because it impacts the charging and discharging processes. Thus, the potential of heat storage is utilised fully or partially. The PCM melting temperature should suit the low solar radiation during winter to boost the heating demand. On the contrary, it should be sufficiently high to restrict the high solar radiation and heat transfer during summer, thereby minimising the cooling load. Jelle and Kalnæs (Jelle and Kalnæs, 2017) suggested that for water heating applications, the optimal PCM melting temperature lies between 29 °C and 60 °C, between 22 °C and 28 °C for human thermal comfort and up to 21 °C for cooling applications. Table 2.3 shows the operating melting temperature of several commercially available PCMs incorporated into the building envelope in different literature studies.

Table 2.3. Operating melting temperature of commercially available PCMs

PCM type	PCM symbol	PCM melting temperature (°C)	Manufacturer
Bulk	RT21 HC	21	Rubitherm
	RT22 HC	22	Rubitherm
	RT25 HC	25	Rubitherm
	RT27	27	Rubitherm
	PureTemp 23	23	Entropy Solutions
Microencapsulated	Micronal DS5040X	23	BASF
	Micronal DS5008X	25	BASF
	MPCM24D	24	BASF
	Micronal DS5038X	25	Microteklabs
Microencapsulated	MacroPCM28	28	Microteklabs
	MacroPCM24	24	Microteklabs

2.2.3.2. PCM quantity/thickness

The quantity of PCM incorporated into building envelopes considerably affects the thermal energy stored during phase transition. For example, when a small amount of PCM is included in building elements to decrease cooling loads during summer, the PCM stores limited heat in the charging phase and quickly reaches the full liquid state. Thus, it cannot absorb more energy. By contrast, larger PCM amount stores more heat during the charging process and restricts the heat from passing through the element. At the same time, larger stored heat requires more time to be discharged in addition to the negative impact on the building element's mechanical strength and the economic concern. This parameter needs to be studied carefully, along with the effect of melting temperature, to guarantee a positive performance of the PCM without affecting the mechanical strength of the building element.

The volume of PCM required for any application (V_{PCM} in m^3) can be easily obtained using Eq. (2.1) by dividing the mass (m) of PCM (in kg) over its density ρ (in kg/m^3).

$$V_{PCM} = m_{PCM}/\rho_{PCM} \quad (2.1)$$

The overall heat storage capacity of the PCM, E_{latent} (kJ) can be determined, considering its amount (i.e., m), the total energy exchange of PCM enthalpy content H_f (kJ/kg). Furthermore, the number of cycles during the day n, in accordance with Eq. (2.2) (Aranda-Usón et al., 2013), as follows:

$$E_{latent} = n \times m \times H_f \quad (2.2)$$

2.2.3.3. PCM position

The position of the PCM layer depends on the location of the building under study and the purpose of PCM implementation, whether used for reducing the heating or cooling loads. Incorporating PCM has shown better cooling load reduction performance than heating load reduction. Moreover, the PCM can work actively under temperatures higher than its melting point (Plytaria et al., 2019).

Many studies reported that the PCM layer should be positioned closer to the heat energy source (Yu et al., 2019). Other studies stated that the mid-element position results in better performance for the building annually (Vukadinović et al., 2020). For cooling purposes, the PCM layer should be installed on the exterior side of the building element. By contrast, it should be installed closer to the interior for heating purposes (Jin et al., 2016). The melting temperature of the PCM layer profoundly influences the optimal position. For instance, Lagou et al. (Lagou et al., 2019) numerically investigated the optimal position of PCM within the building envelope, along with the best melting temperature for six different European cities under summer and winter conditions. The analysis was conducted using COMSOL multiphysics software for walls of nonconditioned rooms at different orientations, locations and building types. The study revealed that the PCM layer should be installed on the interior surface of the walls in all cases and conditions. Furthermore, the PCM should have a melting temperature of 16 °C for the southern locations, 11 °C for the central areas and 20 °C for the northern European cities for optimal PCM thermal performance. Darvishi et al. (Darvishi et al., 2019) numerically investigated the best position of three PCM types with 21 °C, 23 °C and 25 °C melting temperatures for two Iranian cities with different climate conditions. The heating and cooling load reductions and the annual energy saving were considered in their study. They concluded that on an annual basis, placing the PCM in the middle or near the interior zone reduced the thermal load and increased energy saving regardless of the climatic conditions. Fig. 2.7 indicates more details about the best position of PCM, considering the main influential parameters under cold and hot locations.

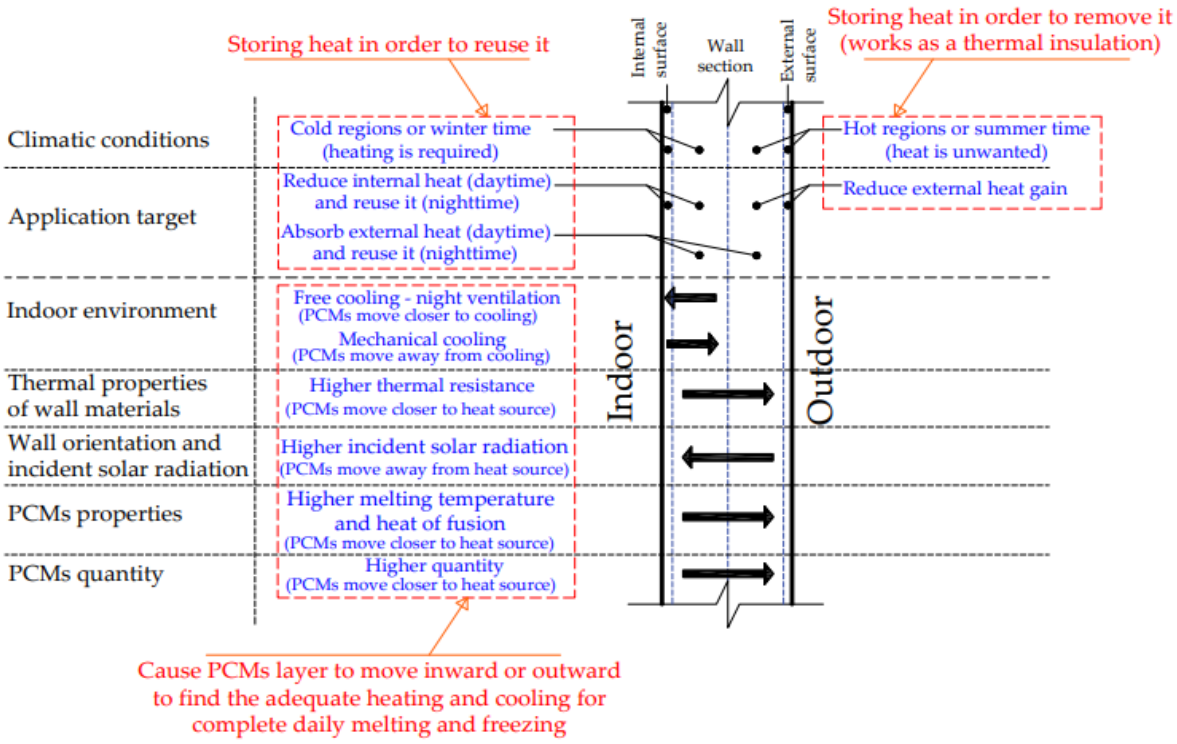

Fig. 2.7. Optimal position of PCM in cold and hot climates for wall application (Al-Absi et al., 2020)

2.2.3.4. Heat transfer fluid

PCM is typically utilised passively or actively. In the passive scenario, the heat is stored in the PCM and released naturally. However, in the active scenario, the heat is stored and/or released by employing pumps, fans and blowers, where the HTF is important. Under hot climate applications, HTF is required to discharge the heat accumulated in the PCM and solidify it for the following cycle. The relatively low temperature during the night period (typically called night cooling) is usually utilised for this purpose because it is free and has good potential to solidify the melted PCM, especially when used in a controlled manner (Soudian and Berardi, 2019)88]. In the usual

design of night cooling systems, the PCM cycle is considered once a day, where the rising temperature during day hours melts the PCM and then solidifies it by using low air temperature at night, as illustrated in Fig. 2.8. The potential of night cooling is limited in severe hot climate regions because it effectively works when the diurnal temperature variation is sufficiently large (up to 15 °C) (Souayfane et al., 2016). Several limitations, such as partial solidification, have been reported in studies that considered natural night cooling an effective HTF for PCM-accumulated heat (Soudian and Berardi, 2019).

In some cases, full solidification of PCM cannot be achieved at night due to the high surface temperature of the building envelope, resulting from high diurnal solar radiation and heat stored by envelope materials. Consequently, the PCM is melted partially in the next cycle and loses its ability to act as a heat storage medium. Furthermore, active night ventilation should be controlled by several parameters, such as the range of night air temperature, the quantity of solidified PCM, air flow rate and ventilation period (Yu et al., 2020).

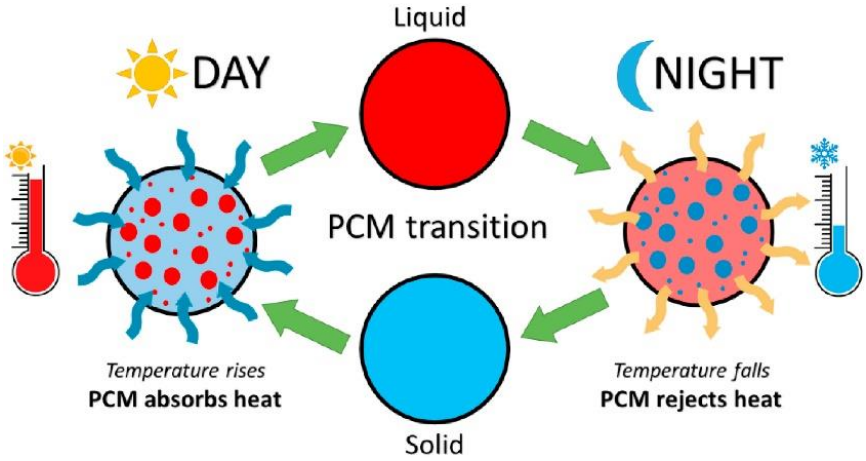

Fig. 2.8. Daily PCM transition cycle (Faraj et al., 2020)

Alternative HTF is recommended to maintain the solidification process, especially in locations with harsh weather conditions during the summer period. The shading and building orientation techniques were investigated and showed to be beneficial in avoiding the direct solar impact and reaching an acceptable night cooling effect (Berardi and Soudian, 2019). The HTF is also required for cold climate applications to improve the charging phase. The solar radiation is poor under cold locations and cannot reach the PCM layer naturally. Therefore, using active means (such as solar collectors, where water or air is implemented as HTF) is necessary to harvest, as much as possible, the heat during day hours to be stored in the PCM.

2.3. Possible incorporation techniques of PCM in building envelope

The literature has many practical techniques to incorporate PCMs into building elements. PCM is usually included during construction or incorporated as a separate layer within the building structure. PCMs of different types, methods, quantities and operational characteristics have been applied in different building elements, such as roofs, exterior walls, floors and windows, thereby showing spectacular enhancements. Studies that deal with PCM incorporating floors and windows are less than those on walls and roofs. As a building envelope element, the floor usually has the least effect on the building's energy on the bases of heating and cooling loads because it is far from the effect of weather conditions and deals with a relatively stable temperature of the ground. Thus, several researchers investigated the role of PCM incorporating floor systems (Lu et al., 2020). Although several PCM applications in windows have been conducted for frame and glazing cavities, serious issues regarding leakage and low transparency of glazed pans were reported, thereby limiting its implementation (Silva et al., 2016). The incorporation of PCM in the building envelope has been assessed, focusing on the roofs and exterior walls, which share the largest

building area and are exposed to changeable weather conditions. Therefore, they represent the primary source of undesired heating and cooling loads (Al-Yasiri et al., 2019).
In this section, up-to-date studies on PCM-incorporated building envelopes have been reviewed and presented in accordance with the PCM installed into the construction materials. These methods are primarily categorised as (i) mixed with concrete, cladding and finishing materials, (ii) inserted separately with building construction in the form of sheets/boards/layers, (iii) contained inside bricks, and (iv) pipe-encapsulated.

2.3.1. PCM-incorporated concrete and cladding/finishing materials

Concrete has been used as a primary construction material worldwide. Similarly, mortars (gypsum and cement mortar in particular) are used widely in construction as exterior and interior finishing materials (Al-Yasiri et al., 2019). Mixing PCM with these materials has shown high potential in regulating and controlling indoor thermal comfort and energy saving for heating and cooling applications (Frigione et al., 2019). However, this method suffers from several limitations, such as the risk of fire, the low mechanical strength of mixed materials and the poor thermal conductivity of PCM because of the polymeric materials used for PCM microencapsulation (the prevalent technique used in this approach) (Rao et al., 2018). Yun et al. (Yun et al., 2019) examined the mixture of PCM/concrete to control the heat within the concrete and evaluate its fundamental properties. The strontium-based powder (Sr(OH)2-8H2O) was selected as PCM given its excellent ability to store heat during phase transition and other desired properties tested by DSC. Results showed that the heat through concrete was reduced by 15%–21%, along with a slight reduction in its compressive strength. Moreover, the results revealed that adding PCM to the concrete mixture remarkably decreased the thermal stresses and cracks. Cabeza et al. (Cabeza et al., 2020) investigated the long-term performance of concrete-based PCM to conduct the thermal and mechanical properties after a decade. They tested built cubicles made in 2005 (one with 5 wt% PCM and the other without PCM) and repeated the same test procedure conducted then to compare the results. The study reported no change in the thermal response, given the heat reduction, time delay and thermal fluctuations between day and night. Furthermore, the mechanical property-based compressive strength test was the same. Although the PCM-incorporated concrete had many thermal advantages, it often showed serious drawbacks, such as subcooling of PCM, thereby leading to segregation and leakage in the case of immersion and direct methods. Furthermore, limited PCM types can only be used due to the concrete alkali nature and the corrosion of steel used for reinforcement (Adesina, 2019). An advanced type of concrete-based PCM in micro- and macroencapsulation forms was introduced by Antonella et al. (D'Alessandro et al., 2018). Fig. 2.9 shows the procedure used in their experiment. The newly produced concrete was reported to have good thermal stability. Moreover, it optimised the thermal insulation effect by up to 9 h compared with the standard concrete. Results reported good mechanical properties, such as compressive strength, ductility, low weight, and reliability.

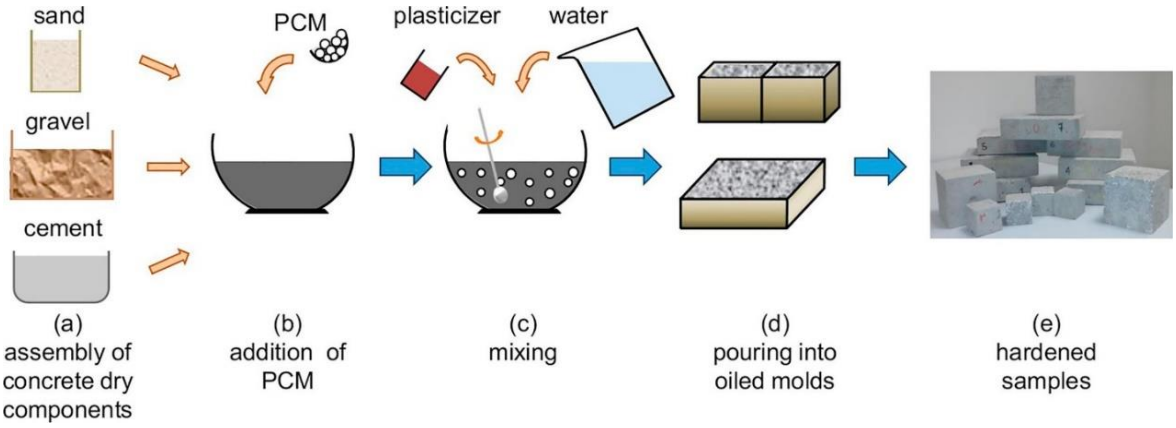

Fig. 2.9. Concrete brick Preparation using micro/macroencapsulated PCM (D'Alessandro et al., 2018)

Mortar-based PCM also had a considerable improvement in terms of thermal comfort and energy saving. Frazzica et al. (Frazzica et al., 2019) numerically and experimentally designed and tested two microencapsulated PCM-based paraffin composites (Micronal 5038X and Micronal 5040X of melting points 25 °C and 23 °C, respectively) mixed with cement mortar in different percentages (Fig. 2.10). The samples were analysed under weather conditions of Sicily, Italy to reduce the energy consumption and maintain suitable comfort conditions inside the building during summer and winter based on ASHRAE comfort conditions. They used COMSOL multiphysics software to validate the results by solving a numerical model and defining the optimal melting point temperature, 27 °C. The results showed that Micronal 5038X had higher heat of fusion than Micronal 5040X. Furthermore, an increase of approximately 15% in the comfort conditions in terms of reduced internal surface temperature was achieved with 15 wt% of PCM-mortar compared with the pure cement mortar sample.

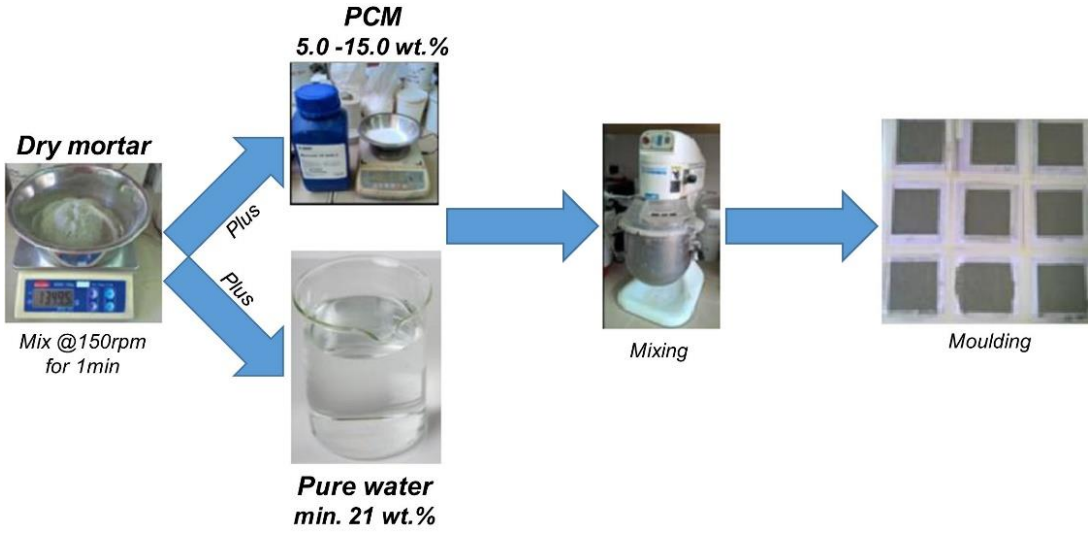

Fig. 2.10. Preparation process of microencapsulated PCM-cement mortar samples (Frazzica et al., 2019)

Younsi and Naji (Younsi and Naji, 2020) numerically investigated the microencapsulated PCM-mortar layer incorporated into the wall to manage the building's thermal comfort, downsize heating/cooling equipment and shift the peak load. The factors examined during the simulation included the mass fraction of PCM, the thickness of the wallboard and the melting temperature, which varied between 24 °C and 28 °C. The results indicated that the microencapsulated PCM–mortar layer reduced the temperature by 3 °C, and the PCM mass fraction of 20%–30% was required for efficient thermal storage and better thermal comfort. The study also concluded that the PCM-mortar layer added to the walls was a good option in the summer period because it reduced the heat transfer entering the building and shifted the cooling peak loads to the late hours of the day. Abden et al. (Abden et al., 2020) experimentally investigated the thermal performance of a composite PCM-incorporated gypsum board false ceiling for cooling load reduction. The composite PCM was prepared from methyl stearate and diatomite mixed with the gypsum mortar to develop a form-stable PCM board with excellent thermal stability and physical properties. The results showed that the temperature was reduced by 4.9 °C during the first day of the experiment. Furthermore, an average reduction of 3.5 °C was obtained during the three-day experiment compared with an identical chamber of standard gypsum board. The study concluded that such board type was efficient in saving the cooling loads by 16.2% and economically feasible with 1.7 years' payback period. Li et al. (Li et al., 2020) fabricated a composite PCM wallboard containing three types of PCMs with different melting points (12 °C, 18 °C and 29 °C) to maintain thermal comfort and increase energy saving under different climate conditions. Two models of PCM boards were fabricated with varying concentrations of PCM and tested considering the heat flux and temperature changes. The results showed high energy saving of up to 30% for the wallboard-based PCM with reasonable thermal control of temperature fluctuations compared with the

standard gypsum wallboard. Kusama and Ishidoya (Kusama and Ishidoya, 2017) investigated the thermal comfort and energy storage efficiency of using the plaster-integrated microcapsuled PCM as a finishing layer for a room's wall and ceiling. The study revealed that the microcapsuled PCM has the potential to store heat that passes through windows and release it to maintain thermal comfort. The PCM plaster was tested in the laboratory to determine the melting temperature and heat storage capacity and then used as a finishing layer in a testing room. The results showed a higher solar radiation utilisation rate of up to 82% of the PCM plaster room than another conventional method. This finding confirmed a stable comfort temperature and humidity level under the cold climate conditions of Japan.

2.3.2. PCM-sheet/board/layer inserted into building element

In this category, the sheets, boards or layers of macroencapsulated PCM are installed as an additional layer in the building structure and activated passively or actively. The main advantage of this method is that a vast amount of PCM could be contained in the building elements without influencing its mechanical properties. Hu and Yu (Hu and Yu, 2019) simulated the performance of a wall-embedded PCM board in five different climate conditions in China using the EnergyPlus tool. The study investigated the total energy saving and CO_2 emission reduction, considering the PCM board type and thickness. The findings stated that incorporating PCM could save energy consumption through building walls by 6% and reduce CO_2 emissions by 1% in warm climate buildings. The study also reported that the position of the PCM layer within the wall is sensitive; thus, placing the PCM layer inside the wall insulation can save 1%–7% more energy than the PCM layer outside the wall insulation. Moreover, increasing PCM thickness can save 2%–6% more energy in severe and hot climate zones. Ahangari and Maerefat (Ahangari and Maerefat, 2019) numerically investigated thermal comfort and building energy-saving by applying double PCM layers in a room at five Iranian climatic conditions (mostly dry and semi-arid). The layers had different melting temperatures installed one by one close to the interior zone, in which the PCM layer with low melting temperature was placed closer to the interior. The thermal performance was evaluated using EnergyPlus software and the Fanger model for thermal comfort. The results pointed out the effectiveness of the double-layer system, where the thermal comfort period improved from 73% to 93% in a dry climate and from 63% to 75% in a semi-arid climate in winter. Moreover, a reduction in heating energy consumption was achieved at 17.5% and 10.4% in a dry and semi-arid climate, respectively. Zhu et al. (Zhu et al., 2019) numerically studied the effectiveness of paraffin compounds as PCMs for a Trombe wall during the summer and winter seasons of Wuhan City, China, using TRNYS software. The study proposed two PCM layers with different melting temperatures to maintain the necessary thermal comfort for the whole year. One of these layers was placed externally concerning the wall and coupled with a solar chimney. By contrast, the other layer was placed internally to the wall and combined with a solar heating system. The simulated results stated that the best melting temperature was 30 °C and 18 °C for the external and internal PCM layers, respectively. Furthermore, the maximum cooling and heating load reduction was 9% and 15%, respectively, compared with the wall without PCM. In addition, the PCM layers decreased the indoor temperature by 3.28 °C in summer and increased the indoor temperature by 0.11 °C.

The location of the PCM layer within the building envelope is essential and affects the thermal performance significantly. Arıcı et al. (Arıcı Bilgin et al., 2020) numerically studied the effect of the PCM layer position, the melting temperature and layer thickness based on the energy-saving of cooling and heating loads of three Turkish locations. They revealed that the optimal exploitation of PCM latent heat could be achieved with a time lag of 10.3 h when the melting temperature of the PCM varies from 6 °C to 34 °C with 1–20 mm PCM layer thickness based on the building climate conditions. Jin et al. (Jin et al., 2016) numerically and experimentally studied the optimal position of a thin PCM layer incorporated with a frame wall to reduce the heat flux that passes through it. The layer was placed in different locations with respect to the exterior and interior wall layers, as shown in Fig. 2.11. The simulated results revealed that the optimal PCM layer position

depended on the thermal properties of the PCM layer and the environmental conditions. Two places were found effective, namely, the one closer to the interior wall surface (case a) when the interior temperature increased and the layer closer to the exterior wall surface (case d) when the PCM layer thickness, the heat of fusion and the melting temperature of PCM increased. Moreover, the heat flux reduction increased with the increased PCM layer thickness.

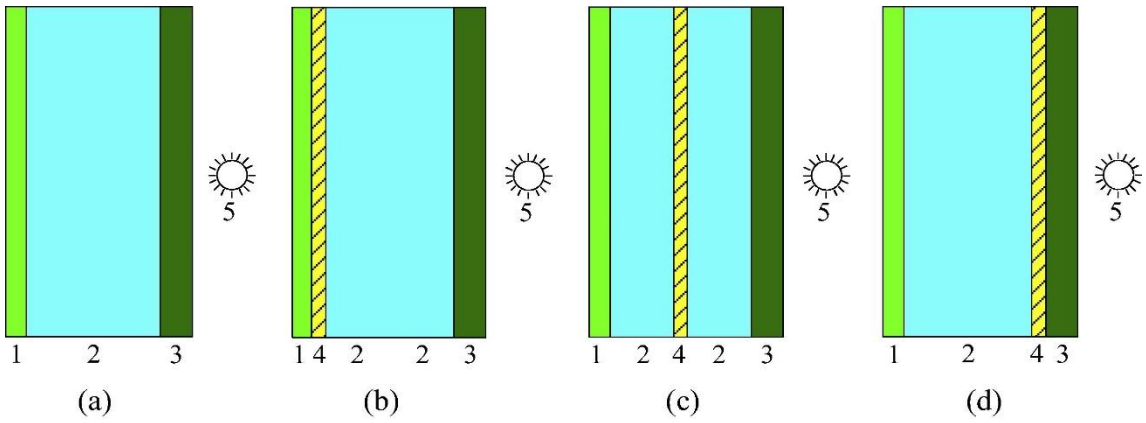

Fig. 2.11. Schematic of PCM positions: (a) regular wall, (b) PCM layer placed close to the interior, (c) PCM layer placed in the middle and (d) PCM layer placed close to the exterior. 1. gypsum board, 2. insulating layer, 3. oriented strand board, 4. PCM layer, and 5. outdoor (Jin et al., 2016)

PCM layer incorporation, together with other technologies, can further enhance the performance of the building envelope and reach better thermal comfort. Zhang et al. (Zhang et al., 2020) investigated the effect of matching PCM sheets with cool paints for roof cooling load reduction and energy saving. They experimentally studied the following types of roofs: normal roof, cool painted roof, PCM-roof and a cool roof coupled with a PCM sheet. The results showed that the roof's performance was enhanced using the PCM sheet, and the cool roof incorporated with the PCM sheet had the best performance. This combination reduced the cooling load of the tested room by 6.6 °C, and the heat entering the room decreased by 52.9%. The study clarified the impact of PCM position and thickness on the roof performance, where the internal position of the PCM sheet inside the roof can reduce the indoor temperature by 1.2 °C compared with the middle position. Furthermore, the thicker PCM layer performed better, where the PCM with 5 mm thickness was sufficient to maintain a comfort level in the range of 22 °C–28 °C for the entire day. The dynamic thermal performance of PCMs combined with the waterproof membrane was investigated by Piselli et al. (Piselli et al., 2019) for temperature reduction of the lightweight roof. Two membrane types (cool and dark coated) were used in the experiment together with different PCM layers of varying melting temperatures under the climate conditions of Rome, Italy and Abu Dhabi, UAE. The results demonstrated that the roof performed well in Rome when the PCMs with melting temperatures of 25 °C and 45 °C were integrated with the cool and dark roof membranes. By contrast, the PCMs with melting temperatures of 35 °C and 55 °C performed better in Abu Dhabi. The study also indicated that the PCM layer with 25 °C and 31 °C melting temperatures combined with cool and dark membranes had the best roofing thermal performance for Rome and Abu Dhabi. Furthermore, the study concluded that the climate conditions, roofing medium, PCM position and its melting temperature should be considered when selecting appropriate PCM to obtain the best cooling effect for roofs. Gracia (De Gracia, 2019) numerically implemented a movable PCM layer (7 mm polymeric sheet) with a changeable position with respect to the insulation layer inside the wall, as shown in Fig. 2.12. The system aimed at reaching full solidification of PCM and avoid heat discharge in the indoor, thereby representing the main practical issue of PCM passively incorporated building. In addition, the system can work as a cooling supplier in hot days. With the optimal control of the system, the researcher claimed that cooling loads can be minimised by 379% compared with a wall without PCM.

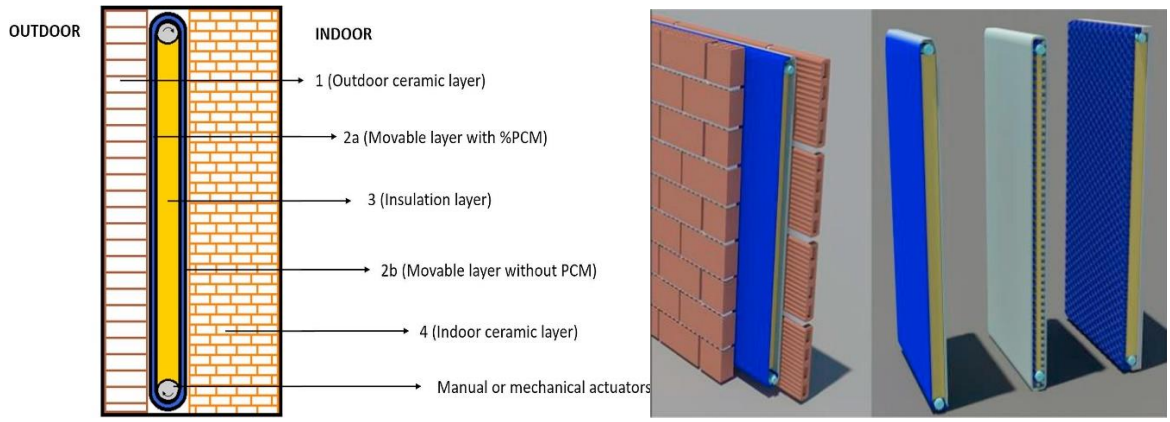

Fig. 2.12. Sketch of the dynamic PCM system (De Gracia, 2019)

Combining PCM with an active solar heating system is a novel technique to utilise the potential of PCM to maintain indoor thermal comfort and increase the efficiency of the building. This technique can effectively be implemented at locations suffering from low solar radiation in winter. Rucevskis et al. (Rucevskis et al., 2019) numerically compared the performance of passive and active incorporation of PCM for cooling load reduction through the building's roof under summer conditions in the Baltic States. They proposed a replaceable PCM layer, which can be installed between the concrete slab and the inside finishing layer. The PCM layer is provided with a capillary pipe system, where cold water flows, utilising the night cooling effect. The system was analysed using ANSYS FLUENT, considering an indoor temperature range of 21 °C–28 °C. The results reported that the indoor air temperature was reduced by a maximum of 4 °C using the passive system (without water flow) and approximately 10.5 °C when actively circulating the night-cold water compared with the standard case without the PCM. The study also indicated that PCM was not fully utilised during the simulation, where 65.7% of PCM was melted during the hottest day compared with only 24.1% on the regular days. This outcome clearly emphasised the need for appropriate calculation of PCM amount to be incorporated with the building envelope, which dramatically affects the cost and thermal performance of the system. Kong et al. (Kong et al., 2020) fabricated a hybrid system composed of perlite-based composite PCM wallboard (passive technique) coupled with a solar heating system (active technique) through capillaries. The system was placed inside the tested room's wall, as shown in Fig. 2.13. The room of the hybrid system was compared with another reference room without PCM over three working days under winter conditions in Tianjin, China. The analysis results showed a reduction of 44.16% in the daily heating energy consumption of the hybrid system in an actual scale room. Moreover, the study concluded that such a hybrid system could maintain the required comfort environment and enhance the efficiency of buildings.

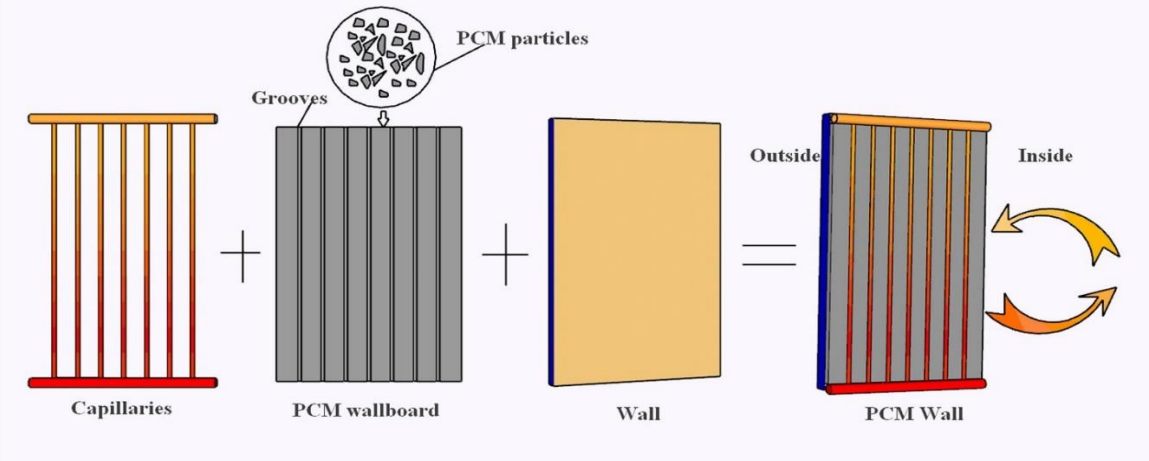

Fig. 2.13. Proposed design of hybrid PCM wall (Kong et al., 2020)

2.3.3. PCM-incorporated bricks

Bricks are important construction elements that are generally available in a rectangular shape. Specifically, fired clay bricks are popular types (particularly for walls) used in different constructions worldwide due to their availability, durability, ease of installation and high mechanical properties (Gentilini et al., 2015). PCM incorporation with bricks effectively increases the thermal mass of the constructed element to control the daily temperature fluctuations. A proposed practical procedure to fabricate bricks based on PCM is illustrated in Fig. 2.14.

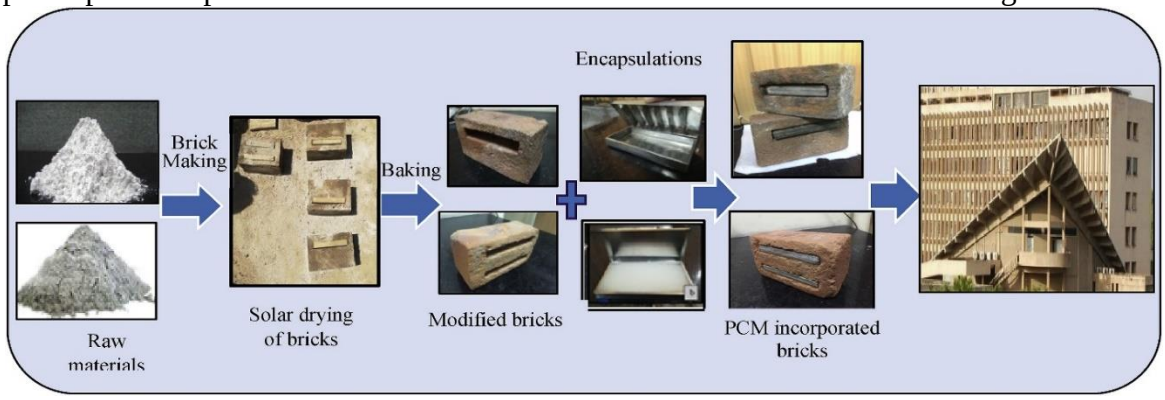

Fig. 2.14. Preparation of PCM-incorporated conventional bricks (Saxena et al., 2020)

The researchers have numerically and experimentally observed the potential of different PCM types containing conventional bricks of different types and configurations. Elnajjar (Elnajjar, 2017) numerically investigated the thermal performance of different types of PCM (n-Octadecane, n-Eicosane and P116 with a melting temperature of 27 °C, 37 °C and 47 °C, respectively) embedded in bricks under the climate conditions of the United Arab Emirates, based on one and seven days of assessment. The research aimed to decrease power consumption and greenhouse gas emissions by decreasing the heat gain through the building envelope and shifting the peak period. The results revealed that the use of PCM for building envelopes should be assessed appropriately and required at least seven-day analysis, given that the one-day assessment is misleading and insufficient to evaluate the thermal behaviour of the PCM. The results also showed that the n-Octadecane PCM had good behaviour on the first day, and the PCM P116 had the best performance with 30% heat flux reduction and energy saving based on the seven-day assessment. Erlbeck et al. Kant et al. (Kant et al., 2017) numerically investigated the latent heat of fusion of PCM embedded in bricks and analysed its effect on the building's thermal comfort under actual solar radiation and ambient temperature conditions. The study compared three cases, namely, the standard bricks, bricks with air filled in the cavity and bricks with PCM filled in the cavity. For the bricks filled with PCM, the performance of the three PCM types (Capric acid, Paraffin and RT-25) was evaluated to identify the best thermal performance. Results presented that the bricks filled with PCM performed well, and the heat flux reduction of Capric Acid, Paraffin, and RT-25 was 8.31%, 6.07% and 3.61%, respectively. The study also pointed out that the reduction of mechanical strength of bricks due to the cavities was the main drawback of PCM incorporation.

Tunçbilek et al. (Tunçbilek et al., 2020) numerically evaluated the seasonal and annual performance of PCM-incorporated bricks and energy saving of its latent heat for cooling and heating load under climate conditions of Marmara, Turkey. They investigated different models of brick-filled gaps with PCM (Fig. 2.16), considering the position of PCM, melting temperature and PCM quantity compared with the conventional air-filled gap brick. The results indicated that the PCM-filled gap, model D, placed near the indoor side, had higher energy saving. The optimal melting temperature depended on the season, which varied between 18 °C and 26 °C. They also conducted an annual analysis to determine the optimum PCM melting temperature for all seasons, which was 18 °C; 17.6% thermal demand reduction is obtained annually. The study revealed that incorporating PCM into bricks could provide better thermal performance in winter more than in

the summer season. Furthermore, an appropriate selection of PCM melting temperature is necessary to avoid overheating, which increases the cooling load considerably.

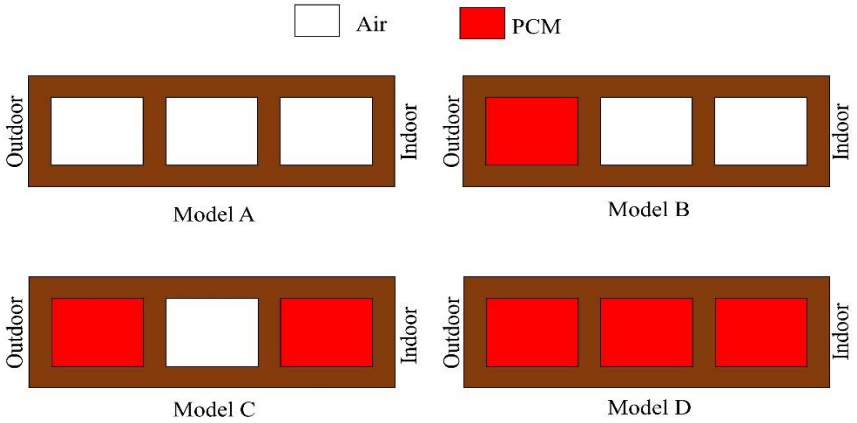

Fig. 2.16. Proposed models of bricks (Tunçbilek et al., 2020)

Saxena et al. (Saxena et al., 2020) experimentally studied the heat transfer and change in temperature across the PCM embedded into bricks under peak summer conditions in Delhi City, India. Two types of PCM, namely, Eicosane and OM35, were selected because they showed good stability and thermo-physical characteristics for melting/solidification processes. The PCMs were weighed and then encapsulated using aluminium containers with appropriate shape and size. Furthermore, the capsules were inserted inside the bricks of single and dual layer arrangements (Fig. 2.17). The proposed bricks were tested and compared with a standard brick without PCM. The results showed a reduction of 4.5 ℃- 7 ℃ in the inner surface temperature of PCM-incorporated bricks compared with the standard material. The heat across the bricks with single and dual PCM layers was reduced by 40% and 60%, respectively. In addition, the heat transfer of bricks containing Eicosane was reduced by 8% and 12% for OM35.

Fig. 2.17. Fabricating steps of PCM-incorporated bricks; (a) Single-slot brick, (b) Encapsulation container, (c) Macroencapsulated PCM, (d) Double-slot brick, (e) Encapsulation container with fins, (f) PCM-incorporated brick with twin slots, (g) Installation of bricks and (h) Final setup (Saxena et al., 2020)

Kumar et al. (Kumar et al., 2019) experimentally investigated the thermal performance of PCM-integrated hollow bricks for walls under warm and humid weather conditions in Chennai, India. One of the two tested identical rooms (3×3×3.65 m) had a macroencapsulated PCM in an aluminium foil packet placed inside the air holes of bricks with a total quantity of 750 kg of PCM (HS 29 type). The results showed a temperature reduction of up to 2 °C–6 °C in the room containing PCM compared with the other room without PCM during the tested months of summer. Therefore, the electric energy consumption for cooling and the greenhouse effect was highly avoided. Compared with the numerical results obtained using Design Builder software, the experimental results revealed good agreement with the experimental work.

Active incorporation of PCM with concrete blocks using air ventilation was investigated by Laaouatni et al. (Laaouatni et al., 2019). The experimental prototype, shown in Fig. 2.18, aims to solve the problem of antisymmetry of heat energy stored in PCM blocks to allow walls to work efficiently under different fixed climates. The study reported that the thermal performance of tested elements was improved by confirmed phase-shifting and increased inertial capability of the elements. The study was validated using two numerical tools and stated that the method could be applied to the actual wall scale, considering several parameters. These parameters are the dimensions of air tubes to the PCM amount, airflow velocity, geometry of tubes, PCM type, PCM melting temperature and the position in the cavities of blocks.

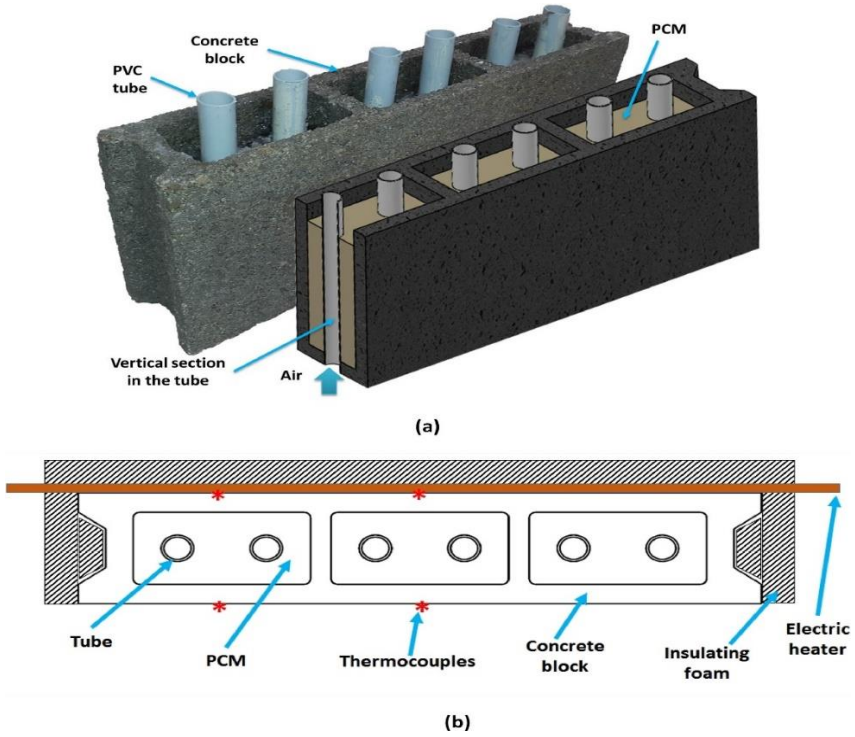

Fig. 2.18. PCM-incorporated block with air ventilation (Laaouatni et al., 2019)

2.3.4. PCM-macroencapsulated pipes

Generally, PCMs have poor thermal conductivity (Drissi et al., 2019; Song et al., 2019). Microencapsulation increases this matter since the PCM is covered using low thermal conductivity polymeric materials. The thermal conductivity of PCM can be improved using metal pipes made from copper, brass and aluminium in addition to their resistance against corrosion over a long term of service (Salgado et al., 2020). The PCM macroencapsulation pipes have better potential than microencapsulation because they can be produced easily at low cost (Cui et al., 2017), they have larger space that allows more PCM quantity to be involved and preserve volumetric change during cycles (Höhlein et al., 2018). In addition, they can be installed into the building envelope as separated elements and do not affect the mechanical or thermo-physical properties of the element, especially for concrete installations (Berardi and Gallardo, 2019). Several experimental studies

were reported in the literature regarding this trend for passive and active techniques. They showed excellent results in minimising cooling loads in summer or maintaining warm thermal comfort in winter. Rathore and Shukla (Rathore and Shukla, 2020) experimentally investigated the thermal response of pipe macroencapsulated PCM into the roof and walls under the outdoor climate conditions of India. Aluminium pipes filled with a commercially manufactured inorganic PCM (OM37) and a melting temperature of 36 °C to °40 °C were incorporated with a building envelope shown in Fig. 2.19. The experiment was conducted to reduce the cooling loads passively by studying the reduction of peak temperature, thermal amplitude and time lag on two cubicles, namely, PCM cubicle and a standard one. The results reported peak temperature reduction in the indoor temperature of PCM cubicle by 7.19%–9.18%, and the thermal amplitude was reduced by 40.67%–59.79%. Moreover, the cooling load of PCM cubicle was minimised by 38.76%, thereby saving electricity by approximately 28.31 Rupees/day (~0.40 US$/day) along with 60–120 min of peak load delay.

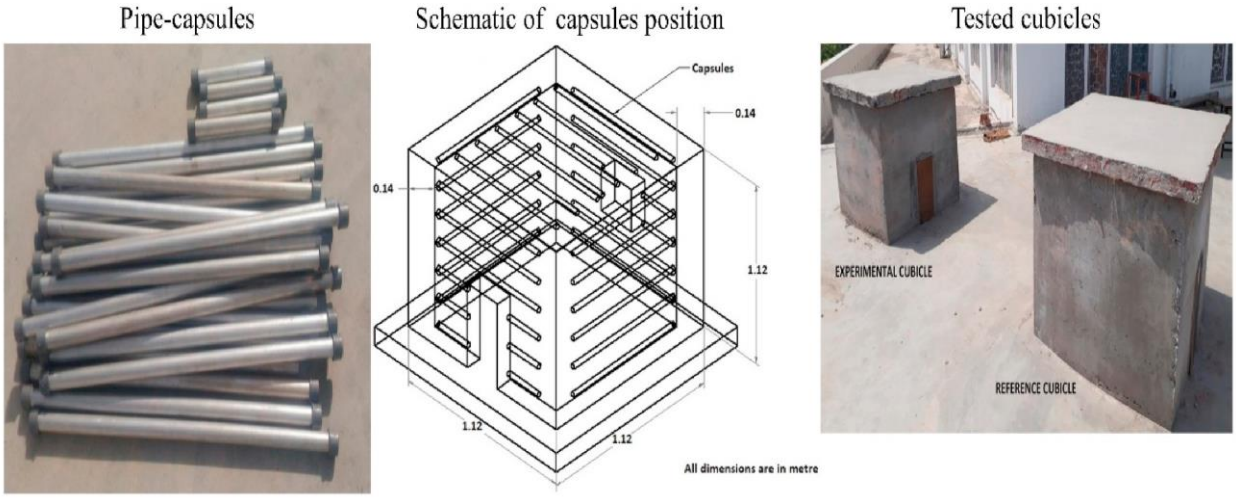

Fig. 2.19. Installation steps of pipe macroencapsulated PCM proposed by (Rathore and Shukla, 2020)

Sun et al. (Sun et al., 2018) experimentally investigated the effect of pipe diameter and its location on the thermal behaviour of PCM passively incorporated walls. Two pipes with sizes 1.27 and 1.9 cm and filled with PCM with melting temperatures ranging from 26 °C to 28 °C were installed horizontally in two positions near the interior and middle. Six light bulbs of 200 W were used as heat flux sources to conduct the experiment's heat reduction and time delay. The results revealed that the small pipe size performed better than the larger pipe size under the same conditions. However, the PCM in the two cases did not fully solidify to complete the cycle on the first day of the experiment. For the pipe with a 1.27 cm diameter installed in the middle position, a maximum heat flux reduction of 36.49% was achieved with a time delay of 89 min when the wall surface temperature was 55 °C. Furthermore, a maximum energy saving of 63.81 W-hr/m^2 and 116 min time delay were recorded at 69 °C for the 1.27 cm compared with 32.67 W-hr/m^2 obtained from the 1.9 cm pipe size. The experiments also concluded that the higher potential of PCM could be achieved at high temperatures, and the optimal pipe position is located between the interior and middle positions to guarantee full-phase transition. Hasan et al. (Hasan et al., 2018) experimentally investigated the potential of paraffin wax at 44 °C melting temperature as an insulation material to minimise the cooling load under hot Iraqi weather conditions. Paraffin wax, in liquid form, was poured inside an aluminium frame (square cross-section area) and installed to the interior of the ceiling and walls of a tested room at a volume of 1.5*1.5*1 m. The results showed that the cooling load reduction across the ceiling was 6.83%. By contrast, the reduction was 19.95%, 14.36%, 7% and 11.7% across the southern, western, northern and eastern walls, respectively. They also found that the maximum cooling load reduction of 20.9% was achieved, equivalent to electricity saving of approximately 1.35 $/day m3 at 1 cm thickness of PCM.

The passive incorporation of PCM into the building envelope is not always sufficient due to the noncompletion of melting or solidification processes either because of the high solar radiation, which overheats the PCM or lacks solidifying medium. In such cases, active techniques are recommended to complete the PCM cycles and prepare for the following day. Sun et al. (Sun et al., 2019) experimentally investigated the effect of active energy charging into the PCM for rectangular slabs. A small wind tunnel was used to supply hot air with various velocities and temperature ranges of 35 °C to 55 °C. The hot air was used to melt paraffin (26 °C–28 °C melting temperature) embedded inside the slab, and their effect on charging speed was investigated. The results indicated that the increase in air temperature from 35 °C to 55 °C increased energy charging by 201.7% (from 36.3 W to 109.4 W). On the contrary, it was slightly enhanced with the increase in air velocity from 4 m/s to 5 m/s. Similarly, the maximum PCM storage capacity of 97.2 Wh was obtained at 55 °C air temperature and 3 m/s air velocity at 109.4 W energy charging speed, thereby showing that the increase in air temperature had a greater effect on charging time than the increase in air velocity.

Navarro et al. (Navarro et al., 2016) experimentally studied the thermal performance of pipes, and encapsulated PCMs were inserted inside a prefabricated concrete slab under severe and mild winter conditions in Spain. Two cubicles with active slab (contains PCM) and conventional slab (reference) were fabricated to compare the energy saving obtained from using PCM. The active slab had 14 cavities incorporated with 52 kg of paraffin (RT-21) of 21 °C-22 °C melting temperature, poured in 1456 tubes of aluminium (12 mm diameter and 100 mm length). The slab, shown in Fig. 2.20, was activated using an air solar collector to reach the melting temperature of PCM and provide a heating stream to the indoor environment by controlled gates. The control system worked based on actual weather conditions to handle the charging and discharging processes, prioritising the latter. The PCM performance varied due to changing weather conditions, and the melting temperature was not reached over time.

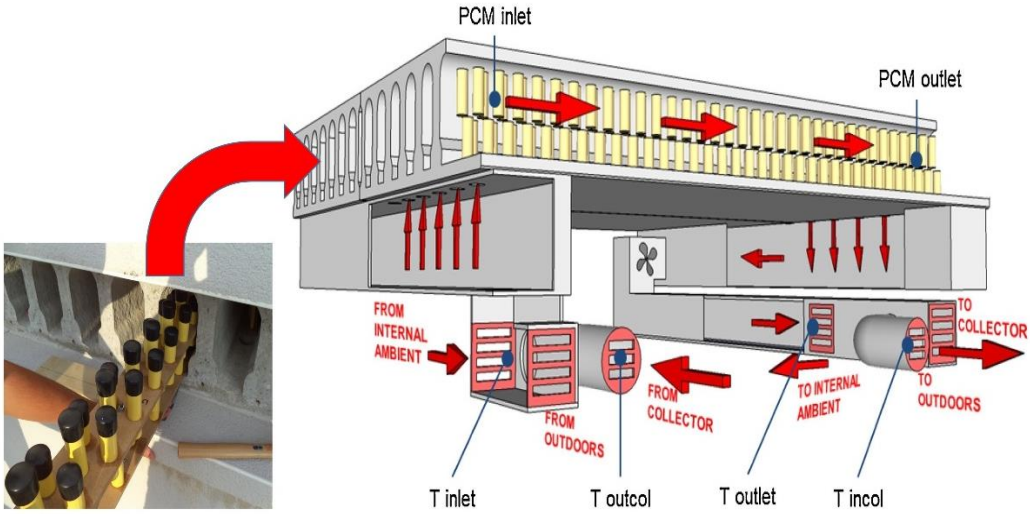

Fig. 2.20. Scheme of active slab system showing the PCM-encapsulated tubes and their position in the slab (Navarro et al., 2016)

The results stated that the energy saving of the active slab reached 20% during the partial melting of the PCM, and 55% was obtained at the complete melting and solidification cycles compared with the referenced slab. Furthermore, the study indicated that the energy-saving achieved was 25% and 40% during severe and mild winter conditions.

A summary of other studies that used different PCM types under different locations is presented in detail in Table 2.4, showing their application, incorporation methods and main findings.

Table 2.4. Summary of recent studies of PCM-incorporated building envelope

PCM type (MT, °C)	Country (city)	Study type	Envelope element	Incorporation method	Findings and remarks	Ref.
BioPCM (26) n-docosane (44)	South Korea	E	Roof	PCM packs	• Indoor temperature reduction up to 5.40°C obtained, • n-docosane was more effective than BioPCM.	(Yoon et al., 2018)
BioPCMs (20-32)	Saudi Arabia, Egypt, India	N	Roof + walls	PCM layer	• The maximum temperature was reduced by 2.04 °C, • ES of 17.97 - 34.26% gained.	(Sovetova et al., 2019b)
Paraffin Wax (58.5)	Thailand	E	Walls	Concrete filled PCM	• CL was reduced by 9%, ES by 31%, and TL of 184 min was obtained.	(Thongtha et al., 2019)
Enerciel 22 (18-29) $CaCl_2$. $6H_2O$ (28.9)	Iran (Isfahan)	N	Walls	PCM layer	• Heat transfer was reduced for Enerciel 22 in the range of 15.6-47.6% and 2-7.8% for CaCl2. 6H2O.	(Li et al., 2019)
BioPCM (25) RUBITHERMPCM (29)	South Korea (Seoul), Japan (Tokyo), and China (Hong Kong)	N	Roof + walls	PCM board	• PCMs showed ES of 4.48-8.21%, 3.81-9.69%, and 1.94-5.15% for Seoul, Tokyo and Hong Kong, respectively.	(Gassar and Yun, 2017)
Nine types PCM19 (19), PCM20 (20), PCM21 (21),..., PCM27 (27)	Canada (McMurray and Val-d'Or), Russia (Bratsk, Arkhangelskand Surgut), Finland (Oulu), and Sweden (Umea)	N	Roof + walls	PCM layer	• PCM23 and PCM24 indicated the highest ES of 4000-10000 kWh, • The payback period for all cities ranged from 16 - 32 years, • PCMs could reduce up to 4817.44 kg/year of CO2 emissions.	(Kenzhekhanov et al., 2020)
PCM (26)	Algeria	N	Walls	PCM clay mixed with stones	• CL reduced by 73%, • The peak load shifted by 5 hours, • Wall inner temperature reduced by 2°C.	(Lakhdari and Chikh, 2019)
RT28 (80 wt%) + Expanded graphite (20 wt%) (26.5-28.5)	China (Wuhan)	N	Walls	Pipe-encapsulated PCM	• Resist 55.6-82.8% of the heat coming from the outdoor, • Reduction of 32.4~55.5% of the accumulated heat entering indoors.	(Yan et al., 2020)
Micronal DS 5038 (25)	Lab. conditions	E	Walls	Cement-based PCM (concrete & mortar)	• The thermal conductivity of mortars decreased by 37% and about 30% for concrete. • The heat capacity increased by 13% for mortars versus 9% for concrete specimens.	(Essid et al., 2020)

PCM_Q21 (21) PCM_Q23 (23) PCM_Q25 (25) PCM_Q27 (27)	Northern Morocco	N+E	Roof + walls	PCM layer	• PCM_Q23 and PCM_Q25 lead to optimal thermal performance, • The east wall showed the best condition (lowest DF = 0.017 and highest TL = 7 13 min), • The worst condition presented by the roof (highest DF = 0.031 and lowest TL = 466 min), • PCM reduced the DF by 60% (north-facing wall) and 35% (roof).	(Kharbouch et al., 2018)
Bio-PCMTM (27)	Australia	N	Ceiling + walls	Cladding layer	• PCM refurbishment can efficiently reduce indoor heat stress risks and improve occupant health and thermal comfort, • The discomfort period was reduced by 65% during extreme heatwave conditions.	(Ramakrishnan et al., 2017b)
Energain® PCM	Lab. conditions	N+E	Wall	Separated PCM layer	• Maximum heat flux reduced by 15% and delayed by 2 h.	(Fateh et al., 2017)
n-octadecane (18.80–37.83) Beeswax (33.41–61.05)	United States (Chicago, Los Angeles, Miami and Phoenix)	N+E	Wall	PCM impregnated gypsum/cement (G/C) board	• n-octadecane and Beeswax-impregnated G/C board increased thermal conductivity by 129% and 150% compared with the original G/C board. • In Chicago, n- octadecane performed better than Beeswax during the cooling season in terms of CL and TL, • In Miami, ES of 7.8% and 6.4% were achieved when n-octadecane and Beeswax were applied during the heating season, • In Miami and Phoenix, CL reduction of 3.6% - 4.3% was obtained using n-octadecane-based G/C board.	(Jeong et al., 2019)
Eicosane (36-38) OM35 (35)	India (Delhi)	E	------	PCM incorporated bricks	• Temperature reduced by 4-7°C during peak hours, • Heat flow reduction by 8% for Eicosane and 12% for OM35.	(Saxena et al., 2019)
OM37 (39.1)	India (Mathura)	E	Roof + walls	Aluminium pipe encapsulated PCM	• Indoor peak temperature reduced by up to 0.2- 4.3 °C, • Annual TL of 97.5 min and the annual DF reduction of 24.69% were obtained. The peak heat flux is reduced by 17.37% annually, • Cost-saving in peak CL of 1.47 rupees/kWh/m2/day obtained.	(Rathore et al., 2020)
PCM24D (21.9) RT21 (21)	Norway (Oslo)	N	Walls	PCM24D integrated concrete and RT21 were added as a separate layer	• The annual ES reached 28%, • Energy reduction during the summer of 32% versus 23% during the winter.	(Cao et al., 2019)
n-octadecane (23.55) n-eicosane (34.99)	China (Hangzhou)	N	Walls	Double PCM layers integrated walls	• Peak indoor temperature reduced by 2.9-6.7°C in summer, thermal comfort hours increased by about 12%, • Thermal energy charge time increased as PCM thickness increased.	(Su et al., 2020)

N: Numerical, E: Experimental, MT: Melting Temperature, ES: Energy Saving, CL: Cooling Load

2.4. Summary of literature review

Incorporating PCMs into building envelopes is still an ongoing research area, with no universal agreement giving a broad insight into this technology. The above work has reviewed the potential of PCM-incorporated building envelope, a growing technology to improve building performance, focusing on the opaque elements (i.e., roofs and walls). PCM technology showed a remarkable enhancement of building thermal energy either by decreasing undesired thermal loads or managing the thermal demand, thereby positively influencing thermal comfort and building energy saving.

A general revision of recent studies has been given, considering the main PCM types, working range, encapsulation methods, influential parameters and incorporation techniques with building envelope materials, mainly for roofs and external walls. It has been observed in the reviewed literature that the PCM has superior potential to enhance the thermal mass of the building envelope, eventually improving the thermal comfort and energy conservation of buildings. The weather conditions were the main factor influencing the PCM incorporation process, including the type of PCM, quantity involved and effective position.

Although reviewed studies showed that passive PCM incorporation techniques are simple and cost-effective, serious drawbacks were pointed out and directly impacted the PCM's effectiveness. These drawbacks were mainly associated with the limitation to exploiting the entire PCM storage capacity, unguaranteed phase transition (charging/discharging) during the thermal cycle and uncontrolled direction of stored heat. This represents a challenging task for further research and deep investigation to reach the maximum benefits of this technology at minimal operational cost and thermal deterioration.

Literature studies also showed that the thermal behaviour and beneficial aspects of PCM-incorporated buildings under harsh weather conditions received little attention. Under severe hot locations, the PCM may reach a full melting state in the early day hours, influencing the benefits and resulting in a negative thermal impact. Since the PCM under such unique locations works as dynamic insulation, its effectiveness could be enlarged using traditional thermal insulations, considering the PCM effectiveness. Furthermore, night cooling/ventilation is an effective method in hot climate applications to recharge the PCM at night and prepare it for the following thermal cycle. However, it may be limited to extremely hot locations where the temperature level of night air is insufficient. Therefore, a deep studying of this method and its interaction with PCM incorporation is worth investigating, considering the possible options.

Based on all research gaps highlighted above, this work will focus on incorporating the PCM into the building envelope, considering all challenging cases. The PCM will be incorporated passively into thermally-poor construction materials under a non-ventilated environment and examined under severe hot weather conditions. The influential parameters of PCM incorporation into the building envelope, such as the PCM position and location, will be studied along with the best PCM-brick wall arrangement. The role of thermal insulation with PCM will be studied from the energetic and thermal points of view to quantify. Finally, natural night ventilation will also be investigated to tackle PCM's negative behaviour during the night and maximise its advantages cost-effectively considering the passive methods.

3. MATERIALS AND METHODS

This chapter presents the research methodology, study location, experimental set-up, materials, instrumentation, mathematical formulation, and evaluation methods carried out in the current research.

3.1. Research methodology

In the current research, the incorporation of PCM into building envelope elements (namely the roof and walls) has been investigated experimentally and numerically under severe hot summer conditions. The follow-up experimental work was conducted under actual weather conditions (outdoor mode) in Al Amarah city, southern Iraq, during 2020 and 2021. The construction materials used and PCM type were locally available in the city, selecting the thermally-poorest combination for residential buildings to show the contribution of PCM. Furthermore, the extended numerical studies were conducted for the same location, building materials and year 2021. The procedure and sequence of experiments carried out in this study are displayed in Fig. 3.1.

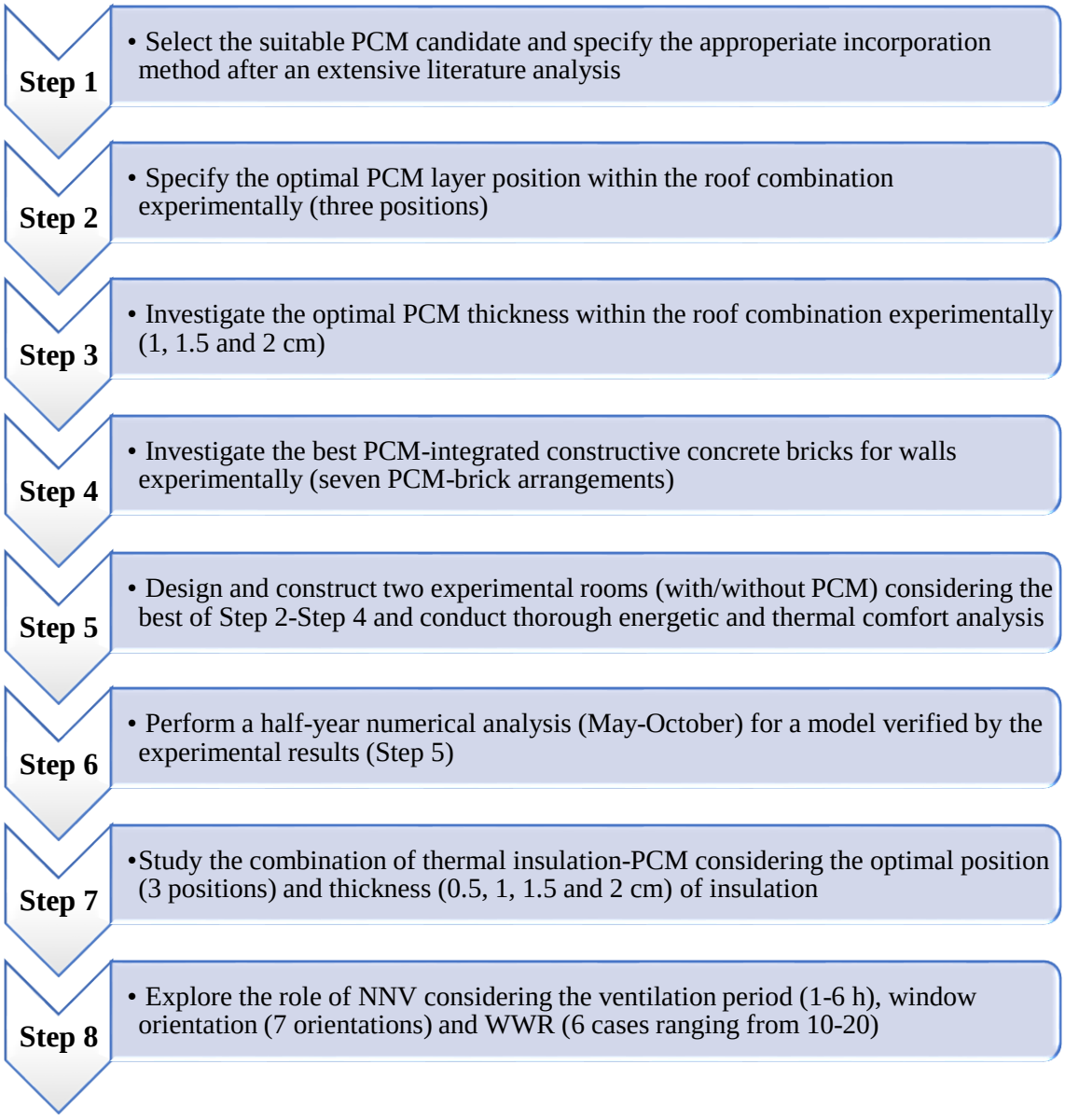

Fig. 3.1. Flowchart for the research methodology

3.2. Study location

The experimental and numerical investigations have been confirmed under the weather conditions of Al Amarah city (Latitude: 31.84°N and Longitude: 47.14°E), Maysan Province, southern Iraq (shown in Fig. 3.2). This location is dominated by a hot summer season and classified as a subtropical desert climate according to the Köppen Geiger climate classification (*Köppen climate classification*, 2022).

Fig. 3.2. Geographical map of Iraq with highlighted study location (Al Amarah city)

The weather in Al Amarah is harsh during the summer season and characterised by high ambient temperatures during the day and night, exceeding the mark of 48 °C and 30 °C, respectively (Fig. 3.3), requiring high-performance air-conditioning systems all day long. July is typically the hottest summer month which usually has long sunshine hours and high ambient temperatures, typically exceeding 45 °C during the day and 30 °C at night. Conversely, October represents a transition month characterised by relatively high diurnal temperatures and cold nights. The experimental days were chosen carefully concerning the clear sky and relatively similar weather conditions to ensure the effective use of PCM with a complete melting phase during the day. Furthermore, most of the experiments were conducted during August and September, suitable hot summer months in the country with typical weather conditions between the hottest (July) and coldest (October). Summer days are generally sunny (more than 29 days/month) with a clear sky and high solar radiation. The latest reports stated that Al Amarah city had the hottest climate in Iraq during the summer of 2021 and amongst the highest recorded high ambient temperatures in the Middle East (Korosec, 2021).

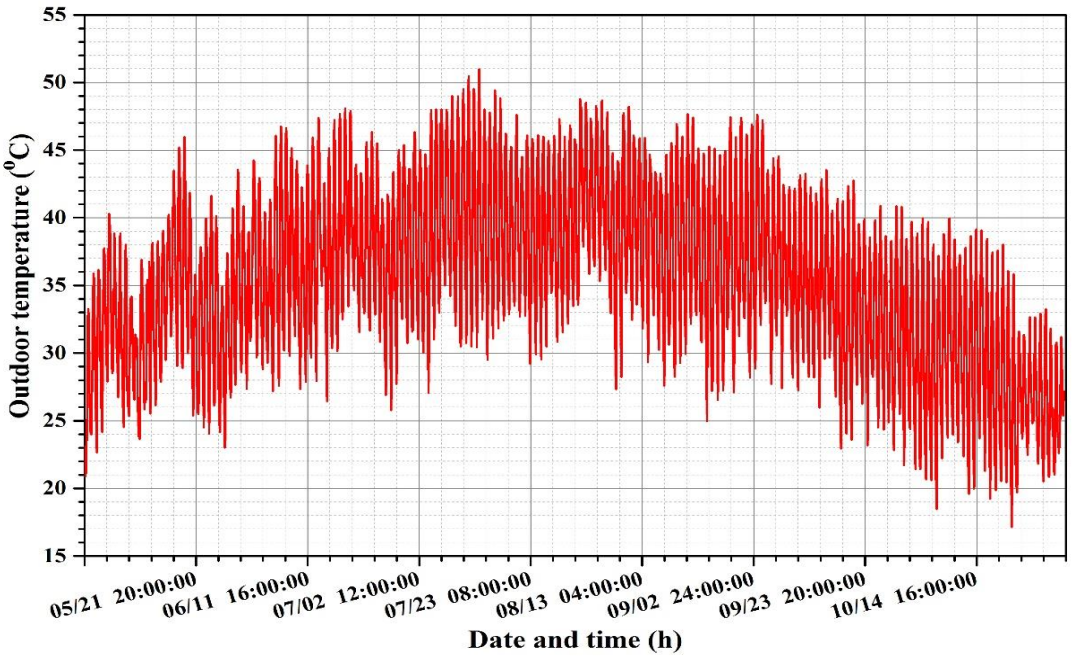

Fig. 3.3. Average hourly outdoor temperature during summer 2021

The incident solar radiation on buildings in the location under study is essential to determine the outside element surface temperature and heat transfer coefficients. In this regard, the average solar radiation rate incident on the room's elements (i.e., the roof and walls) is shown in Fig. 3.4. As observed in the figure, the roof was exposed to high solar radiation rate for a long time a day, namely from 9:00 to 16:00, exceeding 1000 W/m^2 in June, July and August. Besides, the east and west walls receive higher solar radiation rates than the northern and southern walls by about 700-800 W/m^2 in the above three months. However, October shows different solar radiation trends in which the east wall showed higher ratios than the roof, and the south wall received more solar radiation than the previous months.

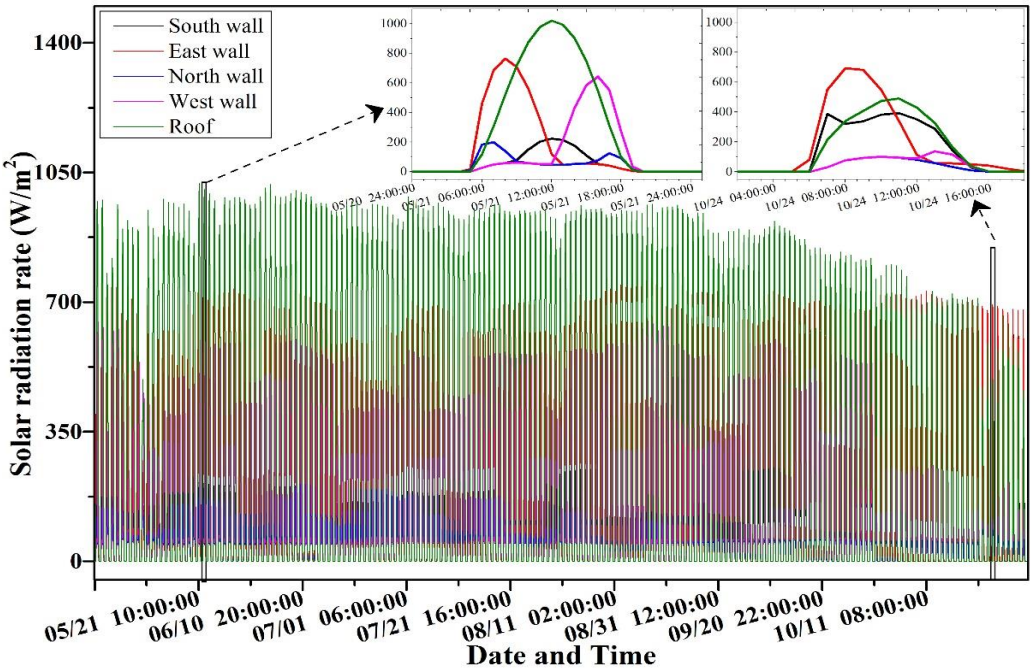

Fig. 3.4. Solar radiation rate incident on room elements

3.3. Experimentation

3.3.1. Construction materials and PCM

First of all, it is worth highlighting that all experiments were performed using the thermally-poorest construction materials used for residential and commercial buildings in Iraq, which resulted in high cooling loads (Al-Yasiri et al., 2019). The main construction materials used in the experimentation are as follows:

Roof combination: The roof was built from a typical combination of flat roofs installed for medium and low-income inhabitants in the city. The roof combination comprised of the following layers, from outside to inside:

- Isogam (roofing layer): Local roofing and waterproof material have been increasingly used in the last 15 years in Iraq as an alternative to concrete tiles and other traditional roofing materials (Al-Yasiri et al., 2019). It is mainly made from bitumen-rubber mastic and laminated from both sides with a thin plastic layer (one coated with silver colour to reflect the solar radiation). This plastic layer is removable and highly influenced by changeable weather conditions, limiting its reflectivity.
- Concrete (main roof layer): Concrete layers were fabricated according to the concrete mix ratio 1:2:3 of raw materials (cement: sand: gravel) used for residential building roofs in Iraq, which has c25-30 Mpa (Resan et al., 2020). Locally used raw materials (i.e., cement, sand and gravel) were mixed with water to fabricate the concrete mixture. The mixture was poured into moulds and left dried naturally. Fig. 3.5 shows the procedure followed to prepare the concrete layers.

Fig. 3.5. Fabrication procedure of concrete layers

- Gypsum mortar (cladding layer): Locally available pre-fabricated gypsum mortar boards were used in the experimental models and rooms. Gypsum mortar is very popular as a cladding material for building interior surfaces in the country.

Walls: The walls of the reference room were built from the following layers, from outside to inside:

- Cement mortar (outdoor cladding layer): This layer is popularly applied on the exterior and interior wall surfaces in Iraqi buildings. The cement mortar layer was applied on the exterior walls in the experiments of the full room to ensure no air leakage could enter the room through brick joints.

- Concrete bricks (main layer): This brick type is widely used in the northern regions of Iraq and is limitedly used in the hot southern regions due to its poor thermal performance. However, low-income inhabitants still use this brick type due to its good mechanical properties and availability with competitive cost. The procedure followed to prepare the bricks (bare and PCM bricks) will be described in subsection 3.3.3.

Window: As stated earlier, a locally available clear single-glazing window was fixed on the east wall of each experimental room. The window in this work has a small size with respect to the wall area since it focuses on the PCM incorporation within the roof and walls, and the only purpose of the window was to provide natural night ventilation for specific cases, as it will be described later.

Floor: A plywood foundation was employed as the floor of each experimental room.

The construction materials and their thermal and physical properties are shown in Table 3.1.

Table 3.1. Materials used for experimental rooms' construction (Ministry of Construction and Housing-Minstry of Planning,Thermal Insulation Blog, 2013)

Material	**Room element**	**Thickness (cm)**	**k (W/m.K)**	**ρ (kg/m^3)**	**C_p (kJ/kg.K)**
Isogam	Roof	0.4	0.35	1400	1100
Concrete layer	Roof	5	1.49	2300	800
Fibreglass insulation	-------	2	0.043	-----	-----
Expanded polystyrene foam (EPS)	Roof + walls	0.5, 1, 1.5 and 2	0.035	25	1400
Gypsum mortar	Roof	0.2	0.23	980	896
Cement mortar	Walls	1-2	0.99	2020	1000
Concrete brick (L:230×W:120)	Walls	7	1.4	1440	750
Plywood	Floor	3	0.18	950	1200
Single glazing (U-Factor=5.48, Solar heat gain coefficient=0.95)	Window	0.6	--------	--------	--------

In this work, a locally available paraffin wax (organic material) was used as a PCM. This PCM type is a petroleum-based product generated during the de-waxing process of Iraqi crude oil at governmental refineries. It has a melting temperature in the range of 40 °C- 44 °C according to the differential scanning calorimeter (DSC) test shown in Fig. 3.6, making it a suitable candidate for the temperature variation in the location under study and the passive technique adopted. The main thermo-physical characteristics of this PCM are listed in Table 3.2.

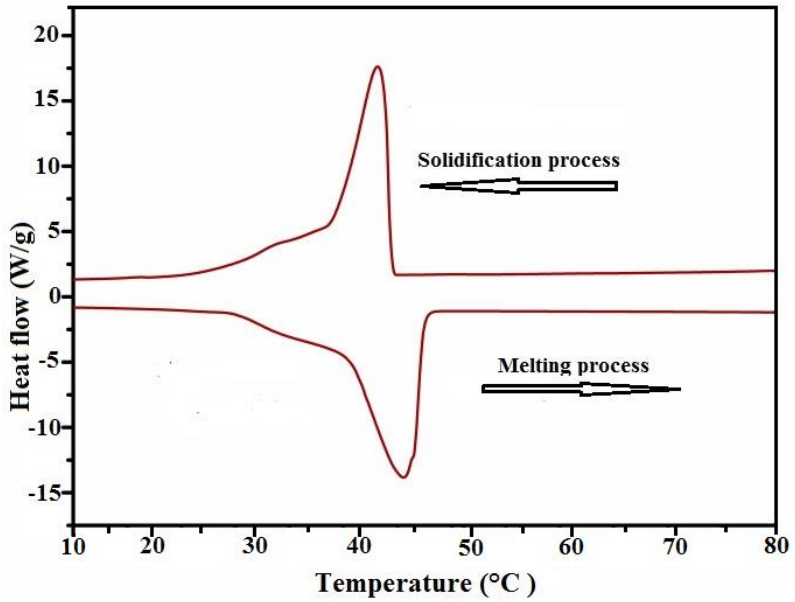

Fig. 3.6. DSC test of used PCM (Ministry of Oil, Midland Refineries Company, 2022)

Table 3.2. Characteristics of PCM used in the experiment

Property/ feature	Unite	Value
Appearance	--------	Whitish
Composition	%	40 oil + 60 wax
Melting temperature range	°C	40-44
Latent heat of fusion	kJ/kg	190
Thermal conductivity (solid & liquid)	W/m.K	0.21
Density (solid/liquid)	kg/m^3	930/830
Specific heat (solid & liquid)	kJ/kg.K	2.1

Moreover, some advantages and disadvantages of this PCM are listed in Table 3.3, making it a good option in the current work. It is worth mentioning that this paraffin type is popular in Iraq and extensively used locally in different thermal applications such as solar desalination (Chaichan et al., 2016), electrical distribution transformers (Hasan, 2017), solar air heating (Habib et al., 2021) and solar photovoltaic modules (Chaichan et al., 2022). Moreover, this PCM has considerable potential to overcome the cooling load issues in Iraqi buildings during summer. It is particularly massively available in Iraqi petroleum refineries as a waste product (Wahid et al., 2017).

Table. 3.3. Advantages and disadvantages of used PCM (Soliman, 2020; Chaichan et al., 2022)

Advantages	Disadvantages
• Locally available at a low price (it can also be provided free for research purposes by the government). • High thermal storage capacity. • Chemically stable after many thermal cycles. • Low flammability. • Compatible with many encapsulation materials. • Environmentally friendly (organic).	• Low thermal conductivity (common disadvantage of paraffin). • Paraffin solidification at the container edges may occur. • Crystallisation may occur at high temperatures.

The macroencapsulation technique using widely available local metallic sheets was adopted to prepare the separate PCM panel for the roof and PCM capsules immersed into bricks. These encapsulation materials are suitable for the application considering the thermal performance provided and compatibility with the PCM type (Ostrý et al., 2020). The PCM panel used in the

roof combination was made of galvanised steel sheet, whereas PCM containers of different shapes and sizes were used for the PCM-concrete bricks, as will be described later in detail.

As mentioned in the research methodology, the final experimental set-up was reached after set of preliminary experiments to investigate the optimal PCM position and thickness within the roof and the best PCM capsule-concrete brick arrangement to be used for constructing the PCM room. The detailed description of the follow-up experiments is as follows:

3.3.2. Optimal PCM layer position in the roof

The optimal position of the PCM layer within the roof was experimentally investigated by considering three different positions of the PCM layer within the roof combination. To this aim, four identical test rooms were fabricated in the experiment, mainly (i) Model A: a reference room consisting of the three traditional layers (finishing layer - main layer - cladding layer), (ii) Model B: a room contains additional PCM layer placed between the finishing layer and the main layer, (iii) Model C: a room contains PCM placed in the middle of the main layer and, (iv) Model D: a room where the PCM layer placed between the main layer and cladding layer (shown in Fig. 3.7). Two cases were investigated in this work in which how the finishing layer affects the absorptivity of a composite roof and results in higher outside surface temperatures. Therefore, the Isogam has been installed in two cases: Case I, in which regular Isogam is used, and Case II, when removing the reflecting layer. The latter case allows high heat to be transferred towards the test room, which is essential in investigating PCM's potential at high temperatures.

As this work focuses on the roof, high-density cork boxes were considered as the floor and sidewalls of tested models. The boxes have a thickness of 30 mm and have length, width and height of 40×30×23 cm, respectively. Boxes are locally available and often used for ice cream storage and low-temperature food preservation due to their high thermal insulation behaviour. The boxes are covered with a high-quality fibreglass insulator for further insulation to guarantee that the heat passes through the roof layers only.

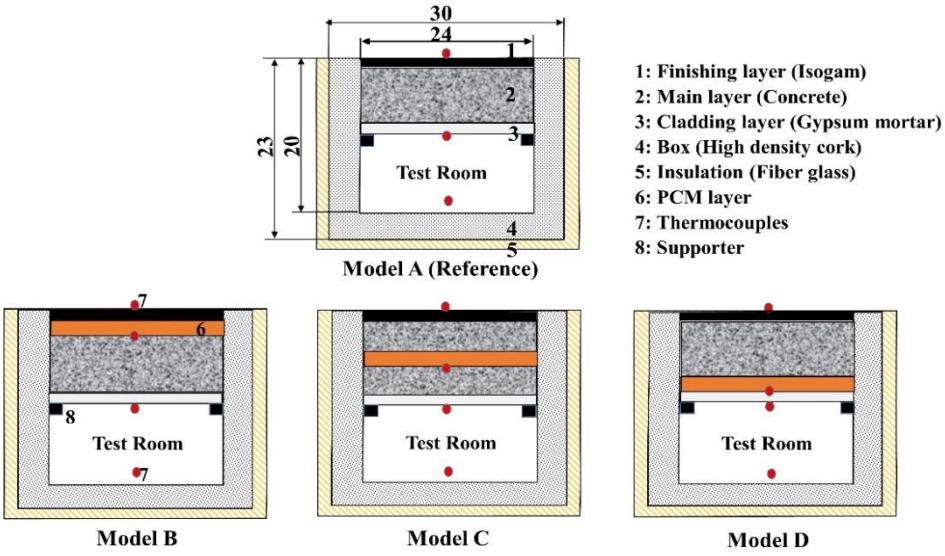

Fig. 3.7. Schematic view of the proposed models for optimal PCM position experiment

Each model's roof comprises three layers: an Isogam layer, a concrete layer and a gypsum mortar layer. This roof type is a popular combination installed in residential buildings in the city, with the worst thermal behaviour and high cooling loads. It is worth mentioning that all layers were smoothed to make sure of perfect contact between each two. Every layer has been sealed separately using high-quality insulation foam during the installation. The foam is essential to guarantee no air infiltration from outside towards the test room, and vice versa, and heat would be exchanged only through the roof layers. The last experimental set-up of this experiment is shown in Fig. 3.8.

Besides, a detailed description of the instruments and measurement devices used in the experiment will be detailed in Section 3.4.

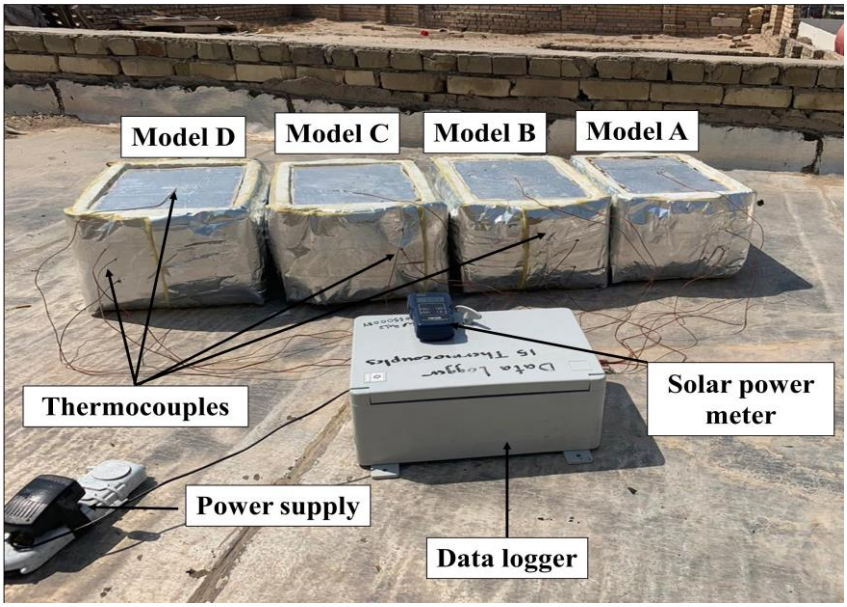

Fig. 3.8. Experimental models of optimal PCM position experiment

3.3.3. Optimal PCM layer thickness in the roof

The optimal PCM layer thickness was also investigated experimentally for three consecutive days considering three different thicknesses, namely 1, 1.5 and 2 cm (Fig. 3.9), placed beneath the Isogam roofing layer. In this regard, the models are composed of a composite roof situated inside a rectangular box made from high-density cork characterised as the insulated floor and walls of the room. Moreover, high-density insulation blanket were insulated boxes to improve the insulation further and guarantee that the heat transfers only through the roof layers. The first model served as a reference room with standard composite roof layers (Model A). The other three models were incorporated with an extra macroencapsulated PCM panel with 1, 1.5 and 2 cm thicknesses termed Model B, Model C and Model D, respectively. The panels were placed beneath the roofing layer as it is the optimal position for the PCM within the building envelope to gain the best thermal performance and energy-saving under hot climate conditions (obtained in the 3.3.2 experiment). The final appearance of the experimental model is similar to those presented in Fig. 3.8.

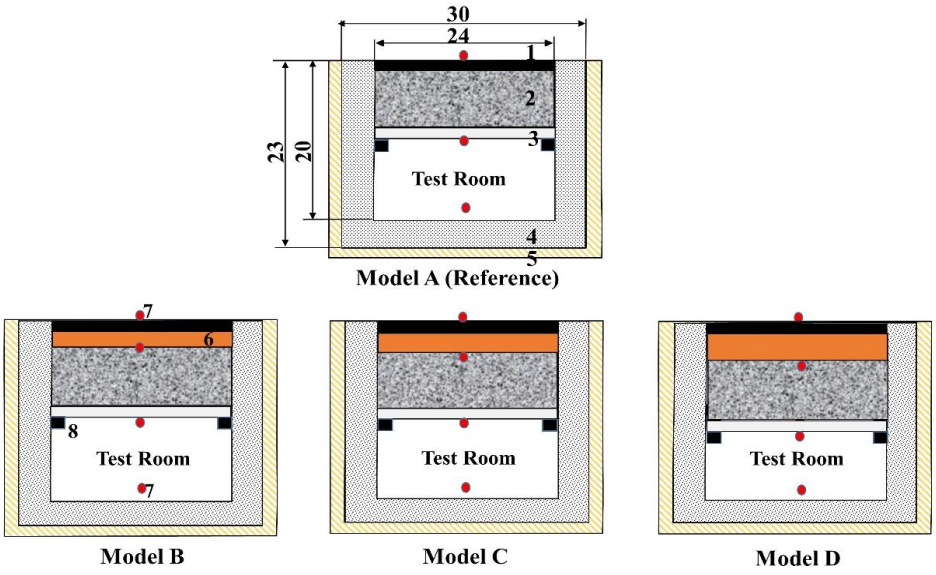

Fig. 3.9. Schematic for the experimental models. (1- Finishing layer, 2- Main roof layer, 3- Cladding layer, 4- Box, 5- Insulation, 6- PCM layer, 7- Thermocouples, 8- Supporter)

Fig. 3.10 shows the procedure to prepare the PCM panels used in the experiments to investigate the optimal position and thickness within the roof combination. The poured paraffin (PCM) inside panels was 0.5 kg for the optimal position experiment, whereas poured with 0.5, 0.75 and 1 kg in the optimal thickness experiment to prepare 1, 1.5 and 2 cm, respectively.

Fig. 3.10. Preparation procedure of PCM panels

3.3.4. Concrete brick-enhanced PCM

Eight concrete bricks were fabricated and tested in this experiment over four consecutive days to specify the best thermally-enhanced concrete brick with PCM. The bricks were mixed with a ratio of 1:1.5:3 (cement/sand/gravel), the popular mixing ratio of concrete bricks in the country of Iraq (Ministry of Construction and Housing- Ministry of Planning,Thermal Insulation Blog, 2013). The bricks were fabricated with 23, 12 and 7 cm (length, width and depth) to control the PCM capsules' position and maintain a suitable experimental set-up. The first brick sample was the reference brick (A), and the other seven samples were made with PCM capsules of different shapes and sizes (B, C, D, E, F, G and H). These PCM bricks were designed, fabricated and immersed inside bricks during preparation. The capsules were made from locally available aluminium of circular, square and rectangular cross-section areas. Aluminium sections were cut into different shapes and sized carefully to hold the same quantity of PCM (~145 g), providing a fair comparison among tested samples. Likewise, the capsules' design also considered the concrete brick size to produce symmetric bricks with maintained mechanical strength. The procedure followed to prepare PCM capsules and test bricks and the schematic view of prepared bricks are shown in Fig. 3.11-3.13. Besides, Table 3.4 lists the main design characteristics of capsules.

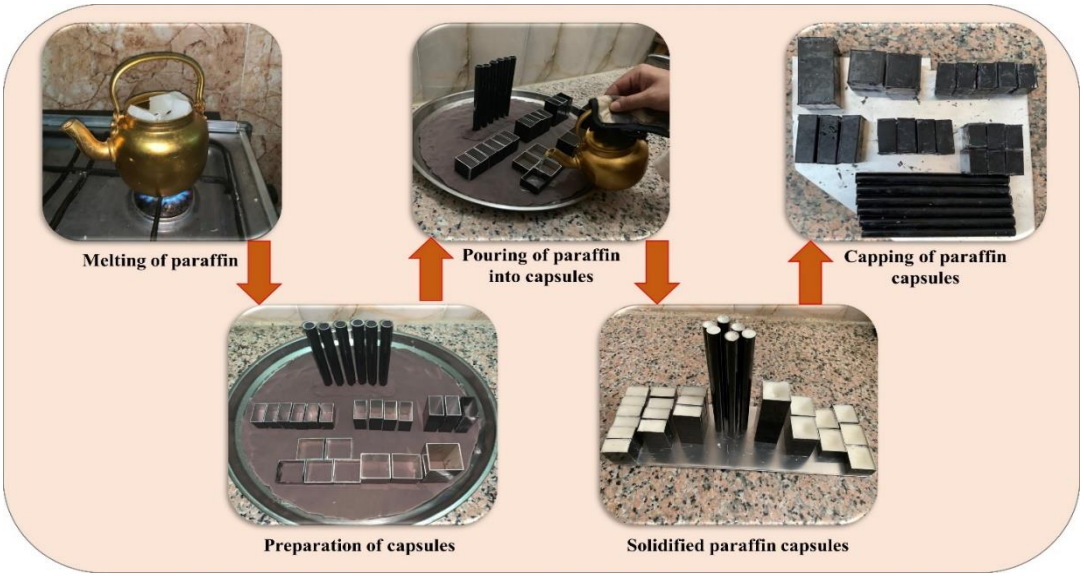

Fig. 3.11. Preparation of PCM capsules

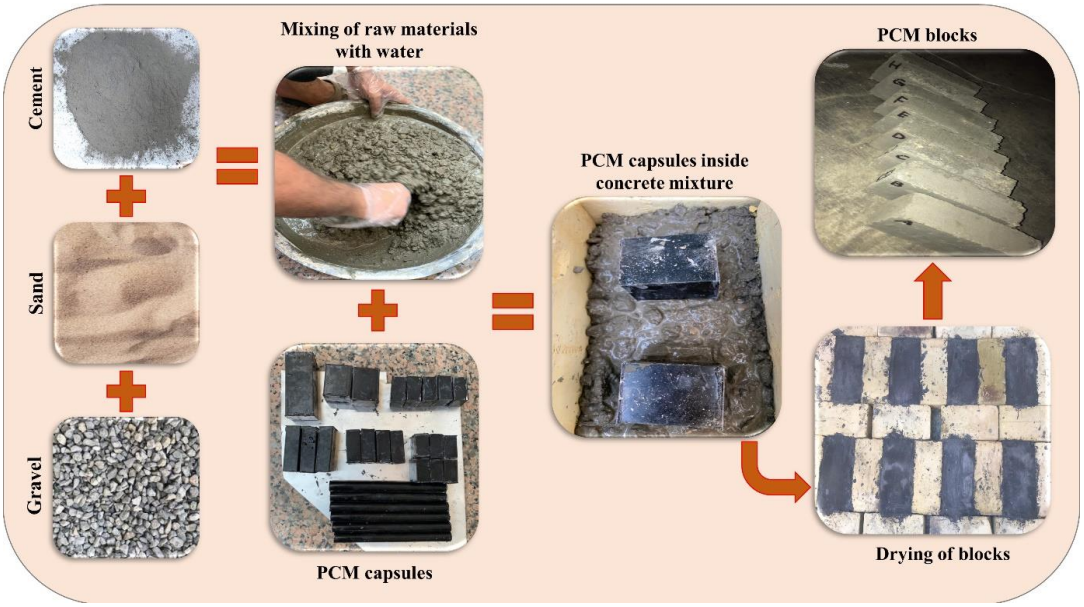

Fig. 3.12. Fabrication procedure of PCM concrete bricks

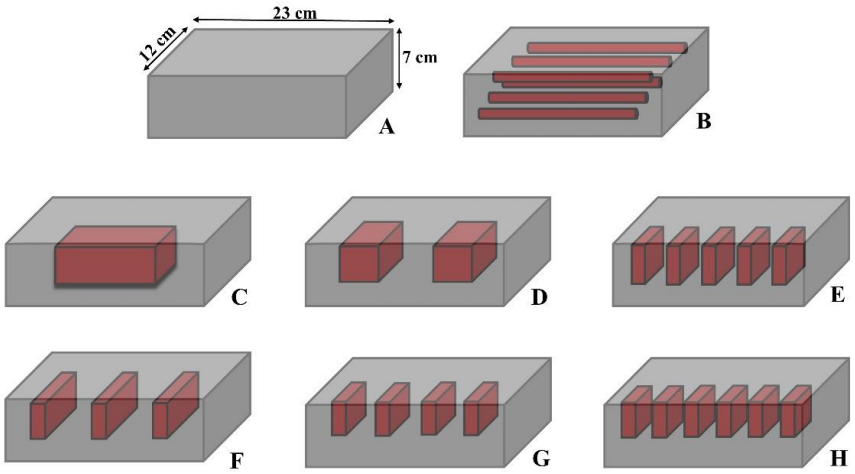

Fig. 3.13. Schematic for PCM capsules incorporated concrete bricks

Table 3.4. Design characterisation of experimental brick samples

Brick sample	Capsule cross-section area	Capsule dimensions (cm)	Number of capsules	Heat transfer area of capsule(s) (cm^2)
A	Reference brick	------	------	------
B	Circular	Ø1.5*18	6	529.9
C	Square	4*4*10.25	1	196
D	Square	4*4*5	2	224
E	Square	4*4*2	5	320
F	Rectangular	4*2*7	3	300
G	Rectangular	4*2*5.125	4	310
H	Rectangular	4*2*3.5	6	348

Experimental bricks were placed inside a high-density cork arrangement (80 mm thickness) and covered with a fibreglass blanket to provide more insulation. Each brick was placed separately, and two thermocouples were installed on both sides to measure the temperature difference during the experiment, as shown in Fig. 3.14. During installation, bricks were sealed using high-quality insulation foam to ensure no air leakage between the interior and exterior environments and guarantee that heat passes only through the bricks.

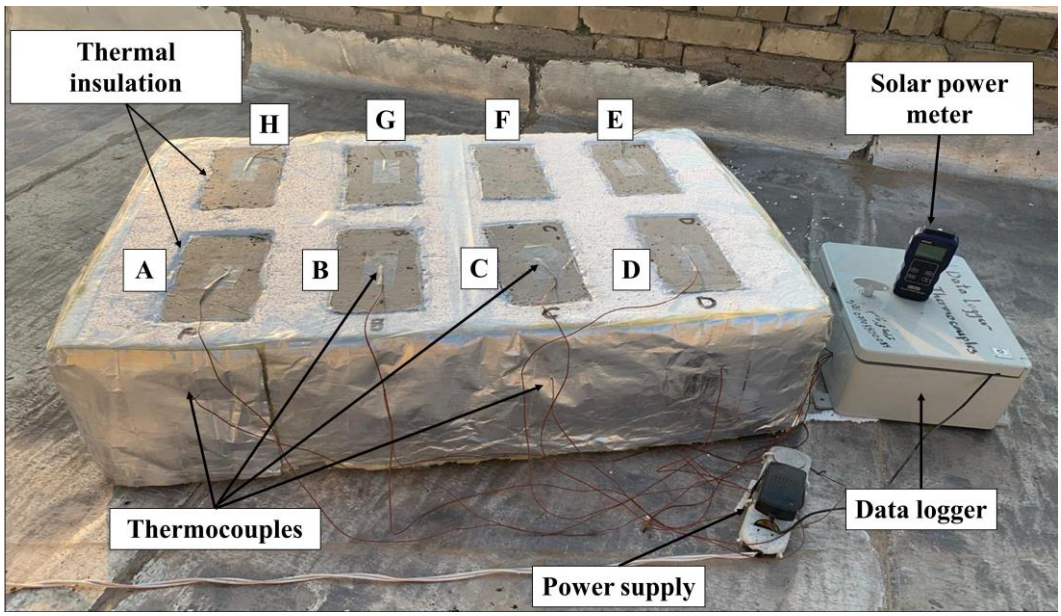

Fig. 3.14. Experimental set-up of the referenced and modified concrete bricks

3.3.5. Experimental rooms

Two identical rooms were built with a size of 1×1×1 m; one included PCM in the roof and walls (PCM room), whereas the other left without PCM for comparison (reference room). The PCM room was constructed considering the best thermally-performed case of the preliminary experiments described in 3.3.2, 3.3.3 and 3.3.4, according to the results presented in Section 4. Both rooms were placed in an open atmosphere, exposed directly to solar radiation all day long, and were east-oriented, as shown in Fig. 3.15. The rooms were situated on a high-density wooden plate to ensure no thermal influence of the foundation and guarantee that the room's ambient temperature is only influenced by the walls and roof. Both rooms were spaced by 120 cm to avoid the shadow effect of one on the other during sun inclination. Furthermore, a small openable window with a wooden frame (25×35 cm) was fixed on the east wall. However, both windows were kept close all day to investigate the thermal behaviour of PCM under a non-conditioned state in some cases and opened for 1-6 h in other cases to investigate the role of night ventilation. All slots of joined elements were closed using high-density foam to ensure no air infiltration between the indoor and outdoor environments.

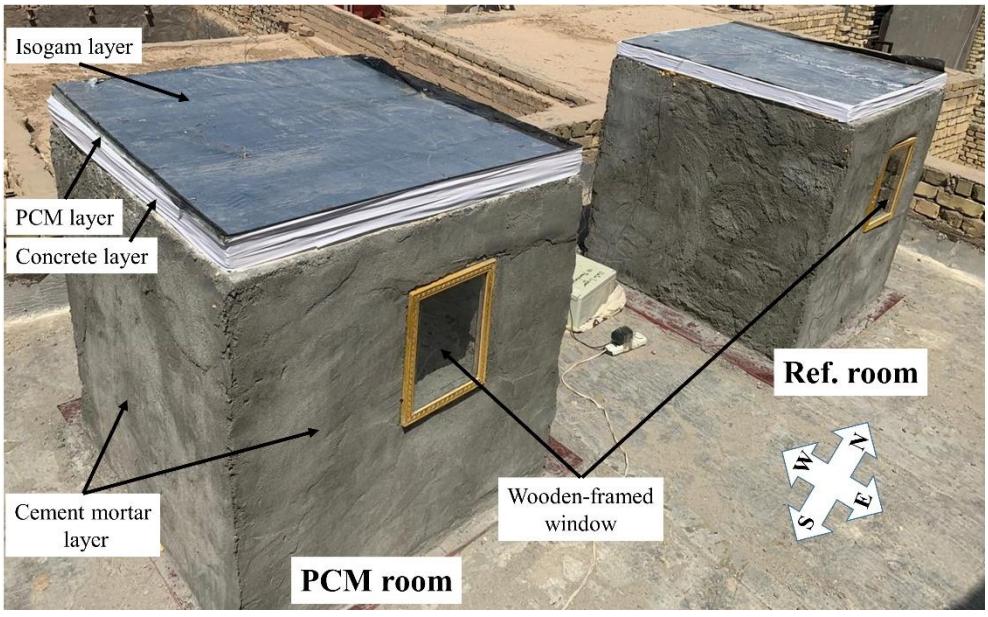

Fig. 3.15. 3D view of final experimental rooms

The PCM panel involved in the roof of the PCM room was made with dimensions of 100×100×1.5 cm and placed between the Isogam and main roof layer. Although the panel could carry more than 10 kg of PCM, only 7 kg was poured to ensure that no leakage occurs during the melting phase that may result from PCM volume change or possible panel inclination during installation.

For the walls of the PCM room, PCM capsules made of aluminium containers of a square cross-sectional area of 4×4×2 cm dimensions were immersed inside each concrete brick. Five PCM capsules were inserted in the centre of each PCM concrete brick. Each PCM brick holds a total PCM quantity of about 145 g. These PCM capsule-immersed concrete bricks are the best thermally-performed among many arrangements, according to the experiment presented in 3.3.4. Fig. 3.16 shows some photos of the preparation of the PCM panel and capsules.

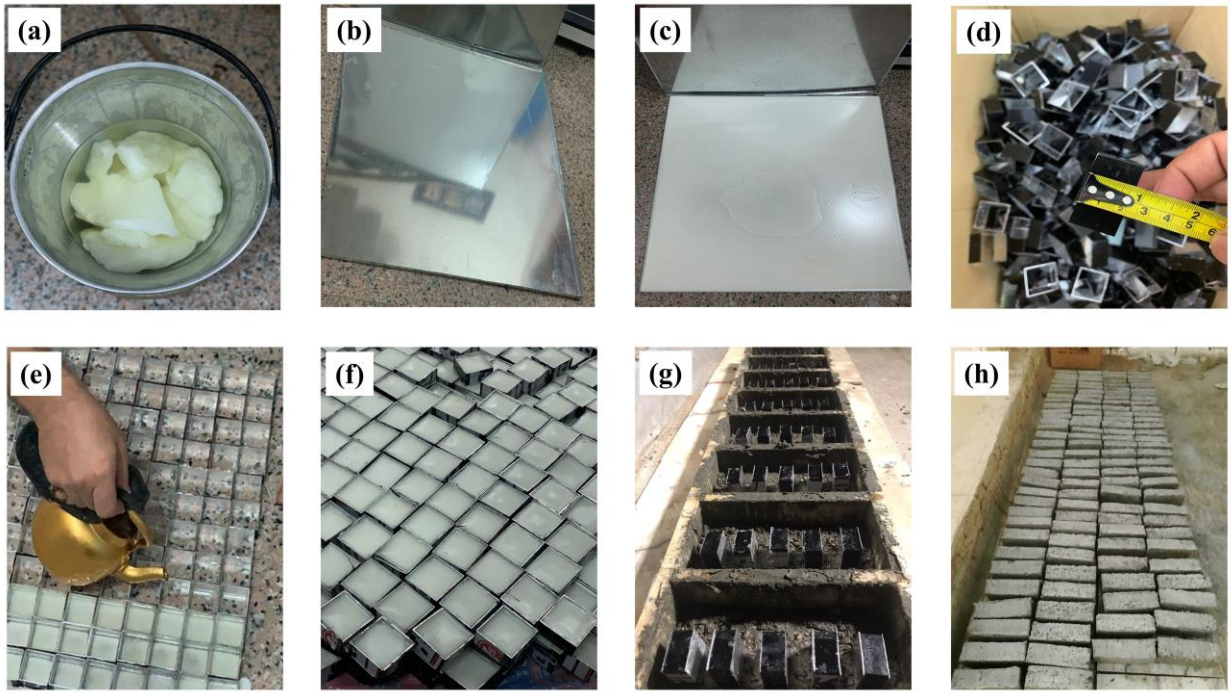

Fig. 3.16. Preparation of PCM panel and capsules (a) melted paraffin (PCM), (b) empty galvanised panel, (c) poured PCM inside the panel, (d) empty capsules, (e) poured PCM inside capsules, (f) solidified PCM capsules, (g) PCM capsules inside concrete during preparation, (h) dried PCM bricks

3.4. Instrumentation

For thermal measurements, a multi-channel Arduino (type Mega 2560) based data logger (manufactured and calibrated by Ardunic Co. (*Ardunic*, 2020)) was connected to thermocouples to measure envelope surface temperature and air temperatures. Ten T-type thermocouples from TEMPSENS of 0.2 mm direct contact bulb with a temperature range of -270 °C to 370 °C and accuracy of ±0.5 °C) were installed on the inside surface centre of roofs and walls for both reference and PCM models/rooms. Besides, one thermocouple was positioned in the space centre of each model/brick/room to measure the indoor air temperature, and another was fixed outside the models/bricks/rooms for outdoor air temperature measurement.

The data logger was programmed to measure and record temperatures every 10/30 min throughout the experiments and store data continuously in a portable micro storage memory connected to the Arduino. On the other hand, a handy solar power meter (Type SM206 with a range of 0.1-399.9 W/m^2 and accuracy of ±10 W/m^2) was used to measure the incident solar radiation during the experiment daytime every 30 min. In addition, a thermal camera (model WB-80VOLTCRAFT®) of a temperature sensor ranging from -20 °C to 600 °C and accuracy of ±2% ±2 °C was used to show the temperature behaviour of outside surfaces temperature of models/bricks/rooms at

different times of the experiment. The data logger arrangement, the solar power meter, and the thermal camera are shown in Fig. 3.17.

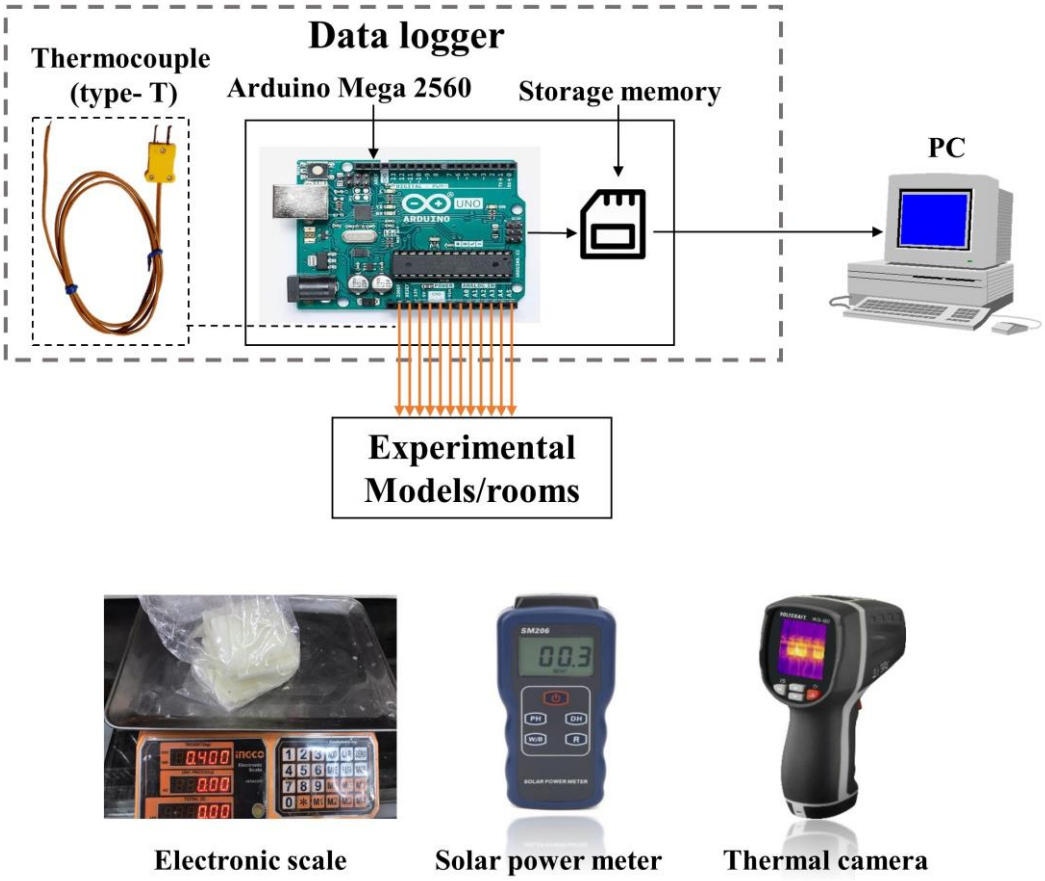

Fig. 3.17. Data logger arrangement and other devices used in the experimentation

As indicated earlier, the PCM layer was integrated with the PCM roof of the model/room as a separate layer, while it was immersed as capsules into wall bricks, which weakened their mechanical properties. Therefore, investigating the mechanical strength of PCM bricks is necessary to provide a complete vision of PCM incorporation into the building structure from the thermal and mechanical point of view. Therefore, the best PCM brick attained in section 3.3.4 and used later to construct the PCM room was tested at the age of 28 days using a compression test machine (type ADR Touch head from ELE International) with a 2000 kN maximum load capacity to specify the crushing strength against bare bricks without PCM. Fig. 3.18 presents some photos of the mechanical test.

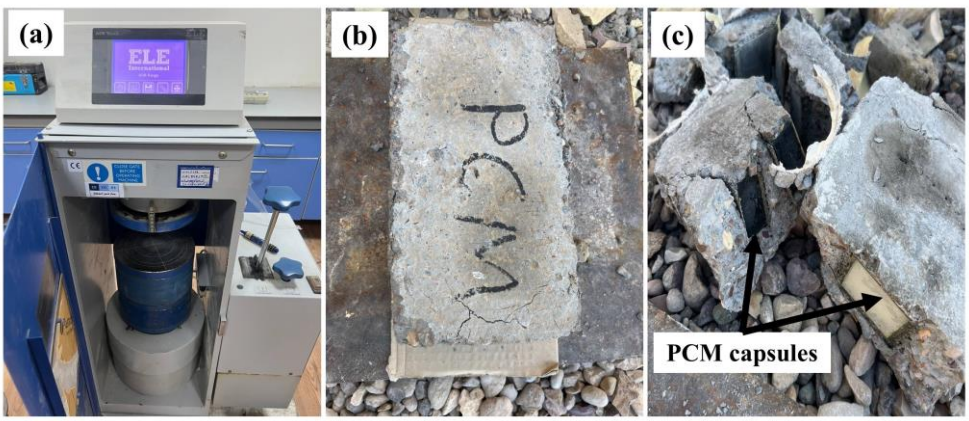

Fig. 3.18. Mechanical test (a) test machine, (b) PCM brick before crushing, (c) crushed PCM brick

3.5. Numerical formulation

3.5.1. Numerical model and modelling

Numerical studies were conducted to extend the results obtained in the experimental studies over the summer period from May to October. Besides, some other studies regarding the effect of night ventilation and thermal insulation were not easy to attain experimentally. In this regard, a PCM room model was developed by SketchUp graphical tool, identical to the PCM room used in the experimental studies, having the same element size and composed from the same construction materials (Fig. 3.19). The room model was simulated using EnergyPlus software, the most popular software in building energy simulation studies. The software was developed by the US Department of Energy, mainly using EnergyPlus weather file (EPW) and information data file (IDF) as editable input files comprising all required data of the weather and thermophysical characteristics of the building. The software relies on advanced heat balance algorithms to produce the heat transfer coefficients of the surface temperature difference of building elements and other output variables.

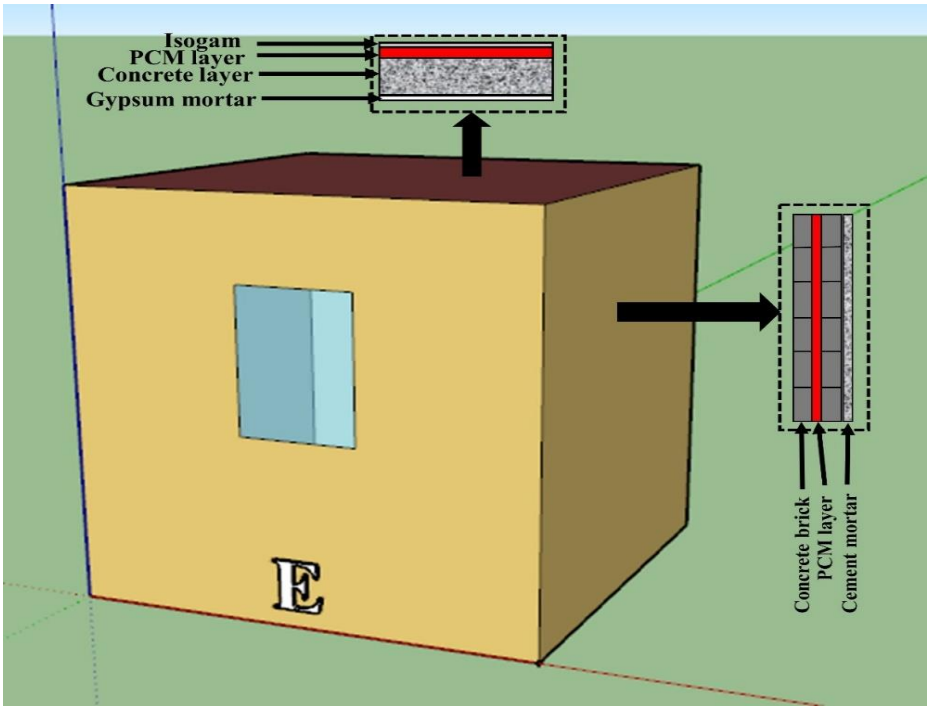

Fig. 3.19. PCM room model

EnergyPlus software can simulate buildings-based PCM via a one-dimensional conduction finite-difference (CondFD) solution algorithm to overcome the phase change phenomenon and interactions with the adjacent construction materials. In this regard, the PCM layer loaded into the building envelope is expressed using a fully-implicit first-order scheme shown in Eq. (3.1) as follows:

$$\rho C_p \Delta x \frac{T_i^{j+1} - T_i^j}{\Delta t} = \left(k_W \frac{\left(T_{i+1}^{j+1} - T_i^{j+1}\right)}{\Delta x} + k_E \frac{\left(T_{i-1}^{j+1} - T_i^{j+1}\right)}{\Delta x} \right) \quad (3.1)$$

where ρ is the layer density (kg/m^3), C_p is the specific heat capacity (kJ/kg.K), Δx is the layer thickness (m), and Δt is the calculation time step (s). T is the node temperature (K), whereas i denotes the modelled node. Subsequently, $i+1$ and $i-1$ represent the adjacent nodes concerning the inner and outer sides, respectively. $j+1$ is the instant time step, whereas j is the previous time step. k_W is the thermal conductivity of the interface between i and $i+1$ nodes, whereas k_E is the thermal conductivity for the interface between the i and the $i-1$ nodes (W/m.K). k_W and k_E could be calculated by Eq.(3.2-a) and Eq.(3.2-b), as follows:

$$kw = \frac{\left(k_{i+1}^{j+1} + k_i^{j+1}\right)}{2} \tag{3.2-a}$$

$$k_E = \frac{\left(k_{i-1}^{j+1} + k_i^{j+1}\right)}{2} \tag{3.2-b}$$

Since the C_p of the PCM layer is a temperature-dependent property every time, its value could be calculated by Eq. (3.3) as follows:

$$C_p = \frac{h_i^j - h_i^{j-1}}{T_i^j - T_i^{j-1}} \tag{3.3}$$

where h is the specific PCM enthalpy (kJ/kg) and could be defined by the auxiliary function with respect to the PCM temperature as presented in Eq. (3.4), as follows:

$$h = h(T) \tag{3.4}$$

To simplify the CondFD algorithm for the transient heat transfer model, the following assumptions were considered:

- The PCM and construction materials are homogeneous and isotropic, with no heat generation within the material.
- The PCM layer is in perfect contact with the roof and wall layers, and the contact resistance is negligible.
- The PCM melting and solidification temperatures are sharp during the simulation, and no hysteresis occurs.
- The outer surface temperature of the room elements was calculated as a sol-air temperature ($T_{sol\text{-}air}$), considering hourly solar radiation incident on each element and outdoor convection heat transfer, according to Eq. (3.5) (American Society of Heating, 2016; Li et al., 2019).

$$\begin{aligned} T_{sol-air} &= T_a + \frac{\alpha I_{inc}}{h_o} - 3.9°C \textit{ for Roof} \\ T_{sol-air} &= T_a + \frac{\alpha I_{inc}}{h_o} \textit{ for walls} \end{aligned} \tag{3.5}$$

where T_a is the ambient temperature (K), α is the element absorptivity coefficient, I_{inc} is the inclined solar radiation on the element (W/m^2), and h_o is the convective-radiative heat transfer coefficient of outer element surfaces (W/m^2.K).

In some cases, it is necessary to explore the effectiveness of PCM within the element during specific times by considering the percentage of liquid and solid states. This is essential, especially when several PCM types are compared with each other or investigating their effective PCM position within the building element. This can be attained by calculating the so-called liquid fraction. The PCM liquid fraction denotes the amount of liquidus PCM out of the total PCM amount, ranging from 0 to 1, in which the value 0 means no liquid found, whereas the value 1 means the PCM is fully melted. Mathematically, the liquid fraction is calculated according to Eq. (3.6) as follows:

$$Liquid\ fraction = \begin{cases} 0 & \text{if } T_n \geq T_l \text{ (Solid phase)} \\ \dfrac{T - T_s}{T_l - T_s} & \text{if } T_l > T \geq T_s \text{ (Mushy zone)} \\ 1 & \text{if } T_n < T_s \text{(Melting phase)} \end{cases} \tag{3.6}$$

where T represents the node temperature within the PCM layer. T_l and T_s are the PCM temperatures at the liquid and solid states (i.e., melting and solidification phases).

3.5.2. Extended numerical studies

Numerical tools usually perform wider investigations than experimentations, extending the understanding of building energy when applying different methods. Therefore, it is easier to conduct several studies that are hard to be accomplished by experiments due to limited physical abilities and the complexity of time and measurements.

Numerically, the basic studies presented in 3.3.4 are verified for long summer periods (6 months) to show PCM's thermal behaviour and contribution to the built environment. Besides, some other studies are conducted in this thesis numerically, to extend the knowledge of PCM incorporation from other thermal aspects. These studies mainly consider the role of natural night ventilation and thermal insulations.

3.5.2.1.Thermal insulation combined PCM room

Combining PCMs with thermal insulation could improve the building's thermal inertia and increase thermal resistance, which potentially improves the building's energy performance. Consequently, the role of traditional thermal insulation (expanded polystyrene, EPS) was investigated following the procedure below:

i. Specify the optimal position of EPS concerning the PCM layer in the roof since it has many layers and highly influences the room performance (Al-Yasiri and Szabó, 2022b). To this aim, a simulation is conducted on a composite roof involving 1 cm of EPS in three different positions for a specific day in July, the hottest month. During simulations, the walls and floor of the room were set as adiabatic, while the roof contained an additional EPS layer placed in different positions (shown in Fig. 3.20), as follows:
   - Between the Isogam and PCM layers (termed as "*EPS-o*", indicating the EPS position near the outdoor environment),
   - Between the PCM and concrete layers (termed as "*EPS-m*", indicating the EPS position in the middle of the roof composition), and
   - Between the concrete and gypsum mortar layers (termed as "*EPS-i*", indicating the EPS position near the indoor zone).

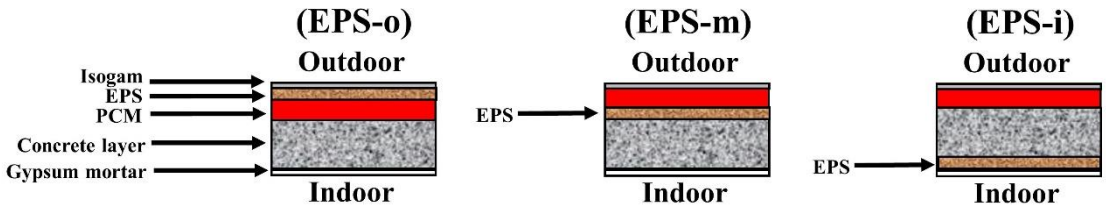

Fig. 3.20. EPS position cases in the roof combination

The best position of the EPS layer was identified by determining the position with minimal influence on the PCM effectiveness in terms of its liquid fraction as the best variable to monitor PCM effectiveness (Arıcı et al., 2020). In other words, the best EPS layer position is considered the position with the lowest influence on the PCM melting and solidification to avoid a negative impact on the PCM phase change during the thermal cycle.

ii. The best position specified for the EPS layer (in i) was adopted to investigate different EPS thicknesses, namely 0.5, 1, 1.5 and 2 cm, installed in the PCM room.

3.5.2.2. Natural night ventilation

The effect of natural night ventilation (NNV) was investigated, considering the role of low ambient temperature at night to minimise the indoor temperature of the PCM room and improve its negative behaviour. For this purpose, the NNV period through a one-side window was first studied to show improvement in the PCM room thermal performance compared with the reference room. Later, the numerical model was verified against the experimental results and applied to show the effect of window direction, building orientation and window-to-wall ratio (WWR) to give a wider look at possible further enhancements that could be applied along with the PCM, following the procedure bellow:

i. The NNV period was investigated experimentally for six consecutive days in which the windows of both reference and PCM rooms were opened for 1h on the first day from 18:00 to 19:00, 2 h on the second day from 18:00 to 20:00, and so on till 6 h in the sixth day from 18:00 to 24:00.
ii. Verified numerical model was used to consider the NNV through opened window for 6 hours from 18:00 to 24:00 when positioned on the south, west and north compared with the original direction towards the east. Besides, the same procedure was applied by rotating the room model towards the south-east, south-west, north-east and north-west directions to specify the best building orientation for NNV.
iii. At the best building orientation attained in the previous point, the effect of WWR of 10-20 WWR was investigated compared with the original case of 8.75 WWR. Fig. 3.21 shows the WWR cases considered in the study.

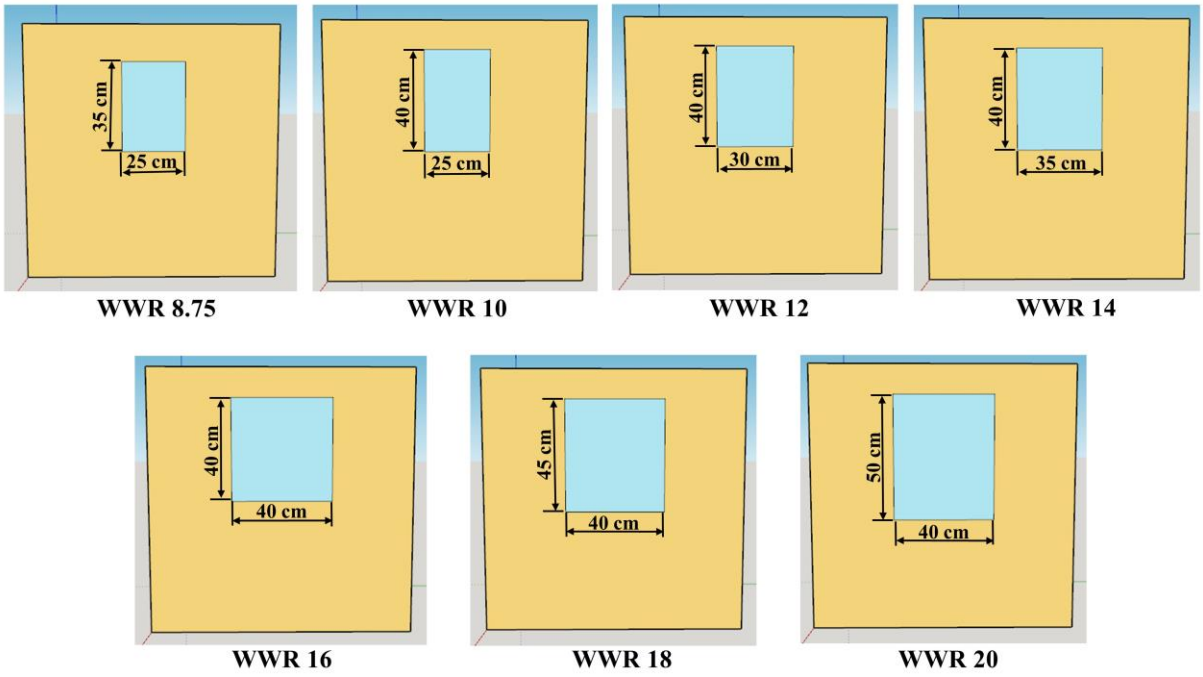

Fig. 3.21. Proposed WWR in the study

3.6. Analysis of the PCM thermal contribution

Several indicators have been presented and discussed to show the thermal behaviour and contribution of the PCM room in comparison with the reference room. These indicators could show the energetic and thermal comfort improvement of the PCM element/room compared with the reference one considering the surface temperature of the building envelope or indoor temperature. These indicators are as follows:

3.6.1. Maximum temperature reduction

Maximum temperature reduction (MTR) is an energetic indicator that describes how high the temperature reduction of the room's elements is considering the indoor and outdoor surface temperatures in the PCM room compared with the reference one. Mathematically, the MTR of an element could be calculated according to Eq. (3.7) as follows (Kenzhekhanov et al., 2020):

$$MTR = T_{out,max.} - T_{in,max.} \tag{3.7}$$

where $T_{out,max.}$ and $T_{in,max.}$ are respectively the maximum outer and inner surface temperature of the element (in °C). Moreover, the MTR difference between elements of reference and PCM rooms can also be calculated to show the contribution of PCM to the element energy enhancement.

The same concept was followed in some cases to indicate the MTR (in %) and referred to as room maximum temperature reduction (RMTR), referring to the maximum reduction in the indoor room temperature when incorporated PCM compared with the reference room. In this regard, the mathematical expression in Eq. (3.8) was as follows:

$$RMTR = \frac{T_{i,max,reference} - T_{i,max,PCM}}{T_{i,max,reference}} \times 100\% \tag{3.8}$$

where $T_{i,max.reference}$ and $T_{i,max.PCM}$ are the maximum indoor temperature for reference and PCM rooms/models. In the RMTR calculations, the outdoor ambient temperature (T_o) is used instead of T_{out} to be compared with the indoor temperature (T_i).

3.6.2. Decrement factor

The decrement factor (DF) is the reduction in the cyclic temperature through the envelope elements (Thiele et al., 2017). This means the envelope element with a lower DF has a higher thermal resistance against outdoor temperature fluctuations. This property is essential for the thermal comfort assessment since it is associated with the mean radiant and operative temperatures. The DF was calculated as the difference between the element's maximum and minimum inner surface temperatures to the difference between the maximum and minimum outer surface temperatures. Mathematically, the DF of any element was calculated according to Eq. (3.9) (Asan, 2006). All other elements followed the same formula.

$$DF = \frac{T_{in,max} - T_{in,min}}{T_{out,max} - T_{out,min}} \tag{3.9}$$

where $T_{in,max}$, $T_{in,min}$, $T_{out,max}$ and $T_{out,min}$ are respectively the maximum and minimum temperatures of an element's interior and exterior surfaces (in °C).

3.6.3. Time lag

The difference between the time at the maximum inner and outer element surface temperatures is identified as the time lag (TL). TL indicates the shifting of peak temperature during the midday to the off-peak period at a late time, which is the main benefit of PCMs in building applications. Accordingly, the TL of the element was calculated according to Eq. (3.10) (Mazzeo and Kontoleon, 2020) as follows:

$$TL = \tau_{T_{in,max}} - \tau_{T_{out,max}} \tag{3.10}$$

where $\tau_{in,max}$ and $\tau_{out,max}$ are respectively, the time at the element's maximum inner and outer surface temperatures (min, h).

The DF and TL are important indicators for building envelope studies since they determine the envelope's performance against outdoor temperature fluctuations. Fig. 3.22 shows those indicators in terms of temperature and time.

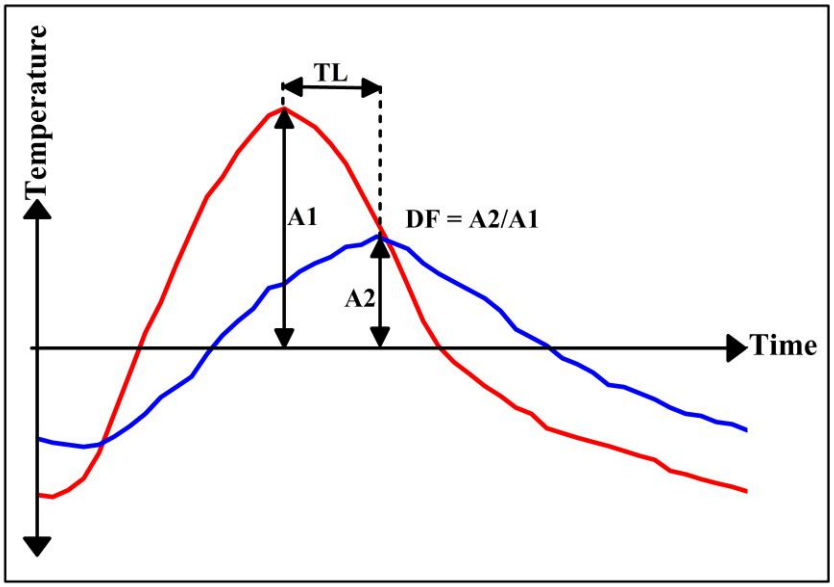

Fig. 3.22. Schematic of DF and TL

3.6.4. Average temperature fluctuation reduction

Average temperature fluctuation reduction (ATFR) is the average reduction in the envelope element layers' temperature considering the interior and exterior temperatures during the whole day cycle. In other words, ATFR is the summation of the average decrease in the envelope temperature during the daytime and the average increase in the envelope element temperature during the nighttime (as a result of non-ventilation). Therefore, the higher the ATFR value, the better the thermal behaviour of PCM (the negative value of ATFR means that the PCM incorporation has adverse thermal behaviour, while zero value means no advantages of PCM incorporation). In this work, the period from 6:00 to 18:00 represents the daytime (denoted by X). The period from 18:00 to the end of the cycle, denoted by Y, represents the nighttime. ATFR could be applied considering the indoor temperature variation during the thermal cycle, giving an equivalent indication of the effect of inner surfaces on indoor thermal comfort. ATFR was calculated according to Eq. (3.11)-Eq. (3.13) (Alam et al., 2014), as follows.

$$ATFR = X + Y \tag{3.11}$$

$$X = T_{in,av.,reference} - T_{in,av.,PCM} \tag{3.12}$$

$$Y = T_{in,av.,PCM} - T_{in,av.,reference} \tag{3.13}$$

where $T_{in,av.,reference}$ and $T_{in,av.,PCM}$ are respectively the average inner surface temperature of the element of the reference and PCM rooms (°C).

3.6.5. Thermal load levelling

The thermal load levelling index (TLL) indicates how the indoor temperature of a room fluctuates during the day, considering the maximum and minimum T_i. Therefore, the lower TLL indicates better building envelope thermal performance to stabilise indoor thermal comfort. The TLL for reference and PCM rooms was calculated according to Eq. (3.14) and (3.15) (Meng et al., 2017), as follows:

$$TLL_{Ref\ room} = \frac{T_{i,reference,max} - T_{i,reference,min}}{T_{i,reference,max} + T_{i,reference,min}} \tag{3.14}$$

$$TLL_{RCM\ room} = \frac{T_{i,PCM,max} - T_{i,PCM,min}}{T_{i,PCM,max} + T_{i,PCM,min}} \tag{3.15}$$

3.6.6. Operative temperature reduction

The operative temperature (OT) is the temperature that occupants feel inside the built environment. Mathematically, Eq. (3.16) is the simplification form to calculate the OT considering the average indoor air and mean radiant temperatures (ANSI/ASHRAE Standard 55-2010, 2010), as follows:

$$OT = \frac{T_i + \bar{T}_{mr}}{2} \tag{3.16}$$

where T_i is the indoor ambient temperature and, $\bar{T}_{mr}$ is the mean radiant temperature (°C). The latter can be calculated by considering the indoor surface temperatures and areas of the roof and walls, according to Eq. (3.17) (Fanger, 1970).

$$\bar{T}_{mr} = \frac{T_1 A_1 + T_2 A_2 + \cdots + T_n A_n}{A_1 + A_2 + \cdots + A_n} \tag{3.17}$$

where T_1, T_2, ..., T_n are the element interior surface temperatures in °C, and A_1, A_2, ..., A_n are the interior area of each element (in m^2). It is worth mentioning that $\bar{T}_{mr}$ is calculated directly by the EnergyPlus software in the numerical investigations.

Accordingly, the operative temperature reduction (*OTR*) is calculated according to Eq. (3.18) (Kenzhekhanov et al., 2020), considering the OT of the reference and PCM rooms.

$$OTR = \frac{OT_{reference} - OT_{PCM}}{OT_{reference}} \times 100\% \tag{3.18}$$

3.6.7. Heat gain reduction

The solar heat gain reduced through the building envelope indicates the cooling load reduction (Sharma and Sengar, 2019). Subsequently, this also specifies the energy-saving obtained from PCM incorporation (Lei et al., 2016). The heat gain (HG) of each element in the reference and PCM room was calculated according to Eq. (3.19) (Al-Rashed et al., 2021a) as follows:

$$HG = h_i \, A \, (T_{in} - T_i) \tag{3.19}$$

Where h_i denotes the combined convective and radiative heat transfer coefficient for the interior element surface and interior room temperature in $W/m^2.K$. In this study, the values 8.29 $W/m^2.°C$ and 6.13 $W/m^2.°C$ are used for walls and roofs, respectively, considering the horizontal/vertical direction of heat flow and surface emittance of concrete (ASHRAE, 1997). T_{in} and T_i refer to the inner surface temperature of the element and the indoor air temperature, respectively. T_i is variable since it is influenced by the heat exchange between the indoor and outdoor temperatures through the envelope elements. Sometimes it becomes higher than T_{in} due to the influence of non-ventilated space, giving adverse results. Therefore, it should be fixed in the calculations refereeing to the design temperature controlled by air-conditioning systems (Al-Rashed et al., 2021b) (T_i assumed to be equal to 24 °C).

Consequently, the heat gain reduction (HGR) can be calculated considering the HG in each element in the PCM room and its corresponding element in the reference room, according to Eq. (3.20) (Fateh et al., 2018). It is worth mentioning that the HGR is sometimes calculated as MHGR when the maximum HG consider or as AHGR when the average HG for elements is considered.

$$HGR = \frac{HG_{reference} - HG_{PCM}}{HG_{reference}} \times 100\% \tag{3.20}$$

3.6.8. CO_2 emission saving

Diminishing CO_2 emissions is a fundamental objective in modern society when dealing with building technologies since it is associated with global warming and climate change anxieties (Uludaş et al., 2022). The CO_2 emission saving (CO_2ES) was quantified considering the total heat

HG of PCM and reference rooms (in kW) and the equivalent quantity of CO_2 produced from each kWh of electricity generated in Iraq, according to Eq. (3.21) (Al-Rashed et al., 2021a), as follows:

$$CO_2\ ES = total\ HG \times \frac{kgCO_2}{kWh\ electricity} \times 24\ h \tag{3.21}$$

The value of 1.00284 kg CO_2/kWh of electricity was considered in this study as a typical value for calculations since Iraq still heavily employs natural gas and petroleum resources for powering governmental power plants and generating electricity (IEA, 2020).

3.6.9. Electricity cost saving

The electricity cost saving (ECS) is another important economic indicator since it determines the technology feasibility. The ECS, in Iraqi dinar (IQD)/day, was calculated considering the total HG of PCM and reference rooms and the cost of each kWh in Iraq according to Eq. (3.22), as follows:

$$ECS = Total\ HG \times electricity\ cost/kWh\ \times 24\ h \tag{3.22}$$

The electricity cost per kWh was taken as 60 Iraqi dinar (IQD)/kWh according to the latest Iraqi electricity tariff provided to commercial buildings (Iraq electricity prices, 2021).

4. RESULTS AND DISCUSSION

The experiments' results are presented in this chapter, along with discussions, suggestions and new findings. The chapter includes the experimental studies conducted to specify the optimal position and thickness of PCM in a composite roof, the optimal PCM capsule-concrete brick arrangement and the thermal evaluation of a scaled room. Moreover, the chapter also involved the extended numerical simulations verified on the room model to study the PCM thermal performance along with the role of thermal insulation and natural night ventilation. In the end, the new findings drawn from the studies are listed.

4.1. Investigation of the optimal PCM position within a composite roof

The experimental work to indicate the optimal PCM layer within the roof described in section 3.3.2 lasted for one week during August and September 2020. The measurements of Case I (regular Isogam layer) were collected for three consecutive days (29-31.08.2020), whereas Case II was conducted for four days from 11-14.09.2020. Fig. 4.1 and Fig. 4.2 show the variation of outer, inner and room temperatures as a function of time for Model A, Model B, Model C and Model D, respectively, in case I and case II experiments with 30 min time step. As expected, it can be noticed that all models containing the PCM layer have better thermal performance than the reference case, thanks to the thermal storage potential of the PCM layer. The maximum value of T_o reached 60.8°C, 59.3°C and 58.2°C in the first, second and third cycle of Case I. Whereas, T_o reach a maximum of 76.4 °C, 75.4°C, 75.5 °C and 73.25 °C respectively in the first, second, third and fourth cycle of Case II. In conjunction with the highest solar radiation, peak temperatures were reached in the midday from 12:30 to 13:00.

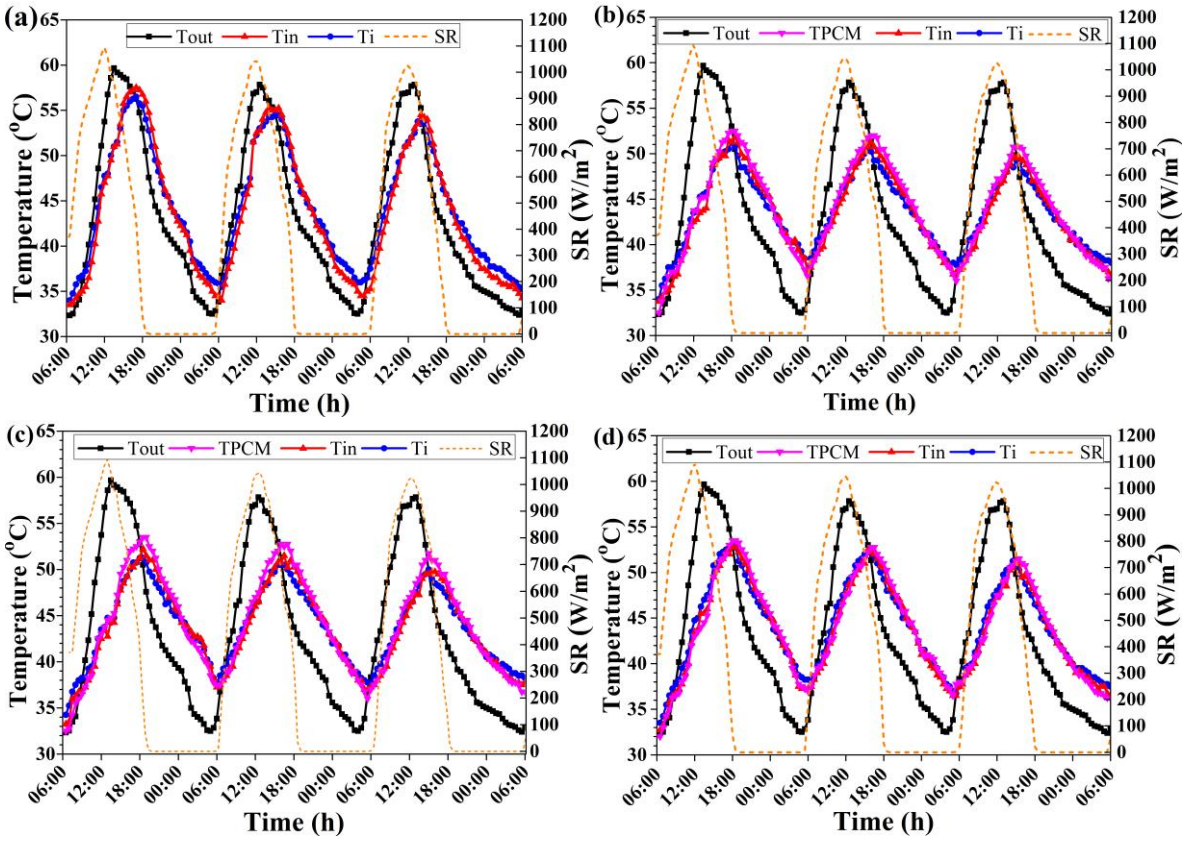

Fig. 4.1. Temperature profile of Case I (a) Model A; (b) Model B; (c) Model C; (d) Model D

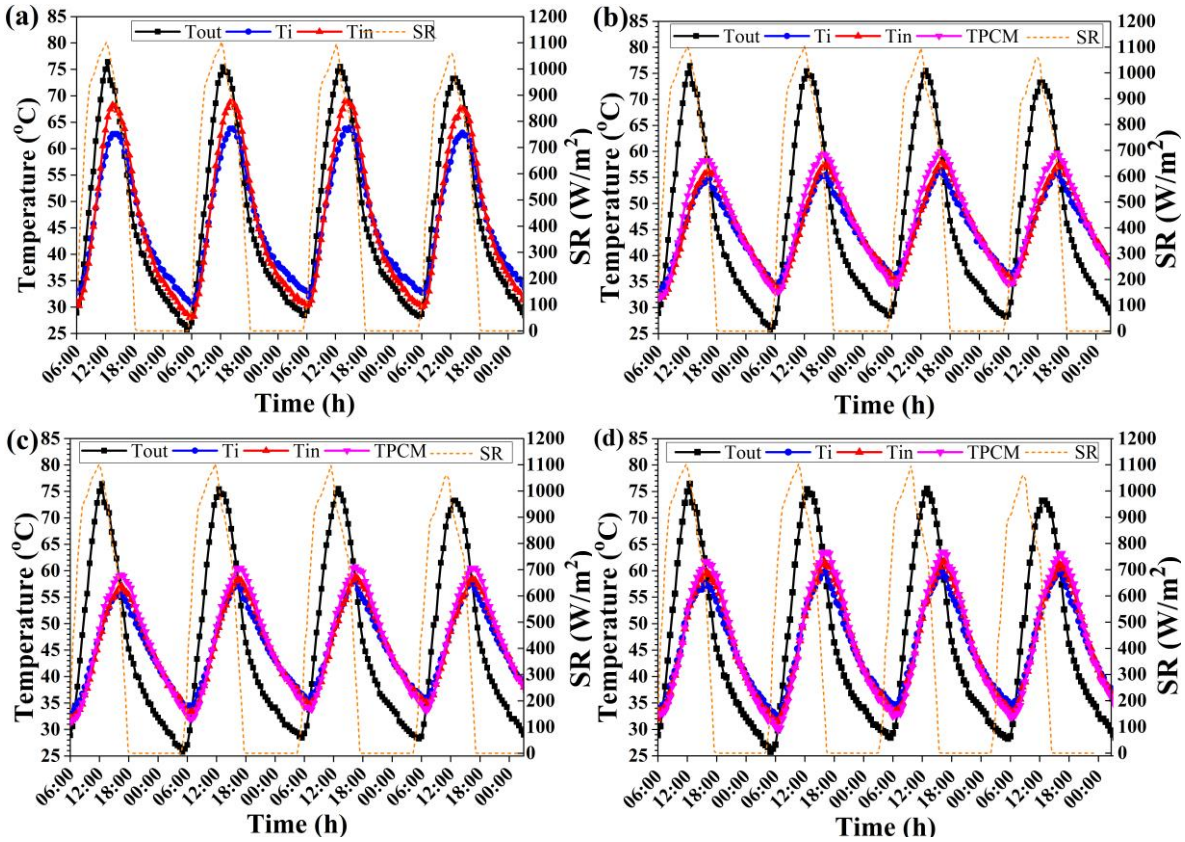

Fig. 4.2. Temperature profile of Case II (a) Model A, (b) Model B, (c) Model C, (d) Model D

By comparing the figures of Case I and Case II, considering the difference between the outdoor and room temperatures, we can recognise that PCM works better at higher outdoor temperatures. This is attributed to the high melting temperature of used PCM, which requires more heat to be utilised sufficiently. The following indicators are discussed to evaluate the best thermal performance amongst Model B, Model C, and Model D resulted from PCM optimal position compared with Model A, as follows:

4.1.1. Room maximum temperature reduction

PCMs can reduce indoor temperatures thanks to their thermal energy storage, which allows working as a dynamic insulation. This can be observed by comparing T_{in} for all models in each case. For instance, the maximum T_i recorded for Model A, Model B, Model C and Model D in the first cycle of Case II (shown in Fig. 4.3) are respectively 62.75 °C, 54.75 °C, 55.75 °C and 57.5 °C against T_{out} equal to 76.4 °C. Those values represent a temperature decrement by 9 °C, 8 °C and 5.25 °C in the T_i of Model B, Model C and Model D compared with Model A.

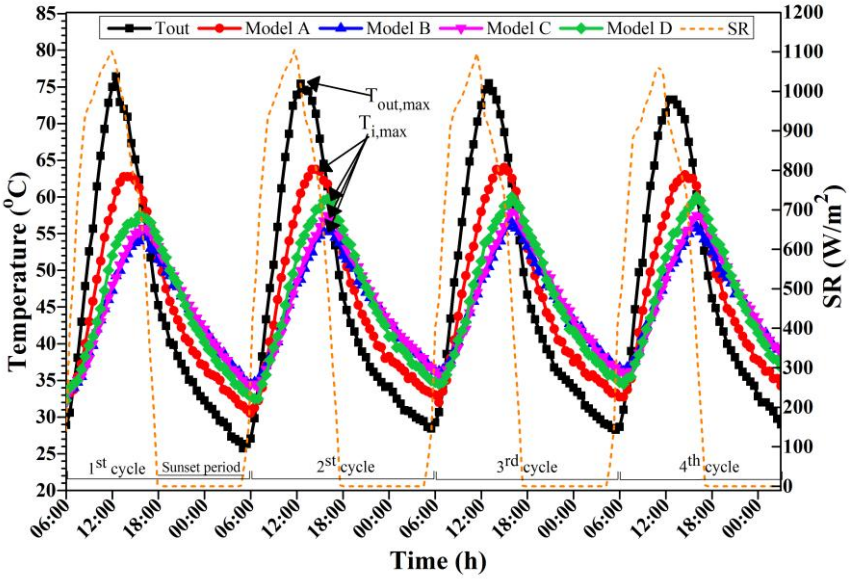

Fig. 4.3. Curves of T_i for test models (Case II)

RMTR shows how high the reduction in T_i inside the PCM room is due to incorporating the PCM layer, which impacts the cooling and air-conditioning systems' reliance on real-scale cases. The calculated RMTR by Eq. (3.8) in Case I and Case II are shown in Fig. 4.4.

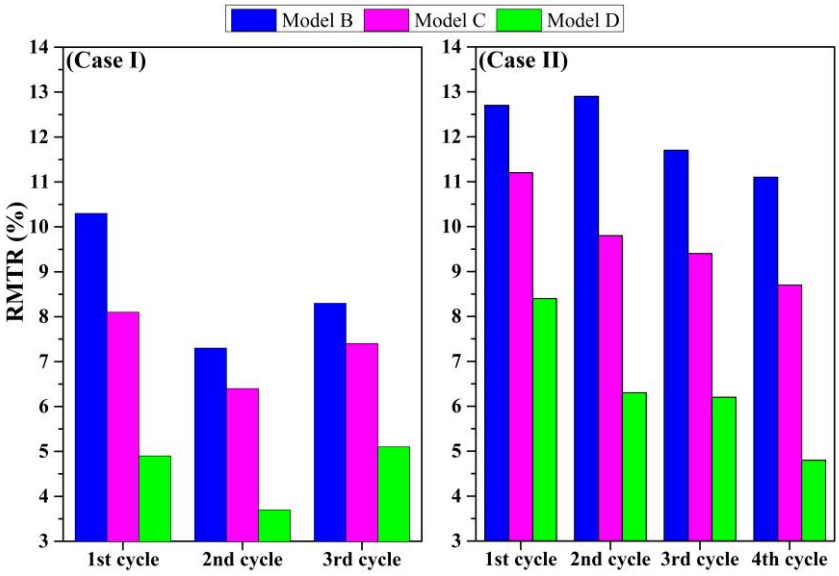

Fig. 4.4. RMTR of PCM models for Case I and Case II

As observed in Fig. 4.4, Model B showed the best thermal performance in all cycles. Furthermore, Model B at a higher temperature case (i.e., Case II) performed better than the lower temperature case, which shows higher utilisation of PCM storage capacity. On the other hand, Model D shows the worst performance amongst other PCM models in RMTR. This indicates the PCM layer's negative effect when placed near the interior of the non-conditioned environment under hot climates. The highest RMTR obtained by Model B, Model C and Model D in Case I was 10.3%, 8.1% and 5.1% higher than Model A at the maximum T_{out} of 60.8 °C and 58.2 °C (first and third cycles), respectively. Likewise, the highest RMTR in Case II reached 12.9%, 11.2% and 8.4% at the maximum T_o in the first and second cycles (i.e., 76.4°C and 75.4 °C, respectively) for PCM models compared with the referenced model.

4.1.2. Decrement factor

As previously stated in section 3.6.2, the lowest DF value indicates lower cyclic fluctuation of the envelope temperature during the thermal cycle as an advantage of PCM layer incorporation. The DF results calculated by Eq. (3.9) of the experimental model in both cases are shown in Fig. 4.5.

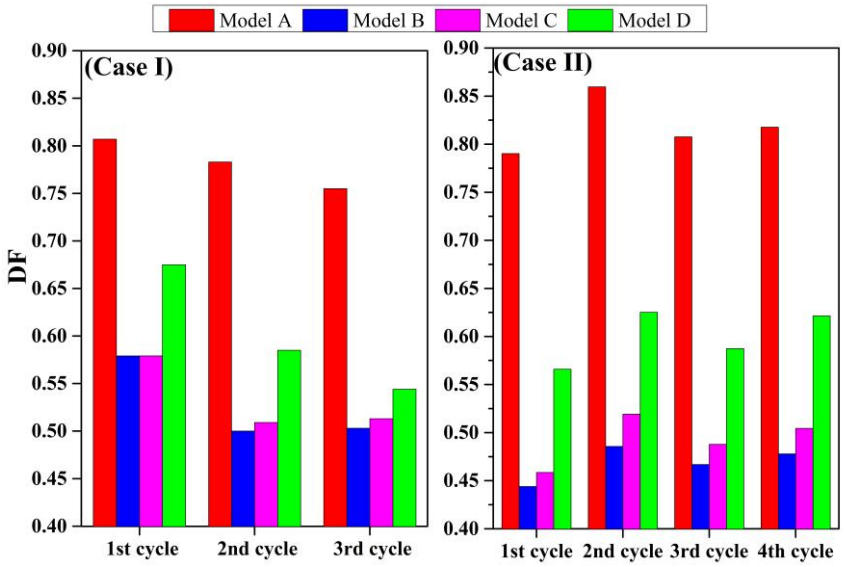

Fig. 4.5. DF of models for Case I and Case II

As shown in the figure and compared with Model A, Model B has the best DF, which indicates the utilisation of PCM storage capacity to moderate the changeable inside surface temperature during the day and night. Model C also showed good behaviour of DF compared with Model D, which was the worst. It is also noted that Model B and Model C have better DF under higher temperatures (i.e., Case II), which points out the better implementation of PCM layers at outside and middle positions under high solar radiation locations. The DF obtained in Case I was 0.5-0.58, 0.51-0.58, 0.54-0.68 for Model B, Model C and Model D compared with 0.76-0.81 for Model A. Likewise, the DF for Model B, Model C, Model D were respectively in the range 0.44-0.49, 0.46-0.52, and 0.57-0.63 against 0.79-0.86 for Model A in Case II.

4.1.3. Time lag

TL is a convincing way to differentiate among the best position of PCM models. This indicator designates the period of shifting peak load to off-load, which determines the effectiveness of PCM in the roof. Fig. 4.6 shows the comparative period at which the TL was achieved in each case.

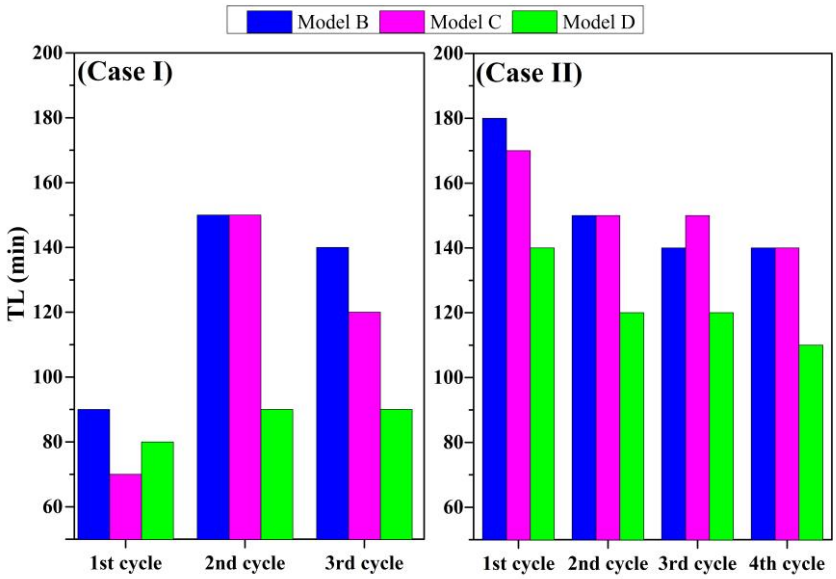

Fig. 4.6. TL of PCM models for Case I and Case II (based on 10 min time step measurements)

Figure 4.6 shows that Model B and Model C have the best TL compared to Model A. In Case I, the TL of Model B, Model C, and Model D ranged from (90-150 min), (80-150 min), and (80-90 min), respectively, more than Model A. Besides, the TL of these models ranged from (140-180 min), (140-170 min) and (110-140 min) in Case II. TL was higher in Case II than Case I because under high $T_{o,}$ the PCM is activated and stored more heat in all PCM models than in the reference model. It means that the heat passed through the envelope of Model A faster than PCM models that utilised the PCM's storage capacity. Whereas, models in Case I were subjected to lower $T_{out,}$ and only a little heat was stored in the PCM models due to the high melting temperature of PCM compared with the passed heat in this case and considering the thermal resistance of roof layers.

Both DF and TL are intrinsic indicators in the building envelope studies as they identify the heat stored in the envelope and influence the required hours for employing the cooling systems (Toure et al., 2019). TL could be calculated twice for peaks during the day cycle, as shown in Fig. 4.7. It is clear from the figure that the TL resulting from the shifting of high solar radiation during the day is more significant than that at the end of the day cycle. It emphasises the PCM layer's role in enhancing the thermal mass of PCM roofs compared with the conventional roof during peak hours.

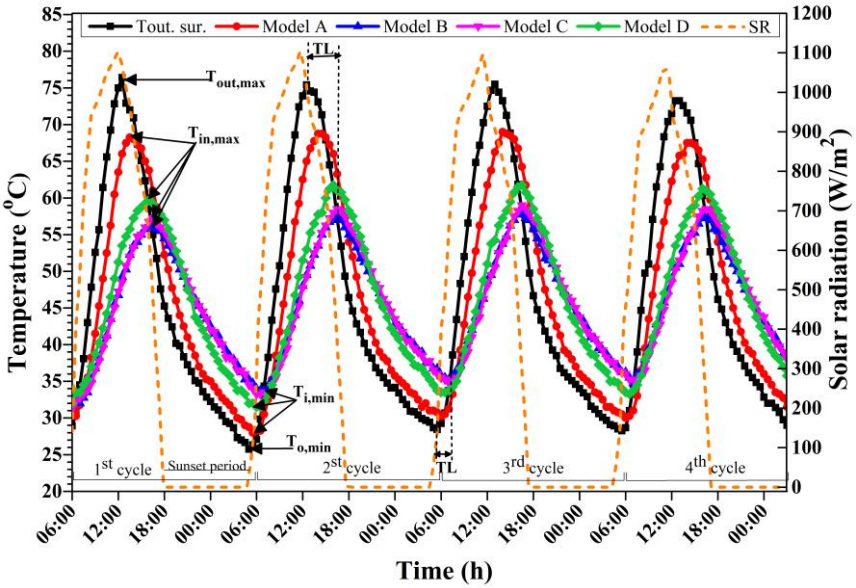

Fig. 4.7. T_{in} vs. T_{out} and SR for tested models (Case II)

4.1.4. Average temperature fluctuation reduction

As indicated earlier in section 3.6.4, ATFR indicates the average decrement of PCM room temperature fluctuation compared with the reference room during the day and night. ATFR of Case I and Case II cycles is represented in Fig. 4.8.

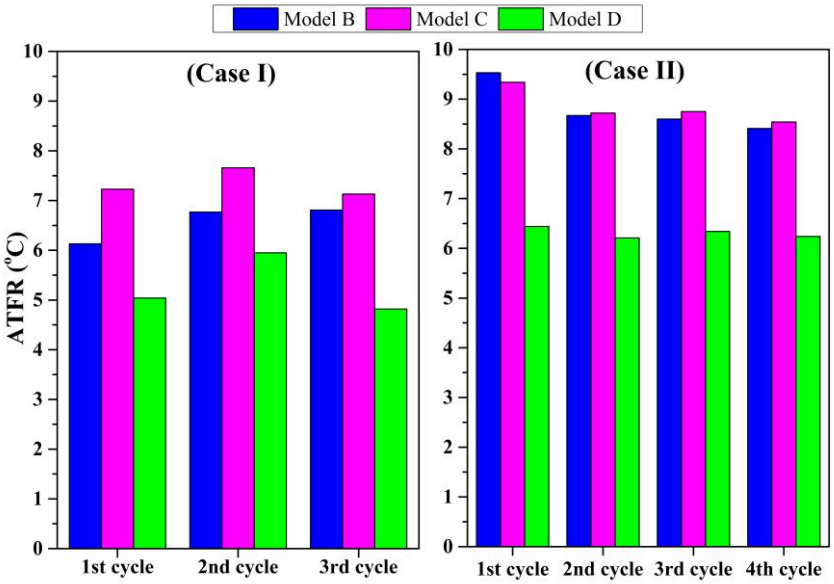

Fig. 4.8. ATFR of PCM models for Case I and Case II

Generally, all positions of PCM models have effectively restrained room temperature fluctuations. Here, it can be noticed that Model C showed the best behaviour, even better than Model B, and then Model D. It is also noted that the PCM layer at all positions had a better thermal performance at high outdoor temperatures, meaning that more heat was stored into the PCM which damping temperature fluctuations. On average, the ATFR was reduced by 6.1 °C- 6.8 °C in Model B, 7.1-7.7 °C in Model C, and by 4.8 °C-5.9 °C in Model D for Case I. Besides, the value of ATFR ranged between 8.4 °C-9.5 °C, 8.5 °C-9.3 °C, and 6.2 °C-6.4 °C for Model B, Model C and Model D, respectively, for Case II. Latter values indicated the advantage of using PCM under hot climates, which is much higher than those obtained in the literature (Kenzhekhanov et al., 2020; Saxena et al., 2020). For instance, the highest values of ATFR ranged between 3-4 °C were obtained in a study conducted under Australian conditions (Alam et al., 2014), which reflects the suitability of used PCM in the current work for the Iraqi solar radiation which effectively exploited the heat storage potential of selected PCM.

As long as ATFR deals with room temperature during the day and night, it is important to study PCM's thermal behaviour during the melting and solidification phases. As shown in Fig. 4.9, it can be appreciated that the PCM temperature of Model B is higher than the temperature of other models in the first half of the day in each cycle. It is attributed to that the PCM layer in Model B is placed close to the exterior environment and restricts the high solar radiation during the early hours of the day, and the heat was charged into the PCM before other models. For Model D, the PCM temperature was high at the beginning of the day, influenced by room high temperature as the thermocouple was placed beneath the PCM layer and close to the test room. The PCM temperature of Model C was between the two models most of the time, which showed more stable room temperatures during the day and night periods and resulted in better ATFR.

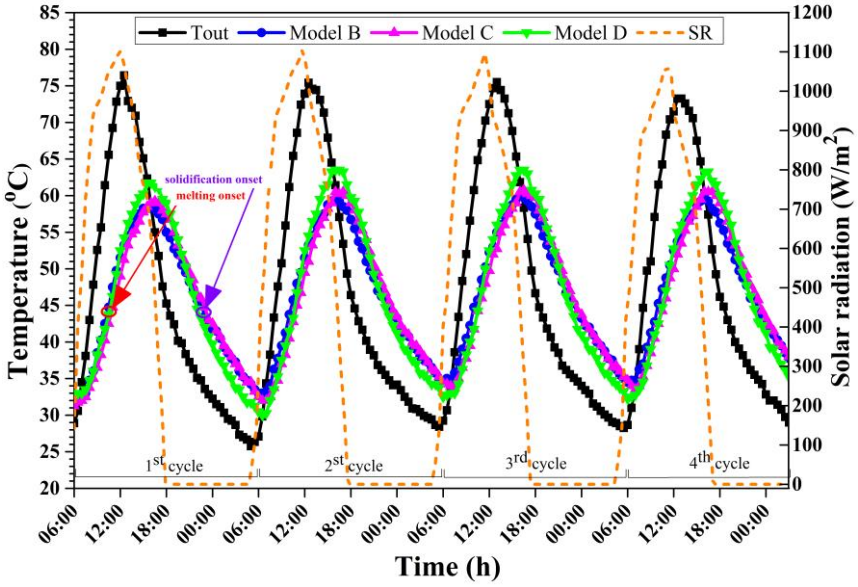

Fig. 4.9. T_{PCM} of PCM models (Case II)

For the solidification phase, the PCM temperature of Model B was decreased as T_o decrease in the second half of the day cycle. This is because of low ambient temperature during late afternoon and evening, which release heat from the PCM layer closer to the finishing layer than in other positions. Nevertheless, the PCM temperature of Model B shows better performance during the solidification phase because the heat stored by the PCM during the day was released towards the outside low temperature. Model D showed a worse thermal performance during the melting phase compared with other PCM models. During the evening period and early morning of the following cycle, the PCM temperature in this model was the closest to T_o, indicating the lack of PCM storage capacity. Following the above analysis, we can emphasise that roof layers' thermal resistance (i.e., Isogam and concrete in the present study) reduces the heat charged into each model's PCM layer and ultimately affects its melting process. Therefore, as proved in Model A, the heat that passes through the roof elements should be high enough to utilise PCM's storage capacity. Tables 4.1 and 4.2 summarise the results obtained in Case I and Case II, respectively.

Table 4.1. Summary of average results of indicators in Case I

Model	Average RMTR (%)	Average DF	Average TL (min)	Average ATFR (°C)
Model A	-----	0.78	-----	-----
Model B	8.6	0.53	126.7	6.6
Model C	7.3	0.53	113.3	7.3
Model D	4.6	0.60	86.7	5.3

Table 4.2. Summary of average results of indicators in Case II

Model	Average RMTR (%)	Average DF	Average TL (min)	Average ATFR (°C)
Model A	-----	0.82	-----	-----
Model B	12.1	0.47	152.5	8.8
Model C	9.8	0.49	152.5	8.8
Model D	6.4	0.59	122.5	6.3

4.2. Investigation of the optimal PCM layer thickness within composite roof

The experiment to investigate the optimal PCM layer thickness presented in section 3.3.3 was conducted for three consecutive thermal cycles, from 3-5/9/2020. As indicated in Fig. 3.9, three PCM layer thicknesses were proposed in this study, placed between the Isogam roofing layer and the main concrete layer since this position was optimal according to the results presented in section 4.1. Fig. 4.10 shows the indoor temperature of PCM rooms (Model B, Model C and Model D) with

different thicknesses than the reference room model (Model A). The maximum T_r was achieved in the second cycle as 64.75 °C, 57.5°C, 56°C, 55.75°C in Model A, Model B, Model C and Model D, respectively, against a maximum T_o of 76.9 °C. This signifies a reduction of 7.25 °C, 8.75 °C and 9 °C for Model B, Model C and Model D compared with the reference case (i.e., Model A).

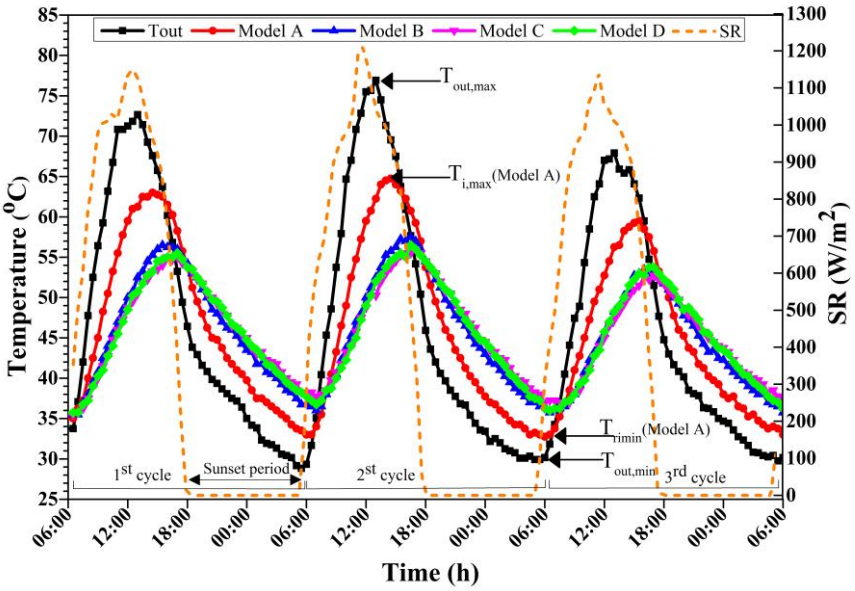

Fig. 4.10. T_i profile of experimental models

Fig. 4.11 shows the temperature profile of experimental models' (Model A, Model B, Model C and Model D) as a function of time during the days of the experiment. In the early hours of each day, T_i was higher than T_{out} due to low solar radiation. Later, the temperatures increased with the solar radiation (SR) increase and reached the maximum around 13:00 in each day-cycle. The maximum T_o achieved was 72.7 °C, 76.9 °C and 67.9 °C, respectively, on the first, second and third day of the experiment encountered with the highest SR of 1149, 1210 and 1139 W/m^2, respectively. It is worth mentioning that the experimental work experienced some hours of partially-clouded weather at midday, especially on the first and third days of the experiment.

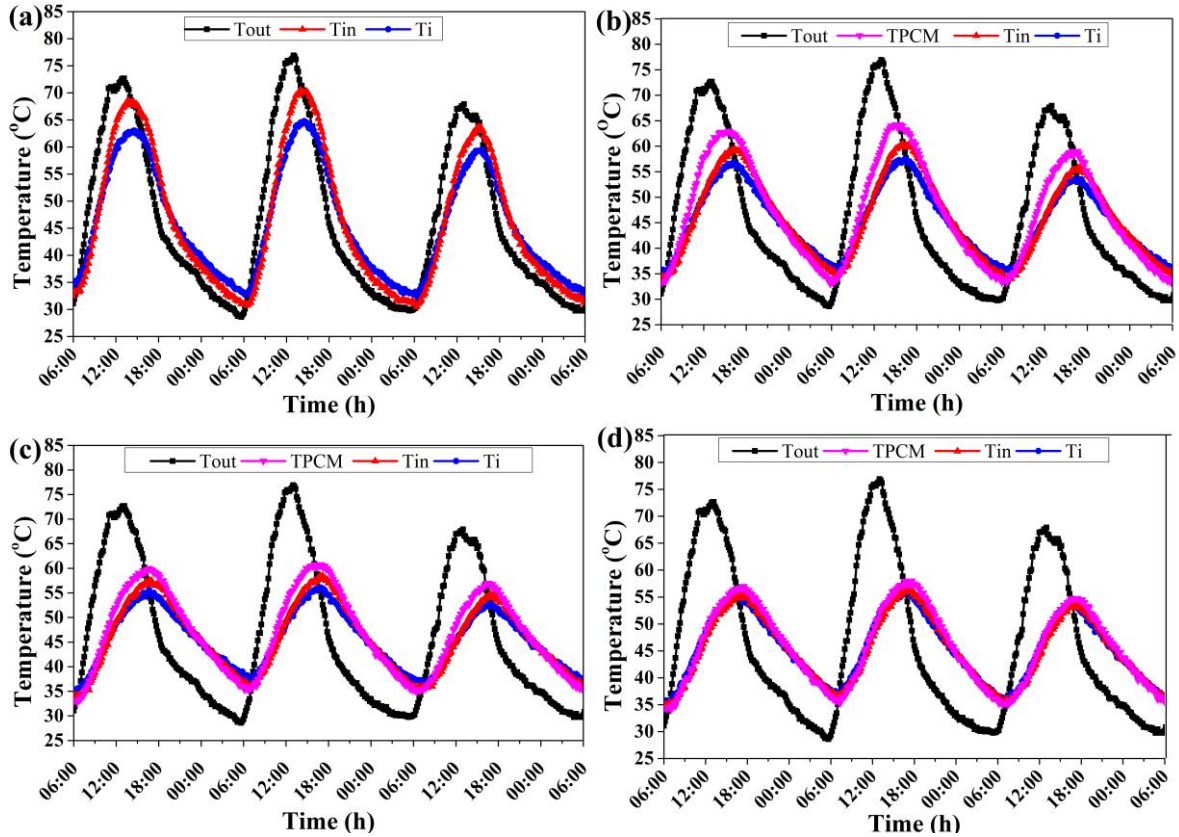

Fig. 4.11. Temperature profile of (a) Model A (b) Model B (c) Model C (d) Model D

Due to PCM heat storage capacity, Tin and Ti in PCM models were generally lower than those of the reference model. In this regard, T_{in} and T_i decreased as the PCM layer's thickness increased, which shows the PCM's ability to shave temperature fluctuations during peak hours.

At night, To values dropped quickly as the SR decreased until sunset around 18:00 each day. T_{out} dropped sharply, followed by T_{PCM} for PCM models with a slight reduction in T_{in} and T_i profiles. Lower T_{out} between 28.6 °C and 29.75 °C was recorded during the late night of the experiment, which was suitable for passively discharging the heat from PCM models and preparing them for the next thermal cycle.

4.2.1. Room maximum temperature reduction

PMTR of PCM models compared with the reference model indicates the effect of increased PCM layer thickness on indoor temperature improvement, which eventually indicated thermal comfort enhancement. The calculated RMTR of PCM models compared with Model A is shown in Fig. 4.12.

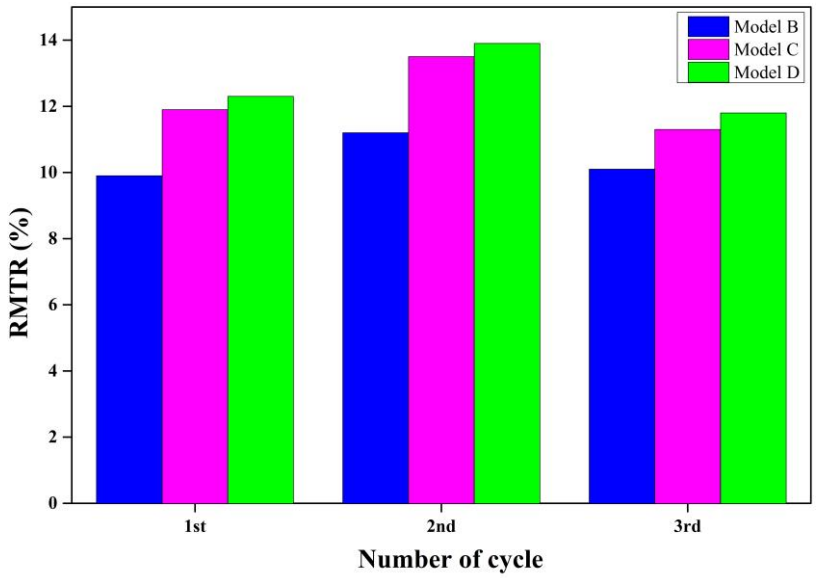

Fig. 4.12. RMTR for tested models

Model D showed the best RMTR compared with the other PCM models. The better performance obtained at the second cycle indicates a better utilisation of PCM thermal storage at higher temperatures resulting from using PCM of high melting temperature. At this cycle, a maximum RMTR of 11.2%, 13.5, and 13.9% for Model B, Model C and Model D were calculated at the highest T_{out}. Increasing PCM thickness from 1 to 1.5 cm has reduced T_i by 2.3%, whereas increasing the thickness from 1.5 to 2 cm has only reduced T_i by 0.4%. Although increased PCM layer thickness has thermal advantages, it is worth studying its impact on the building structure and economic point of view to specify the optimal integration of PCM at a minimal cost.

4.2.2. Decrement factor

The thermal resistance of roof layers is easy to quantify using the DF indicator, especially when the PCM layer temperature variation cannot be measured. Fig. 4.13 shows the calculation results of DF for experimental models.

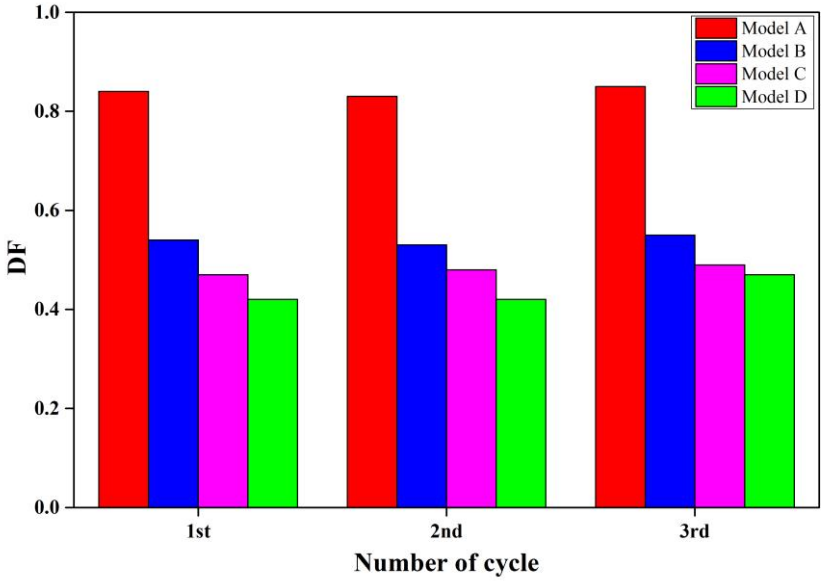

Fig. 4.13. DF of experimental models

As shown in the figure and compared with Model A, Model D has the best DF in all cycles, followed by Model C and then Model B. The maximum DF was obtained in the third-day cycle,

which was 0.85, 0.55, 0.49 and 0.47 for Model A, Model B, Model C and Model D, respectively. That means reducing the cyclic interior surface temperature by 35.3%, 42.4% and 44.7% for Model B, Model C and Model D compared with Model A. This reduction positively influences thermal comfort in real case studies as it affects the mean radiant temperature and operative temperature (ANSI/ASHRAE Standard 55-2010, 2010). Conclusively, the DF decreases linearly with the increased PCM layer thickness, as shown in Fig. 4.14.

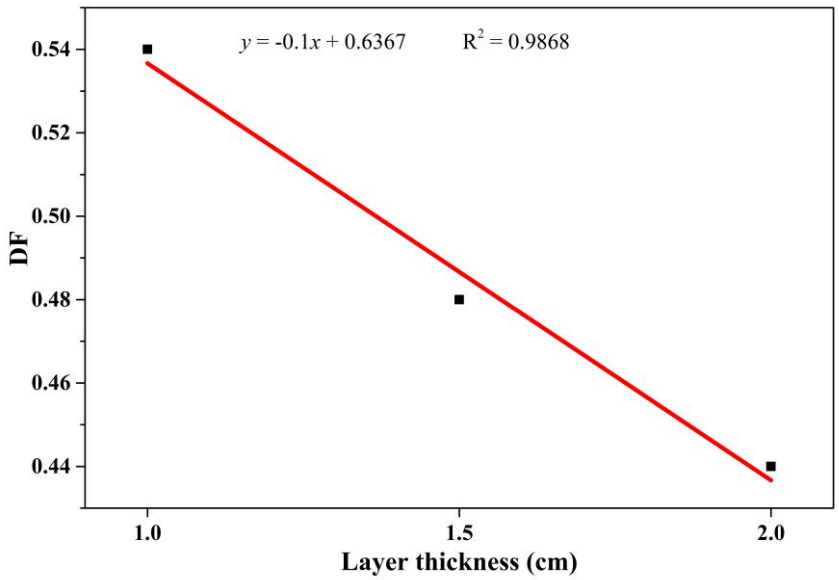

Fig. 4.14. Relationship of DF with PCM layer thickness

4.2.3. Time lag

The time delay of temperature during peak hours is an essential indicator to investigate the roof's thermal resistance against the heat flow from outside. The TL owing to incorporating PCM with different thicknesses in each thermal cycle is presented in Fig. 4.15.

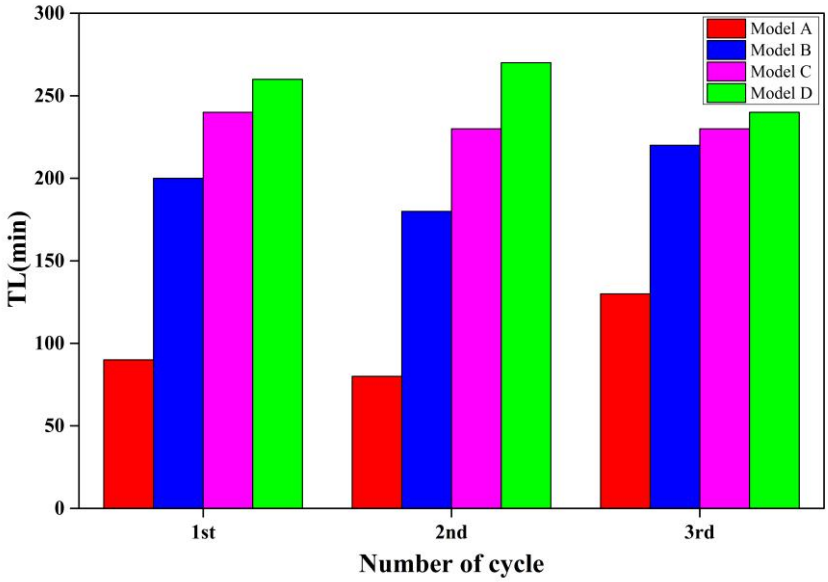

Fig. 4.15. TL of the experimental models

As indicated in the figure, peak hours were shifted in all PCM models to the late time compared with the reference model. Results showed that the TL ranged between 80-130 min for Model A, 180-220 min for Model B, 230-240 min for Model C and from 240-270 for Model D. The highest

TL for Model D was obtained in the second day-cycle at the highest outdoor temperature in the experiment. At this cycle, the time in Model B, Model C and Model D was extended by 100 min, 150 min and 190 min, respectively, compared with Model A.

It is well known that TL can be calculated for the crests during peak and off-hours, as shown in Fig. 4.16. The TL during peak hours is more important because they show the shifting of high temperatures as an advantage of incorporating the PCM layer. Moreover, after the SR drops, a higher reduction in the interior surface temperatures also can be recognised during the daytime compared with the nighttime.

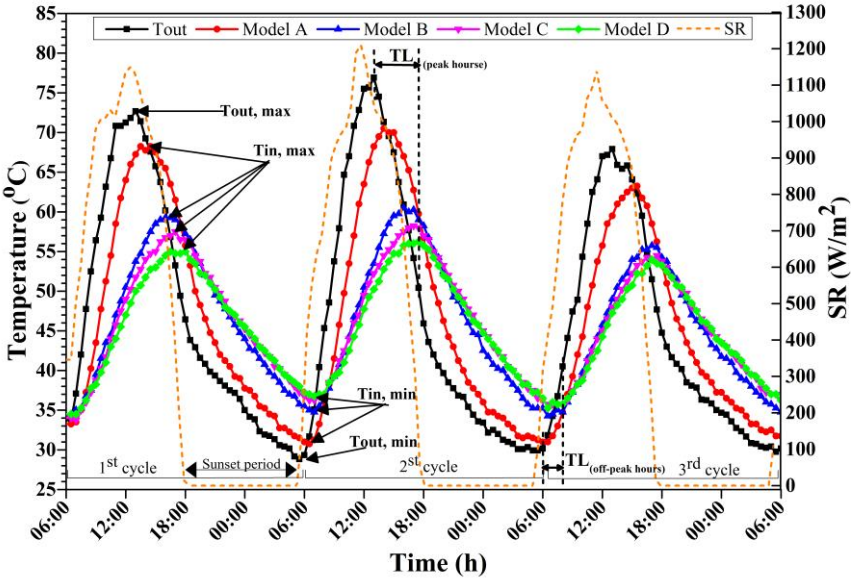

Fig.4.16. T_{in} profile for experimental models

TL and the DF are essential to study PCM's influence on the thermal performance of the building envelope. They could analyse the building's thermal inertia and show how the building envelope restricts the high outside temperatures that are not felt inside buildings (Toure et al., 2019).

4.2.4. Average temperature fluctuation reduction

The ATFR indicator could provide a clear vision of how the indoor temperature fluctuates inside tested rooms during the thermal cycle. The calculated results of ATFR in this experiment are shown in Fig. 4.17.

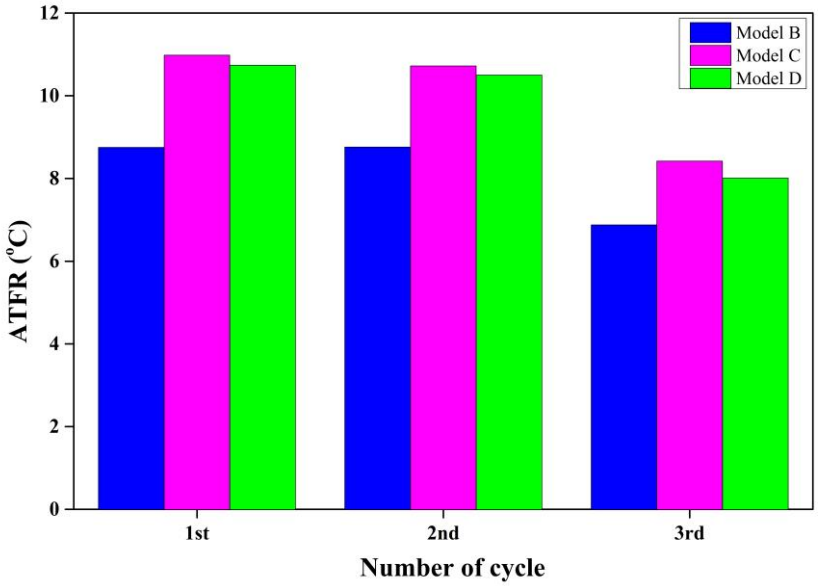

Fig. 4.17. ATFR of PCM models

The results showed that ATFR was high for Model C compared with Model B and Model D, where the maximum value obtained in the first-day cycle was 8.75°C, 10.98°C and 10.74°C for Model B, Model C and Model D, respectively. The reason is attributed to the effect of passive incorporation on the solidification phase during night hours in which the stored heat in Model D was not released. The calculation of ATFR values in all cycles showed that the X value was higher for Model D than for Model B and Model C. In reverse, the value of Y was much high for Model C than for Model B and Model D. Therefore, the summation of X and Y resulted in higher ATFR for Model C than Model B and Model D. This indicator informs us that the thicker PCM (i.e. 2 cm) can save more heat during day hours and reduce the room temperature. However, at the same time, it has lower thermal performance during the nighttime and cannot release all stored heat passively. The main reason behind that is the low thermal conductivity of PCMs in nature, particularly paraffin, which slows down the time to melt and solidify fully. Several techniques were reported in the literature to enhance the low thermal conductivity of PCMs using different enhancers such as fins, metallic foams and the presence of nanoparticles (Li et al., 2018; Qureshi et al., 2018).

ATFR results indicated a high thermal performance of PCM in the present work in which the values were in the range 6 °C < ATFR < 11 °C, which is much higher than the results reported in the literature. For instance, a study reported that the value of ATFR ranged between 3 °C -4 °C under Australian climate conditions (Alam et al., 2014).

As the value of ATFR is influenced by the temperatures during the daytime and nighttime, it is worth analysing the thermal performance of PCM in each PCM model. As shown in Fig. 4.18, it can be realised that the T_{PCM} in all PCM models was increased as the SR increased and decreased at lower SR and night periods. Model B showed a faster increase in $T_{PCM,}$ which was close to T_{out} followed by Model C and then Model D. This logically means that the PCM melted earlier in Model B because of its small quantity, and the heat later passed towards the test room. Consequently, the heat took more time to pass through Model C and Model D, which had more PCM quantity to be melted. Considering the melting temperature of the used PCM, we can say that the PCM melted earlier in Model B than in Model C and Model D, around 9:00, 10:00 and 11:00, respectively, in the first-day cycle.

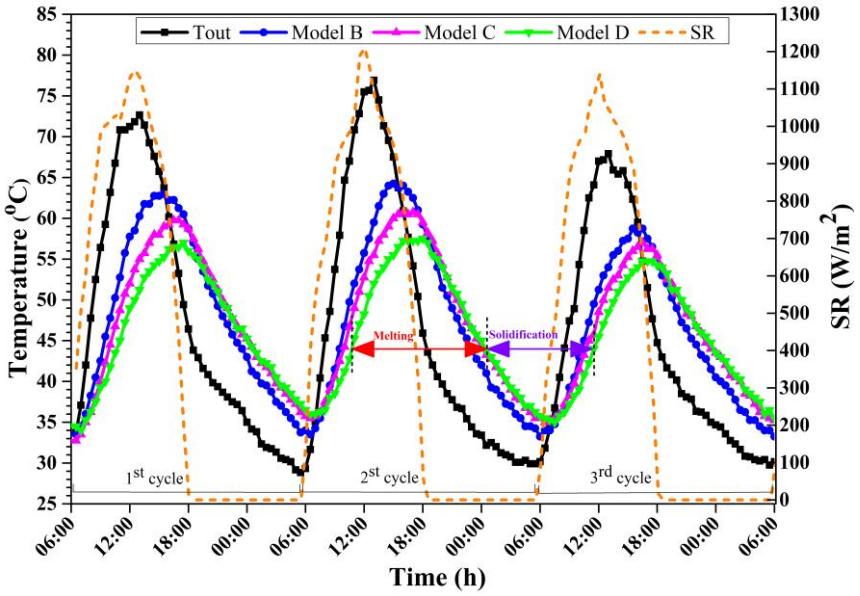

Fig. 4.18. T_{PCM} profile of experimental models

On the other hand, during the solidification period, the TPCM of Model B was the closest to $T_{out,}$ meaning that the thickness of PCM was solidified faster in Model B than in the other models. Likewise, the solidification in Model C was faster than in Model D due to its lower PCM quantity. Accordingly, the lower the PCM quantity, the faster it is solidified. Table 4.3 summarises the results of the above indicators.

Table 4.3. Comparative summary of the indicators results discussed in the study

Model	Average RMTR (%)	Average DF	Average TL (min)	Average ATFR (°C)
Model A	-----	0.84	-----	-----
Model B	10.4	0.54	100.1	8.13
Model C	12.2	0.48	133.3	10.04
Model D	12.7	0.44	156.7	9.75

4.3. Investigation of the optimal PCM capsule-incorporated concrete brick

This experimental work was conducted to specify the best PCM-concrete brick arrangement, described in subsection 3.3.4, and lasted for four hot days, from 16.09.2020 to 6:00 of 20.09.2020. This experiment is necessary to specify the best PCM brick from the thermal point of view to be used to construct the walls of the PCM room in the latter experiments.

Fig. 4.19 presents the T_{in} and T_{out} variation and SR for PCM brick samples against reference brick (shown in Fig. 3.13 and Fig. 3.14) as a function of time. T_{in} was increased in conjunction with the increase of T_{out} and reached the highest values with a time delay varied in each PCM brick compared with the reference brick. The bricks' temperature increased considerably as the SR increased and reached the highest of 1059, 1053, 1062 and 925 W/m^2 on the first, second, third and fourth day of the experiment. This is encountered with the highest T_{out} of 63.5 °C, 63.67 °C, 62.96 °C and 59.3 °C in the midday.

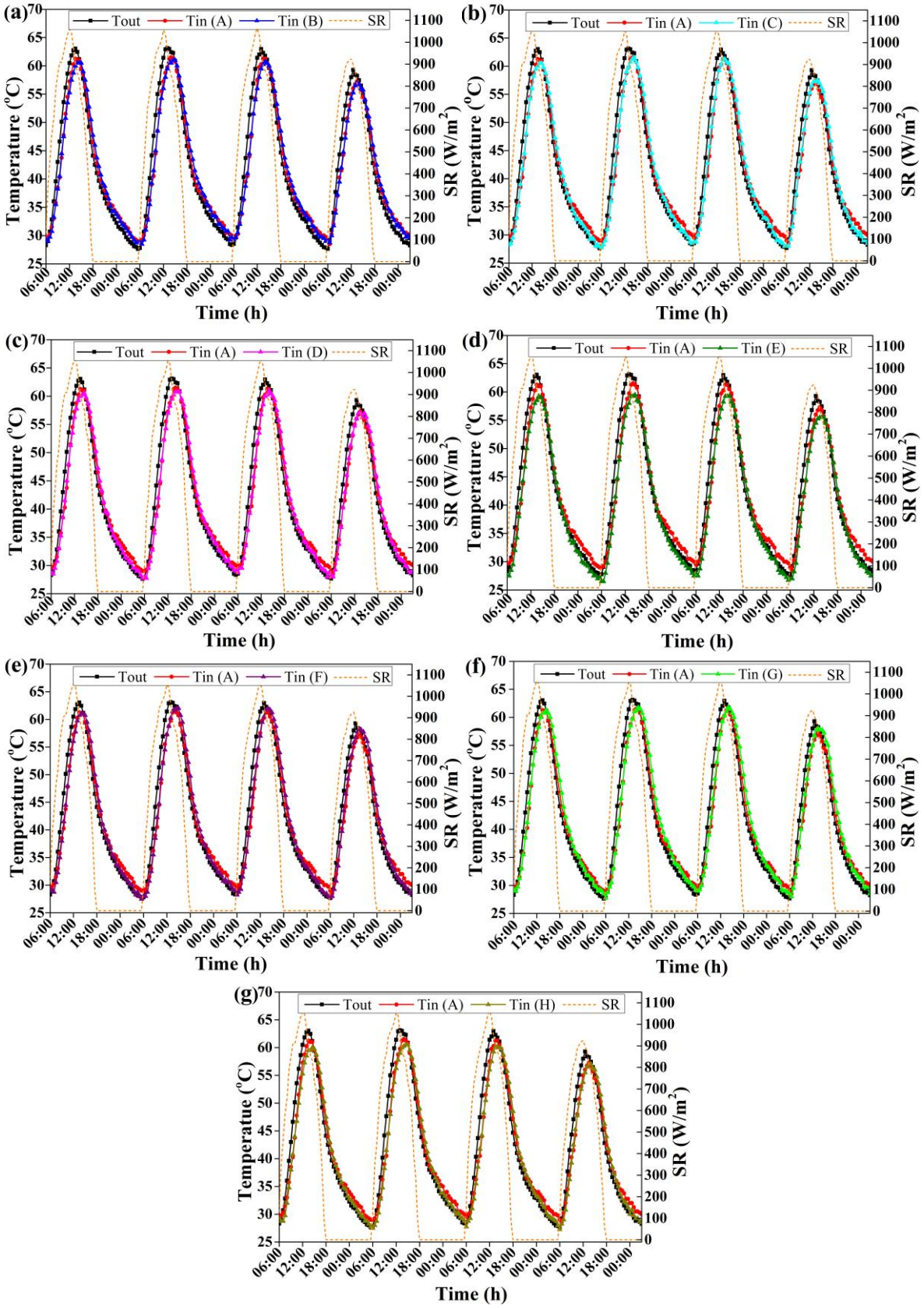

Fig. 4.19. Temperature profile for (a) A vs. B, (b) A vs. C, (c) A vs. D, (d) A vs. E, (e) A vs. F, (f) A vs. G, (g) A vs. H

The following indicators have been discussed to compare among tested PCM bricks and specify PCM's contribution to each one.

4.3.1. Maximum temperature reduction

Measurements of the current experiment showed that the maximum interior surface temperature during peak hours was reduced in all PCM bricks compared to the reference brick, as shown in Fig. 4.20. This reduction reflects the positive contribution of PCM to concrete bricks.

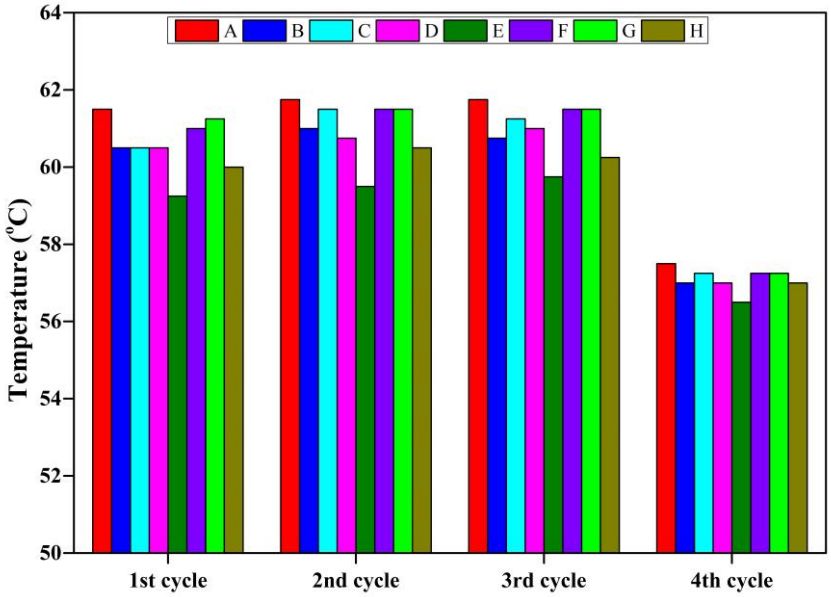

Fig. 4.20. Maximum T_{in} of tested concrete bricks at peak hours

As designated in the figure, concrete bricks with many PCM capsules (i.e., B, E and H) showed the highest reduction in T_{in} than other PCM bricks, even though there was a slight reduction. Expressly, E, followed by H, showed the best thermal performance.
Quantitively, the MTR results for each PCM brick compared with the reference brick (A) are shown in Table 4.4.

Table 4.4. MTR for PCM bricks during peak hours

No. of cycle	MTR (°C)						
	B	**C**	**D**	**E**	**F**	**G**	**H**
1st	1	1	1	2.25	0.5	0.25	1.5
2nd	0.75	0.25	1	2.25	0.25	0.25	1.25
3rd	1	0.5	0.75	2	0.25	0.25	1.5
4th	0.5	0.25	0.5	1	0.25	0.25	0.5

Table 4.4 indicated that the MTR of PCM bricks that involved many PCM capsules was the best. Besides, bricks of bulky PCM capsules showed lower MTR and poorer thermal performance. The average MTR can be calculated for each PCM brick during all cycles to quantify the best PCM brick performance. The average MTR of B, C, D, E, F, G and H compared with A during all cycles was ~0.81 °C, 0.50 °C, ~0.81 °C, ~1.88 °C, ~0.31 °C, 0.25 °C, and ~1.19 °C, respectively. These results showed that the bricks that included many PCM capsules (i.e., E and H) got the highest MTR compared with bricks with larger PCM capsules.

The main reason behind this disparity of MTR values is the overall heat exchange area of each PCM capsule(s). It can be noticed that the E and H samples have a larger number of PCM capsules compared with the other samples (except for B). Therefore, their heat transfer area was enlarged, maximising the PCM melting rate. On the other hand, sample B also has many PCM capsules. Accordingly, it has a huge heat transfer area compared with E and H samples, which might influence the PCM melting process, raising the brick temperature. However, the B sample also showed better MTR than other PCM bricks with bulk PCM capsules.

4.3.2. Decrement factor and time lag

Investigating the DF and TL of PCM bricks is important in this experiment to show the ability of PCM bricks to store and release heat during melting and solidification and also their ability to dampen the T_{out} towards T_{in} for a longer time. Fig. 4.21 shows the calculated DF for experimental brick samples for all cycles.

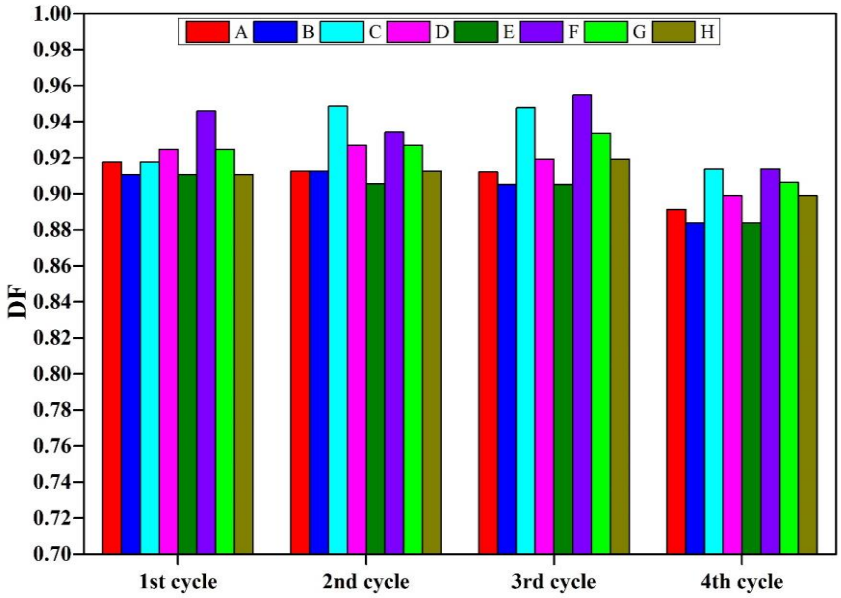

Fig. 4.21. DF of brick samples at peak hours

Fig. 4.21 shows that the E sample has the lowest DF in all cycles, representing the best case. However, B and H samples also showed a good DF compared to other PCM brick samples. Bulky PCM capsules (i.e., samples C and F) designated high DF even higher than the reference brick, meaning that the PCM was not melted or solidified completely, resulting in negative thermal behaviour. Therefore, the interior temperature fluctuations were not maintained during peak hours. The average DF of A, B, C, D, E, F, G and H was 0.908, 0.903, 0.932, 0.917, 0.901, 0.937, 0.923 and 0.910, respectively.

Fig. 4.22 shows the TL of all brick samples during the peak hours. The results fluctuated even for the same brick type over the experiment days. However, all PCM bricks showed longer TL than the reference concrete brick by 30 min at least. This advantage is attributed to PCM's ability to restrict the heat from the exterior towards the interior surface during the melting phase, which shaved and shifted the heat flux.

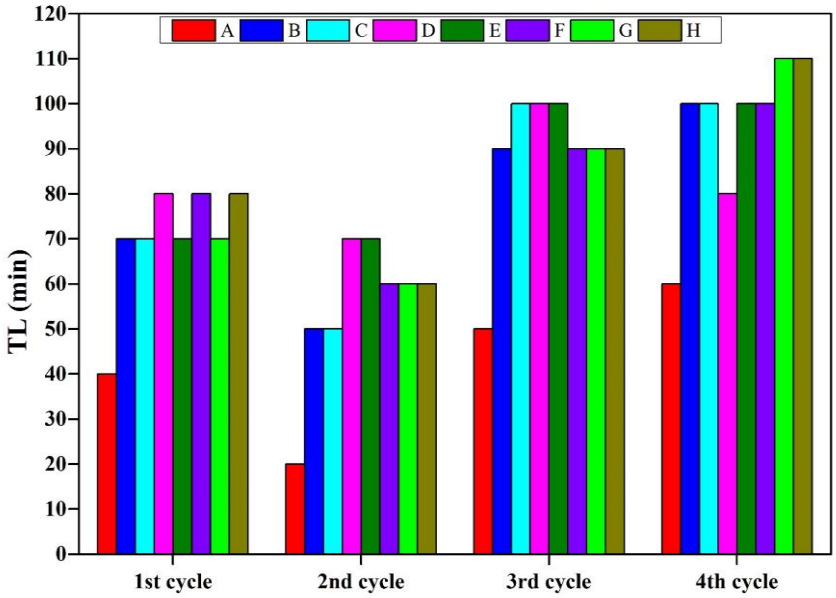

Fig. 4.22. TL of brick samples at peak hours

The average TL can be presented to make a fair comparison among the PCM brick samples and point out the best TL during all days of the experiment. Compared with the reference brick, TL obtained from each PCM brick was varied between 20-50 min. The average TL obtained from PCM bricks compared with the reference brick during all cycles is shown in Fig. 4.23. The average TL was calculated by taking the average four days for each PCM brick sample extracted from the average of TL for the reference brick.

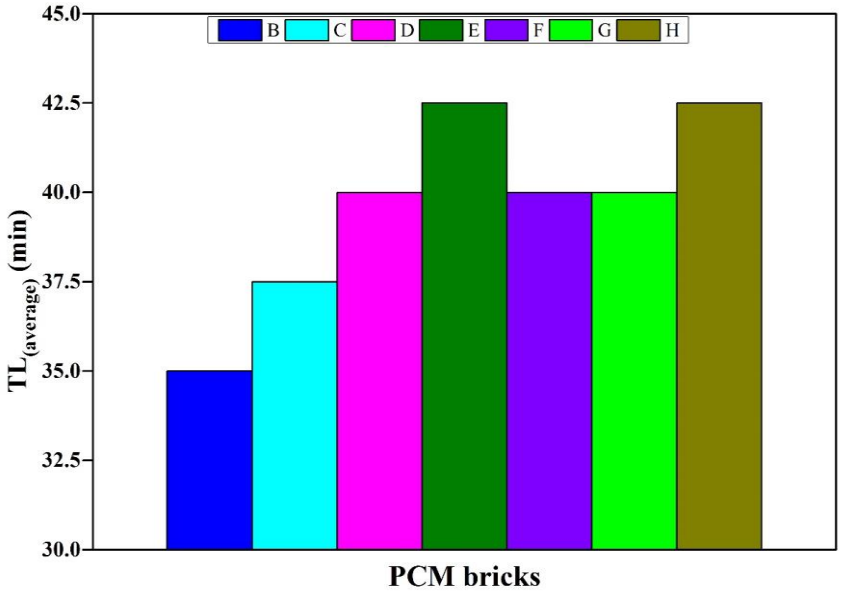

Fig. 4.23. Average TL of PCM bricks

Among PCM brick samples, E and H samples showed the highest average TL by about 42.5 min during the experiment, more than the reference brick, indicating efficient utilisation of PCM incorporation. D, F and G also indicated a good TL of 40 min compared with the brick of bulk PCM (i.e., C) that reported a 37.5 min delay. Surprisingly, the B brick sample showed the lowest TL, compared to other PCM samples, by 35 min more than A. The reason might be attributed to the considerable heat transfer area of PCM capsules of the B sample, which resulted in fast PCM melting and kept the brick heated for a longer time. Hence, the brick cannot restrict heat flow towards the interior environment as it reaches a full melting state.

4.3.3. Thermal behaviour of bricks during melting and solidification phases

PCM thermal behaviour varies during heat charging and discharging phases, influencing the PCM brick interior temperature accordingly. To investigate the thermal performance, a comparison among PCM bricks can be made against the reference brick during peak and off-peak hours of the first-day cycle.

Specifically, in this study, the heat charging and discharging rate depends highly on PCM capsules' heat transfer area as long as we deal with the same PCM quantity and position of capsules (Erlbeck et al., 2018). This parameter (i.e., heat transfer area) influences the rate of heat flows towards PCM capsules during day hours and out of them during off-peak hours at night.

All bricks showed nearly equal interior temperature during the early hours of the day when the melting phase did not occur yet, and all PCM bricks behaved like reference bricks. The interior temperature decreased for PCM bricks compared with the reference brick around 10:00, wherein the heat passing through the bricks reached the melting temperature of PCM (i.e., 40 °C- 44 °C). Here, the melting phase of PCM was started, and the heat was stored in PCM capsules. The capsule heat transfer area influences the rate of heat stored in each PCM capsule due to the increased heat exchange interface. In other words, the PCM melting and solidification rate will be fast as the encapsulation heat transfer area increases. Due to completed PCM melting, PCM bricks of large heat transfer areas have stored more heat faster than those of a small area. Therefore, it is clear that sample E performed better than the bricks of the square cross-section area shown in Fig. 4.24-a, and sample H showed the best performance compared with the bricks of the rectangular cross-section area (Fig.4.24-b). A comparison can be made among the PCM bricks with the highest heat transfer area (i.e., B, E and H) against the reference brick, as shown in Fig. 4.24-c. In this regard, it was evident that all PCM bricks have better thermal performance than the reference brick during peak hours.

Furthermore, brick E has the lowest T_{in} during all hours compared with B and H bricks. Simultaneously, B brick showed poorer thermal performance than E and H bricks, although it has a larger heat transfer area. It is logical as the heat transfer area speeds up the time to reach full PCM melting; thus, capsules cannot store more heat and behave as the reference brick.

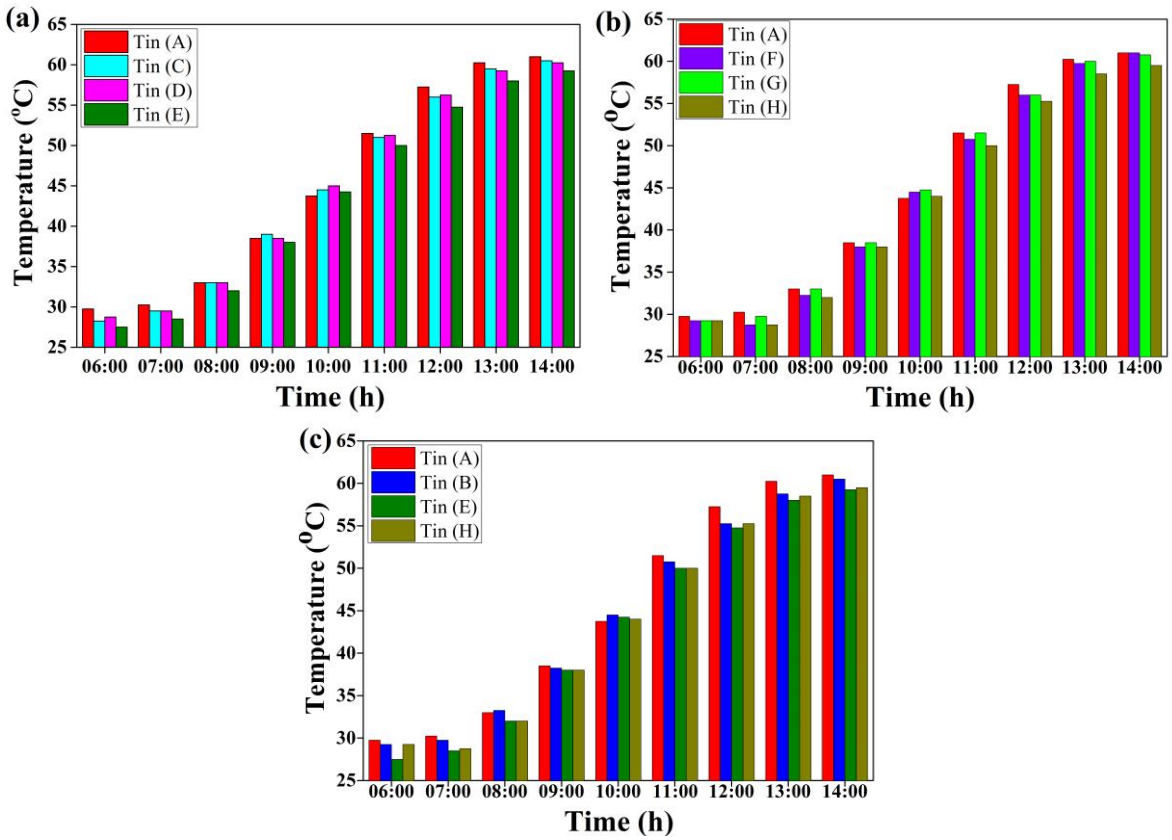

Fig.4.24. Hourly T_{in} during the peak period in the first cycle for (a) A vs C, D and E, (b) A vs F, G and H, (c) A vs B, E and H

In the solidification phase, the bricks' thermal behaviour was reversed. The reference brick performed better than PCM bricks as the ambient temperature decreased, but this behaviour was limited. As indicated in Fig.4.25-a, the reference brick performed better than PCM bricks of square cross-sectional capsules until around 21:00 in the late evening. Later, the temperature of PCM bricks performed better till the end of the cycle. Likewise, PCM bricks of rectangular cross-section capsules also showed a reversed thermal performance compared with the reference brick till around 21:00 - 22:00, as indicated in Fig.4.25-b. In both cases (i.e., Fig.4.25-a and b), bricks of a higher number of capsules (i.e., E and H) performed better than bulky PCM bricks due to their immense heat transfer area accelerating the time of PCM solidification. Fig. 4.25-c compares PCM bricks of a large number of PCM capsules (i.e., B, E and H), indicating that E was reported with the best thermal behaviour over time compared with B and H samples. Moreover, the H sample showed better performance than the B sample in comparison with A.

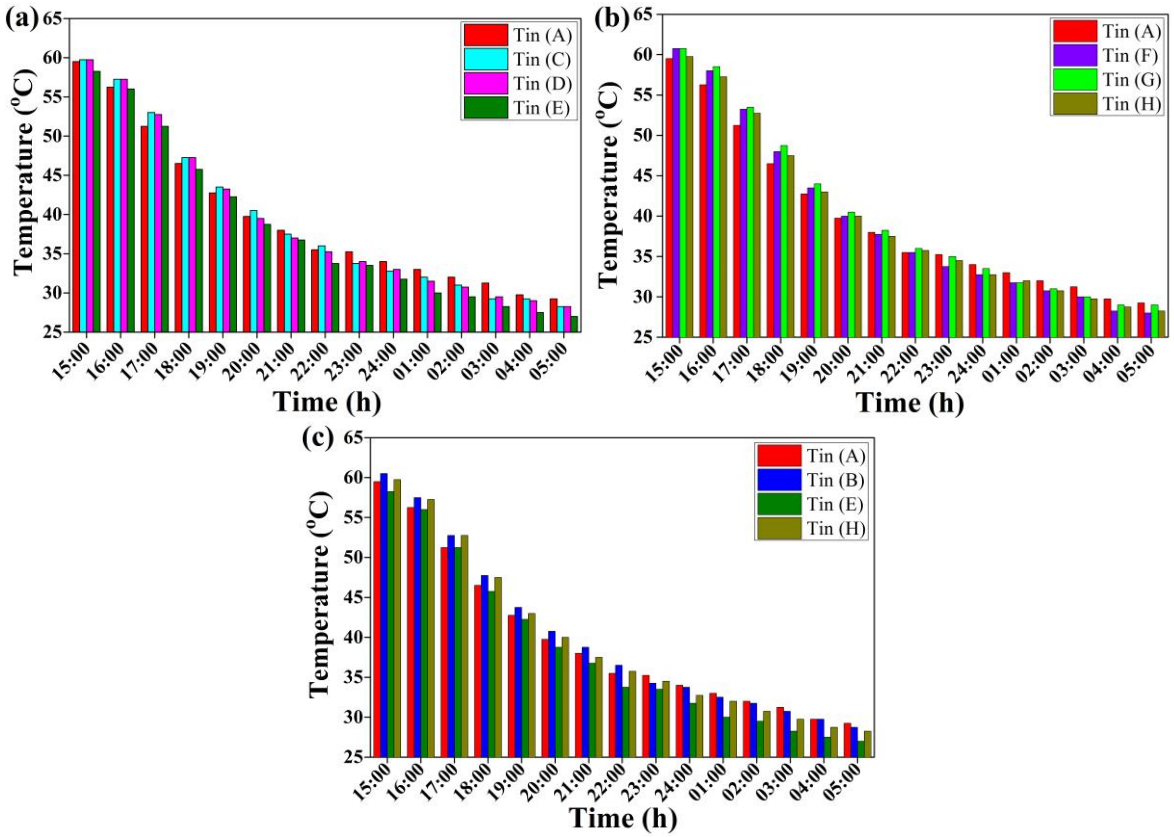

Fig. 4.25. Hourly T_{in} during the off-peak period in the first cycle for (a) A vs C, D and E, (b) A vs F, G and H, (c) A vs B, E and H

Generally, the results of tested PCM concrete bricks considering all the above indicators are tabulated in Table 4.5.

Table 4.5. Summary of the experiment results

Brick sample	Overall heat transfer area (cm^2)	Average MTR (°C)	Average DF	Average TL (min)
B	529.9	0.8	0.903	35
C	196	0.5	0.932	37.5
D	224	0.8	0.917	40
E	320	1.9	0.901	42.5
F	300	0.3	0.937	40
G	310	0.3	0.923	40
H	384	1.2	0.910	42.5

4.3.4. Mechanical behaviour of PCM bricks

As indicated earlier, the PCM layer was integrated with the PCM roof as a separate layer, while it was immersed as capsules into wall bricks, weakening their mechanical properties. Therefore, it is necessary to investigate the mechanical strength of PCM bricks and their thermal performance to provide a clear vision of PCM incorporation into the building structure. For this purpose, a crushing strength test was made for the PCM and bare bricks using a compression test machine (type ADR Touch head from ELE International) with a 2000 kN maximum load capacity, as described in Section 3.4 and Fig. 3.18. The mechanical test was applied on the concrete brick containing many square cross-section capsules (E sample) since it was the best thermally-performed brick, compared with the reference brick. Therefore, six bricks were tested (three from each brick type), and the results showed that the maximum compression strength at the failure of

bare bricks were 496.1, 481.5 and 503.2 kN, against 411, 3, 15.2 and 338 kN for PCM bricks. These values are averagely equivalent to 17.88 and 12.84 N/mm^2 compression strength, considering the brick area of 27600 mm^2. Therefore, the compression strength of PCM bricks was reduced by ~28.2% compared with the bare bricks. The decline of PCM brick strength is attributed to the poor mechanical strength of aluminium containers used for PCM encapsulation.

4.4. Thermal performance of a scaled experimental PCM room

This experiment has been conducted with three concepts: one-day evaluation, hourly analysis and long-term investigation. In the one-day evaluation, the PCM performance was evaluated experimentally daily, whereas the hourly analysis considered an hour-by-hour experimental analysis of PCM thermal performance. Besides, the long-term analysis was verified numerically for six summer months using the EnergyPlus software model validated by the one-day evaluation experiment.

4.4.1. One-day assessment of PCM room thermal performance

The experiment to investigate the thermal performance of the PCM room compared with the reference one was conducted for 24 h on 16th September 2021. The measured outdoor ambient temperature and SR on the experiment day are shown in Fig. 4.26. As indicated in the figure, the outdoor ambient temperature exceeded the mark of 47 °C at midday, with high SR values exceeding 1200 W/m^2. Moreover, the ambient temperature exceeded 30 °C in the late night and early morning hours, indicating how HVAC systems are needed during the whole day in such locations to maintain suitable thermal comfort for residents.

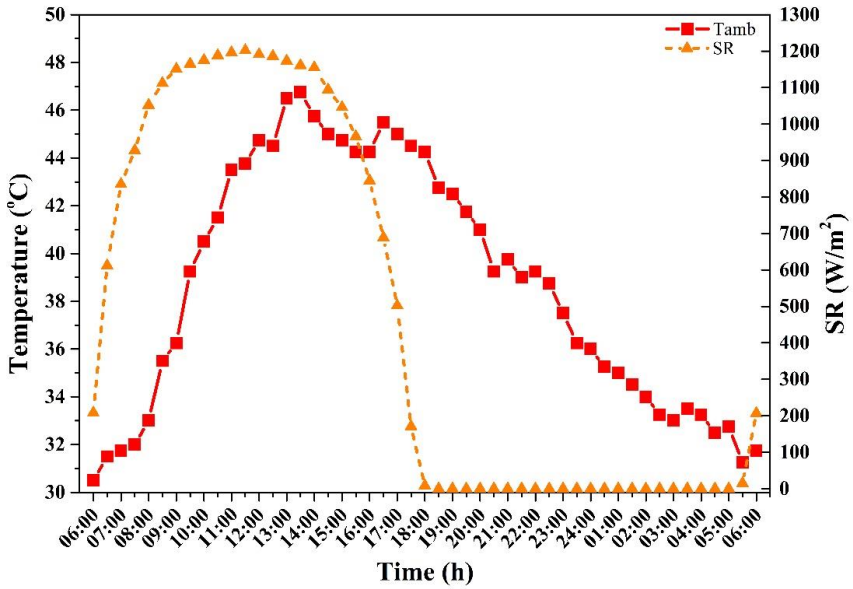

Fig. 4.26. Outdoor ambient temperature (Tamb) and SR during the experimental day measured in-site

Fig. 4.27 shows the recorded T_{in} and T_{out} for the roof, east wall, north wall, west wall, south wall and the indoor ambient temperature of PCM and reference rooms, respectively, with a 10 min time step. The outdoor temperature recorded a minimum of 30.5 °C in the early morning and a maximum of 47.5 °C in the midday at 13:40. The maximum T_{out} reached 56.5 °C, 56 °C, 52.75 °C, 59.25 °C and 53.75 °C for the east wall, west wall, north wall, south wall and roof, respectively.

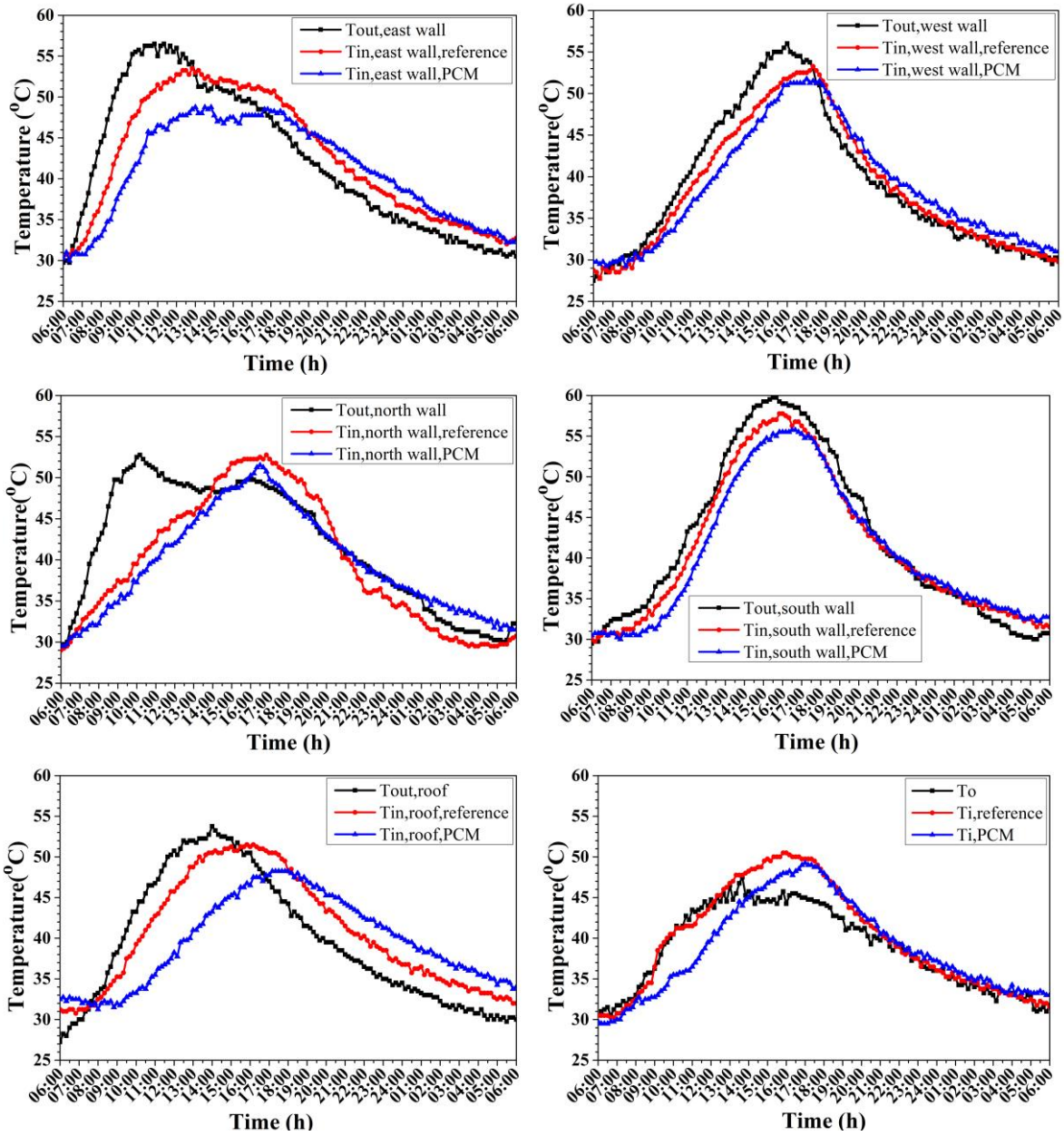

Fig. 4.27. T_{in}, T_{out} and T_i variation of PCM and reference rooms

The east, west, north and south walls of the reference room reach maximum T_{in} marks of 53.5 °C, 52.5 °C, 52.25 °C and 57.75 °C, respectively. In comparison, they recorded a maximum of 50.75 °C, 51.25 °C, 51.5 °C and 55.5 °C, respectively, in the PCM room. Moreover, the maximum indoor roof surface temperature and indoor ambient temperatures were 51.5 °C and 50.5 °C in the reference room compared with 48.25 °C and 49.25 °C in the PCM room.

It is evident from Fig. 4.27 that each element has its temperature variation trend depending on the time during the day and sun position. However, two intrinsic summaries are noticed in these figures, namely:

- All elements of the PCM room, more or less, have stable temperature behaviour than the reference room, which showed more temperature fluctuations. This fact is attributed to the PCM potential that traps the heat, making the envelope element more thermally stable against changeable weather conditions than local construction materials without PCM.
- The PCM elements showed negative thermal behaviour after sunset (after 18:00 till the beginning of the next day), in which the inside surface temperature of all elements was increased. This is mainly due to the PCM inclusion in the PCM room with a non-conditioned

case wherein the stored heat starts to transfer towards the outdoor low ambient temperature during the peak period.

It is worth mentioning that the thermal behaviour of roofs was different than that of walls during the night. As indicated in Fig. 4.27, the roofs' inside surface temperatures stay with a remarkable gap till the end of the next day. This is because the roof has more layers than walls, so the heat needs more time to be released from the PCM roof than the walls.

At night, mainly soon after 18:00, the indoor surface temperature of PCM room elements was higher than that of the reference room. This means that PCM starts releasing its heat as the ambient temperature falls, and it needs an average of 6-8 hours to discharge all stored heat (Guarino et al., 2017). Besides, the non-conditioned/ventilated rooms slowed the heat release from the indoor environment to the outdoor ambient, which is undoubtedly faster in ventilated cases. Therefore, ventilation is recommended for passive PCM building applications in hot locations (Arumugam et al., 2022).

Although Energy-saving earned from PCM incorporation into building envelopes is a commonly studied topic on a seasonal or annual basis (Frota de Albuquerque Landi et al., 2020), a detailed energetic analysis can be made for a shorter period considering several indicators showing the main advantages of PCM. To this aim, the previously discussed energetic and thermal comfort indicators are presented and analysed below to show the thermal behaviour of the PCM room against the reference room.

4.4.1.1. Maximum temperature reduction

Fig. 4.28 shows the MTR of each element of reference and PCM rooms together with the MTR difference for each element. As observed in the figure, the east wall, followed by the south wall, shows the highest MTR and MTR difference compared with other walls. Moreover, the roof showed higher MTR and MTR difference than the walls.

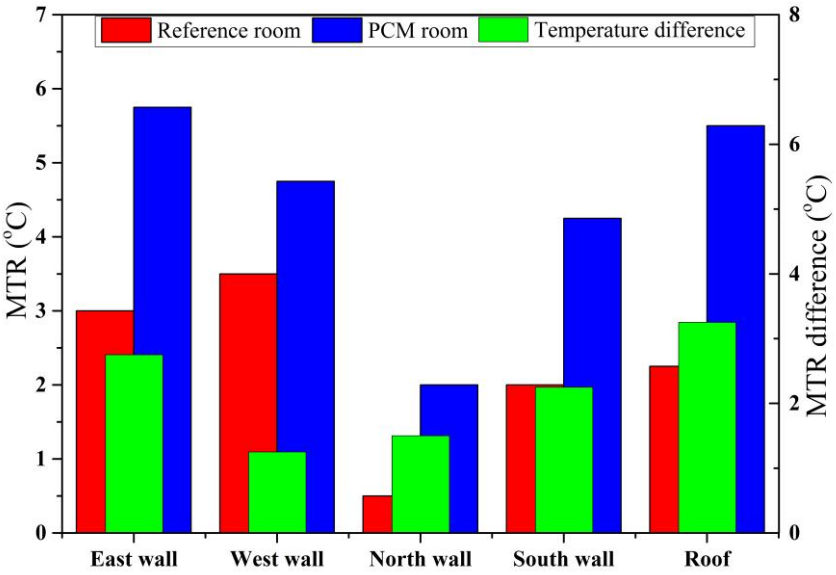

Fig. 4.28. MTR of reference and PCM rooms' elements

The MTR of east, west, north and south walls in the reference room was 3 °C, 3.5 °C, 0,5 °C and 2 °C compared with 5.75 °C, 4.75 °C, 2 °C and 4.25 °C in the PCM room, respectively. Moreover, the MTR of the roof in the reference room was 2.25 °C compared with 5.5 °C in the PCM roof.

The MTR difference between the reference and PCM rooms are 2.75 °C, 1.25 °C, 1.5 °C, 2.25 °C and 3.25 °C, respectively, for the east wall, west wall, north wall, south wall and the roof. These MTR difference values influence the thermal comfort inside the room and energy consumed during

the peak period. Besides, they indicated positive, energetic behaviour, although the rooms were built with limited sizes and no ventilation.

It is known that the MTR of the roof and walls all influence the indoor temperature inside rooms. Accordingly, MTR can be calculated for the indoor air of both rooms, considering the difference in the outdoor ambient temperature. MTR difference of indoor air inside the PCM room compared with the reference one (also researchers referred to as indoor temperature reduction (ITR) or indoor temperature drop) ranged between 0.25 °C to 5.75 °C during day hours. These values align with those of studies verified under hot weather conditions. For instance, Sovetova et al. (Sovetova et al., 2019a) conducted a numerical study under hot weather in Sharjah and Al-Ain cities in the United Arab Emirates and found that the optimal PCM can decrease the MTR by up to 1.09 °C when incorporated with the building envelope. Moreover, recent studies found that ITR reached about 0.2 °C to 4.3 °C under Indian hot weather conditions (Rathore et al., 2020) and about 3.4 °C under Danish summer conditions (Hagenau and Jradi, 2020).

4.4.1.2. Average temperature fluctuation reduction

ATFR calculation results are presented in Fig. 4.29. ATFR of the PCM room roof was much higher than all walls. The maximum ATFR of the east wall, west wall, north wall, south wall and the roof were ~2.4 °C, ~2.3 °C, 3.3 °C, 2.1 °C and 6.5 °C, respectively. Moreover, the ATFR of the indoor air of the PCM room compared with the reference one reached 3.45 °C, influenced by the values obtained for the room's elements. This value reflects the remarkable advantage of incorporated PCM as it was exceeded by a mark of 3 °C (Nurlybekova et al., 2021). Alam et al. (Alam et al., 2014) found that ATFR ranged between 3 °C- 4 °C in tested PCM-enhanced envelope in different Australian cities (Canberra, Melbourne and Hobart) from September to April. Kenzhekhanov et al. (Kenzhekhanov et al., 2020) verified ATFR values between 1.59 °C- 2.65 °C during the summer season of different cities worldwide, namely Bratsk, Arkhangelsk and Surgut in Russia, Fort McMurray and Val-d'Or in Canada, Oulu in Finland, Umea in Sweden and Anchorage in the United States.

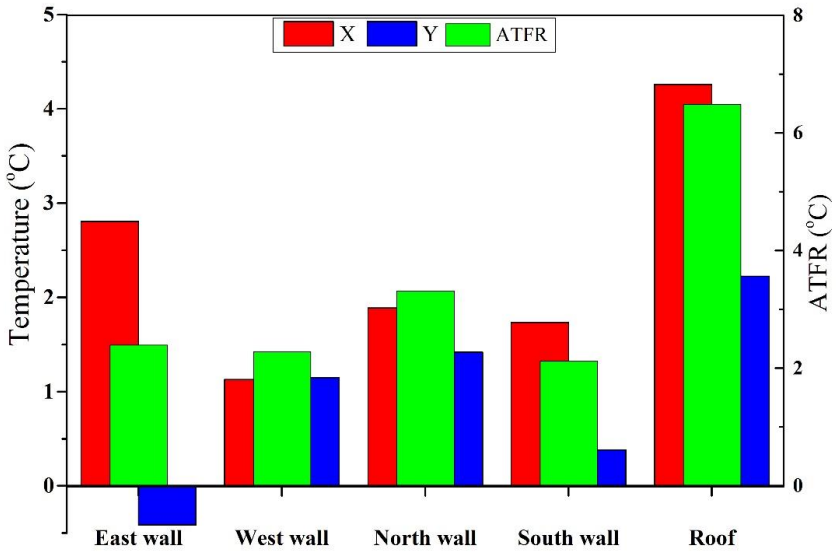

Fig. 4.29. ATFR of reference and PCM rooms

The figure shows that the PCM incorporation was beneficial as all ATFR values were more than 0 °C. This means that all X-values were higher than Y-values in every element, indicating the better performance of PCM during the daytime. Fig. 4.29 also indicates a negative Y value for the east wall of the PCM room, which was the best thermally performed amongst walls in terms of MTR. This could be attributed to the fact that the east PCM wall was effective during the day hours, which resulted in a high X (average temperature difference between the reference and PCM

east walls). Therefore, the average surface temperature of the PCM wall is still lower than the reference wall, even during the solidification phase.

4.4.1.3. Decrement factor

The calculation results of DF for the reference and PCM room elements are shown in Fig. 4.30.

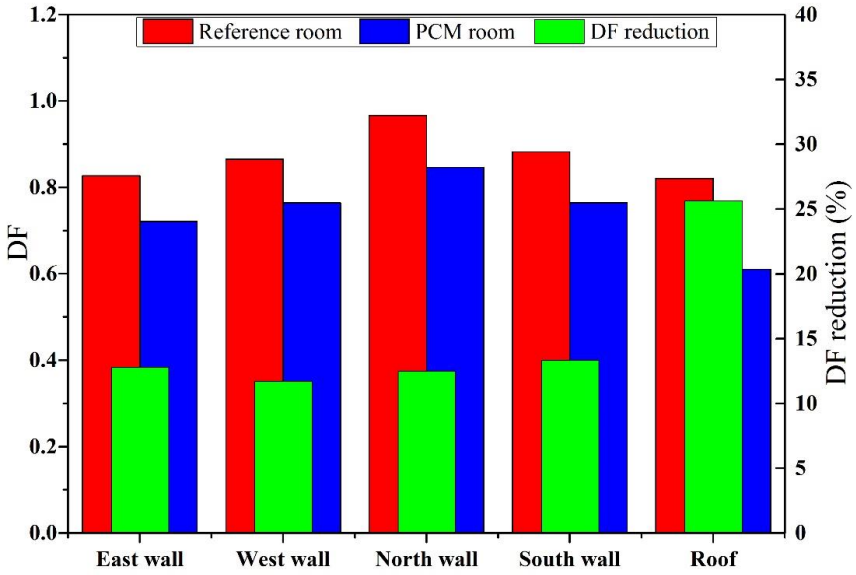

Fig. 4.30. DF of reference and PCM rooms

Generally, PCM room elements showed better DF, as expected, thanks to the PCM thermal potential, which literarily worked as dynamic insulation. The DF reduction of the east wall, west wall, north wall, south wall and the roof of the PCM room was better than the reference room by about 12.8%, 11.7%, 12.5%, 13.3% and 25.6%, respectively. DF of the PCM room roof was almost double of each wall, indicating the better performance of PCM in the roof compared with walls. This is mainly due to the better thermal performance of the roof's layers and the position of the PCM in the roof close to the outdoor environment, which charge and discharges heat far from the indoor environment, compared with the middle position in walls. Saafi and Daouas confirmed this fact, reporting that the DF of a PCM applied on a north wall was reduced from 39.41% to 27.3% by changing the PCM position from an internal to an external location (close to the outdoor environment). On the contrary, Jia et al. (Jia et al., 2021) claimed that PCM-filled inner cavities of concrete blocks had reduced DF from 12.3%-17.0% to 1.7%–2.2%. In another approach, Kontoleon et al. (Kontoleon et al., 2021) studied the effect of PCM thickness on the DF and found that the PCM-enhanced cement mortar can reduce the DF of a standard concrete wall by 17.4%, 22.1% and 29.1% when 1, 1.5, and 2 cm of PCM layers applied, respectively.

4.4.1.4. Time lag

Fig. 4.31 shows the TL and TL difference in the reference and PCM rooms' elements. The TL differs from one element to another. For instance, the north wall had the maximum TL among other walls by 320 and 340 min in the reference and PCM rooms. This TL is quite large and is not logical compared with other rooms' elements. By considering the temperature trend of the outdoor surface temperature of the north walls presented in Fig. 4.27, we recognise that the maximum outdoor surface temperature reached around 10:00 in the morning, as expected, as the solar radiation was high near the north walls in the early morning hours. In contrast, the maximum indoor surface temperature of the north walls was reached after 16:00, in the afternoon, due to the accumulated heat during the whole day and the influence of the other elements' temperature on it due to non-ventilated conditions.

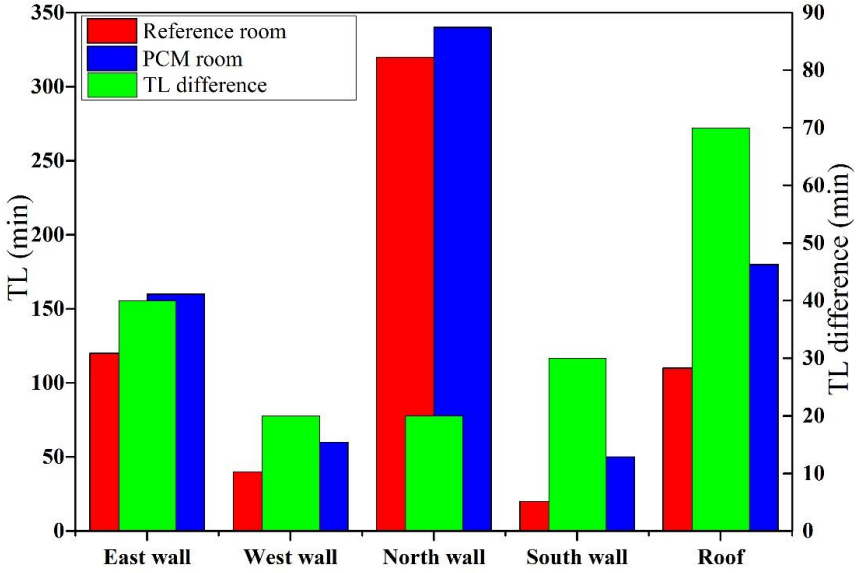

Fig. 4.31. TL of reference and PCM rooms

On the other hand, a more logical explanation can be observed when considering the TL difference between the reference and PCM rooms. In this regard, the east wall followed by the south walls, had the maximum TL difference (40 min and 30 min, respectively) compared with the west and north walls, which had only 20 min. This is expected as long as the east and south walls experienced direct high solar radiation for a longer time than the other walls, in which the PCM was activated sufficiently. The MTR indicator also supports this, which shows the best thermal behaviour of the east and west walls. Moreover, the roof of the PCM room showed the highest TL difference/increment with 70 min compared with the roof of the reference room. Wu et al. (Wu et al., 2021) exhibited that applying PCM on walls resulted in TL in the range of 3.33 h- 4.17 h and was affected by the thickness and position of PCM. In this regard, Zhang et al. (Zhang et al., 2016) stated that the TL of PCM-incorporated hollow concrete brick wall was reduced by 0.5 h- 3 h under China weather conditions depending on the PCM position within the bricks. In the same approach, Jia et al. (Jia et al., 2021) claimed that PCM filling the interior gaps of concrete bricks can reduce the TL from 1.50 h- 2.00 h to 6.17 h- 6.50 h under Shanghai city weather conditions. Another study showed that TL was decreased by 0.14 h, 0.66 h, and 1.30 h when 5, 10 and 15 mm PCM thickness was incorporated compared with a base case with no PCM (Zhang et al., 2020). Imghoure et al. (Imghoure et al., 2021) found that the TL for building walls incorporated Bio-PCM ranged from 2 h to 3 h compared with the base case regardless of PCM thickness and position under the summer climate of the Marrakech region.

4.4.1.5. Operative temperature reduction

Fig. 4.32 shows the OT variation of the reference and PCM rooms against the outdoor ambient temperature. The figure shows that the outdoor ambient temperature was higher than the OT in both rooms until noon. It then gets lower as the interior surface temperature of rooms' elements increases with a noticeable time delay between the PCM and reference room. Moreover, the heat accumulated inside rooms throughout the experiment (due to non-ventilation) continuously increases the indoor air temperature. It was also evident that the OT of the PCM room was lower than that of the reference room during the daytime, and the trend reversed in the evening (after 18:00) till the next day. This is attributed to PCM integration into elements that release heat uncontrollably as the ambient temperature falls below 40-44 °C during the day. The maximum OT difference reached 4.6 °C at 10:10 due to the PCM activation involved in the PCM rooms' elements that were the most in the period from 9:20 to 11:30. This period is critical in actual buildings in Iraq as it represents the peak period of electric power consumption for powering air-conditioning

systems. Besides, the rooms required suitable ventilation after sunshine to overcome the indoor temperature increment that occurs due to the PCM discharging phase.

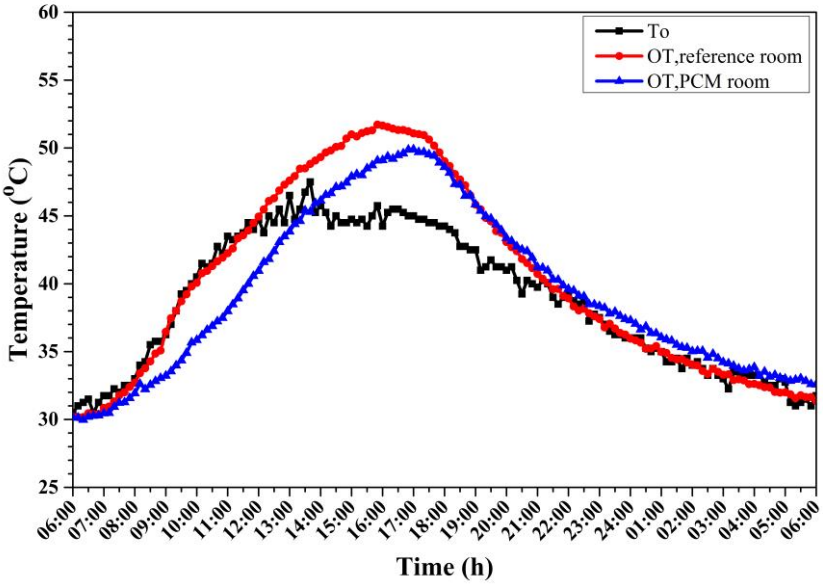

Fig. 4.32. OT variation of reference and PCM rooms

The OT difference/reduction results obtained in the current work are remarkable compared with those found in the literature. For instance, Costanzo et al. (Costanzo et al., 2018) conducted a study under three different climates, namely Rome (Italy), Wien (Austria) and London (United Kingdom), to show the effectiveness of commercial PCM-enhanced office building walls considering the OT reduction. Numerical results exhibited OT reduction by 0.5 °C during the day hours in a conditioned environment. Touma and Ouahrani (Touma and Ouahrani, 2018) examined the thermal behaviour of PCM-incorporated floor and wall tiles applied to typical Majlis living space in Qatar. Results showed that the PCM enhanced the space OT that was in the range from 25.7 °C to 29.4 °C and became in the range of 26.1 °C to 29 °C after PCM incorporation, indicating OT enhancement by 21.6% on average. Ramakrishnan et al. (Ramakrishnan et al., 2017a) conducted an experimental and numerical study for form-stable PCM-enhanced plastering mortar applied as a cladding layer for a multi-story office building in Milbourn, Australia. Considering the OT, results indicated that the applied method reduced the indoor OT by up to 2.5 °C. The above literature studies indicate that the PCM macroencapsulated panel and capsules adopted in the current study were more effective than other incorporation methods. However, this effectivity could be more improved when dealing with the negative behaviour at night, as stated by Adilkhanova et al. [82] that OT could be enhanced by more than 5 °C with a suitable night cooling control under all conditions cities of Kazakhstan.

The OTR in the PCM room compared with the reference room could be considered according to Eq. (3.20) to quantify the contribution of the PCM. The hourly OTR resulting from the PCM incorporation into the PCM room during the daytime is listed in Table 4.6.

According to the reslts shown in Table 4.6, the maximum OTR was reached in the first half of the day between 10:00 and 11:00 in the range of 10.1% to 11.2%. This period experienced high solar radiation and outdoor temperature levels, as the PCM inside the roof and walls in the heat charging phase. In contrast, the OTR is getting low in the late afternoon, during which the outdoor ambient temperature gets lower than the melting temperature of PCM. Thus, the heat discharging phase of PCM starts with no control of heat dissipation towards the indoor environment, and the OT of the PCM room increased near that of the reference room.

Table 4.6. Hourly OT and OTR of reference and PCM rooms during day hours

Time (h)	$OT_{ref.\ room}$ (°C)	$OT_{PCM\ room}$ (°C)	OTR (%)
06:00	30.20	30.13	0.25
07:00	30.85	30.45	1.30
08:00	32.70	31.93	2.37
09:00	36.45	33.23	8.85
10:00	40.08	35.85	10.54
11:00	42.25	37.98	10.12
12:00	44.95	40.95	8.90
13:00	47.6	43.85	7.88
14:00	49.33	46.13	6.45
15:00	51	47.9	6.08
16:00	51.65	49.10	4.94
17:00	51.08	49.9	2.31
18:00	49.03	48.60	0.87

4.4.1.6.MHGR

The solar heat gain reduced through the building envelope could indicate the cooling load reduction (Sharma and Sengar, 2019). Subsequently, this also specifies the energy-saving obtained from PCM incorporation (Lei et al., 2016). Fig. 4.33 shows the maximum HGR (MHGR) of each element considering the HG of PCM and reference rooms.

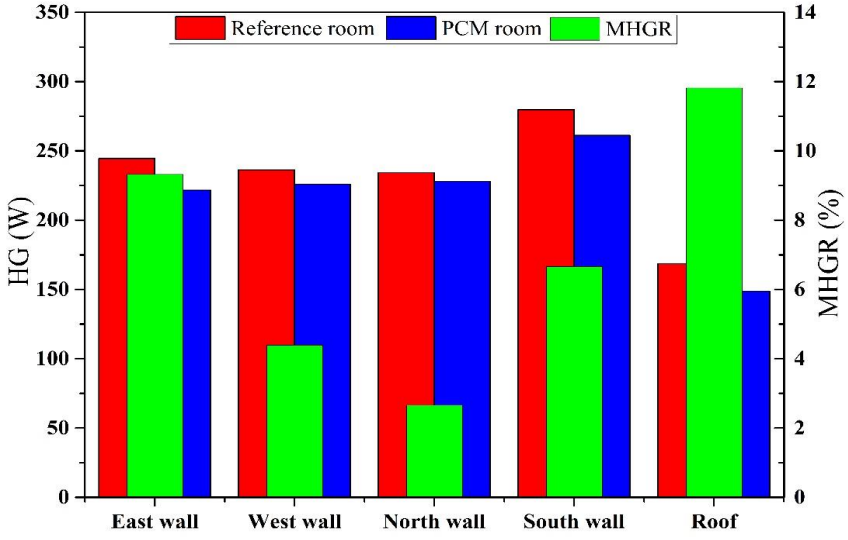

Fig. 4.33. HG and MHGR in the reference and PCM rooms

In general, Fig. 4.33 showed that the east wall had better HG compared with the other walls, followed by the south walls. However, the latter exhibited more HG in reference and PCM rooms. This indicates that the heat across these walls was high as they were exposed to high solar radiation for a long time, which allowed more heat to transfer. On the other hand, the roof of the PCM room minimised the HG more than the reference room, thanks to the PCM layer, which interrupted the heat flowing towards the indoor zone. Considering the MHGR, the east and south walls showed

MHGR of 9.3% and 6.7%, respectively. These percentages are higher than those of the west and north walls, which showed only 4.4% and 2.7%, respectively, indicating that these walls received less solar radiation, particularly the north wall. In contrast, the roof showed the best MHGR of about 11.8%.

The calculations show that the roofs had reduced the HG more than the walls. This is mainly due to the thicker roof combination than the walls, which provides more thermal resistance against the heat flow. In addition, the PCM quantity incorporated into the roof was higher than that incorporated walls (7 kg in the roof against ~4 kg in each wall). Thus, more heat would be stored in the PCM roof than in PCM walls, especially since the roof was exposed to direct solar radiation longer than any wall. In view of that, the total MHGR in the PCM room was about 34.8% compared with the reference room. This percentage is realistic compared with those obtained under different locations worldwide. For instance, the MHGR ranged by 3.5%–47.2% according to a study conducted under the United States weather conditions (Kishore et al., 2020) and by up to 35% under Saudi Arabia's climate conditions (Khdair et al., 2022). Besides, an optimisation study for building with insulation and PCM reported 33.5% MHGR under hot Indian climate conditions (Saikia et al., 2020). A summary of the above results is shown in Table 4.7.

Table 4.7. Summary of experimental results obtained in the current study

Element	MTR(°C)	ATFR(°C)	DF reduction(%)	TL(min)	MHGR(%)
East wall	2.75	2.4	12.8	40	9.3
West wall	1.25	2.3	11.7	20	4.4
North wall	1.5	3.3	12.5	20	2.7
South wall	2.25	2.1	13.3	30	6.7
Roof	3.25	6.5	25.6	70	11.8

4.4.2. Hourly analysis of PCM room thermal performance

The experimental work of evaluating the hourly thermal performance of the PCM room compared with the reference one was conducted on a hot summer day, 15 September 2022, from 6:00 to 24:00. Fig. 4.34 shows the temperature variation with 30 min time intervals of the indoor air temperature and inside surface temperatures for roofs and walls of the reference and PCM rooms. In addition, the outdoor ambient temperature and SR are presented in each figure. As can be observed in all figures, the inside surface temperature of the elements of the reference room was high compared with that of the PCM room during daytime hours. In contrast, the temperature behaviour was adverse as soon as the daytime ended. This phenomenon occurs due to the PCM thermal behaviour that decreases the heat flow through the envelope elements in the daytime during the heat charging phase (melting phase). Besides, the charged heat (the heat accumulated inside the PCM) had released at night, increasing the elements' temperature in the PCM room until they became at the same temperature level late at night. This temperature behaviour has resulted from the non-ventilated rooms throughout the experiment, which keeps the outdoor temperature controlling the temperature variation during the day and night.

Fig. 4.34 also indicated that both room elements' highest inside surface temperature was shifted (compared to the outdoor ambient temperature and solar radiation) due to the thermal resistance of room elements. However, the PCM room’s elements indicated noticeably longer time-shifting than the reference room elements.

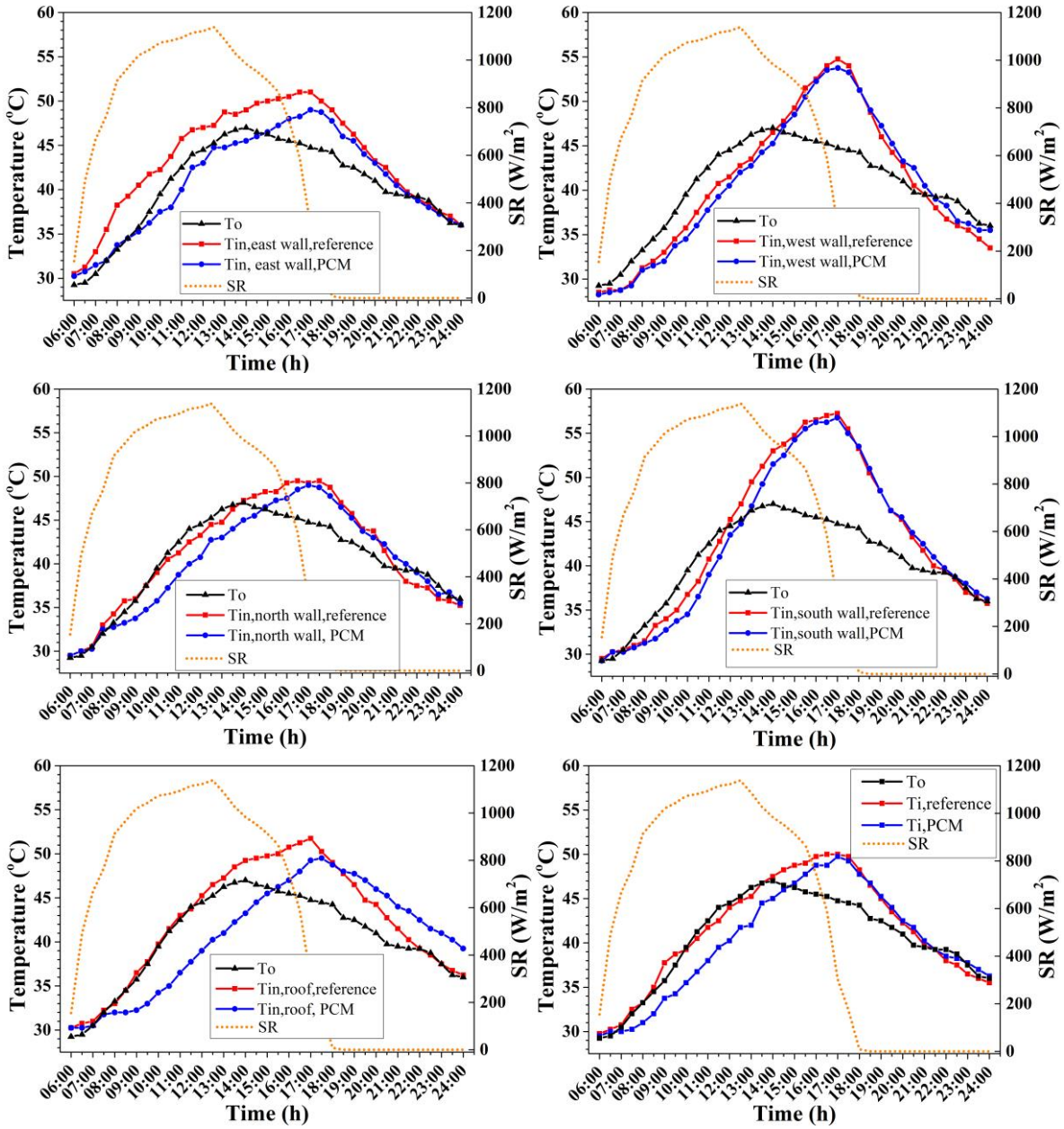

Fig. 4.34. T_{in} and T_i variation of reference and PCM rooms against T_o and SR

Fig. 4.34 shows that east-oriented walls exhibited the highest temperature gap of 2 °C-5.25 °C between 8:00 and 17:00, with the highest mark between 9:00 and 10:00. This temperature gap rapidly shrinks after 18:00, affected by the low ambient temperature at night. On the other hand, south-oriented walls showed a lower temperature gap of 1.25 °C- 2.75 °C from 8:30 to 14:30, showing poorer PCM potential utilisation than the case of east-oriented walls. These walls have severely influenced the indoor environment temperature as they reached the mark of 57 °C around 17:00. The temperature behaviour of south-oriented walls was reversed earlier, even before the sunset at 18:00, till midnight. As indicated in Fig. 4.34, the west-oriented walls showed the poorest temperature behaviour regarding PCM utilisation, wherein the temperature gap was between 0.25 °C and -1.5 °C during the day. In contrast, north-oriented walls indicated a better temperature gap by an average of 2.25 °C from 8:30 to 14:30.

The temperature variation of roofs shown in Fig. 4.34 designated different temperature trends than walls. The temperature gap of roofs was large by up to 4.25 °C - 6.5 °C between 9:00 to 15:00, showing a notable utilisation of PCM storage capacity. However, the PCM solidification phase (i.e., heat discharging) in the PCM rooms' roof was not finished as in the walls and required more

time to release the stored heat. This may be attributed to the fact that the roof stored more heat than any wall in the PCM room as it was exposed to direct solar radiation all daytime long compared with the time-dependent walls. Besides, the thermal mass of the PCM roof was larger than that of PCM walls due to the high incorporated PCM quantity that needed more time to be released completely.

The temperature variation of the indoor air of both rooms (shown in Fig. 4.34) followed the same temperature variation trend as the roofs and walls, and the indoor temperature was always above the comfort level range. The temperature gap was between 2.25 °C and 4.5 °C in the period 7:30-14:30 due to the accumulated heat of all elements. However, the temperature trend of indoor air was primarily similar to east walls and roofs during the daytime, indicating the considerable influence of these elements on indoor air temperature during the peak period.

Fig. 4.35 shows numerous thermal camera images of the outside surface temperature of rooms at different times of the day. Starting from 6:00, the sun was partially incident on the north walls at a low rate, heating the outer surfaces equally by about 28 °C. At 9:00, the sun rises vertically, and most solar radiation incident on the east walls with a high ratio; thus, the outer surfaces are warming up with lots of heat passing towards the inside space. At this time, the PCM is in a charging phase, and heat is stored inside PCM capsules, making the middle of the brick hotter than the outside and inside surfaces. This is observed clearly in the slight temperature difference of about 0.6 °C between the reference and PCM east walls at 9:00. Besides, the night coolness stored by PCM during the late night hours is released, making PCM elements colder than reference elements in the first few hours of the morning. The sun's position at noon is perpendicular to rooms where the roofs and south walls receive high solar radiation. At this time, the PCM is expected to be in a full liquid state inside the capsules of the PCM room south wall, and heat charging is continuous. Therefore, some heat is dissipated uncontrollably towards inside and outside spaces due to the heat transfer difference between PCM capsules and indoor/outdoor environments. This behaviour is noticed in the relevant photos where the outer surface temperature difference between the reference and PCM south walls is about 0.4 °C. At 15:00, the sun is perpendicular on the roofs and west walls, and the ambient temperature reaches high limits encountered with a high solar radiation rate. Therefore, the PCM liquid is at a high temperature, at this time, in the west wall and roof, resulting in a high outside surface temperature compared with their corresponding elements in the reference room. This is shown by the outside surface temperature difference of about 1.7 °C and 1.8 °C between the west walls and roofs, respectively.

At 18:00, when the sun rises and ambient temperature drops, the discharging heat from PCM is expected to start due to the conductive and convective heat transfer difference between the PCM capsules and outdoor ambient temperature. As a result, the outside surfaces of the PCM room dissipate heat at a larger rate than the reference room's outer surfaces. The temperature limit and heat dissipation time depend mostly on the outdoor conditions (mainly the ambient temperature and wind speed) and the amount of heat stored in the roof and walls. This can be detected considering the inside surface temperature difference between PCM and reference roofs in Fig. 4.34 and their outside temperature difference of about 1.9 °C in Fig. 4.35.

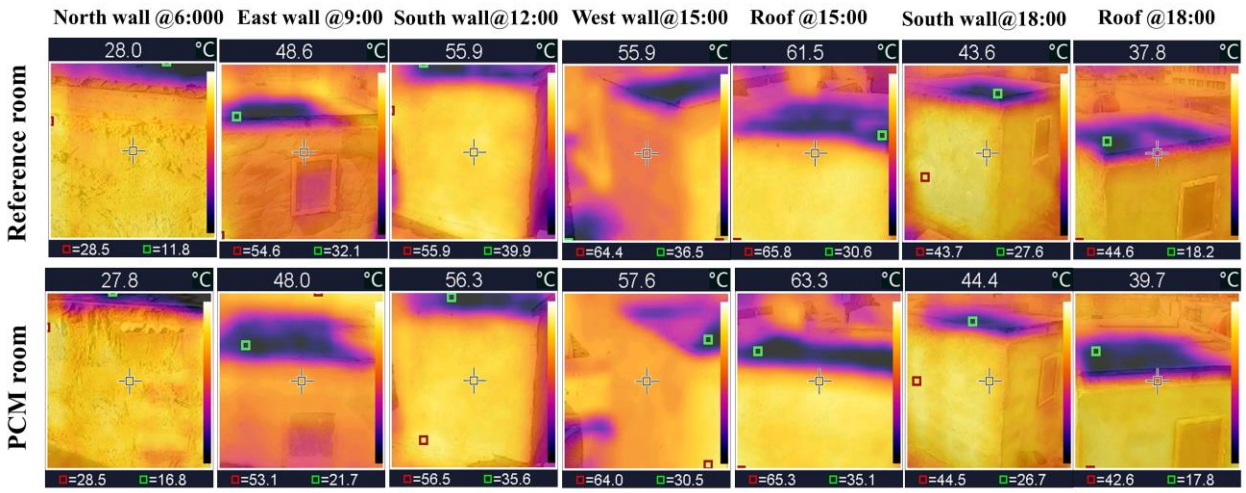

Fig. 4.35. Thermal images for outside elements at different times

4.4.2.1. Analysis of hourly temperature reduction

Reduced inside surface temperature is the main benefit of PCM when incorporated into building elements under hot locations, working as dynamic thermal insulation (Toure et al., 2019). This reduction considerably influences occupants' thermal comfort and decreases the reliance on cooling and air-conditioning systems. Besides, it may avoid the need for such systems in transition seasons (i.e., spring and autumn).

In this research, a comparison between PCM and reference rooms is studied during day time considering the inside surface temperature decrement and the impact on the indoor temperature. In this regard, the hourly temperature reduction (HTR) is calculated following the same concept of MTR presented in Eq. (3.7) but considering the hourly temperature difference (HTD) instead of the maximum temperature difference to explore the hourly contribution of PCM. Accordingly, the HTD was simply calculated as the difference between the T_{in} of every element in the reference and PCM rooms each hour (indoor HTD was calculated considering the T_o and T_i). Besides, the HTR was calculated as the ratio of HTD of each element in rooms to the corresponding element surface temperature, the same as the equation RMTR described in section 3.6.1. Fig. 4.36 shows the HTD and HTR of each element. It is worth mentioning that the HTR was calculated during the day hours only since the PCM temperature behaviour is adverse during nighttime due to the heat discharging phase of the PCM room, as indicated earlier.

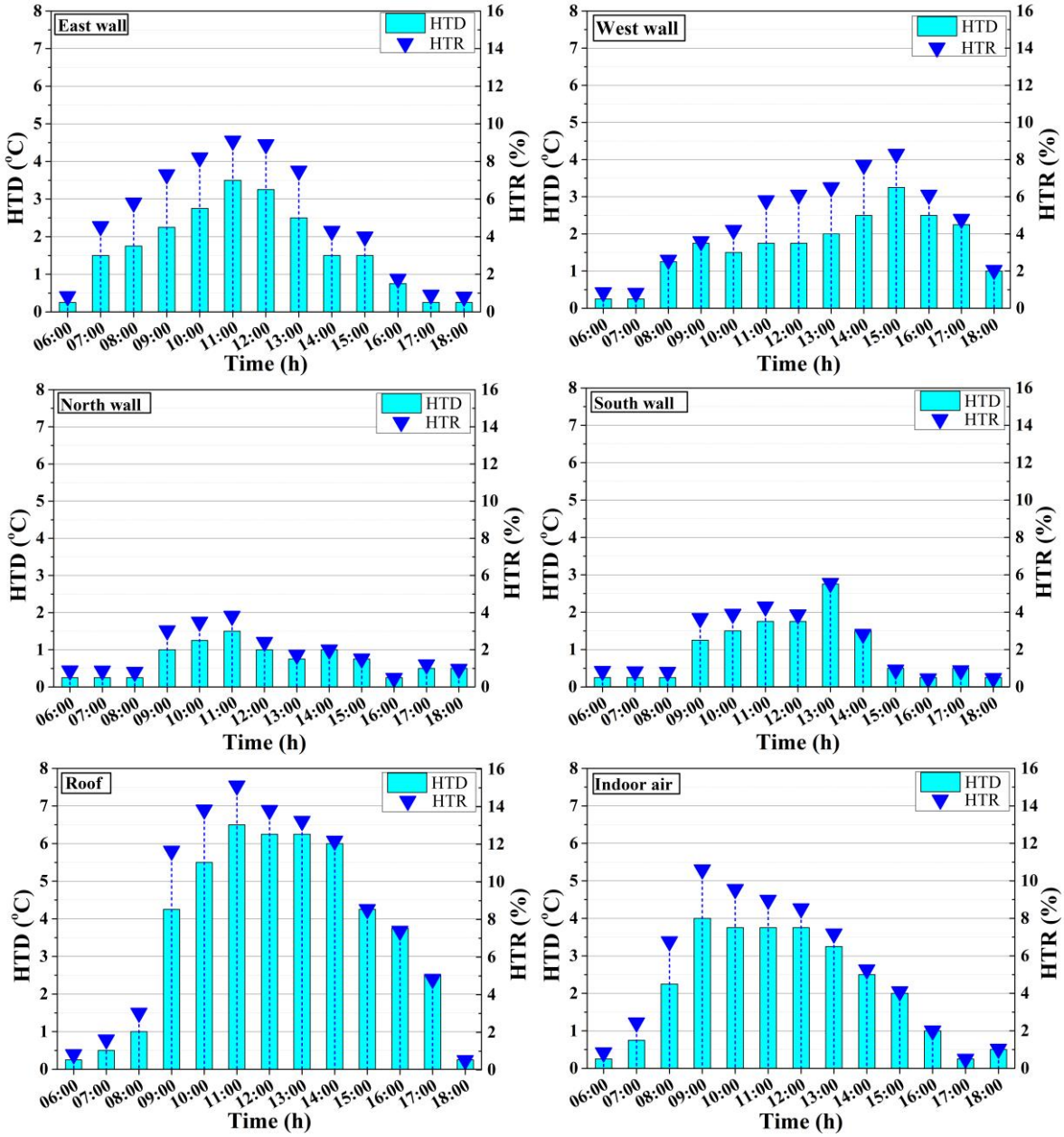

Fig. 4.36. HTD and HTR during daytime hours

As shown in the figure, all elements of the PCM room recorded HTD and HTR by at least 0.25 °C and ~0.5%, respectively. The east-oriented wall was designated the highest HTD and HTR compared with the other walls. The maximum HTD was attained at 11:00, reaching HTR by 9.1% with HTD of 3.5 °C. The east walls were exposed to direct solar radiation at this time with an inclined sun position, resulting in the PCM melting phase earlier than other walls. On the other hand, the west-oriented wall showed the second-best thermal behaviour compared with the southern and northern walls. The highest HTR of the western wall reached at 13:00 with 8.5% and HTD of 3.2 °C, as expected, since the solar radiation was hitting the west walls in the late afternoon. However, the PCM in the west wall was also effective before this time, influenced by the high ambient temperature from 9:00 to 13:00, as obviously shown in the HTR and HTD indicated in the relevant figure.

Surprisingly, the south-oriented wall indicated low HTR with a maximum of 5.6% (HTD of 2.75 °C) at 13:00, although the sun was perpendicular in the midday period. The main reason behind this behaviour is that the accumulated heat by the other elements in both rooms during the first half of the day has influenced the temperature of the inside surfaces of the south walls, making

slight HTD between them. Fig. 4.35 supports this claim, showing that the inside surface temperature of the south walls exceeded 55 °C. Besides, the incident solar radiation hit the roofs when the sun was perpendicular at midday, with a minimal direct solar radiation rate on the south-oriented walls. Likewise, the north-oriented PCM wall showed poor thermal performance in terms of HTR, and this was expected since the solar radiation with a low rate was incident only in the early hours on the north walls. Therefore, the PCM involved in the north PCM wall did not reach its melting point, especially since the ambient air temperature was also low.

The roof of the PCM room showed the best thermal performance compared with the walls during all daytime. The best performance was between 10:00 and 2:00, recording the highest HTD of 6.5 °C and HTR of about 15.1% at 11:00. The considerable performance of the PCM roof compared with the walls is attributed to two main reasons. Firstly, the high PCM quantity involved in the roof than walls stored more heat. Secondly, the roofs were exposed to direct solar radiation for a long time, which was advantageous for the PCM roof that utilised the PCM thermal storage potential compared with a negative impact on the reference roof.

The improvement of the inside surface temperature attained by PCM influences the indoor air temperature of the PCM room, even though the experiment was conducted with no ventilation. In this regard, the heat accumulated continuously through the room elements inside the PCM space and considerably lowered the indoor air temperature compared with the reference room. This indicates PCM's benefits in reducing the peak load even during high outdoor temperatures and non-ventilated building envelopes. The highest HTD and HTR in the indoor air were obtained at 9:00 with 4 °C and 10.6%, respectively. Later, the HTR was decreased as the outdoor ambient temperature increased and more heat crossed the rooms' envelope towards the inside space. The HTR after 9:00 was linear with time till 18:00, as shown in Fig. 4.37. The reduction of such values significantly influences the indoor environment when considering the energy-saving for air-conditioning usage and thermal comfort attained. The HTD and HTR were adverse in the PCM room during the night due to the PCM solidification phase, when stored diurnal heat was released passively and uncontrollably as the outdoor ambient temperature decreased.

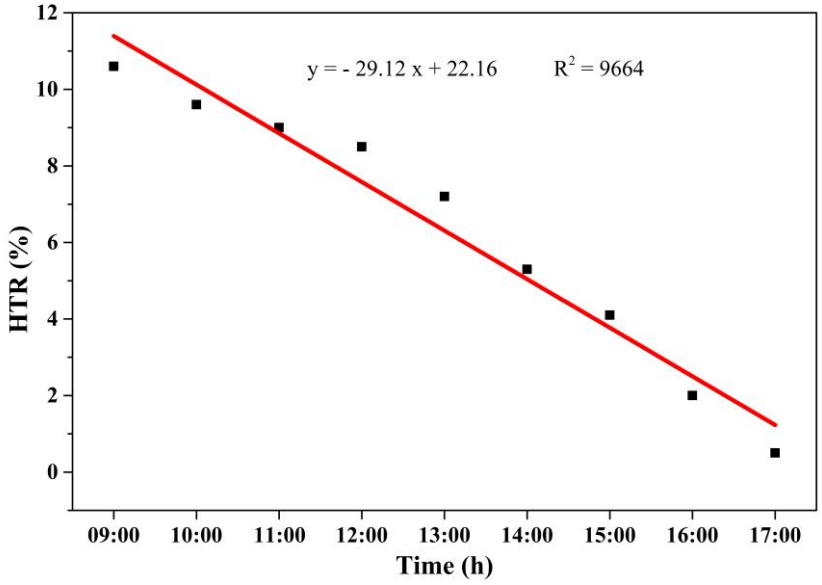

Fig. 4.37. Relationship of the indoor HTR of PCM room with time

The results of HTD and HTR accomplished in this study are in good agreement (sometimes better) with the results of literature studies conducted in different hot locations. For instance, Rathore et al. (Rathore and Shukla, 2020) performed an experimental study under Indian weather conditions (Mathura city) to determine the HTR for pipe-macroencapsulated PCM buried in a concrete room compared with another without PCM. Regardless of the low PCM melting temperature and the

experimental site's outdoor ambient temperature compared with the current study, all room elements reported HTD and HTR in the range of 3.1 °C- 3.7 °C and 7.19%–9.18%, respectively. Under weather conditions of Chennai city, Beemkumar et al. (Nagappan Beemkumar et al., 2020) analysed the HTD of a concrete building roof integrated with PCM macroencapsulated inside rectangular-shaped aluminium containers. The results showed an average HTD of 1 °C- 2 °C compared with the standard concrete roof. Sovetova et al. (Sovetova et al., 2019a) analysed thirteen PCMs with melting temperatures ranging from 20 °C to 32°C, applied as a separate PCM panel of 20 mm thickness in the roof and walls of a typical building located in the United Arab Emirates. Numerical results showed that the indoor air temperature could be reduced by up to 1.09 °C at the optimum PCM melting temperature of 32 °C. Ramakrishnan et al. (Ramakrishnan et al., 2019) conducted research on shape-stabilised PCM (SSPCM) consisting of paraffin (RT27) combined with hydrophobic expanded perlite (PCM carrier) to be used as plastering mortar for cladding interior walls and floors under Melbourne (Australia) climate conditions. The main findings reported HTD in the inner surface and indoor air by 3.7 °C and 2.4 °C, respectively. Following the same incorporation method, Wi et al. (Wi et al., 2020) have also investigated SSPCM fabricated from *n*-Octadecane/expanded vermiculite and expanded perlite in a panel form applied for the interior envelope. The experimental results were performed using a climate chamber and revealed that the HTD of the SSPCM panel surface was reduced by up to 1.6 °C compared with the standard panel without SSPCM.

4.4.2.1. Analysis of hourly HGR

The hourly heat gain reduction (HHGR) attained in the PCM room compared with the reference room followed the same concept used to calculate the MHGR but for hourly values this time. The calculated results of the HHGR of the PCM room elements compared to the reference room during daytime hours are shown in Fig. 4.38. The HHGR during the nighttime was not considered due to the reversed behaviour of PCM room elements during the solidification phase due to non-ventilation, as highlighted previously.

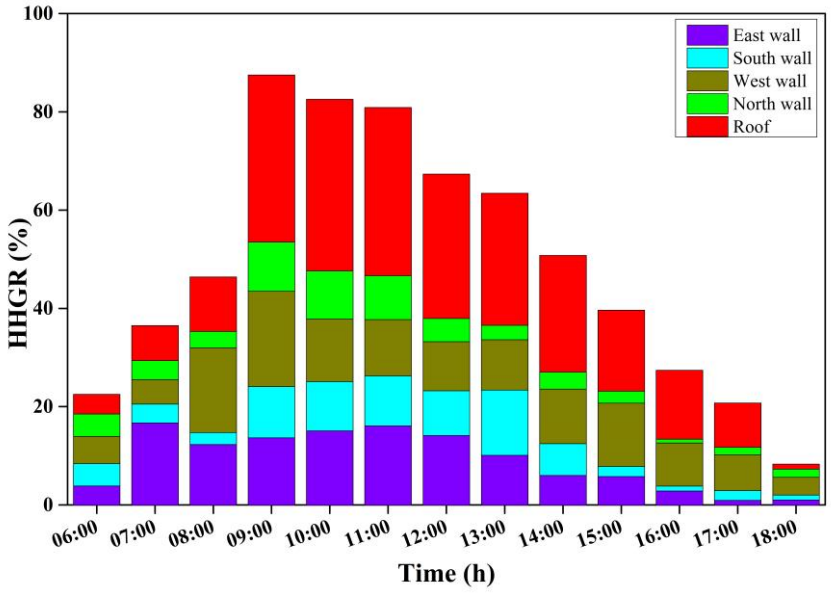

Fig. 4.38. HHGR during the daytime of the PCM room compared with the reference room

As a general finding in Fig. 4.38, the roof showed HHGR higher than all elements, whereas the east-oriented wall showed higher HHGR than the other walls. The HHGR of the eastern wall was high between 9:00 and 13:00 since the east walls were exposed to the incident solar radiation during this period. The PCM wall was interrupting and storing the heat from the outdoor while passing quickly through the reference wall. The highest HHGR was achieved at 11:00 and 12:00 by about 16% and 14.1%, respectively. Later, the HHGR dropped for the rest of the day when PCM reached a full melting state and could not store more heat.

Similarly, the west-oriented PCM wall showed high HHGR reaching the highest reduction of about 12.9% at 15:00 since the west walls were exposed to direct solar radiation in the afternoon. This behaviour is apparently due to increased outdoor air temperature during midday that influences the PCM inside the west wall of the PCM room. Nevertheless, the PCM was expected to reach its melting temperature at midday, and the PCM was in the melting phase along late afternoon. It is worth mentioning that the accumulated heat inside rooms resulting from the other walls and windows in the first half of the day influenced the inside surface temperature of all elements in the second half of the day, including the west walls.

The south-oriented PCM wall exhibited relatively poorer HHGR than the east-oriented wall. However, it experienced a high ambient temperature for a long time as the east PCM wall. This may be elucidated that the south PCM wall did not receive direct solar radiation as much as the east PCM wall (as indicated in Fig. 4.34), which influenced the PCM effectiveness. However, the south PCM wall reached the highest HHGR of 13.3% at 13:00 and drastically decreased after that time. This is shown in Fig. 4.35, wherein the south walls' highest inside surface temperature difference was reached. The north walls, from the other side, showed the poorest HHGR compared with other walls, as expected, since these walls were exposed to low solar radiation only in the early morning. The highest HHGR attained by the north PCM wall was 10% at 9:00, influenced by the increased ambient temperature. Referring to the HHGR trend of the north PCM wall in Fig. 4.37, it can be stated that the PCM was ineffective at this wall and should be considered when conducting optimisation studies.

The roof, as expected, showed the highest HHGR, reaching a maximum of 34.9% at 10:00, making this element the main contributor to the total HHGR by about one-third. However, the east-oriented PCM wall showed higher HHGR from 7:00 to 8:00 than the PCM roof due to the sun's position concerning these elements. Besides, the solar absorptivity difference of Isogam (in the roof) compared with the cement plaster of the wall has speeded the heat transfer in the latter element, which activated the PCM earlier. The continuously increased HHGR of the roof compared with the walls might be attributed to the high amount of PCM involved in the PCM panel and the thermal resistance of the roof layers compared with the thin layers of walls. These reasons expand the time to reach a complete PCM melting state inside the panel (compared with the capsules), which offers more insulation for the PCM roof. However, the positive behaviour of the PCM panel on the roof negatively influenced the HHGR during the night, which was the poorest compared with walls due to the considerable amount of stored heat. This keeps the inside surface temperature of the PCM roof high until the end of the thermal cycle, as indicated in Fig. 4.34.

Total HHGR can be quantified by summing the HHGR of all elements following the same concept of Rathore and Shukla (Rathore and Shukla, 2020) to calculate the total cooling load reduction through building elements. Accordingly, the PCM-incorporated room resulted in an average HHGR of 48.7% during day hours compared with the reference room. These findings are remarkable compared with the studies conducted in different locations worldwide. For instance, Lei et al. (Lei et al., 2016) reported that the HG reduction (HGR) could attain the mark of 40.7% under tropical Singapore weather conditions when PCM of 28 °C melting temperature of 10 mm layer thickness applied to the exterior building walls surface. Rai (Rai, 2021) investigated the HGR when PCM incorporated different brick masonry wall configurations under Indian summer conditions and found that peak HGR of 9.9% to 45.2% could be achieved considering the wall orientation, outdoor ambient temperature and night ventilation effect. Kishore et al. (Kishore et al., 2020) conducted a numerical study on the PCM-integrated building walls in various locations in the United States, considering different PCM melting temperatures, layer thicknesses and positions within the walls and reported an annual HGR of 3.5%-47.2% could be achieved. In the Middle Eastern countries, Amirahmad et al. (Amirahmad et al., 2021) numerically analysed PCM loading (RT-27) into the building walls in parallel with an absorption chiller driven by a solar system considering the hot and arid climate for Najran, Saudi Arabia. They reported HGR by up to 21% during July. In comparison, Alqallaf and Alawadhi (Alqallaf and Alawadhi, 2013)

conducted a numerical and experimental study under Kuwait city weather conditions for PCM integration with cylindrical holes in the roof. They reported HGR by 9%-17.26% depending on the PCM type, working hours and month of operation. Table 4.8 summarises the main average results obtained in this study.

Table 4.8. Summary of average results of the PCM elements compared with the reference ones

Element	Average MTD (°C)	Average HTR (%)	Average HHGR (%)
East wall	1.69	4.9	16.9
West wall	1.67	4.6	5.4
North wall	0.71	1.8	9.8
South wall	0.98	2.3	6.2
Roof	3.63	8.2	18.9

4.4.3. Long-term numerical investigation of PCM room thermal performance

The experimental results obtained in sections 4.4.1 and 4.4.2 analysed the thermal performance of PCM when incorporating building envelope elements for a short time. This may not give a broad insight into this technology since it is associated with changeable weather conditions throughout the year. Therefore, the experimental results extended numerically to show the PCM thermal performance over a long-term summer period. As indicated in section 3.5.2, the numerical study was conducted for six summer months under the same weather conditions where the experimental studies were conducted, namely from May to October 2021.

Firstly, the room model presented in subsection 3.5.1 (Fig. 3.19) has been verified against the experimental results detailed in subsection 4.4.1. The IDF file adopted the same construction materials used to construct experimental rooms as inputs. It is worth mentioning that an equivalent PCM brick with 0.7 mm layer thickness has been proposed instead of the PCM brick (with PCM capsules) used in experimental studies since the EnergyPlus software deal with a layered envelope. The proposed brick held the same PCM quantity (~45 g) as the brick-based PCM capsules and sowed roughly similar thermal behaviour. Both PCM bricks showed similar TL, but the PCM-layer brick showed slightly better DF and surface temperature reduction by 4.39% and 0.5 °C, respectively, based on our recently conducted experimental study (A2, Ref. 17).

The model showed good agreement considering the room indoor air temperature in both the reference and PCM rooms, as presented in Fig. 4.39. However, a maximum difference of 6.1% and 7.9% was observed between the experimental and simulation curves of the reference and PCM rooms, respectively. This divergence can be attributed to the inconsistency of weather data measured during the experimental work compared with that predicted in the weather file used for the simulation. Besides, the thermal and physical properties of construction materials used as inputs in the software do not have the exact values as the room constructed in experimental work, which eventually influences the simulation outcomes.

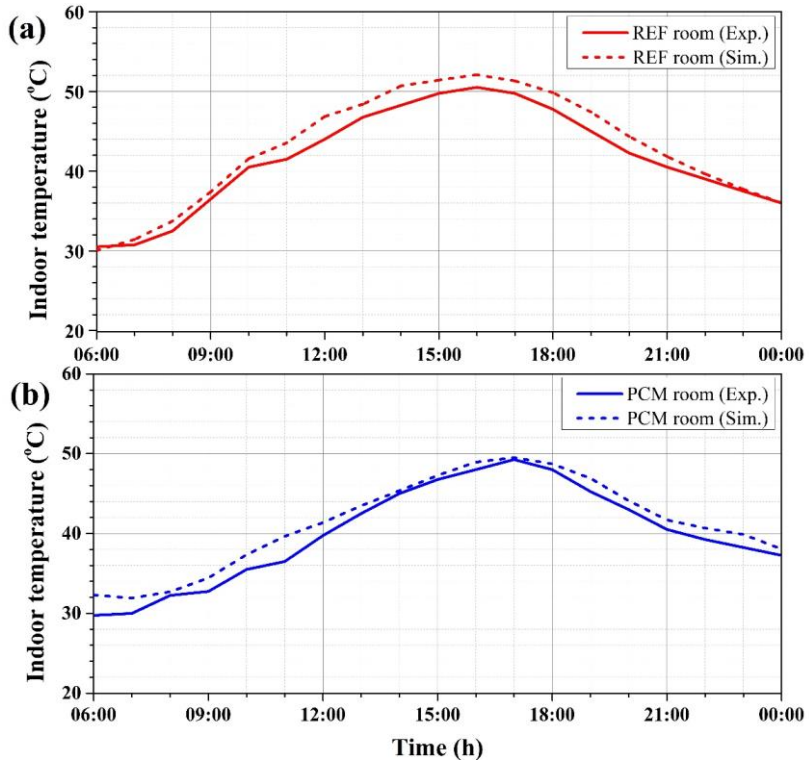

Fig. 4.39. Validation of the numerical model against experimental results presented in (Al-Yasiri and Szabó, 2022a) for (a) reference room, (b) PCM room

EnergyPlus software has many output variables to analyse the building performance, including climatic data summary, envelope summary, zone summary and other energy metrics. The output variables set in this study were the inside and outside face temperatures of walls and roofs in addition to the zone indoor mean temperature and mean radiant temperature. Therefore, several concepts were adopted to quantify the energy contribution of PCM to the room considering the indoor thermal comfort enhancement and stemmed energy-saving at the hottest day of every month, namely 19 May, 18 June, 12 July, 1 August, 4 September and 2 October.

The improvement in indoor thermal comfort is the main purpose of integrating PCMs with building envelope due to increased envelope thermal inertia and enhanced thermal performance (Suresh et al., 2022). Fig. 4.40 shows the hourly average indoor temperature variation of reference and PCM rooms during the simulation period. As expected, numerical results exhibited low indoor temperatures for the PCM room compared with the reference room during day hours, with obvious time shifting of the highest values by approximately one hour. However, May and October indicated a relatively higher difference in the indoor temperature between the reference and PCM rooms attributed to low outdoor ambient temperatures at night in these two months, compared with June-September. The highest indoor temperature of the reference room was 54.8 °C, 56.3 °C, 57.3 °C, 57.8 °C, 56.7 °C and 49.1 °C in May, June, July, August, September and October, against 50.7 °C, 52.8 °C, 53.9 °C, 54.2 °C, 52.8 °C and 43.7 °C inside the PCM room, respectively.

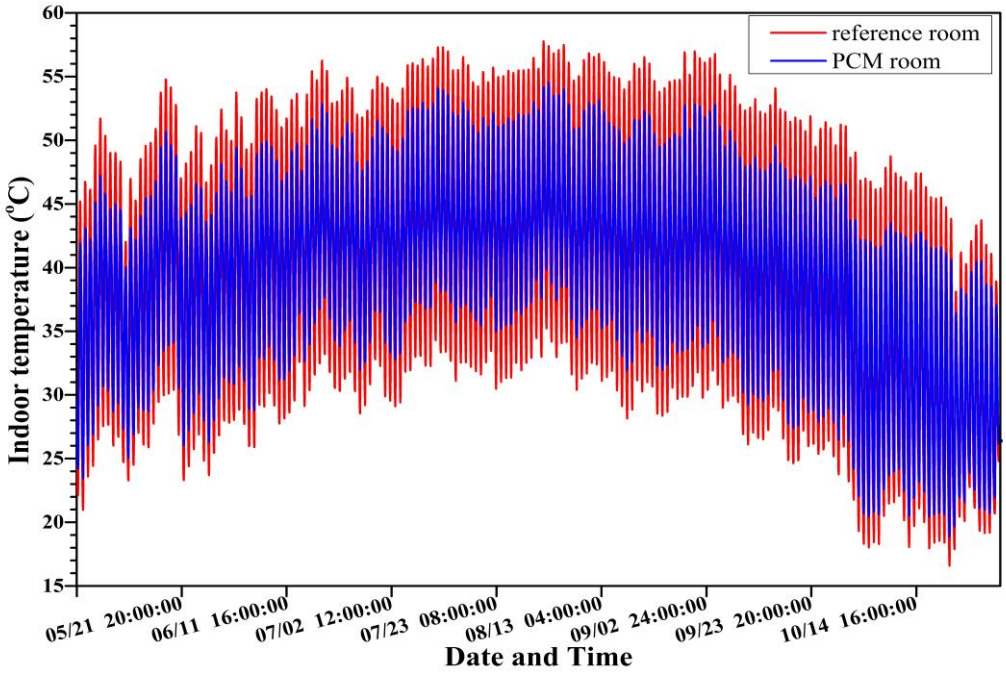

Fig. 4.40. Hourly indoor temperature variation of reference and PCM rooms

As mentioned previously, the role of PCM in enhancing indoor thermal comfort and energy-saving can be quantified in terms of several concepts. For this purpose, the concept of ATFR, TLLR, OTR and AHGR will be discussed and analysed in this numerical study.

4.4.3.1. Average temperature fluctuation reduction

The calculation results of ATFR of the PCM room compared with the reference room on the hottest day of each month are presented in Fig. 4.41.

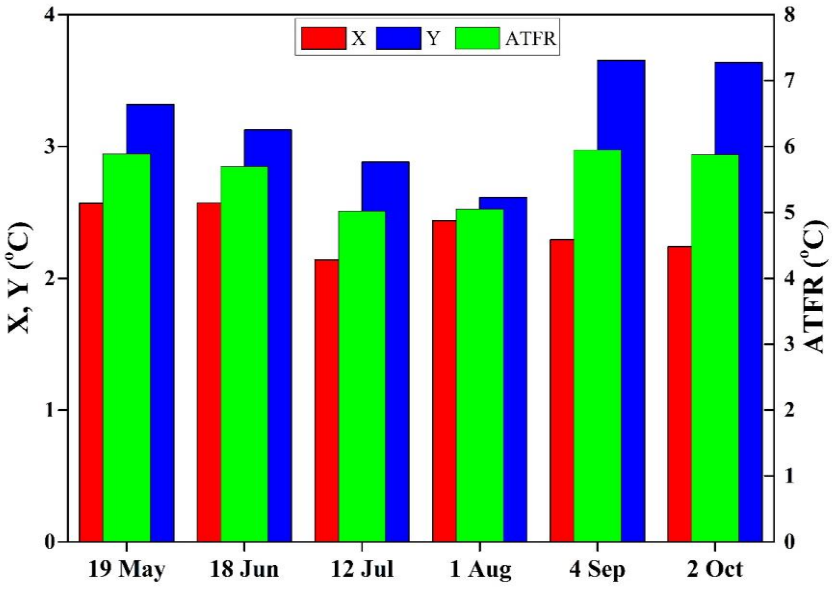

Fig. 4.41. ATFR of PCM room compared with reference room

As designated in the figure, the PCM room showed positive ATFR on all days, indicating PCM effectiveness in all summer months. In general, the PCM showed remarkable contribution regarding the ATFR reaching 5.89 °C in May, 5.70 °C in June, 5.02 °C in July, 5.05 °C in August, 5.95 °C in September and 5.88°C in October. Besides, it can be observed that Y values were always higher than X values, meaning that the average temperature difference between simulated rooms during no-sun hours (solidification period) was higher than their difference during sun hours (PCM

melting period). In this regard, X values ranged from 2.14 °C in July to 2.57 °C in May and June, whereas Y values ranged from 2.61 °C in August to 3.65 °C in September. The main reason behind this behaviour is that rooms were non-ventilated, and the heat accumulated inside zones takes time to be removed at night since the heat transfer rate is associated with the temperature difference between outdoor and indoor environments. Therefore, ATFR could be increased by adopting ventilation means, especially at night, with suitable ventilation air rate (quantity) and temperature level.

4.4.3.2. Thermal load levelling reduction

The TLL of reference and PCM rooms and TLL reduction (TLLR) during the hottest days of the simulated period are shown in Fig. 4.42.

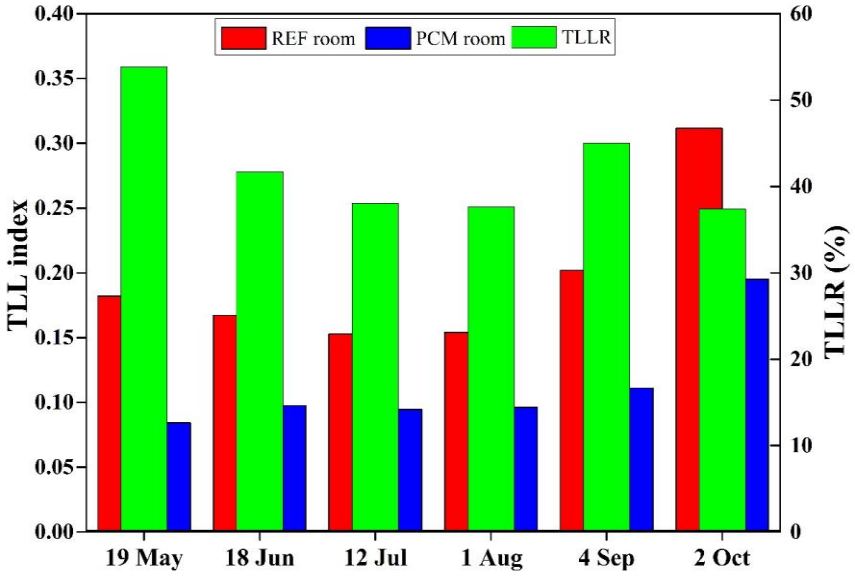

Fig. 4.42. TLL and TLLR of rooms over summer months

Fig. 4.42 indicated remarkable TLL for the PCM room compared with the reference room, meaning that the indoor temperature was diminished in the PCM room more than in the case of the reference room. The TLL of the PCM room was relatively equal for all months, ranging between 0.08 and 0.1, except for October, which showed a high TLL of 0.2. In contrast, the TLL of the reference room ranged from 0.15 and 0.2 in May-September, whereas October showed a higher TLL of 0.31. Considering the TLLR, the hottest day of May showed the highest TLLR of about 58.8%, followed by 45% in August and 41.7% in June. In contrast, July, August and October reported lower TLLR by about 38%, 37.6% and 37.4%, respectively. According to these findings, the PCM was more effective in terms of TLLR during May in dampening the temperature fluctuation inside the zone due to low outdoor temperatures at night. This could be supported by the fact that the PCM reaches melting point quickly on hot days (Wang et al., 2020) due to the high heat charging rate and become less effective when integrated passively till the outdoor temperature drops towards the solidification point. However, October showed a similar TLLR as July, although the TLL was highly different. This could be attributed to the fact that October's diurnal outdoor ambient temperature was relatively equal to the PCM melting temperature, which partially utilised PCM potential. Therefore, the TLL index was high (see Fig. 4.42) for both reference and PCM rooms, showing high indoor temperature fluctuations. On the contrary, high outdoor ambient temperature during the thermal cycle in July has kept the PCM in a melting state most of the time while providing a poor cooling medium (at night) due to the low-temperature difference between indoor and outdoor temperatures.

4.4.3.3. Average heat gain reduction

The AHGR in the reference room elements compared with those of the PCM room was estimated according to Eq. (3.15) averagely for day hours from 6:00 to 18:00. Fig. 4.43 shows the AHGR attained over the simulation period.

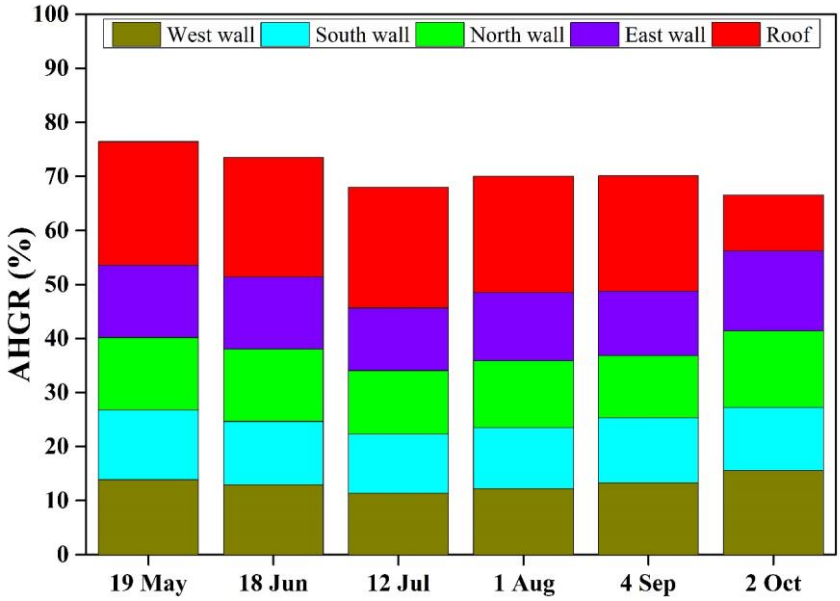

Fig. 4.43. AHGR of envelope elements on the hottest month day

As observed in Fig. 4.43, the roof achieved the highest AHGR every month, except in October, compared with the walls. In this regard, the roof shared about 22.9% in May, 22.1% in June, 22.3% in July, 21.5% in August, and 21.4% in September. This high share indicates the effectiveness of PCM in the roof more than with walls, which is mainly attributed to the high PCM thickness incorporated into the roof (1.5 cm) compared with walls (~0.7 cm). Besides, since the roof was receiving a high solar radiation rate for a longer time, it was the hottest element in the room. This increased the PCM effectiveness in the PCM room compared with the reference room roof, which was at a high surface temperature. However, the roof showed a different trend in October, where the AHGR reached a slight reduction of only 10.4%, which is relatively lower than that of walls. This is attributed to the fact that the roof received lower solar radiation in October than in other months, as shown in Fig. 3.4, which affected the PCM melting phase.

Although the walls were constructed from a thin combination, they showed good AHGR for the PCM room compared with the reference room. In general, all PCM room walls showed relatively similar AHGR during the simulated period, with a higher share for the east and west walls, followed by the south wall. This behaviour has the same attribution as the PCM roof since the east and west walls received higher solar radiation rates than the south and north walls (as indicated in Fig. 3.4). The east wall was more effective in June, July and August than the west wall, whereas the latter was better in May, September and October.

The total AHGR of the PCM room compared with the reference room reached 76.5%, 73.5%, 68.2%, 70.1%, 70.2% and 66.6% on the hottest day of May, June, July, August, September and October, respectively. May showed the highest total AHGR, followed by June. In contrast, October achieved the lowest, indicating that the outdoor ambient temperature variation during the day and night was the main factor behind PCM effectiveness. However, these outcomes eventually indicate a decent contribution of PCM to building energy saving, resulting from effective melting temperature, and can significantly reduce the cooling loads in hot climate buildings. In the average of six months, the total AHGR linearly increased with the increased EPS layer thickness, as shown in Fig. 4.44.

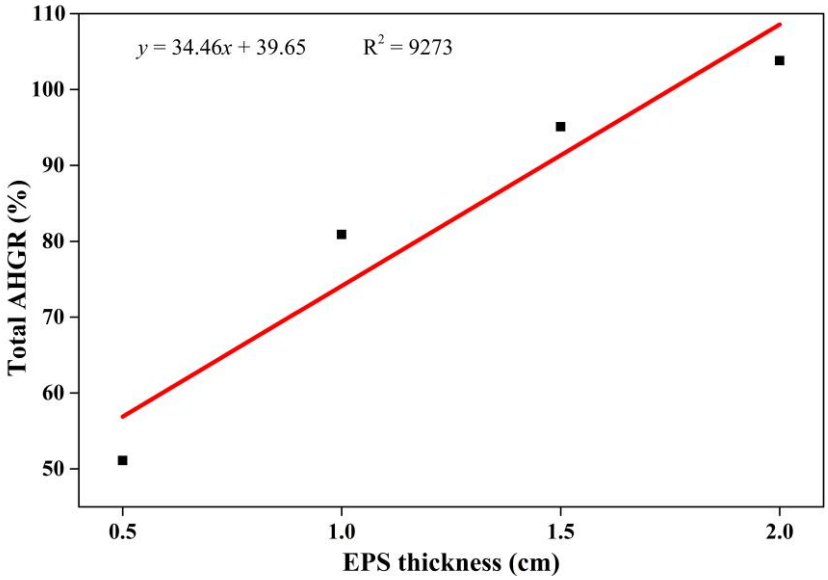

Fig. 4.44. Relationship of total AHGR EPS and layer thickness

4.4.3.4. CO_2 emission and energy cost saving

The CO_2ES and ECS have been calculated considering the average HG difference of reference and PCM rooms according to Eq. (3.21) and (3.22). The results of CO_2ES and ECS are shown in Fig. 4.45.

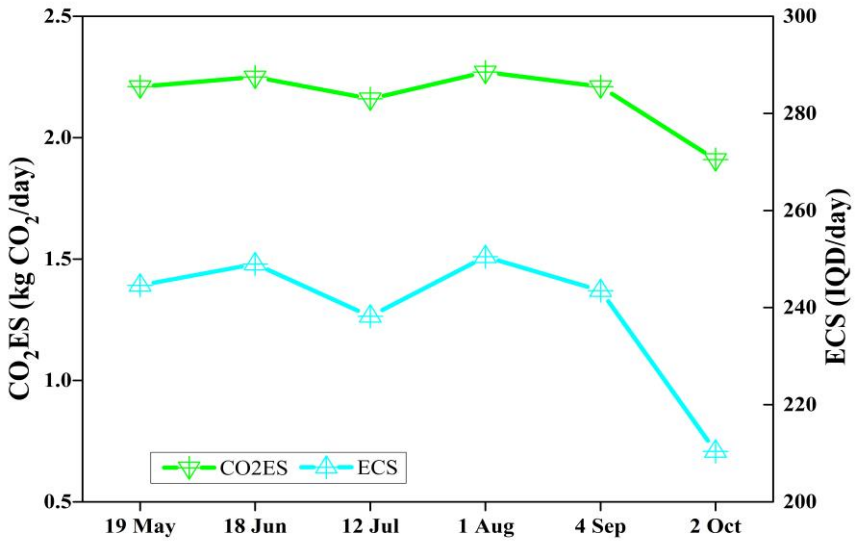

Fig. 4.45. CO_2ES and ECS during the hottest days

The results presented in Fig. 4.45 indicated remarkable saving of CO_2 emission by about 2.21, 2.25, 2.16, 2.27, 2.21 and 1.91 kg CO_2/day in May, June, July, August, September and October, respectively. The figure also showed that ECS of about 245, 249, 238, 250, 244, and 210 IQD/day could be achieved on the hottest day of May, June, July, August, September, and October, respectively.

Such values have a huge environmental and economic impact on the building sector, considering the performance of PCM over a building lifespan of about 50 years. Besides, the benefits could be maximised when incorporating PCM for larger building envelope areas. Table 4.9 list the average results of indicators analysed in this study.

Table 4.9. Summary of study findings

Month	ATFR (°C)	TLLR (%)	Total AHGR (%)	CO_2ES (kg CO_2/day)	ECS (IQD/day)
May	5.89	53.83	169.84	2.21	244.6
Jun	5.70	41.69	172.92	2.25	249
Jul	5.02	38.04	165.39	2.16	238.2
Aug	5.05	37.63	173.96	2.27	250.5
Sept	5.95	45.01	169.07	2.21	243.5
Oct	5.88	37.37	146.14	1.91	210.4

4.5. Performance assessment of PCM room-combined thermal insulation

The simulations for this numerical study were confirmed for six summer months for the same location and weather conditions investigated in the previous experimental studies. As described in subsection 3.5.2.1, a thermal insulation of type expanded polystyrene (EPS) with different thicknesses (namely 0.5, 1, 1.5 and 2 cm) was proposed. However, the optimal position of the EPS layer involved in the PCM room should be specified first with respect to the PCM layer. Next, the EPS thicknesses will be evaluated at the optimal EPS layer position considering several energetic and thermal comfort indicators, as will describe in detail in the following subsections.

4.5.1. Optimal position of thermal insulation

The EPS layer was placed in different positions to investigate the best position with the lowest effect on the PCM activation considering the PCM liquid fraction. To reach this aim, a simulation was verified for the three proposed EPS positions within a roof construction (highlighted in Fig. 3.20) on the 21st of July, the typical summer design day in the thermal calculations made under Iraqi weather conditions (Al-Mudhafar et al., 2021). The simulation results in terms of the liquid fraction of the PCM layer in each case (i.e., EPS-i, EPS-m and EPS-o) are shown in Fig. 4.46.

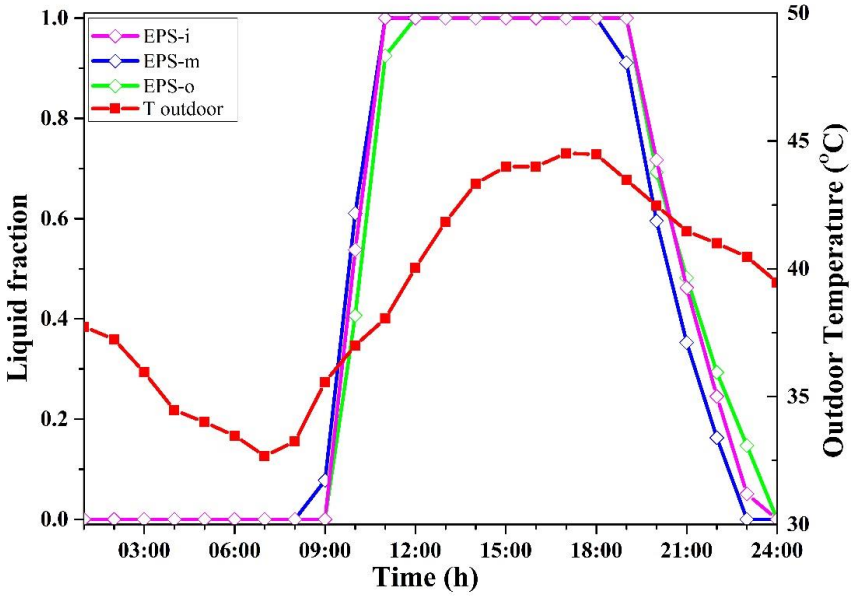

Fig. 4.46. Liquid fraction of PCM layer within roof combination

On the whole, the cases where the EPS layer was placed near the indoor environment (i.e., EPS-i and EPS-m) showed better PCM liquid fraction evolution than the case where the EPS layer was placed outside (i.e., EPS-o). The PCM started the melting phase at 9:00 with about 0.08 melting fraction in the case of EPS-m, while it was in a solidification phase in the EPS-i and EPS-o. At 10:00, the PCM was partially melted in all cases, reaching 0.54, 0.61 and 0.41 in the EPS-i, EPS-m and EPS-o, respectively. The PCM was in a liquid state (i.e., melting fraction equal to 1)

at 11:00 in the EPS-i and EPS-m cases, while it was partially melted with a liquid fraction of 0.92 in the EPS-o case.

The PCM was in a liquid state at 12:00-18:00 in all cases, indicating no influence of the EPS layer on the PCM in this period. However, the PCM solidified at 19:00 in the EPS-m case with 0.91 liquid fraction, whereas the PCM was in a liquid state in the EPS-i and EPS-o cases. The PCM was partially melted from 20:00 till 22:00 with better solidification in the case of EPS-m followed by EPS-i and then EPS-o. Later, the PCM layer was fully solidified at 23:00 in the case of EPS-m, while it was partially solidified in the case of EPS-i and EPS-o with a liquid fraction of 0.05 and 0.15, respectively. At midnight, the PCM was in a solid phase in all cases, indicating the suitability of the high PCM melting temperature (40-44 °C) with the temperature level at night even though the PCM was involved passively within the roof structure.

The above analysis shows that the PCM was activated better when placed after the EPS layer towards the outdoor environment. The best EPS position is in the middle of the roof construction. This is logical since the outdoor ambient temperature is the main controller of PCM melting and solidification in passive PCM applications. Besides, the insulation layer will decrease the temperature necessary for PCM activation, which impacts the melting and solidification phases. Besides, installing the insulation layer near the outside environment would affect the phase change of PCM; thus, it should be incorporated towards the inside with a lower melting temperature (Rai, 2021). Based on the above analysis, the EPS layer will be positioned directly after the PCM layer towards the indoor environment (i.e., in the EPS-m case) to investigate the role of the EPS layer with different thicknesses, namely 0.5, 1, 1.5 and 2 cm, on the PCM room thermal performance.

4.5.2. Analysis of thermal performance at different insulation thicknesses

Literature studies have confirmed the potential of PCM to shave and shift the indoor peak temperature if properly incorporated with the building envelope (Tunçbilek et al., 2020; Al-Absi et al., 2022). Besides, thermal insulations could improve the thermal resistance of buildings, minimising heat transfer towards the indoor environment. However, installing thermal insulation could maximise the benefits of PCM since the thermal insulation increases the building's thermal resistance, whereas the PCM improves the building's thermal inertia (Jia et al., 2021). This combination of PCM/thermal insulation is critical in severe hot location buildings where the PCM has limited effectiveness when reaching full melting early. In contrast, increasing PCM quantity could cause economic worries and negative behaviour during solidification.

Thermal insulation thickness could impact PCM's effectiveness since the phase transition associated with the temperature variation across the PCM layer and increasing the insulation thickness may reduce the temperature below the necessary phase change level. Therefore, the optimal thermal insulation thickness should be specified to ensure the effective use of PCM and promote the thermal storage benefits.

This section investigates the advances in indoor air temperature when different thermal insulation (EPS) thicknesses are installed in a PCM room, placed directly after the PCM layer near the indoors. The simulation performed for the reference room model in comparison with the room with PCM only and PCM combined with EPS of 0.5, 1, 1.5 and 2 cm thicknesses, termed as PCM-EPS(0.5), PCM-EPS(1), PCM-EPS(1.5) and PCM-EPS(2), respectively. The indoor temperature variation of studied cases each month is shown in Fig. 4.47.

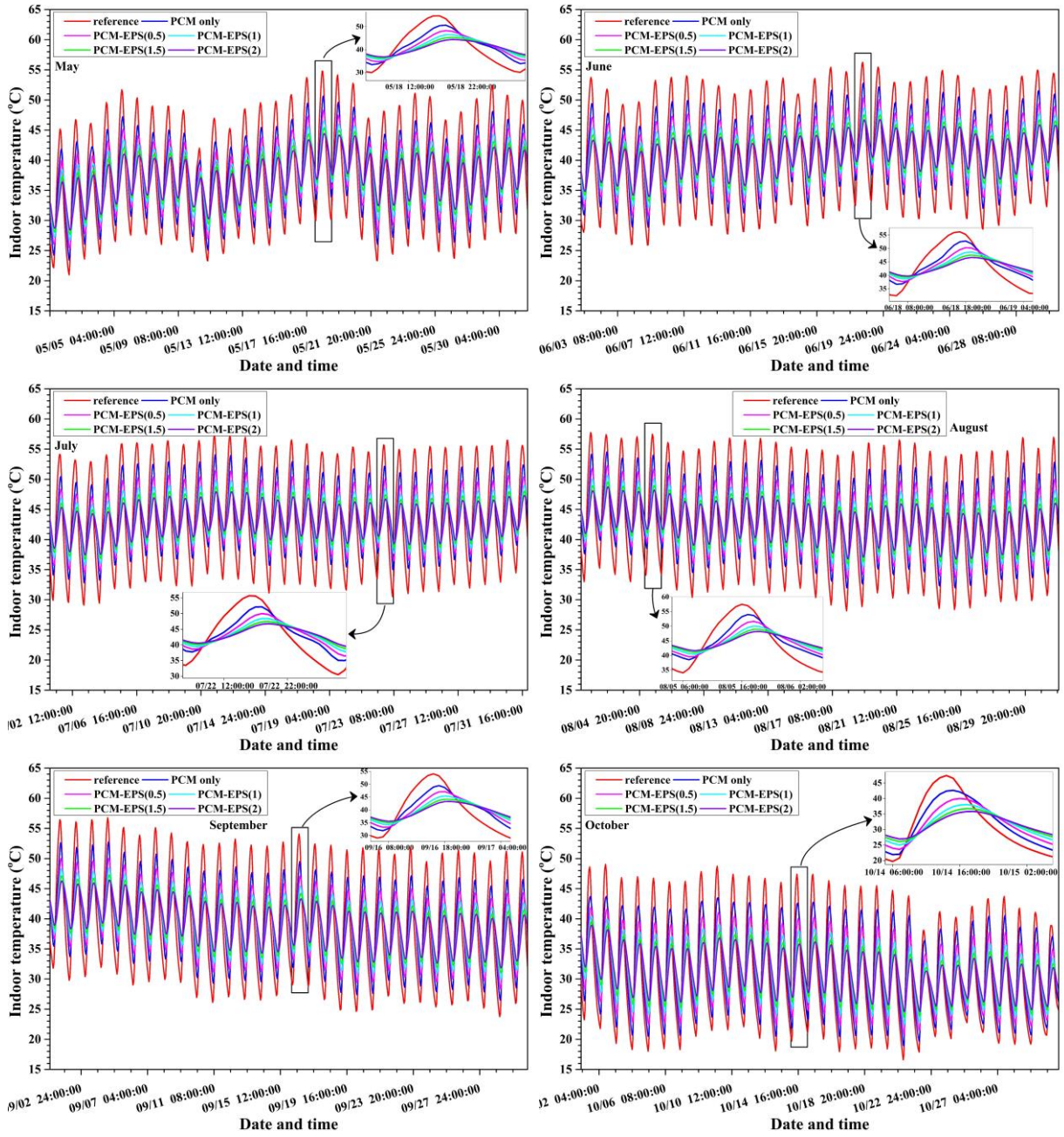

Fig. 4.47. Hourly indoor temperature variation in each month (May-October)

According to the results presented in Fig. 4.47, the increased EPS layer thickness has reduced the indoor temperature and shaved the maximum temperature at midday hours. This behaviour is expected since increasing the envelope thickness (of any material) usually reduces the heat transfer rate and indoor temperature due to increased envelope resistance, according to Fourier's law (Garrido et al., 2001). However, the indoor temperature showed reversed behaviour during night hours in which the thicker EPS layer caused worsen performance than the thinner one since the indoor space was not ventilated. Thus, the indoor temperature behaviour and its correlation with the PCM activation during the thermal cycle should be evaluated well to indicate the best EPS thickness. Consequently, the following subsections briefly discuss several indicators to show the PCM contribution, including the RMTR, TL, ATFR, OTR and AHGR.

4.5.2.1. Room maximum temperature reduction

The RMTR indoor temperature of modified rooms (PCM-EPS rooms) compared with the PCM room gives a fair indication of the contribution of EPS over incorporated PCM. However, it is

worth showing first the MTR (maximum indoor temperature difference between the PCM/PCM-EPS rooms and the reference one) over the simulated period. This is shown in Fig. 4.48 below.

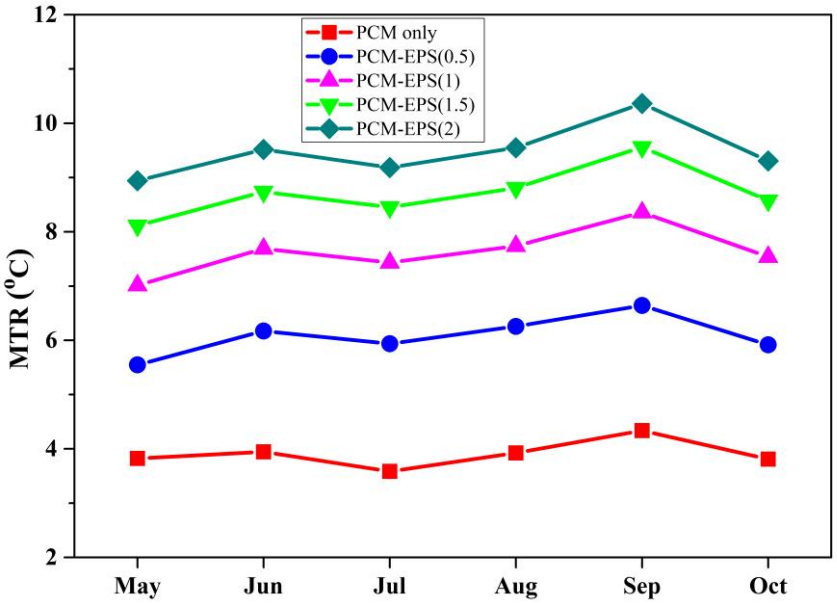

Fig. 4.48. MTR of modified rooms compared with the reference room

In general, the MTR trend was relatively similar in all months, even though the temperature variation during the day was different (e.g., July was the hottest and October the coldest month). This is because the MTR calculations considered the average of highest temperatures, which were relatively similar, exceeding 45 °C, except for October. However, this figure could provide a reasonable indication of the building's ability to cope with heat waves and increase in ambient temperature in the future as globally expected due to climate change (Liu et al., 2021). It is obvious in Fig. 4.47 that the indoor temperature decreased as the insulation thickness increased, resulting from the improved envelope's thermal resistance against outdoor heat flow. Amongst months, May exhibited lowest MTR by about 3.8 °C, 5.5 °C, 7.1 °C, 8.1 °C and 8.9 °C respectively in the PCM, PCM-EPS(0.5), PCM-EPS(1), PCM-EPS(1.5) and PCM-EPS(2) rooms, whereas September showed the highest by 4.3 °C, 6.6 °C, 8.4 °C, 9.6 °C and 10.4 °C, respectively. The RMTR shown in Fig. 4.49 may present the role of EPS over the PCM contribution.

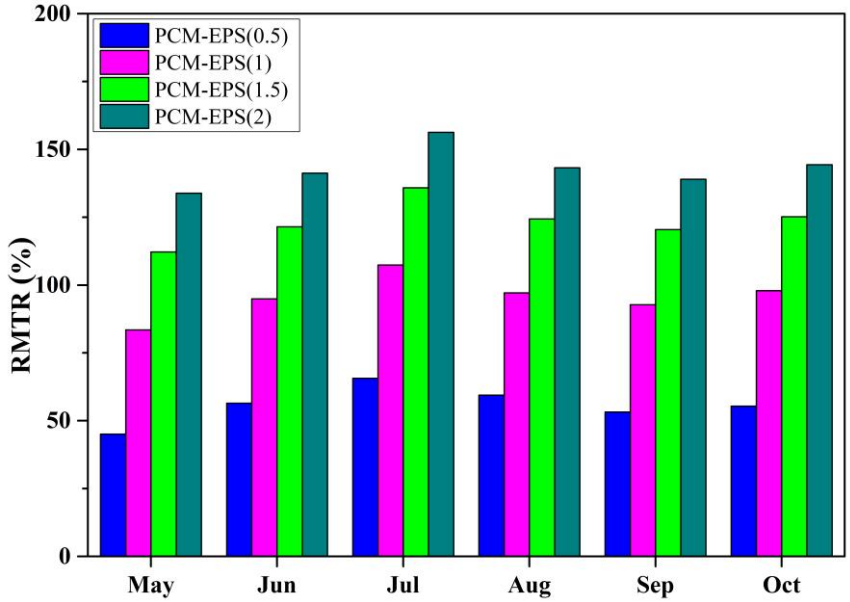

Fig. 4.49. RMTR of PCM-EPS rooms compared with PCM room

Fig. 4.49 displays that installing EPS layer with 0.5 cm over the PCM room could improve indoor thermal comfort by about 50%. Likewise, increasing the EPS layer could attain better advantages. Conclusively, installing an EPS layer of increased thickness by 0.5 cm with the PCM room has reduced the RMTR by 55.9%, 95.6%, 123.3% and 142.9%, respectively, as an average of simulated months.

4.5.2.2. Time lag

The TL generally refers to the daily time delay of peak (maximum) indoor temperature compared with the peak outdoor temperature, representing an essential indicator of building envelope thermal resistance. This indicator and the MITR provide a crucial indication of building envelope physical performance to stabilise indoor temperature and contribute mostly to NZEBs (Rathore et al., 2020). The TL in this study was calculated as the average daily time delay difference between the peak indoor temperature of the modified room (with PCM only or with PCM-EPS) compared with that of the reference room (in min). The calculation results of TL are presented in Fig. 4.50.

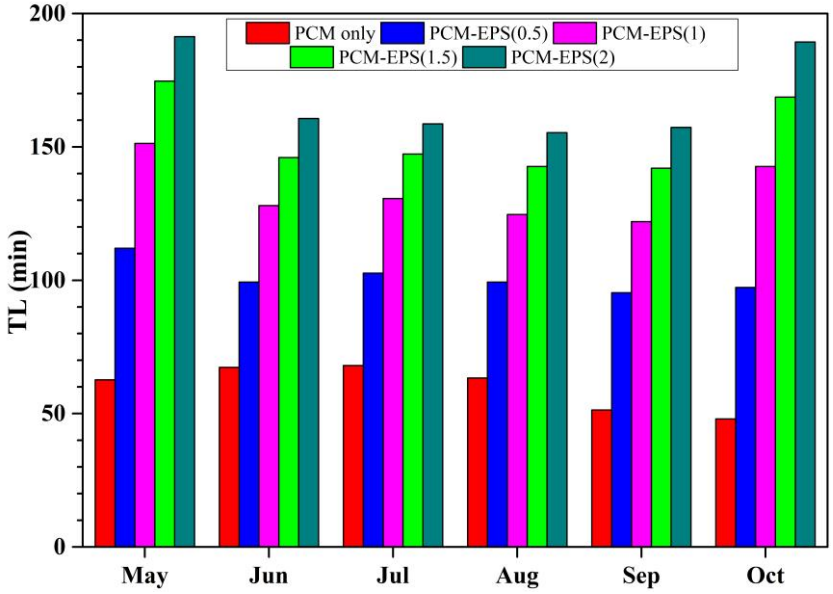

Fig. 4.50. TL of modified rooms compared with the reference room

All modified rooms showed TL by at least one hour compared with the reference room. Nevertheless, incorporating PCM into the room showed lower TL than PCM-EPS cases. Moreover, the thicker EPS layer installed in the PCM room has extended the TL due to increased room thermal resistance. In this regard, the PCM room showed maximum TL by about 1 h compared with 1.9 h for the PCM-EPS(0.5), 2.5 h for PCM-EPS(1), 2.9 h for the PCM-EPS(1.5) and 3.2 h for the PCM-EPS(2) during the simulation period. Considering all months, the TL in May was longer than in other months, except October, whereas September showed a shorter TL. Besides, the PCM room showed better TL during June and July against poor TL in September and October. These results are associated with the peak diurnal temperature and PCM effectiveness each month in which the higher outdoor temperatures had shown priority for PCM incorporation compared with the reference room. Therefore, October indicated lower utilisation of PCM, which was working as an additional insulation layer with no thermal storage potential.

On average of the simulated period, the PCM room displayed TL by an average of ~1 h compared with the reference room against 1.7 h, 2.2 h, 2.6 h and 2.8 h in the PCM-EPS(0.5), PCM-EPS(1), PCM-EPS(1.5) and PCM-EPS(2) rooms, respectively. These results are equivalent to an extended TL period in the PCM room by 68.3%, 117.8%, 157.4% and 177.2% when installing an extra EPS layer of 0.5, 1, 1.5 and 2 mm, respectively.

4.5.2.3. Average temperature fluctuation reduction

Considering the thermal behaviour of PCM and its impact on the daily indoor temperature is necessary to determine the best thermal insulation thickness and ensure the PCM's full melting/solidification cycle. Fig. 4.51 presents the average ATFR values during each simulated month.

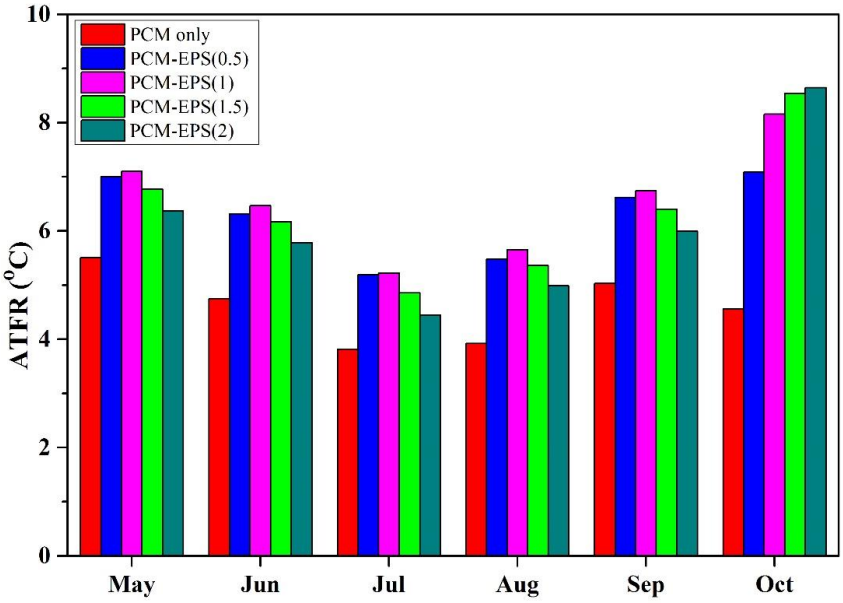

Fig. 4.51. ATFR of modified rooms compared with the reference room

The ATFR results presented in Fig. 4.51 indicated crucial thermal behaviour of the simulated room under different thermal insulation thicknesses. The ATFR outcomes exhibited different behaviour than the MITR and TL that were discussed lastly. The ATFR was relatively similar in May-September, then totally different in October. In May-September, the PCM-EPS(1) displayed the highest ATFR, followed by PCM-EPS(0.5) compared with the PCM-EPS(1.5) and PCM-EPS(2) cases. The average ATFR during simulated months was 4.6 °C, 6.1 °C, 6.2 °C, 5.9 °C and 5.5 °C respectively in the room with PCM, PCM-EPS(0.5), PCM-EPS(1), PCM-EPS(1.5) and PCM-EPS(2). Equivalently, these values represent an enhancement in the indoor temperature during the thermal cycle in the PCM room by 32.9%, 35.4%, 28.4% and 19.8% when adding EPS layers with 0.5, 1, 1.5 and 2 cm thickness. This is because the EPS restricts the indoor heat dissipation towards outdoor ambient due to EPS' low thermal conductivity, keeping the indoor zone at a high temperature for a long time during the night. This thermal behaviour will worsen as the EPS layer thickness increases. Although the PCM-EPS(1) room has higher EPS thickness than the PCM-EPS(0.5) room, the average indoor temperature of the PCM-EPS(1) room compared with the reference room during day time (i.e., X) was higher than that of the PCM-EPS(0.5). This was against a slight difference in the nighttime (i.e., Y) between PCM-EPS(0.5) and PCM-EPS(1), resulting in a better ATFR for the PCM-EPS(1) throughout the thermal cycle.

The thermal performance of ATFR was different in October, as indicated in Fig. 4.51, in which the thicker EPS layer incorporated with the PCM room resulted in better ATFR. This is attributed to the fact that the PCM did not activate well during most of October due to low outdoor ambient temperature; hence, the PCM layer behaved as a traditional construction layer with low thermal conductivity. Besides, the outdoor ambient temperature in October was low enough to accelerate heat dissipation from inside the thermal zone towards outside, regardless of EPS thickness, resulting in low Y values against high X values of increased EPS thickness. The latter reason confirms the ATFR results during July, for instance, which showed the worsening behaviour due to high outdoor ambient temperature at night that influenced the heat transfer rate between the

indoor and outdoor environments, which eventually negatively impacted the rooms with thicker EPS layers.

4.5.2.4. Operative temperature reduction

The average OTR is discussed in this subsection as an essential thermal comfort indicator. The OTR was calculated for modified rooms (with PCM and with PCM-EPS) compared with the reference room during day hours from 6:00 to 18:00. The calculation results of the OTR of the simulated rooms are shown in Fig. 4.52.

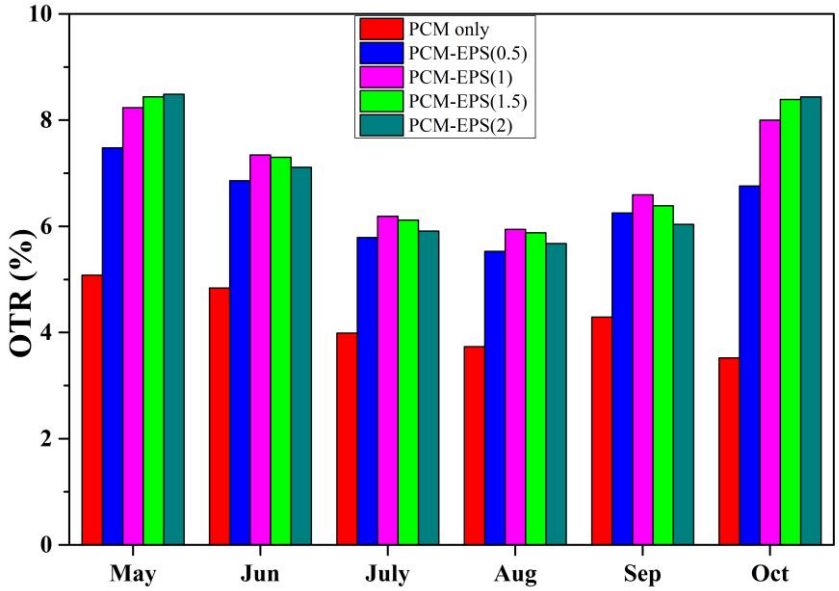

Fig. 4.52. OTR of modified rooms compared with the reference room

Fig. 4.52 indicates better OTR for the modified rooms than the reference room, with superior behaviour for PCM-EPS over the PCM layer during the simulation months. The rooms integrated with EPS showed different enhancement trends in which the thicker EPS layer performed better during May and October. In contrast, the EPS with 1 cm thickness showed better behaviour during June-September. The OTR in May and October was around 4.3%, 7.1%, 8.1%, 8.4% and 8.5% for the room with PCM, PCM-EPS(0.5), PCM-EPS(1), PCM-EPS(1.5) and PCM-EPS(2), respectively. In contrast, the average OTR in June-September was 4.2%, 6.3%, 6.6%, 6.4% and 6.1% for the mentioned cases, respectively. This diverse trend could be attributed to the nighttime outdoor temperature level. In this regard, May and October had lower outdoor ambient temperatures than the other months (June-September), leading to full solidification of PCM and complete dissipation of indoor heat before the next thermal cycle. Therefore, the OTR associated with the average decrease in room indoor and interior surface temperature was better for the PCM-EPS of higher thickness.

In contrast, the relatively high outdoor ambient temperature during the nights of June-September had delayed the heat dissipation from the indoor zone of thicker EPS cases, resulting in poor OTR in the following thermal cycle. This can be noticed from the negative OT difference between the modified and reference rooms at the beginning day hours (around 6:00 till 8:00) of June-September, due to poor heat dissipation at night in the room with thick EPS. In conclusion, the EPS with 0.5 and 1 cm thickness were suitable for installation with the PCM to keep the zone OT within acceptable level during June-September more than EPS with 1.5 and 2 cm thickness. Besides, the thicker EPS layer installed in the PCM room could improve indoor OT during low outdoor temperatures.

4.5.2.5. Average heat gain reduction

Analysing the thermal performance of building elements is vital to quantify the energy-saving owing to installing the thermal insulation with PCM, especially for the current case, since it focuses on building envelope enhancement regardless of other cooling load sources (lighting, equipment, appliances, etc.).

Since the current study focuses on the role of thermal insulation when combined with a PCM room, the total average heat gain reduction (AHGR) was calculated for the PCM-EPS room cases compared with the PCM room. The AHGR is quantified by considering the heat gain difference between each element in the PCM-EPS room compared with the corresponding elements of the PCM room during the day hours. Fig. 4.53 presents the AHGR of each PCM-EPS case over simulated months.

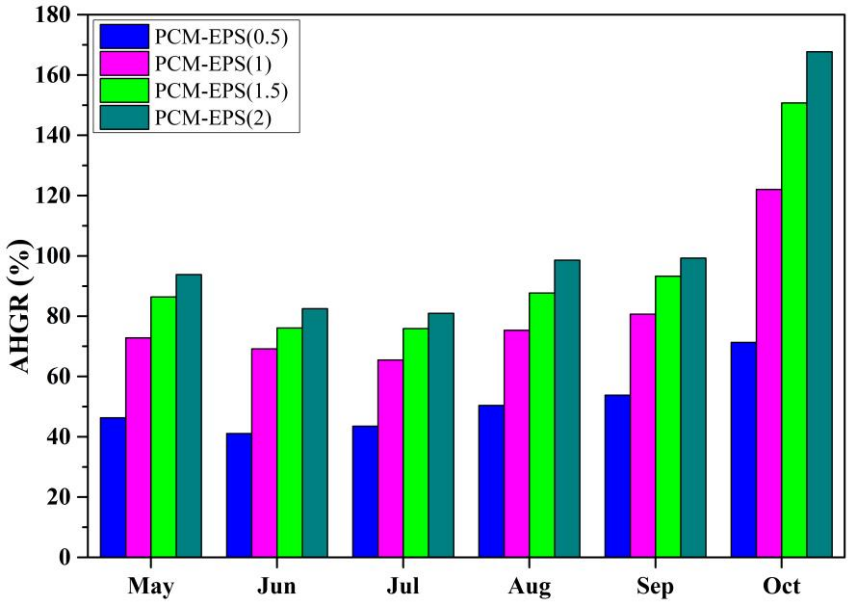

Fig. 4.53. AHGR of PCM-EPS rooms compared with PCM room

As observed in Fig. 4.53, the AHGR increased as the insulation layer thickness increased compared to the PCM layer. On average, the AHGR was increased by 51.1%, 80.9%, 95.1%, and 103.8%, respectively, when EPS layer of 0.5, 1, 1.5 and 2 cm thickness was installed in the PCM room. This is evident since the HG of the envelope element is dependent on the thermal resistance of element layers (i.e., R-value), which is specified by the layer's thermal conductivity and thickness (Holman, 2011).

The AHGR varied during the simulation months, showing the lowest values in July against the higher ones in October. Incidentally, increasing EPS layer thickness by 0.5 cm over the PCM-EPS(0.5) has increased the AHGR by about 50.5%, 74.5% and 86.1% in July, in contrast to 71.2%, 114.4% and 135.2%, respectively in October. The reason is that the PCM was more effective in July due to phase change phenomena, which lessened the importance of EPS layer thickness increment in the PCM-EPS cases compared with the case of PCM only. In contrast, the PCM was useless during October and acted as a traditional construction material of fixed thermal conductivity (i.e., no phase change phenomena). Therefore, increasing EPS layer thickness has augmented the thermal resistance of the envelope compared with the element with PCM only, as stated previously by Solgi et al. (Solgi et al., 2019) and others. Table 4.10 summarise the main results of the above indicators for PCM and PCM-EPS cases.

Table 4.10. Summary of results obtained for modified rooms compared with the reference room

Month	RMTR (%)				TL (min)					ATFR (°C)					OTR (%)					AHGR (%)			
	PCM-EPS(0.5)	PCM-EPS(1)	PCM-EPS(1.5)	PCM-EPS(2)	PCM	PCM-EPS(0.5)	PCM-EPS(1)	PCM-EPS(1.5)	PCM-EPS(2)	PCM	PCM-EPS(0.5)	PCM-EPS(1)	PCM-EPS(1.5)	PCM-EPS(2)	PCM	PCM-EPS(0.5)	PCM-EPS(1)	PCM-EPS(1.5)	PCM-EPS(2)	PCM-EPS(0.5)	PCM-EPS(1)	PCM-EPS(1.5)	PCM-EPS(2)
May	45.1	83.4	112.2	133.9	62.7	112	151.3	174.7	191.3	5.5	6.9	7.1	6.8	6.4	5.1	7.5	8.2	8.4	8.5	46.3	72.8	86.4	93.8
Jun	56.4	94.9	121.	141.	67.3	99.3	128	146	160.	4.8	6.3	6.5	6.2	5.8	4.8	6.9	7.3	7.3	7.1	41.1	69.2	76.1	82.5
Jul	65.6	107.4	135.9	156.3	68	102.7	130.7	147.3	158.7	3.9	5.2	5.2	4.9	4.4	3.9	5.8	6.2	6.1	5.9	43.5	65.5	75.9	80.9
Aug	59.4	97.2	124.4	143.2	63.3	99.3	124.7	142.7	155.3	3.9	5.5	5.7	5.4	4.9	3.7	5.5	5.9	5.9	5.7	50.4	75.3	87.7	98.6
Sep	53.2	92.8	120.5	138.9	51.3	95.3	122	142	157.3	5.1	6.6	6.7	6.4	5.9	4.3	6.3	6.6	6.4	6.0	53.8	80.7	93.3	99.3
Oct	55.4	97.9	125.2	144.4	48	97.3	142.7	168.7	189.3	4.6	7.1	8.2	8.5	8.6	3.5	6.8	8.0	8.4	8.4	71.3	122.1	150.8	167.7

4.6. Effect of natural night ventilation on the indoor thermal comfort

Buildings with passively integrated PCM suffer from high inside surface temperature of elements when the ambient temperature falls below the operating range of applied PCM (i.e. melting and solidification range). This period is usually designed to be occurred at night by selecting a suitable PCM considering the daily ambient temperature variation and the optimal PCM position within the building structure that controls the PCM activation (Piselli et al., 2020). At night, the relatively low outdoor ambient temperature is often employed to remove undesired PCM heat (heat discharging), enhance the indoor environment, and ensure complete PCM solidification for the next day's cycle. For this purpose, passive and active means provide NV through openings (i.e., windows) or using designed air channels considering the amount of air used and time for ventilation.

In this section, the effect of NNV will be studied considering the improvement in the indoor temperature enhancements, mainly considering the effect of the NNV period, window orientation and role of WWR, as will be analysed in the following subsections.

4.6.1. Effect of NNV period on the indoor thermal comfort

The effect of the NNV period, through the window, on the indoor thermal comfort was investigated in this section experimentally to show the indoor temperature improvement considering one to six hours opened window over six consecutive days. The experiments were performed for six consecutive days, from 18th to 23rd September 2021. Windows of reference and PCM rooms were kept open for one hour from 18:00 to 19:00 on 18.09.2021, for two hours from 18:00 to 20:00 on 19.09.2021, and up to six hours from 18:00 to 00:00 on 23.09.2021, as indicated in Fig. 4.54.

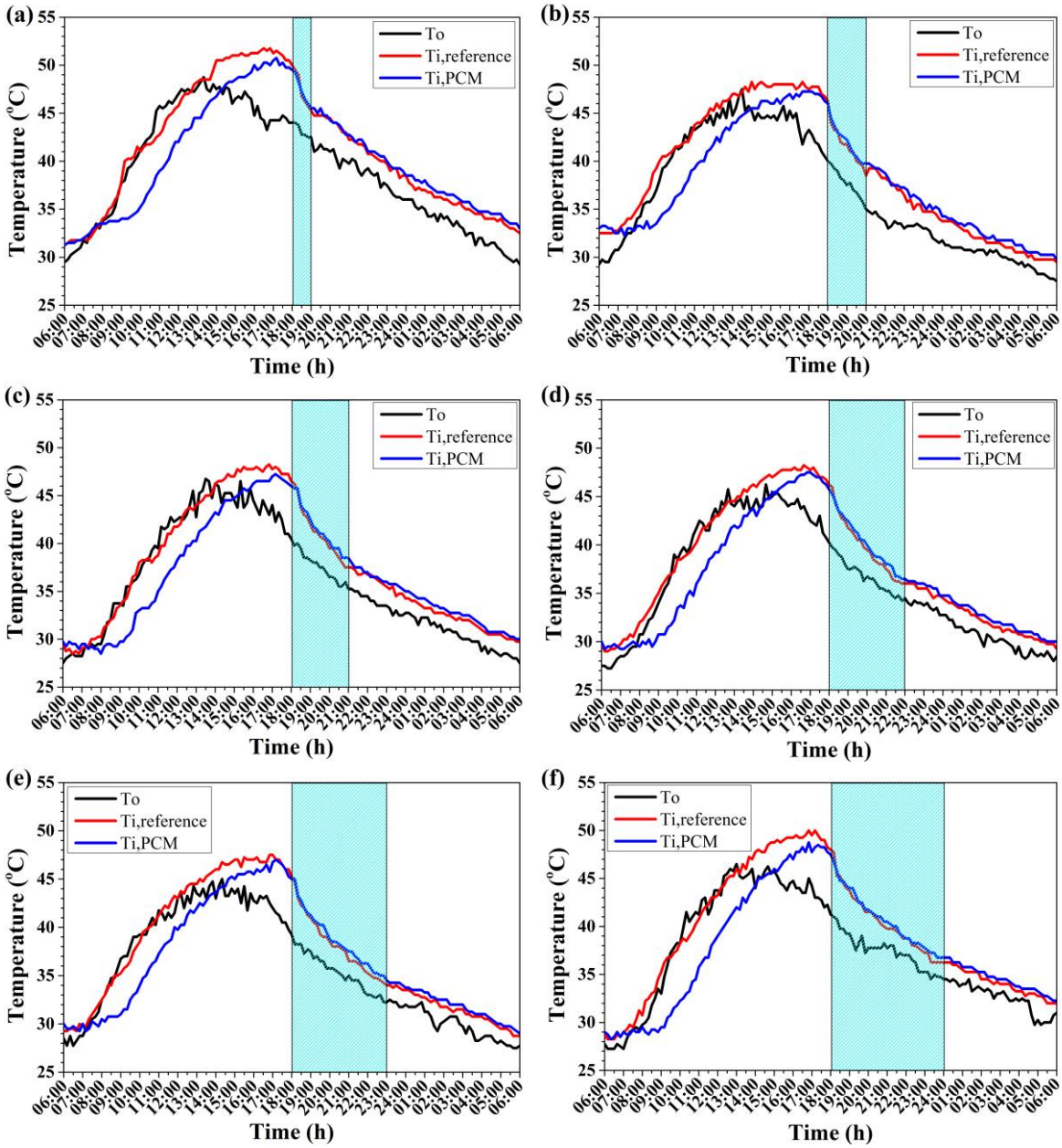

Fig. 4.54. T_i and T_o of reference and PCM rooms over NNV periods, (a) 1h, (b) 2h, (c) 3h, (d) 4h, (e) 5h, (f) 6h

The effect of the NNV period was analysed by considering the indoor temperature behaviour in terms of the room average temperature reduction (AITR) and OTR.

4.6.1.1. Average indoor temperature reduction

The AITR concept is similar to the concept of Y presented in subsection 3.6.4, Eq. (3.13); both consider the average indoor temperature difference between the PCM and reference rooms during the night period. AITR shows how the indoor temperature of the PCM room was influenced by the NNV period compared to the reference room indoor temperature. The average indoor temperature variation during the last six hours of each thermal cycle (i.e., from 00:00 to 6:00) was considered to study the effect of every NNV period on the temperature variation of the next cycle.

Moreover, the difference between the average indoor temperature of reference and PCM rooms could also quantify the indoor temperature reduction due to NVV utilisation, as shown in Fig. 4.55.

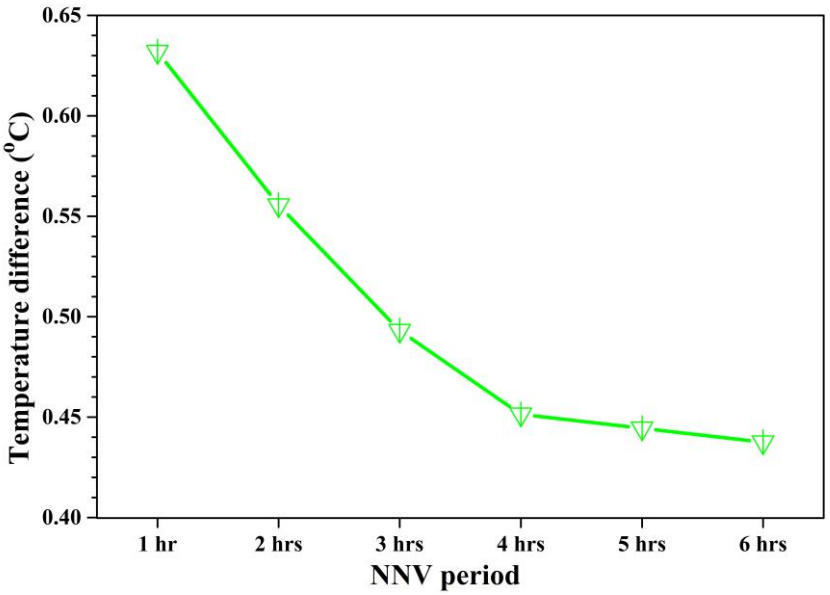

Fig. 4.55. Temperature difference between PCM and reference room during each NNV period

Although the indoor temperature of the PCM room is still higher than that of the reference room in the night period, a positive enhancement can be noticed in both rooms when NNV is applied. However, this enhancement was relatively slight regardless of the NNV period due to the high outside ambient temperature at night compared with the indoor temperature of the room and the dependency on the buoyancy forces to transfer the heat through the window (natural ventilation).

The AITR of PCM and reference rooms decreased sharply and linearly in the first four cycles, as shown in Fig. 4.56, while a slight reduction could be noticed in the 5th and 6th cycles. The temperature difference in the 1st, 2nd, 3rd, 4th, 5th and 6th cycle was 0.632 °C, 0.555 °C, 0.493 °C, 0.451 °C, 0.444 °C and 0.438 °C, respectively. These values are equivalent to AITR in the PCM room by 12.2%, 21.9%, 28.6%, 29.7% and 30.7%, respectively, when 2 hrs, 3 hrs, 4 hrs, 5 hrs and 6 hrs of NNV are applied compared with 1 hr NNV. This reveals that applying NNV for 4, 5, and 6 hours has nearly the exact indoor temperature enhancement percentages.

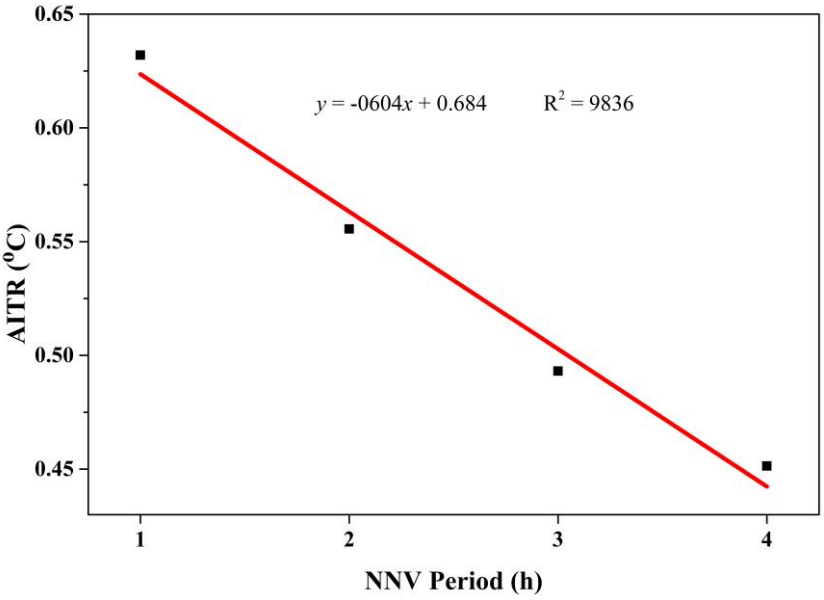

Fig. 4.56. AITR between PCM and reference rooms in the first four NNV periods

4.6.1.2. Operative temperature reduction

The OTR is essential in this study to consider the effect of the NNV period on both the indoor air and inside surface temperatures. Fig. 4.57 shows the OT and OTR of rooms during the experimental days.

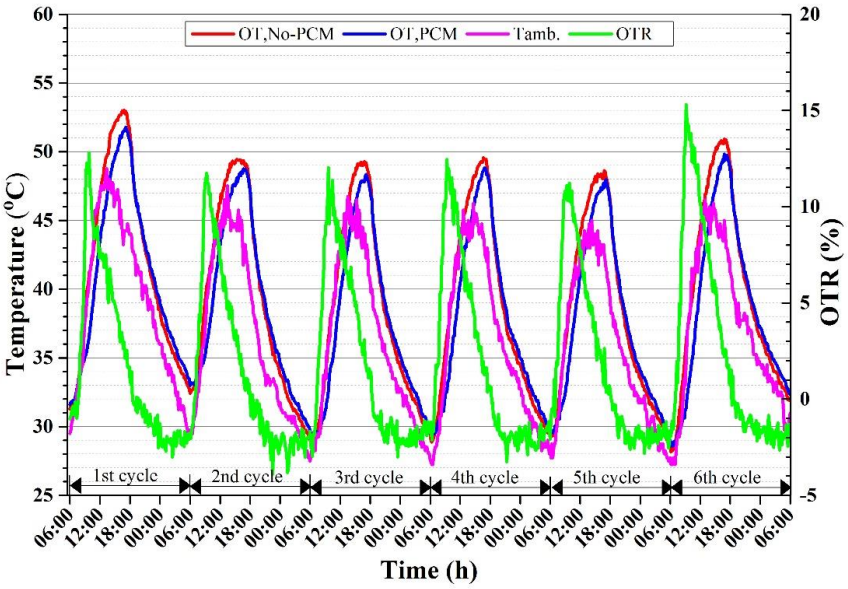

Fig. 4.57. OT and OTR of PCM and reference rooms

Fig. 4.57 shows that the ambient temperature was lower than the OT in the PCM and no-PCM rooms from 12:00 to 6:00 in each day cycle. This occurs because the inside surface temperature of elements affected the OT, and heat accumulated inside rooms in the first half of each cycle (i.e. from 6:00 to 12:00). However, the PCM room's OT was consistently lower than that of the reference room from 6:00 to 18:00, resulting from the activated PCM inside the roof and walls. Considering the OT difference between the PCM and reference rooms, a maximum temperature mark of 4.68 °C, 4.23°C, 3.9°C, 4°C, 3.94 °C and 4.8 °C was calculated in the 1st, 2nd, 3rd, 4th, 5th and 6th cycle, respectively during the period from 9:20 to 10:10.

Fig. 4.57 also indicates that the maximum OTR has increased inconsistently from 6:00 to 12:00, achieving 12.8%, 11.74%, 12%, 12.45%, 11.2% and 15.2%, respectively, in the 1st, 2nd, 3rd, 4th, 5th and 6th day-cycle. These OTR values indicate no influence of NNV on the OT of the PCM room in the next cycle compared with the reference room, which was more affected by the outdoor ambient temperature and solar radiation during the day. This is attributed to the relatively high ambient temperature at night, which cannot be utilised to discharge the entire PCM heat and store coolness for the next cycle. Therefore, the PCM room still shows a negative indoor temperature behaviour during the nighttime regardless of the NNV period applied.

4.6.2. Effect of window orientation

The effect of window direction compared with the reference case, east direction (E), was studied numerically considering the other three wall directions; south (S), west (W) and north (N). The other orientations are also studied by rotating the room 45° clockwise (i.e. north-east (NE), south-east (SE), south-west (SW) and north-west (NW), as previously indicated in subsection 3.5.2.2-ii. The NNV was applied for six hours, starting from 18:00 to 24:00, over the simulation period of six summer months. The improvement in the indoor temperature of the PCM room during the NNV period in terms of AITR is considered in the calculations to specify and analyse the best window direction, which will be adopted in subsection 4.6.3.

Fig. 4.58 shows the AITR of the PCM room under NNV and different orientations compared with the non-ventilated case.

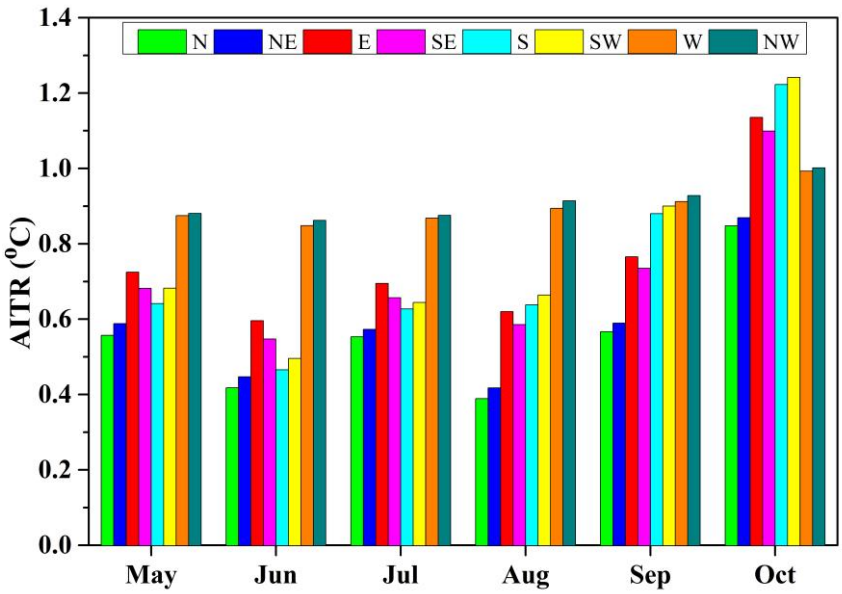

Fig. 4.58. AITR of PCM room with different window orientations compared with non-ventilated one

The results presented in Fig. 4.58 showed that the NNV through a single-sided window could not improve the indoor temperature of the PCM room by more than 1 °C during May-September, regardless of window orientation. This is attributed to the high outdoor air temperature at night, which was insufficient to release heat from the PCM room considering the wind speed only. Besides, the figure displayed that the W and NW orientations are the best for NNV compared with the others during May-October, whereas the N and NE were the worst. The trend differed in October, where the S and SW orientations showed better AITR than the other orientations by more than 1.2 °C. Considering the wind speed and direction presented in Fig. 4.59, it could be observed that the wind direction is mostly from NW and W at the location under study. This is the main reason behind the best AITR at these orientations since the NNV depends mainly on the wind and buoyancy effect to ventilate the simulated room (Aflaki et al., 2015).

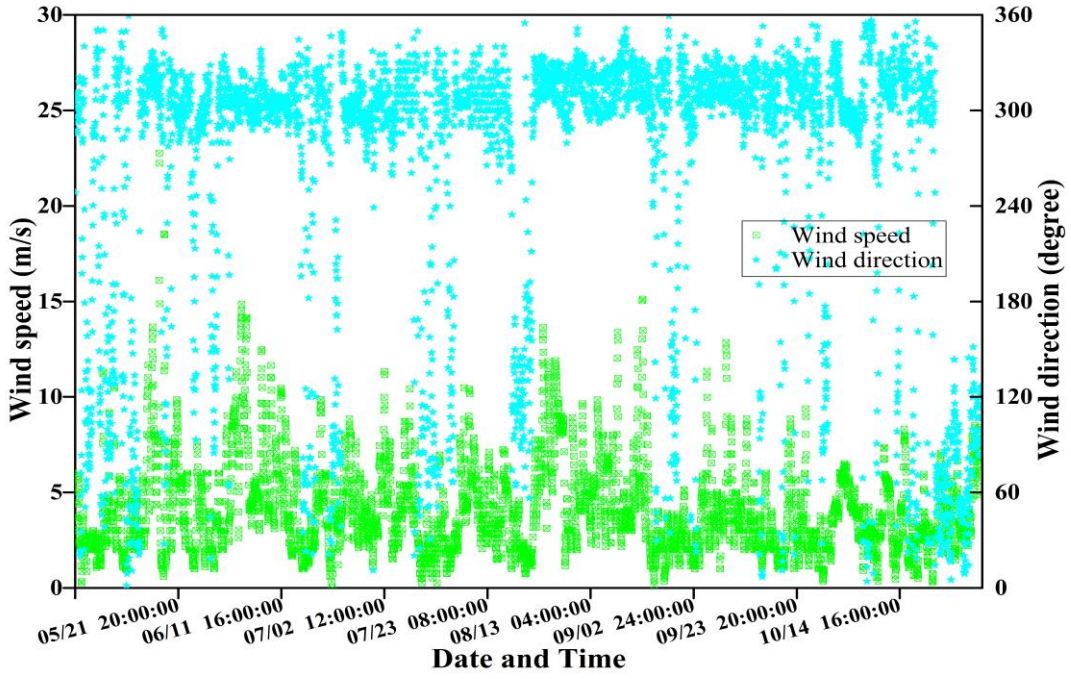

Fig. 4.59. Wind speed and direction during the simulation period

In summary, during hot months (May to September), the non-ventilated PCM room could be enhanced by an average AITR of about 0.51 °C 0.52 °C, 0.68 °C, 0.64 °C, 0.65 °C, 0.68 °C, 0.88 °C and 0.89 °C at the N, NE, E, SE, S, SW, W and NW orientations, respectively. Besides, in comparison with the original case investigated in subsection 4.6.1 (i.e., E orientation), only the W and NW orientations could improve the indoor thermal comfort over the PCM room with an E-oriented window by 29.3% and 31.1%, respectively.

4.6.3. Effect of the window-to-wall ratio

As highlighted in subsection 3.5.2.2-iii, the WWR was analysed considering WWR10, WWR12, WWR14, WWR16, 18 WWR and 20 WWR compared with the reference case of 8.75 WWR for the PCM room with NW orientation, the best case obtained in subsection 4.6.2. The effect of WWR on indoor thermal comfort was analysed considering the AITR of the PCM room with NNV at different WWRs compared with the PCM room with no ventilation, as shown in Fig. 4.60.

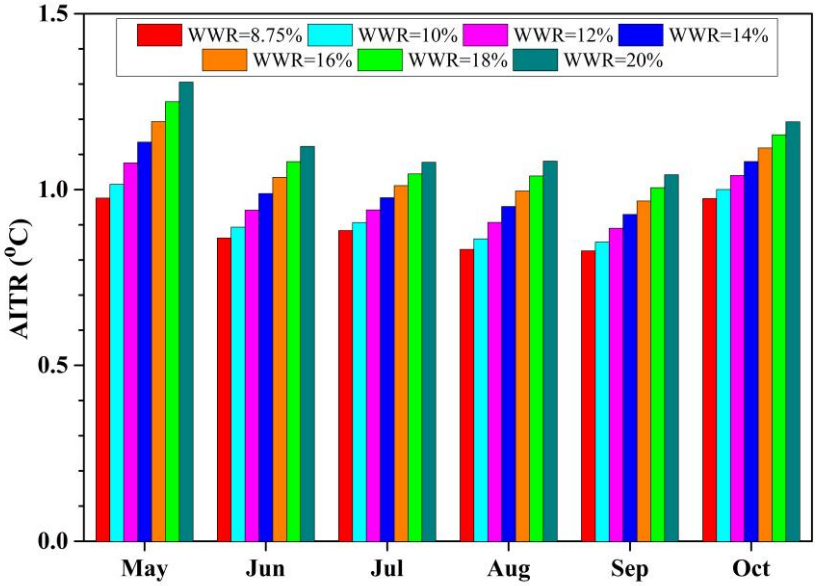

Fig. 4.60. AITR of PCM room with NW orientation and different WWR compared with non-ventilated PCM room

Fig. 4.60 displayed that the AITR of the PCM room decreased as the WWR increased during the simulated period, indicating better thermal comfort. However, the influence of WWR was relatively similar during all months, except during May and October, which showed better AITR influenced by the colder nights. In an average of all months, the AITR of the PCM room was enhanced by 0.89 °C at WWR=8.75%, 0.92 °C at WWR=10%, 0.97 °C at WWR=12%, 1.01 °C at WWR=14%, 1.05 °C at WWR=16%, 1.09 °C at WWR=18% and 1.14 °C at WWR=20%. These AITR values are equivalent to 3.2%, 8.4%, 13.5%, 18.1%, 22.9% and 27.5% at WWR of 10%, 12%, 14%, 16%, 18% and 20%, respectively, compared with the reference case of WWR=8.75%. Considering the average of all simulated months, it can be concluded that the AITR of the PCM room is in a positive linear relationship with the increased WWR, as shown in Fig. 4.61.

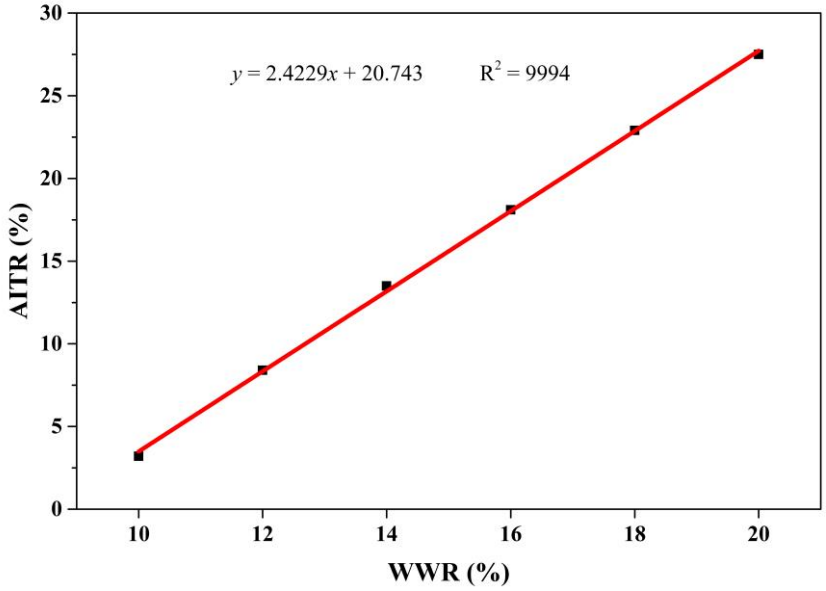

Fig. 4.61. Relationship of average AITR in the PCM room with WWR

The above results showed that applying NNV for 6 h at the best window orientation (NW) and WWR (20%) could reduce the PCM room indoor temperature by only 1.14 °C over the case of a non-ventilated PCM room directed towards NW. This temperature reduction is too slight compared to the heat released from the PCM at night. Therefore, applying forced NV is suggested for such harsh weather locations considering the ventilation time and amount of ventilated air. Besides, an alternative cooling medium could be processed to expedite the PCM solidification phase.

4.7. New scientific results

This section presents the new scientific findings from this research work as follows:

1. Effect of phase change material position on the thermal performance of a roof

I have pointed out that the optimal position of phase change material (PCM) strongly influences the roof's thermal performance from both energetic and thermal comfort viewpoints. Besides, I proved experimentally that the PCM was more beneficial as the outer surface temperature increased.

Based on the experimental findings, I found that positioning the PCM layer near the outer roof side (between the roofing and main layers) has reduced the inner surface temperature and indoor ambient temperature regardless of the roof’s outer surface temperature at non-ventilated conditions. Besides, positioning the PCM layer in the middle of a composite roof could enhance the indoor thermal comfort superior to the position near the inner roof layer (near indoor).

Compared with the roof without PCM, I proved that the PCM layer at the outside position had reduced the maximum indoor temperature by 12.9%, along with average indoor temperature fluctuation reduction by 9 °C during the thermal cycle and time delay by 140-180 min. At the highest outer surface temperatures, the roof's inner surface temperature decreased as the PCM layer moved from the inner towards the outer position by 36.5%, 66.3% and 74.8%.

2. Effect of phase change material thickness on the thermal performance of a roof

I experimentally investigated the optimal thickness of the PCM layer incorporated in a roof and its effect on thermal performance. I found that increasing PCM layer thickness from 1 cm to 1.5 and 2 cm has increased the roof's thermal performance and improved indoor thermal comfort. In this regard, the PCM layer thickness of 2 mm has reduced the maximum indoor temperature by

about 13.9% and extended the temperature time lag by 240-270 min compared with the roof without PCM. However, I found that increasing PCM layer thickness has descending effectiveness in which increasing thickness from 1 to 1.5 cm has reduced the indoor temperature by 20.5% while increasing the thickness from 1.5 to 2 cm has reduced it by about 3% only.

I noticed that increasing PCM layer thickness "*x*" by 0.5 cm has enhanced the roof thermal resistance in terms of the decrement factor "y" according to the linear equation:

$$y = -0.1x + 0.6367 \; R^2 = 0.9868$$

I observed that increasing PCM thickness in the non-ventilated roof has limited advantages in passive applications due to the poor PCM solidification phase at night. According to the experimental results, I found that the average temperature fluctuation reduction at 2 cm PCM layer thickness had poorer thermal performance than 1.5 cm thickness, considering the full thermal cycle. I discovered that the PCM layer of 1.5 cm could reduce the indoor temperature fluctuations by an average of 10.04 °C compared with the bare roof. In contrast, 1 and 2 cm PCM thicknesses could reduce the fluctuations by 8.13 °C and 9.75 °C, respectively.

3. The influence of encapsulation heat transfer area on bricks-based PCM capsules

I have examined and justified the effect of encapsulation area on the PCM thermal performance when immersed into concrete bricks. I have proven that in passive novel bricks containing PCM capsules with different shapes and sizes, the overall heat transfer encapsulation area was the main influential parameter of PCM performance during the thermal cycle since the same PCM quantity was involved.

Based on the experimental results, I observed that concrete bricks with many PCM capsules had lower inner surface temperatures than those based on bulky PCM capsules, thanks to the high PCM heat transfer area. However, although increased encapsulation area has improved the melting/solidification phases, I noticed that increasing encapsulation area was critical and excessive area could reach a fast melting phase and decline heat storage early regardless of the capsules' shape.

I found that 320 cm^2 overall heat transfer area was the best for ~45g PCM in the concrete brick, reducing the maximum inner surface temperature by ~1.88 °C and lagging peak temperature by 42.5 min on average. Technically, the mechanical strength of this PCM brick type declined by 28.2% compared with the reference one.

4. Thermal comfort and energetic evaluation of scaled PCM room

I assessed the contribution of PCM to the indoor thermal comfort and energy saving of a scaled room under no ventilation compared with a reference room. I showed that the PCM had improved indoor thermal comfort and energy saving remarkably during day hours. According to experimental results, I showed that the maximum indoor temperature has decreased by up to 5.75 °C in the PCM room compared to the reference room. From the energetic view point, I found that the PCM effectiveness during the day is time-dependent with respect to the sun's position. Considering walls, the east-oriented wall performed better in the first half of the day, whereas the west-oriented wall performed well in the afternoon. The maximum temperature reduction of the east wall reached 2.75 °C, whereas the west wall showed a 2.25 °C temperature reduction. Besides, all PCM walls showed roughly similar decrement factor of 11.7%-13.3% compared with the reference walls. I confirmed that the roof was the most effective element in the room, responsible for an average surface temperature reduction of 3.25 °C, a decrement factor of 25.6% and a total heat gain reduction of 35%-40% over the reference roof.

Based on the hourly analysis, I noticed that the best effectiveness hour for the PCM room is at 9:00, in which the indoor temperature reduction "*y*" after this hour was linearly declined with time "*x*", according to the following equation:

$$y = -29.12x + 22.16\ R^2 = 0.9664$$

Energetically, I had seen that the PCM was most effective during the first half of the day, particularly from 9:00 to 11:00, more than the rest day hours. Besides, the PCM involved in walls should vary, considering their orientation and period of exposure to solar radiation.

Considering the long-term numerical analysis, I observed that the average indoor temperature fluctuations were minimised during summer by up to 6 °C in the PCM room compared to the reference room. Moreover, I found that the thermal load levelling during the thermal cycle was reduced by 38%-59%, with superior performance observed in May and lower in October. From the energetic standpoint, I showed that the average heat gain reduction during the hottest summer months ranged between 66.6%- 76.5%. Accordingly, I estimated that the PCM incorporated could save CO_2 emission by up to 2.27 kg CO_2/day and electricity by up to 250 IQD/day.

5. Effect of thermal insulation with PCM room

I presented the positive effect of traditional thermal insulation (expanded polystyrene, EPS) on the PCM thermal performance of the PCM room. Numerically, I proved that the optimal position of the EPS layer is in the middle of an element, directly next to the PCM layer from the indoor side, in which the melting and solidification phases of PCM expedited by one hour compared with the position near indoor or outdoor sides.

I investigated the optimal thickness of the EPS layer (0.5, 1, 1.5 and 2 cm) installed in the PCM room at the optimal position. I proved that increasing EPS layer thickness had improved the thermal performance of the PCM room noticeably from the energetic and thermal comfort perception. However, I observed that increasing EPS layer thickness is limited when considering the full thermal cycle and had adverse behaviour under a non-conditioned PCM room. On average summer months, I disclosed that installing EPS with 0.5, 1, 1.5 and 2 cm layer thickness had increased the maximum indoor temperature reduction over the PCM room by 55.7%, 95.4%, 123.1% and 142.8%, respectively.

I evidenced that the average temperature fluctuation during May-September was reduced by up to 35% when installing a 1 cm thickness of EPS with PCM room, compared with only 20% when 2 cm was installed. I also exhibited that the thicker EPS layer than 1 cm installed in the PCM room has performed poorly compared with that of EPS layer thickness equal to/or lower than 1 cm during June-September.

From the energetic viewpoint, I showed that the envelope total heat gain reduction "*y*" linearly increases with the increased EPS layer thickness by 0.5 mm "*x*", according to the following positive relationship:

$$y = 34.46x + 39.65\ R^2 = 0.9273$$

6. Role of natural night ventilation to enhance thermal comfort of PCM room

I explored the role of natural night ventilation (NNV) experimentally through a single-side window to enhance the PCM room thermal comfort. I showed that increasing the NNV period from 1 h to 6 h could slightly decrease the PCM room temperature compared to that of the reference room. I observed that increasing the NNV period to 4 h has narrowed the indoor temperature difference between PCM and reference rooms noticeably, according to the following linear equation. However, a slight temperature difference was attained at 5 and 6 h.

$$y = -0.0604x + 0.684\ R^2 = 0.9836$$

I also revealed that the daily maximum operative temperature in the PCM room was inconsistently increased by 11.2%-12.8% in the first half of the next day, indicating no influence of the NNV on the following thermal cycle.

Considering the window orientation, I proved that the NNV could improve the thermal performance of the PCM room further when directing the room towards the northwest direction. At this orientation, the indoor temperature of the PCM room has decreased by 1.2 °C at night compared with the PCM room without NV.

I also investigated the effect of NNV through an enlarged window-to-wall ratio (WWR) from 10% to 20% with a 2% increment factor on the PCM room indoor temperature. At the north-west room orientation, I disclosed a positive linear relationship between increasing WWR "*x*" and decreasing the indoor temperature of PCM room "*y*", according to the following equation:

$$y = 2.4229x + 20.743 \; R^2 = 0.9994$$

Considering the above statements, I improved the average indoor thermal comfort of the PCM room by about 27.5% when enlarging WWR from 8.75% (reference WWR) to 20% during summer.

5. CONCLUSION AND SUGGESTIONS

The thermal performance of phase change material (PCM) incorporated into building envelope has been investigated experimentally and numerically under severe hot location. The PCM was incorporated passively into the roof and walls to quantify the advantages in terms of thermal comfort and energy saving for non-ventilated rooms. The study involved follow-up experiments to first study the optimal PCM layer position and thickness into the roof and the best thermally-acted PCM brick. Afterwards, the best case attained from each experiment was considered to build a scaled PCM room, which was examined and compared with a reference one. The experiments were extended by EnergyPlus software to show the role of thermal insulation and natural night ventilation (NNV) in the PCM room, considering several aspects. Based on the results obtained, the following conclusions can be drawn:

- Positioning the PCM layer near the outdoor edge of the roof (between the roofing and main roof layer) performed better than the position in the middle or near the indoor zone.
- Increasing PCM layer thickness in the roof from 1 cm to 1.5 and 2 cm has increased the PCM effectiveness. However, adverse PCM thermal behaviour was observed during the solidification period (at night) at 2 cm PCM layer thickness.
- The overall heat transfer area is the main influential parameter on the thermal performance regardless of the shape of the capsules. Immersed many PCM capsules into concrete bricks had better thermal performance than bulky containers during melting/solidification phases. The mechanical strength of PCM brick declined, irrespective of thermal enhancement.
- The PCM effectiveness is time-dependent, where the PCM elements exposed to solar radiation for a long time are more beneficial than their corresponding ones. Energy saving of up to 40% could be attained through the roof than walls.
- The indoor temperature of the PCM room was stabilised, shaved and shifted considerably compared with the reference one, although the investigations were verified under non-ventilation conditions and the outdoor conditions controlled the whole process.
- The thermal insulation could maximise PCM's effectiveness and achieve further energy saving. However, the position and thickness of the thermal insulation should be studied properly to ensure no influence on the PCM melting/solidification phases. It was found that positioning 1 cm of insulation next to the PCM layer from the indoor side is optimal.
- NNV through a single-side window could slightly improve the indoor temperature during night hours due to high outdoor temperatures. NNV for 4 h was critical to reduce the PCM room indoor temperature, in which a slight improvement was observed with 5 and 6 h. The window orientation has a certain effect on the thermal comfort in which the orientation towards the wind direction is the best. Besides, the higher WWR resulted in better thermal comfort in the PCM room. Nevertheless, the influence of window size on indoor heat gain during day hours should be considered along with the architectural and economic concerns.

The scope of this dissertation could be extended to consider the PCM incorporation with the transparent elements (i.e., windows), which normally have an essential influence on the built environment in hot locations. The PCM effectiveness under real conditions, involving the impact of occupants and equipment under controlled conditions (mechanical ventilation), is extremely advised. Coupling PCM with solar thermal system for space heating has many research gaps need to be addressed. Besides, study of PCM contribution for both cooling and heating load reductions is suggested considering composite PCM layers with different melting temperatures. Finally, the study of real buildings considering the economic and environmental aspects is also crucial to foretell the technology feasibility.

6. SUMMARY

INCORPORATION OF PHASE CHANGE MATERIAL INTO BUILDING ENVELOPE UNDER HOT LOCATION

In summary, experimental and numerical investigations have been conducted in this piece of work to evaluate the thermal performance of phase change material (PCM) incorporated building envelope under severe hot conditions. To this aim, two rooms, one passively incorporated with PCM into the roof and walls (PCM room) and the other left without PCM (reference room), were built and examined under summer conditions of Al Amarah city (Latitude: 31.84° & Longitude: 47.14°), Iraq at no ventilation.

In the PCM room, the optimal PCM layer position and thickness into the roof were considered along with the best thermally-performed PCM brick after a set of preliminary experiments. Furthermore, several energetic and thermal comfort indicators were considered to quantify the thermal comfort and energy saving earned from PCM incorporation. Numerical studies have been verified on a validated model (with the experimental studies above) to investigate the PCM effectiveness over the summer months. Besides, the role of thermal insulation at different positions and thicknesses was investigated along with the effect of natural night ventilation (NNV) at different periods, window orientation and window-to-wall ratio (WWR).

The experimental and numerical results indicated notable effectiveness of PCM under severe hot summer conditions, even with passive incorporation and non-ventilated rooms. The PCM layer was better positioned near the outdoor environment where the melting and solidification phases were guaranteed. Besides, increased PCM layer thickness in the roof has decreased the inner surface temperature and increased the time lag. However, the PCM layer of 2 cm showed poor thermal performance during the solidification phase due to high outdoor temperature and high accumulated heat inside the PCM during the day hours. The PCM showed good enhancement in the thermal performance of concrete bricks. However, the PCM involved in capsules performed better than bulky PCM capsules due to increased heat transfer area. Besides, the mechanical strength of the PCM brick declined compared with that of the reference brick.

The PCM room generally showed better thermal comfort and energy saving than the reference room on an hourly, daily and monthly basis. Experimental studies showed that the roof performed much better than the walls due to long-time exposure to solar radiation and the PCM quantity incorporated. Moreover, the walls that experienced high solar radiation, namely the east and west, performed better than the others. Long-term numerical investigation showed that the PCM was effective on the hottest day of May-September, while it behaved as an extra layer with low thermal conductivity during October.

Numerical results also showed that installing thermal insulation with the PCM is beneficial to enhance thermal comfort and energy saving. It was shown that positioning the thermal insulation next to the PCM layer from the indoor side is optimal to ensure the full effectiveness of PCM during the thermal cycle. Besides, the insulation layer of 1 cm was better than thicker layers to guarantee maximum dissipation of indoor heat during the night.

Experimental and numerical investigations also showed that the NNV could slightly enhance the indoor temperature regardless of the NNV period. Moreover, numerical studies displayed that the NNV through a single-side window could reduce the temperature by about one degree at the best window orientation and size with respect to the non-ventilated case. Therefore, forced/mechanical NV could be advised as a better means to overcome PCM negative behaviour during the night, considering the ventilation time and quantity of ventilated air.

7. ÖSSZEFOGLALÁS (SUMMARY IN HUNGARIAN)

ÉPÜLETHATÁROLÓ SZERKEZETBE INTEGRÁLT FÁZISVÁLTÓ ANYAG ALKALMAZÁSA FORRÓ ÉGHAJLATON

A kutatómunka az épület külső határolószerkezetébe integrált fázisváltó anyag (PCM) hőteljesítményének értékelésére irányult kísérleti és numerikus vizsgálatokkal szélsőségesen forró éghajlati körülmények között. A kísérlethez Al Amarah városban (Irak, (FSZ: 31.84° FH: 47.14°)) megépített két helyiség (az egyik (PCM helyiség) fázisváltó anyagot integráló fal- és tetőszerkezettel, míg a másik (referencia helyiség) fázisváltó anyag nélkül) vizsgálatára került sor, nyári időszakban.

A PCM helyiség határoló szerkezetének kialakítása az előzetesen elvégzett kísérletek eredménye alapján meghatározott optimális PCM-réteg elhelyezés és –vastagság figyelembevételével, valamint hőtechnikailag legkedvezőbb kialakítású PCM téglával történt. Számos energetikai és hőkomfort mutatót alkalmaztam a PCM beépítéséből származó termikus komfort és energiamegtakarítás számszerűsítésére. A fenti kísérletek eredményei alapján igazolt validált modellel végzett numerikus vizsgálatokkal elemeztem a PCM hatékonyságát a nyári hónapokban. Megvizsgáltam a különböző elhelyezésű és vastagságú hőszigetelés, valamint a természetes éjszakai szellőzés (NNV) hatását különböző időszakokban, figyelembe véve az ablak tájolását és az ablak-fal arányt (WWR).

A kísérleti és numerikus eredmények egyaránt igazolták a PCM jelentős hatékonyságát szélsőséges forró nyári körülmények között, passzív beépítés és nem szellőztetett helyiségek esetén is. A PCM réteg elhelyezése kedvezőbb a határoló szerkezet külső környezet közelében lévő rétegében, ahol az olvadási és megszilárdulási fázisok egyaránt garantáltak. A tetőn a PCM rétegvastagság növelésével csökken a belső felületi hőmérséklet, nő az időeltolódás. Azonban 2 cm-es PCM-réteg már gyengébb teljesítményt nyújt a megszilárdulási fázisban, a magas külső hőmérséklet és a PCM-ben a nappali órákban akkumulált hőmennyiség miatt. A beton téglákba integrált PCM a hőteljesítményt javítja. A kisebb kapszulákban jelenlévő fázisváltó anyag a nagyobb hőátadási felület miatt kedvezőbb, mint a nagyobb kiterjedésű PCM kapszulák. A PCM-et tartalmazó tégla mechanikai szilárdsága azonban csökken a referencia tégláéhoz képest.

A PCM helyiség órai, napi és havi hőkomfort- és energiamegtakarítás mutatói általánosan kedvezőbbek voltak, mint a referenciahelyiségé. A kísérleti vizsgálatok azt mutatták, hogy a fázisváltó anyagot tartal-mazó tető teljesítménye jobb volt, mint a falaké - a napsugárzásnak való hosszú idejű kitettség és a beépített PCM-mennyiség miatt. Továbbá a nagyobb mértékű napsugárzásnak kitett falak (keleti és nyugati tájolásúak) teljesítménye meghaladta a többiét. A hosszú távú numerikus vizsgálat kimutatta, hogy a PCM a május-szeptemberi időszak legmelegebb napjain volt hatékony, míg októberben alacsony hővezető képességű extra rétegként viselkedett.

A numerikus eredmények alapján kijelenthető, hogy hőszigetelés alkalmazása fázisváltó anyaggal együtt előnyös a hőkomfort és az energiatakarékosság növelése érdekében. Kimutatható, hogy a hőszigetelés elhelyezése a PCM réteg beltéri oldalán az optimális, így a PCM hatékonysága a teljes termikus ciklus alatt biztosítható. Továbbá az 1 cm-es szigetelőréteg a nagyobb rétegvastagsághoz viszonyítva jobban biztosítja a beltéri hő maximális elvezetését éjszaka.

A kísérleti és numerikus vizsgálatok azt is kimutatták, hogy a természetes éjszakai szellőzés (NNV) –függetlenül annak hosszától- kismértékben javítja a beltéri hőmérsékletet. Az elvégzett numerikus vizsgálatok alapján megállapítható, hogy az egy ablakkal végzett NNV közel egy fokkal csökkentheti a hőmérsékletet a nem szellőztetett esethez képest az ablak legkedvezőbb tájolása és mérete mellett. Ezért éjszaka - figyelembe véve a szellőztetési időt és a szellőző levegő mennyiségét - mesterséges/ gépi NV alkalmazása ajánlott a PCM negatív hatásának leküzdésére.

8. APPENDICES

A1: Bibliography

1. Abden, M. J., Tao, Z., Pan, Z., George, L., and Wuhrer, R. (2020): Inclusion of methyl stearate/diatomite composite in gypsum board ceiling for building energy conservation, Applied Energy, 259(November 2019), 114113. https://doi.org/10.1016/j.apenergy.2019.114113
2. Adesina, A. (2019): Use of phase change materials in concrete: current challenges, Renewable Energy and Environmental Sustainability, 4, 9. https://doi.org/10.1051/rees/2019006
3. Aflaki, A., Mahyuddin, N., Al-Cheikh Mahmoud, Z., and Baharum, M. R. (2015): A review on natural ventilation applications through building façade components and ventilation openings in tropical climates, Energy and Buildings, 101, 153–162. https://doi.org/https://doi.org/10.1016/j.enbuild.2015.04.033
4. Ahangari, M., and Maerefat, M. (2019): An innovative PCM system for thermal comfort improvement and energy demand reduction in building under different climate conditions, Sustainable Cities and Society, 44(May 2018), 120–129. https://doi.org/10.1016/j.scs.2018.09.008
5. Al-Absi, Z. A. A. S., Isa, M. H. M., and Ismail, M. (2018): Application of Phase Change Materials (PCMs) in building walls: a review, in International Conference on Architecture and Civil Engineering Conference: Springer, 73–82
6. Al-Absi, Z. A., Hafizal, M. I. M., and Ismail, M. (2022): Experimental study on the thermal performance of PCM-based panels developed for exterior finishes of building walls, Journal of Building Engineering, 52, 104379. https://doi.org/https://doi.org/10.1016/j.jobe.2022.104379
7. Al-Absi, Z. A., Isa, M. H. M., and Ismail, M. (2020): Phase change materials (PCMs) and their optimum position in building walls, Sustainability (Switzerland), 12(4), 1294. https://doi.org/10.3390/su12041294
8. Al-Mudhafar, A. H. N., Hamzah, M. T., and Tarish, A. L. (2021): Potential of integrating PCMs in residential building envelope to reduce cooling energy consumption, Case Studies in Thermal Engineering, 27, 101360. https://doi.org/https://doi.org/10.1016/j.csite.2021.101360
9. Al-Rashed, A. A. A. A., Alnaqi, A. A., and Alsarraf, J. (2021a): Energy-saving of building envelope using passive PCM technique: A case study of Kuwait City climate conditions, Sustainable Energy Technologies and Assessments, 46, 101254. https://doi.org/https://doi.org/10.1016/j.seta.2021.101254
10. Al-Rashed, A. A. A. A., Alnaqi, A. A., and Alsarraf, J. (2021b): Usefulness of loading PCM into envelopes in arid climate based on Köppen–Geiger classification - Annual assessment of energy saving and GHG emission reduction, Journal of Energy Storage, 43, 103152. https://doi.org/https://doi.org/10.1016/j.est.2021.103152
11. Al-Yasiri, Q., Al- Furaiji, M. A., and Alshara, A. K. (2019): Comparative study of building envelope cooling loads in Al-Amarah city, Iraq, Journal of Engineering and Technological Sciences, 51(5), 632–648. https://doi.org/10.5614/j.eng.technol.sci.2019.51.5.3
12. Al-Yasiri, Q., and Szabó, M. (2022a): Energetic and thermal comfort assessment of phase change material passively incorporated building envelope in severe hot Climate: An experimental study, Applied Energy, 314, 118957. https://doi.org/https://doi.org/10.1016/j.apenergy.2022.118957
13. Al-Yasiri, Q., and Szabó, M. (2022b): Phase change material coupled building envelope for thermal comfort and energy-saving: Effect of natural night ventilation under hot climate, Journal of Cleaner Production, 365, 132839. https://doi.org/https://doi.org/10.1016/j.jclepro.2022.132839

14. Alam, M., Jamil, H., Sanjayan, J., and Wilson, J. (2014): Energy saving potential of phase change materials in major Australian cities, Energy and Buildings, 78, 192–201. https://doi.org/10.1016/j.enbuild.2014.04.027
15. Alqallaf, H. J., and Alawadhi, E. M. (2013): Concrete roof with cylindrical holes containing PCM to reduce the heat gain, Energy and Buildings, 61, 73–80. https://doi.org/https://doi.org/10.1016/j.enbuild.2013.01.041
16. Amaral, C., Vicente, R., Marques, P. A. A. P., and Barros-Timmons, A. (2017): Phase change materials and carbon nanostructures for thermal energy storage: A literature review, Renewable and Sustainable Energy Reviews, 79(May), 1212–1228. https://doi.org/10.1016/j.rser.2017.05.093
17. American Society of Heating, R. and A.-C. E. (2016): *2016 ASHRAE Handbook-HVAC Systems and Equipment (IP Edition).* ASHRAE
18. Amirahmad, A., Maglad, A. M., Mustafa, J., and Cheraghian, G. (2021): Loading PCM Into Buildings Envelope to Decrease Heat Gain-Performing Transient Thermal Analysis on Nanofluid Filled Solar System, Frontiers in Energy Research, 9, 727011. https://doi.org/10.3389/fenrg.2021.727011
19. ANSI/ASHRAE Standard 55-2010 (2010): *Thermal environmental conditions for human occupancy*, Encyclopedia of Finance. https://doi.org/10.1007/0-387-26336-5_1680
20. Aranda-Usón, A., Ferreira, G., López-Sabirón, A. M., Mainar-Toledo, M. D., and Zabalza Bribián, I. (2013): Phase change material applications in buildings: An environmental assessment for some Spanish climate severities, Science of the Total Environment, 444, 16–25. https://doi.org/10.1016/j.scitotenv.2012.11.012
21. *Ardunic* (2020): Ardunic Sinaa, Baghdad, Iraq. Available at: https://ardunic.com/auth
22. Arıcı, M., Bilgin, F., Krajčík, M., Nižetić, S., and Karabay, H. (2022): Energy saving and CO_2 reduction potential of external building walls containing two layers of phase change material, Energy, 252, 124010. https://doi.org/https://doi.org/10.1016/j.energy.2022.124010
23. Arıcı, M., Bilgin, F., Nižetić, S., and Karabay, H. (2020): PCM integrated to external building walls: An optimization study on maximum activation of latent heat, Applied Thermal Engineering, 165(January 2020), 114560. https://doi.org/10.1016/j.applthermaleng.2019.114560
24. Arıcı, M., Tütüncü, E., Yıldız, Ç., and Li, D. (2020): Enhancement of PCM melting rate via internal fin and nanoparticles, International Journal of Heat and Mass Transfer, 156, 119845. https://doi.org/https://doi.org/10.1016/j.ijheatmasstransfer.2020.119845
25. Arumugam, P., Ramalingam, V., and Vellaichamy, P. (2022): Effective PCM, insulation, natural and/or night ventilation techniques to enhance the thermal performance of buildings located in various climates – A review, Energy and Buildings, 258, 111840. https://doi.org/https://doi.org/10.1016/j.enbuild.2022.111840
26. Asan, H. (2006): Numerical computation of time lags and decrement factors for different building materials, Building and Environment, 41(5), 615–620. https://doi.org/https://doi.org/10.1016/j.buildenv.2005.02.020
27. ASHRAE, H.-F. (1997): Chapter 22, Thermal and Moisture Control in Insulated Assemblies—Fundamentals, American Society of Heating, Refrigerating and Air-Conditioning Engineers, Inc., Atlanta
28. Baetens, R., Jelle, B. P., and Gustavsen, A. (2010): Phase change materials for building applications: A state-of-the-art review, Energy and Buildings, 42(9), 1361–1368. https://doi.org/10.1016/j.enbuild.2010.03.026
29. Bao, X., Yang, H., Xu, X., Xu, T., Cui, H., Tang, W., Sang, G., and Fung, W. H. (2020): Development of a stable inorganic phase change material for thermal energy storage in buildings, Solar Energy Materials and Solar Cells, 208(May 2019), 110420. https://doi.org/10.1016/j.solmat.2020.110420
30. Beemkumar, Nagappan, Yuvarajan, D., Arulprakasajothi, M., Elangovan, K., and

Arunkumar, T. (2020): Control of room temperature fluctuations in the building by incorporating PCM in the roof, Journal of Thermal Analysis and Calorimetry, 30, 101536. https://doi.org/10.1007/s10973-019-09226-0

31. Beemkumar, N., Yuvarajan, D., Arulprakasajothi, M., Ganesan, S., Elangovan, K., and Senthilkumar, G. (2020): Experimental investigation and numerical modeling of room temperature control in buildings by the implementation of phase change material in the roof, Journal of Solar Energy Engineering, Transactions of the ASME, 142(1). https://doi.org/10.1115/1.4044564
32. Berardi, U., and Gallardo, A. A. (2019): Properties of concretes enhanced with phase change materials for building applications, Energy and Buildings, 199, 402–414. https://doi.org/10.1016/j.enbuild.2019.07.014
33. Berardi, U., and Soudian, S. (2019): Experimental investigation of latent heat thermal energy storage using PCMs with different melting temperatures for building retrofit, Energy and Buildings, 185, 180–195. https://doi.org/10.1016/j.enbuild.2018.12.016
34. Bhave, A. G., and Kale, C. K. (2020): Development of a thermal storage type solar cooker for high temperature cooking using solar salt, Solar Energy Materials and Solar Cells, 208(May 2019), 110394. https://doi.org/10.1016/j.solmat.2020.110394
35. Bista, S., Hosseini, S. E., Owens, E., and Phillips, G. (2018): Performance improvement and energy consumption reduction in refrigeration systems using phase change material (PCM), Applied Thermal Engineering, 142(July), 723–735. https://doi.org/10.1016/j.applthermaleng.2018.07.068
36. Bland, A., Khzouz, M., Statheros, T., and Gkanas, E. I. (2017): PCMs for residential building applications: A short review focused on disadvantages and proposals for future development, Buildings, 7(3). https://doi.org/10.3390/buildings7030078
37. Byron Craig Owens ; Jeffrey Neal Cox ; Peter Franz Horwath ; Reyad I (2018): THERMAL ENERGY STORAGE SYSTEMS INCLUDING A SHIPPING CONTAINER , A HEAT EXCHANGE APPARATUS , AND A PHASE CHANGE MATERIAL. United States
38. Cabeza, L. F., Navarro, L., Pisello, A. L., Olivieri, L., Bartolomé, C., Sánchez, J., Álvarez, S., and Tenorio, J. A. (2020): Behaviour of a concrete wall containing micro-encapsulated PCM after a decade of its construction, Solar Energy, 200(July 2018), 108–113. https://doi.org/10.1016/j.solener.2019.12.003
39. Cao, V. D., Bui, T. Q., and Kjøniksen, A. L. (2019): Thermal analysis of multi-layer walls containing geopolymer concrete and phase change materials for building applications, Energy, 186, 115792. https://doi.org/10.1016/j.energy.2019.07.122
40. Cellat, K., Tezcan, F., Beyhan, B., Kardaş, G., and Paksoy, H. (2017): A comparative study on corrosion behavior of rebar in concrete with fatty acid additive as phase change material, Construction and Building Materials, 143, 490–500. https://doi.org/10.1016/j.conbuildmat.2017.03.165
41. Chaichan, M. T., Abaas, K. I., and Kazem, H. A. (2016): Design and assessment of solar concentrator distillating system using phase change materials (PCM) suitable for desertic weathers, Desalination and Water Treatment, 57(32), 14897–14907. https://doi.org/10.1080/19443994.2015.1069221
42. Chaichan, M. T., Zaidi, M. A. H., Kazem, H. A., and Sopian, K. (2022): Photovoltaic Module Electrical Efficiency Enhancement Using Nano Fluids and Nano-Paraffin, IOP Conference Series: Earth and Environmental Science, 961(1), 012065. https://doi.org/10.1088/1755-1315/961/1/012065
43. Chandel, S. S., and Agarwal, T. (2017): Review of current state of research on energy storage, toxicity, health hazards and commercialization of phase changing materials, Renewable and Sustainable Energy Reviews, 67, 581–596. https://doi.org/10.1016/j.rser.2016.09.070
44. Cheng, W., Xie, B., Zhang, R., Xu, Z., and Xia, Y. (2015): Effect of thermal conductivities

of shape stabilized PCM on under-floor heating system, Applied Energy, 144, 10–18. https://doi.org/10.1016/j.apenergy.2015.01.055

45. Costanzo, V., Evola, G., Marletta, L., and Nocera, F. (2018): The effectiveness of phase change materials in relation to summer thermal comfort in air-conditioned office buildings, Building Simulation, 11(6), 1145–1161. https://doi.org/10.1007/s12273-018-0468-2
46. Cui, H., Tang, W., Qin, Q., Xing, F., Liao, W., and Wen, H. (2017): Development of structural-functional integrated energy storage concrete with innovative macro-encapsulated PCM by hollow steel ball, Applied Energy, 185(2017), 107–118. https://doi.org/10.1016/j.apenergy.2016.10.072
47. D'Alessandro, A., Pisello, A. L., Fabiani, C., Ubertini, F., Cabeza, L. F., and Cotana, F. (2018): Multifunctional smart concretes with novel phase change materials: Mechanical and thermo-energy investigation, Applied Energy, 212(January), 1448–1461. https://doi.org/10.1016/j.apenergy.2018.01.014
48. Darvishi, F., Markarian, E., Ziasistani, Niloufar, Ziasistani, Nastaran, and Javanshir, A. (2019): Energy performance assessment of PCM buildings considering multiple factors, 5th International Conference on Power Generation Systems and Renewable Energy Technologies, PGSRET 2019, 1–5. https://doi.org/10.1109/PGSRET.2019.8882672
49. Drissi, S., Ling, T.-C., and Mo, K. H. (2019): Thermal efficiency and durability performances of paraffinic phase change materials with enhanced thermal conductivity–a review, Thermochimica Acta, 673, 198–210. https://doi.org/https://doi.org/10.1016/j.tca.2019.01.020
50. Elnajjar, E. (2017): Using PCM embedded in building material for thermal management: Performance assessment study, Energy and Buildings, 151, 28–34. https://doi.org/10.1016/j.enbuild.2017.06.010
51. Elsheniti, M. B., Hemedah, M. A., Sorour, M. M., and El-Maghlany, W. M. (2020): Novel enhanced conduction model for predicting performance of a PV panel cooled by PCM, Energy Conversion and Management, 205(January), 112456. https://doi.org/10.1016/j.enconman.2019.112456
52. Erlbeck, L., Schreiner, P., Schlachter, K., Dörnhofer, P., Fasel, F., Methner, F. J., and Rädle, M. (2018): Adjustment of thermal behavior by changing the shape of PCM inclusions in concrete blocks, Energy Conversion and Management, 158(October 2017), 256–265. https://doi.org/10.1016/j.enconman.2017.12.073
53. Essid, N., Eddhahak-Ouni, A., and Neji, J. (2020): Experimental and Numerical Thermal Properties Investigation of Cement-Based Materials Modified with PCM for Building Construction Use, Journal of Architectural Engineering, 26(3), 1–9. https://doi.org/10.1061/(ASCE)AE.1943-5568.0000399
54. Fallahi, A., Guldentops, G., Tao, M., Granados-Focil, S., and Van Dessel, S. (2017): Review on solid-solid phase change materials for thermal energy storage: Molecular structure and thermal properties, Applied Thermal Engineering, 127, 1427–1441. https://doi.org/10.1016/j.applthermaleng.2017.08.161
55. Fanger, P. O. (1970): *Thermal comfort: Analysis and applications in environmental engineering*. Copenhagen: Danish Technical Press. https://doi.org/ISBN:0898744466 9780898744460
56. Faraj, K., Khaled, M., Faraj, J., Hachem, F., and Castelain, C. (2020): Phase change material thermal energy storage systems for cooling applications in buildings: A review, Renewable and Sustainable Energy Reviews, 119(December 2018), 109579. https://doi.org/10.1016/j.rser.2019.109579
57. Fateh, A., Borelli, D., Devia, F., and Weinläder, H. (2018): Summer thermal performances of PCM-integrated insulation layers for light-weight building walls: Effect of orientation and melting point temperature, Thermal Science and Engineering Progress, 6(October 2017), 361–369. https://doi.org/10.1016/j.tsep.2017.12.012
58. Fateh, A., Klinker, F., Brütting, M., Weinläder, H., and Devia, F. (2017): Numerical and

experimental investigation of an insulation layer with phase change materials (PCMs), Energy and Buildings, 153, 231–240. https://doi.org/10.1016/j.enbuild.2017.08.007

59. Frazzica, A., Brancato, V., Palomba, V., La Rosa, D., Grungo, F., Calabrese, L., and Proverbio, E. (2019): Thermal performance of hybrid cement mortar-PCMs for warm climates application, Solar Energy Materials and Solar Cells, 193(December 2018), 270–280. https://doi.org/10.1016/j.solmat.2019.01.022
60. Frigione, M., Lettieri, M., and Sarcinella, A. (2019): Phase change materials for energy efficiency in buildings and their use in mortars, Materials, 12(8). https://doi.org/10.3390/ma12081260
61. Frota de Albuquerque Landi, F., Fabiani, C., and Pisello, A. L. (2020): Palm oil for seasonal thermal energy storage applications in buildings: The potential of multiple melting ranges in blends of bio-based fatty acids, Journal of Energy Storage, 29. https://doi.org/10.1016/j.est.2020.101431
62. Gan, V. J. L., Lo, I. M. C., Ma, J., Tse, K. T., Cheng, J. C. P., and Chan, C. M. (2020): Simulation optimisation towards energy efficient green buildings: Current status and future trends, Journal of Cleaner Production, 254, 120012. https://doi.org/https://doi.org/10.1016/j.jclepro.2020.120012
63. Garrido, P. L., Hurtado, P. I., and Nadrowski, B. (2001): Simple One-Dimensional Model of Heat Conduction which Obeys Fourier's Law, Phys. Rev. Lett., 86(24), 5486–5489. https://doi.org/10.1103/PhysRevLett.86.5486
64. Gassar, A. A. A., and Yun, G. Y. (2017): Energy saving potential of PCMs in buildings under future climate conditions, Applied Sciences (Switzerland), 7(12). https://doi.org/10.3390/app7121219
65. Gentilini, C., Franzoni, E., Graziani, G., and Bandini, S. (2015): Mechanical properties of fired-clay brick masonry models in moist and dry conditions, in Key Engineering Materials. Trans Tech Publ, 307–312. https://doi.org/https://doi.org/10.4028/www.scientific.net/KEM.624.307
66. Giro-Paloma, J., Barreneche, C., Martínez, M., Šumiga, B., Cabeza, L. F., and Fernández, A. I. (2015): Comparison of phase change slurries: Physicochemical and thermal properties, Energy, 87, 223–227. https://doi.org/10.1016/j.energy.2015.04.071
67. De Gracia, A. (2019): Dynamic building envelope with PCM for cooling purposes – Proof of concept, Applied Energy, 235(November 2018), 1245–1253. https://doi.org/10.1016/j.apenergy.2018.11.061
68. Guarino, F., Athienitis, A., Cellura, M., and Bastien, D. (2017): PCM thermal storage design in buildings: Experimental studies and applications to solaria in cold climates, Applied Energy, 185, 95–106. https://doi.org/https://doi.org/10.1016/j.apenergy.2016.10.046
69. Habib, N. A., Ali, A. J., Chaichan, M. T., and Kareem, M. (2021): Carbon nanotubes/paraffin wax nanocomposite for improving the performance of a solar air heating system, Thermal Science and Engineering Progress, 23, 100877. https://doi.org/https://doi.org/10.1016/j.tsep.2021.100877
70. Hagenau, M., and Jradi, M. (2020): Dynamic modeling and performance evaluation of building envelope enhanced with phase change material under Danish conditions, Journal of Energy Storage, 30, 101536. https://doi.org/10.1016/j.est.2020.101536
71. Hasan, M. I. (2017): Improving the cooling performance of electrical distribution transformer using transformer oil – Based MEPCM suspension, Engineering Science and Technology, an International Journal, 20(2), 502–510. https://doi.org/https://doi.org/10.1016/j.jestch.2016.12.003
72. Hasan, M. I., and Abduladheem, A. A. (2019): Modifying the thermal performance of electrical distribution transformers using phase change materials (paraffin wax), Heat Transfer—Asian Research, 48(6), 2440–2455. https://doi.org/https://doi.org/10.1002/htj.21503

73. Hasan, M. I., Basher, H. O., and Shdhan, A. O. (2018): Experimental investigation of phase change materials for insulation of residential buildings, Sustainable Cities and Society, 36(October 2017), 42–58. https://doi.org/10.1016/j.scs.2017.10.009
74. Hirmiz, R., Teamah, H. M., Lightstone, M. F., and Cotton, J. S. (2020): Analytical and numerical sizing of phase change material thickness for rectangular encapsulations in hybrid thermal storage tanks for residential heat pump systems, Applied Thermal Engineering, 170(January), 114978. https://doi.org/10.1016/j.applthermaleng.2020.114978
75. Höhlein, S., König-Haagen, A., and Brüggemann, D. (2018): Macro-Encapsulation of Inorganic Phase-Change Materials (PCM) in Metal Capsules, Materials, 11(9), 1752. https://doi.org/10.3390/ma11091752
76. Holman, J. P. (2011): *Heat transfer*. 10th edn, Mc-GrawHill Higher education. 10th edn. Edited by Bill Stenquist. MC GRAW HILL INDIA. Available at: https://www.academia.edu/36379481/Heat_Transfer_Tenth_Edition_Jack_P_Holman_
77. Hu, J., and Yu, X. (2019): Thermo and light-responsive building envelope: Energy analysis under different climate conditions, Solar Energy, 193(August), 866–877. https://doi.org/10.1016/j.solener.2019.10.021
78. Hu, J., and Yu, X. (Bill) (2020): Adaptive building roof by coupling thermochromic material and phase change material: Energy performance under different climate conditions, Construction and Building Materials, 262, 120481. https://doi.org/10.1016/j.conbuildmat.2020.120481
79. IEA (International Energy Agency) (2018): *The future of cooling: opportunities for energy-efficient air conditioning*, IEA. Available at: https://pronto-core-cdn.prontomarketing.com/449/wp-content/uploads/sites/2/2018/06/Melanie-Slade-The-Future-of-Cooling-Opportunities-for-Energy-Efficient-Air-Conditioning.pdf
80. IEA (International Energy Agency) (2020): *Data and statistics: CO2 emissions*. Available at: https://www.iea.org/data-and-statistics/data-browser?country=IRAQ&fuel=CO2 emissions&indicator=ElecIndex
81. IEA (International Energy Agency), and UN Environment Programme (2019): *2019 global status report for buildings and construction: Towards a zero-emission, efficient and resilient buildings and construction sector*. Available at: https://www.worldgbc.org/news-media/2019-global-status-report-buildings-and-construction
82. Imghoure, O., Belouaggadia, N., Ezzine, M., Lbibb, R., and Younsi, Z. (2021): Performance evaluation of phase change materials for thermal comfort in a hot climate region, Applied Thermal Engineering, 186, 116509. https://doi.org/https://doi.org/10.1016/j.applthermaleng.2020.116509
83. *Iraq electricity prices* (2021): Available at: https://www.globalpetrolprices.com/Iraq/electricity_prices/#:~:text=Iraq%2C December 2021%3A The price,of power%2C distribution and taxes.
84. Javadi, F. S., Metselaar, H. S. C., and Ganesan, P. (2020): Performance improvement of solar thermal systems integrated with phase change materials (PCM), a review, Solar Energy, 206, 330–352. https://doi.org/https://doi.org/10.1016/j.solener.2020.05.106
85. Jelle, B. P., and Kalnæs, S. E. (2017): Phase Change Materials for Application in Energy-Efficient Buildings, in Cost-Effective Energy Efficient Building Retrofitting: Materials, Technologies, Optimization and Case Studies. Elsevier Ltd, 57–118. https://doi.org/10.1016/B978-0-08-101128-7.00003-4
86. Jeong, S. G., Wi, S., Chang, S. J., Lee, J., and Kim, S. (2019): An experimental study on applying organic PCMs to gypsum-cement board for improving thermal performance of buildings in different climates, Energy and Buildings, 190, 183–194. https://doi.org/10.1016/j.enbuild.2019.02.037
87. Jia, C., Geng, X., Liu, F., and Gao, Y. (2021): Thermal behavior improvement of hollow sintered bricks integrated with both thermal insulation material (TIM) and Phase-Change

Material (PCM), Case Studies in Thermal Engineering, 25(March), 100938. https://doi.org/10.1016/j.csite.2021.100938

88. Jin, X., Medina, M. A., and Zhang, X. (2016): Numerical analysis for the optimal location of a thin PCM layer in frame walls, Applied Thermal Engineering, 103, 1057–1063. https://doi.org/10.1016/j.applthermaleng.2016.04.056
89. Kant, K., Shukla, A., and Sharma, A. (2017): Heat transfer studies of building brick containing phase change materials, Solar Energy, 155, 1233–1242. https://doi.org/10.1016/j.solener.2017.07.072
90. Kenzhekhanov, S., Memon, S. A., and Adilkhanova, I. (2020): Quantitative evaluation of thermal performance and energy saving potential of the building integrated with PCM in a subarctic climate, Energy, 192, 116607. https://doi.org/https://doi.org/10.1016/j.energy.2019.116607
91. Kharbouch, Y., Ouhsaine, L., Mimet, A., and El Ganaoui, M. (2018): Thermal performance investigation of a PCM-enhanced wall/roof in northern Morocco, Building Simulation, 11(6), 1083–1093. https://doi.org/10.1007/s12273-018-0449-5
92. Khdair, A. I., Abu Rumman, G., and Basha, M. (2022): Developing building enhanced with PCM to reduce energy consumption, Journal of Building Engineering, 48, 103923. https://doi.org/https://doi.org/10.1016/j.jobe.2021.103923
93. Kishore, R. A., Bianchi, M. V. A. A., Booten, C., Vidal, J., and Jackson, R. (2020): Optimizing PCM-Integrated Walls for Potential Energy Savings in US Buildings, Energy and Buildings, 226, 110355. https://doi.org/https://doi.org/10.1016/j.enbuild.2020.110355
94. Kishore, R. A., Bianchi, M. V. A., Booten, C., Vidal, J., and Jackson, R. (2021): Enhancing building energy performance by effectively using phase change material and dynamic insulation in walls, Applied Energy, 283, 116306. https://doi.org/10.1016/j.apenergy.2020.116306
95. Kong, X., Wang, L., Li, H., Yuan, G., and Yao, C. (2020): Experimental study on a novel hybrid system of active composite PCM wall and solar thermal system for clean heating supply in winter, Solar Energy, 195(February 2019), 259–270. https://doi.org/10.1016/j.solener.2019.11.081
96. Kontoleon, K. J., Stefanidou, M., Saboor, S., Mazzeo, D., Karaoulis, A., Zegginis, D., and Kraniotis, D. (2021): Defensive behaviour of building envelopes in terms of mechanical and thermal responsiveness by incorporating PCMs in cement mortar layers, Sustainable Energy Technologies and Assessments, 47, 101349. https://doi.org/https://doi.org/10.1016/j.seta.2021.101349
97. *Köppen climate classification* (2022): Available at: https://www.weatherbase.com/weather/weather-summary.php3?s=56604&cityname=Al+Amarah%2C+Maysan%2C+Iraq&units=
98. Korosec, M. (2021): *A record-breaking heatwave with almost +50 °C across the Middle East, the Arabian peninsula, and the Caucasus, forecast to head into Iran and Pakistan this week*, Global weather. Available at: https://www.severe-weather.eu/global-weather/record-breaking-heatwave-russia-middle-east-arabian-peninsula-mk/#
99. Köse Murathan, E., and Manioğlu, G. (2020): Evaluation of phase change materials used in building components for conservation of energy in buildings in hot dry climatic regions, Renewable Energy, 162, 1919–1930. https://doi.org/https://doi.org/10.1016/j.renene.2020.09.086
100. Kośny, J. (2015): PCM-Enhanced Building Components: An Application of Phase Change Materials in Building Envelopes and Internal Structures. Edited by Brian Derby. Springer. https://doi.org/10.1007/978-3-319-14286-9
101. Koukou, M. K., Dogkas, G., Vrachopoulos, M. G., Konstantaras, J., Pagkalos, C., Stathopoulos, V. N., Pandis, P. K., Lymperis, K., Coelho, L., and Rebola, A. (2020): Experimental assessment of a full scale prototype thermal energy storage tank using paraffin for space heating application, International Journal of Thermofluids, 1–2, 100003.

https://doi.org/10.1016/j.ijft.2019.100003
102. Kumar, S., Arun Prakash, S., Pandiyarajan, V., Geetha, N. B., Antony Aroul Raj, V., and Velraj, R. (2019): Effect of phase change material integration in clay hollow brick composite in building envelope for thermal management of energy efficient buildings, Journal of Building Physics, 43(4), 351–364. https://doi.org/10.1177/1744259119867462
103. Kusama, Y., and Ishidoya, Y. (2017): Thermal effects of a novel phase change material (PCM) plaster under different insulation and heating scenarios, Energy and Buildings, 141, 226–237. https://doi.org/10.1016/j.enbuild.2017.02.033
104. Laaouatni, A., Martaj, N., Bennacer, R., Lachi, M., El Omari, M., and El Ganaoui, M. (2019): Thermal building control using active ventilated block integrating phase change material, Energy and Buildings, 187, 50–63. https://doi.org/10.1016/j.enbuild.2019.01.024
105. Lagou, A., Kylili, A., Šadauskienė, J., and Fokaides, P. A. (2019): Numerical investigation of phase change materials (PCM) optimal melting properties and position in building elements under diverse conditions, Construction and Building Materials, 225, 452–464. https://doi.org/10.1016/j.conbuildmat.2019.07.199
106. Lakhdari, Y. A., and Chikh, S. (2019): Integration of Phase Change Materials in Traditional Building for Cooling Purposes Under Mediterranean Climate, SSRN Electronic Journal, (November). https://doi.org/10.2139/ssrn.3371764
107. Lei, J., Yang, J., and Yang, E.-H. (2016): Energy performance of building envelopes integrated with phase change materials for cooling load reduction in tropical Singapore, Applied Energy, 162, 207–217. https://doi.org/https://doi.org/10.1016/j.apenergy.2015.10.031
108. Li, C., Yu, H., Song, Y., Tang, Y., Chen, P., Hu, H., Wang, M., and Liu, Z. (2020): Experimental thermal performance of wallboard with hybrid microencapsulated phase change materials for building application, Journal of Building Engineering, 28(June 2019), 101051. https://doi.org/10.1016/j.jobe.2019.101051
109. Li, D., Wu, Y., Liu, C., Zhang, G., and Arıcı, M. (2018): Energy investigation of glazed windows containing Nano-PCM in different seasons, Energy Conversion and Management, 172(April), 119–128. https://doi.org/10.1016/j.enconman.2018.07.015
110. Li, M., and shi, J. (2021): Mechanical and thermal performance assessment of paraffin/expanded vermiculite-diatomite composite phase change materials integrated mortar: Experimental and numerical approach, Solar Energy, 227, 343–353. https://doi.org/https://doi.org/10.1016/j.solener.2021.09.014
111. Li, Z. X., Al-Rashed, A. A. A. A., Rostamzadeh, M., Kalbasi, R., Shahsavar, A., and Afrand, M. (2019): Heat transfer reduction in buildings by embedding phase change material in multi-layer walls: Effects of repositioning, thermophysical properties and thickness of PCM, Energy Conversion and Management, 195(April), 43–56. https://doi.org/10.1016/j.enconman.2019.04.075
112. Liu, T. *et al.* (2021): Ambient Temperature and Years of Life Lost: A National Study in China, The Innovation, 2(1), 100072. https://doi.org/https://doi.org/10.1016/j.xinn.2020.100072
113. Liu, Z., Yu, Z. (Jerry), Yang, T., Qin, D., Li, S., Zhang, G., Haghighat, F., and Joybari, M. M. (2018): A review on macro-encapsulated phase change material for building envelope applications, Building and Environment, 144(August), 281–294. https://doi.org/10.1016/j.buildenv.2018.08.030
114. Lu, S., Li, Y., Kong, X., Pang, B., Chen, Y., Zheng, S., and Sun, L. (2017): A Review of PCM Energy Storage Technology Used in Buildings for the Global Warming Solution, in Zhang, X. and Dincer, I. (eds) Energy Solutions to Combat Global Warming. Cham: Springer International Publishing, 611–644. https://doi.org/10.1007/978-3-319-26950-4_31
115. Lu, S., Xu, B., and Tang, X. (2020): Experimental study on double pipe PCM floor heating system under different operation strategies, Renewable Energy, 145, 1280–1291.

https://doi.org/10.1016/j.renene.2019.06.086
116. Mazzeo, D., and Kontoleon, K. J. (2020): The role of inclination and orientation of different building roof typologies on indoor and outdoor environment thermal comfort in Italy and Greece, Sustainable Cities and Society, 60(January), 102111. https://doi.org/10.1016/j.scs.2020.102111
117. Mazzeo, D., Oliveti, G., and Arcuri, N. (2017): Definition of a new set of parameters for the dynamic thermal characterization of PCM layers in the presence of one or more liquid-solid interfaces, Energy and Buildings, 141, 379–396. https://doi.org/10.1016/j.enbuild.2017.02.027
118. Mendecka, B., Cozzolino, R., Leveni, M., and Bella, G. (2019): Energetic and exergetic performance evaluation of a solar cooling and heating system assisted with thermal storage, Energy, 176, 816–829. https://doi.org/10.1016/j.energy.2019.04.024
119. Meng, E., Yu, H., and Zhou, B. (2017): Study of the thermal behavior of the composite phase change material (PCM) room in summer and winter, Applied Thermal Engineering, 126, 212–225. https://doi.org/https://doi.org/10.1016/j.applthermaleng.2017.07.110
120. Mevada, D., Panchal, H., Sadasivuni, K. kumar, Israr, M., Suresh, M., Dharaskar, S., and Thakkar, H. (2020): Effect of fin configuration parameters on performance of solar still: A review, Groundwater for Sustainable Development, 10(October 2019), 100289. https://doi.org/10.1016/j.gsd.2019.100289
121. Milián, Y. E., Gutiérrez, A., Grágeda, M., and Ushak, S. (2017): A review on encapsulation techniques for inorganic phase change materials and the influence on their thermophysical properties, Renewable and Sustainable Energy Reviews, 73(December 2016), 983–999. https://doi.org/10.1016/j.rser.2017.01.159
122. *Ministry of Construction and Housing- Minstry of Planning,Thermal Insulation Blog (Iraqi Construction Blog)* (2013): Available at: https://amanatbaghdad.gov.iq/amanarules/pict/مدونات/blog20-مدونة العزل الحراري.pdf
123. *Ministry of Oil, Midland Refineries Company* (2022): Available at: https://mrc.oil.gov.iq/?dispatch
124. Nada, S. A., Alshaer, W. G., and Saleh, R. M. (2020): Experimental investigation of PCM transient performance in free cooling of the fresh air of air conditioning systems, Journal of Building Engineering, 29, 101153
125. Navarro, L., Gracia, A. de, Castell, A., and Cabeza, L. F. (2016): Experimental study of an active slab with PCM coupled to a solar air collector for heating purposes, Energy and Buildings, 128, 12–21. https://doi.org/10.1016/j.enbuild.2016.06.069
126. Navarro, L., Solé, A., Martín, M., Barreneche, C., Olivieri, L., Tenorio, J. A., and Cabeza, L. F. (2019): Benchmarking of useful phase change materials for a building application, Energy and Buildings, 182, 45–50. https://doi.org/10.1016/j.enbuild.2018.10.005
127. Nicholas, A. F., Hussein, M. Z., Zainal, Z., and Khadiran, T. (2018): Activated carbon for shape-stabilized phase change material, in Synthesis, Technology and Applications of Carbon Nanomaterials. Elsevier Inc., 279–308. https://doi.org/10.1016/B978-0-12-815757-2.00013-9
128. Nurlybekova, G., Memon, S. A., and Adilkhanova, I. (2021): Quantitative evaluation of the thermal and energy performance of the PCM integrated building in the subtropical climate zone for current and future climate scenario, Energy, 219, 119587. https://doi.org/https://doi.org/10.1016/j.energy.2020.119587
129. Ortega Del Rosario, M. D. L. Á., Chen Austin, M., Bruneau, D., Nadeau, J.-P., Sébastian, P., and Jaupard, D. (2020): Operation assessment of an air-PCM unit for summer thermal comfort in a naturally ventilated building, Architectural Science Review, 1–10. https://doi.org/https://doi.org/10.1080/00038628.2020.1794782
130. Ostrý, M., Bantová, S., and Struhala, K. (2020): Compatibility of Phase Change Materials and Metals: Experimental Evaluation Based on the Corrosion Rate, Molecules, 25(12), 2823. https://doi.org/10.3390/molecules25122823

131. Pasupathy, A., Velraj, R., and Seeniraj, R. V. (2008): Phase change material-based building architecture for thermal management in residential and commercial establishments, Renewable and Sustainable Energy Reviews, 12(1), 39–64. https://doi.org/10.1016/j.rser.2006.05.010
132. Pereira da Cunha, J., and Eames, P. (2016): Thermal energy storage for low and medium temperature applications using phase change materials - A review, Applied Energy, 177, 227–238. https://doi.org/10.1016/j.apenergy.2016.05.097
133. Piselli, C., Castaldo, V. L., and Pisello, A. L. (2019): How to enhance thermal energy storage effect of PCM in roofs with varying solar reflectance: Experimental and numerical assessment of a new roof system for passive cooling in different climate conditions, Solar Energy, 192(January 2018), 106–119. https://doi.org/10.1016/j.solener.2018.06.047
134. Piselli, C., Prabhakar, M., de Gracia, A., Saffari, M., Pisello, A. L., and Cabeza, L. F. (2020): Optimal control of natural ventilation as passive cooling strategy for improving the energy performance of building envelope with PCM integration, Renewable Energy, 162, 171–181. https://doi.org/https://doi.org/10.1016/j.renene.2020.07.043
135. Plytaria, M. T., Tzivanidis, C., Bellos, E., Alexopoulos, I., and Antonopoulos, K. A. (2019): Thermal behavior of a building with incorporated phase change materials in the South and the North Wall, Computation, 7(1). https://doi.org/10.3390/computation7010002
136. PureTemp Company (2020): *PureTemp ® Thermal Energy Storage Materials PureTemp 48 Technical Information*. Available at: https://www.puretemp.com/stories/puretemp-23-tds
137. Qureshi, Z. A., Ali, H. M., and Khushnood, S. (2018): Recent advances on thermal conductivity enhancement of phase change materials for energy storage system: A review, International Journal of Heat and Mass Transfer, 127, 838–856. https://doi.org/10.1016/j.ijheatmasstransfer.2018.08.049
138. Rai, A. C. (2021): Energy performance of phase change materials integrated into brick masonry walls for cooling load management in residential buildings, Building and Environment, 199, 107930. https://doi.org/https://doi.org/10.1016/j.buildenv.2021.107930
139. Ramakrishnan, S., Sanjayan, J., and Wang, X. (2019): Experimental Research on Using Form-stable PCM-Integrated Cementitious Composite for Reducing Overheating in Buildings, Buildings, 9(3), 57. https://doi.org/10.3390/buildings9030057
140. Ramakrishnan, S., Wang, X., Sanjayan, J., and Wilson, J. (2017a): Thermal performance assessment of phase change material integrated cementitious composites in buildings: Experimental and numerical approach, Applied Energy, 207, 654–664. https://doi.org/https://doi.org/10.1016/j.apenergy.2017.05.144
141. Ramakrishnan, S., Wang, X., Sanjayan, J., and Wilson, J. (2017b): Thermal performance of buildings integrated with phase change materials to reduce heat stress risks during extreme heatwave events, Applied Energy, 194, 410–421. https://doi.org/https://doi.org/10.1016/j.apenergy.2016.04.084
142. Rao, V. V., Parameshwaran, R., and Ram, V. V. (2018): PCM-mortar based construction materials for energy efficient buildings: A review on research trends, Energy and Buildings, 158, 95–122. https://doi.org/10.1016/j.enbuild.2017.09.098
143. Rathore, P. K. S., and Shukla, S. K. (2019): Potential of macroencapsulated PCM for thermal energy storage in buildings: A comprehensive review, Construction and Building Materials, 225, 723–744. https://doi.org/10.1016/j.conbuildmat.2019.07.221
144. Rathore, P. K. S., and Shukla, S. K. (2020): An experimental evaluation of thermal behavior of the building envelope using macroencapsulated PCM for energy savings, Renewable Energy, 149, 1300–1313. https://doi.org/10.1016/j.renene.2019.10.130
145. Rathore, P. K. S., Shukla, S. K., and Gupta, N. K. (2020): Yearly analysis of peak temperature, thermal amplitude, time lag and decrement factor of a building envelope in

tropical climate, Journal of Building Engineering, 31(April), 101459. https://doi.org/10.1016/j.jobe.2020.101459

146. Ren, Q., Guo, P., and Zhu, J. (2020): Thermal management of electronic devices using pin-fin based cascade microencapsulated PCM/expanded graphite composite, International Journal of Heat and Mass Transfer, 149, 1–16. https://doi.org/10.1016/j.ijheatmasstransfer.2019.119199
147. Resan, S. F., Chassib, S. M., Zemam, S. K., and Madhi, M. J. (2020): New approach of concrete tensile strength test, Case Studies in Construction Materials, 12, 1–13. https://doi.org/10.1016/j.cscm.2020.e00347
148. Rommel, M., Hauer, A., and Van Helden, W. (2015): Compact Thermal Energy Storage: Material Development for System Integration, (August). Available at: http://task42.iea-shc.org/data/sites/1/publications/Task42-Annex-29-Position-Paper-and-All-Final-Deliverable-Papers.pdf
149. Rucevskis, S., Akishin, P., and Korjakins, A. (2019): Performance Evaluation of an Active PCM Thermal Energy Storage System for Space Cooling in Residential Buildings, Environmental and Climate Technologies, 23(2), 74–89
150. Saffari, M., de Gracia, A., Ushak, S., and Cabeza, L. F. (2017): Passive cooling of buildings with phase change materials using whole-building energy simulation tools: A review, Renewable and Sustainable Energy Reviews, 80, 1239–1255. https://doi.org/https://doi.org/10.1016/j.rser.2017.05.139
151. Saikia, P., Azad, A. S., and Rakshit, D. (2018): Thermal performance evaluation of building roofs embedded PCM for multi-climatic zones, Green Energy and Technology, (9789811071874), 401–423. https://doi.org/10.1007/978-981-10-7188-1_18
152. Saikia, P., Pancholi, M., Sood, D., and Rakshit, D. (2020): Dynamic optimization of multi-retrofit building envelope for enhanced energy performance with a case study in hot Indian climate, Energy, 197, 117263. https://doi.org/https://doi.org/10.1016/j.energy.2020.117263
153. Salgado, R., Akbari, H., Brown, M. C., Reid, I., and McCormack, S. J. (2020): Study of Corrosion Effect of Micronal® Phase Change Materials (PCM) with Different Metal Samples, in Renewable Energy and Sustainable Buildings. Springer, 709–717
154. Saxena, R., Rakshit, D., and Kaushik, S. C. (2019): Phase change material (PCM) incorporated bricks for energy conservation in composite climate: A sustainable building solution, Solar Energy, 183(October 2018), 276–284. https://doi.org/10.1016/j.solener.2019.03.035
155. Saxena, R., Rakshit, D., and Kaushik, S. C. (2020): Experimental assessment of Phase Change Material (PCM) embedded bricks for passive conditioning in buildings, Renewable Energy, 149, 587–599. https://doi.org/10.1016/j.renene.2019.12.081
156. Sharma, A., and Sengar, N. (2019): Heat Gain Study of a Residential Building in Hot-Dry Climatic Zone on Basis of Three Cooling Load Methods, European Journal of Engineering Research and Science, 4(9), 186–194. https://doi.org/10.24018/ejers.2019.4.9.1508
157. Silva, T., Vicente, R., Amaral, C., and Figueiredo, A. (2016): Thermal performance of a window shutter containing PCM: Numerical validation and experimental analysis, Applied Energy, 179, 64–84. https://doi.org/10.1016/j.apenergy.2016.06.126
158. Singh Rathore, P. K., Shukla, S. K., and Gupta, N. K. (2020): Potential of microencapsulated PCM for energy savings in buildings: A critical review, Sustainable Cities and Society, 53, 101884. https://doi.org/10.1016/j.scs.2019.101884
159. Solgi, E., Hamedani, Z., Fernando, R., and Mohammad Kari, B. (2019): A parametric study of phase change material characteristics when coupled with thermal insulation for different Australian climatic zones, Building and Environment, 163, 106317. https://doi.org/https://doi.org/10.1016/j.buildenv.2019.106317
160. Soliman, A. R. V. E.-F. S. (2020): Paraffin as Phase Change Material, in. Rijeka: IntechOpen, Ch. 5. https://doi.org/10.5772/intechopen.90487

161. Song, S., Qiu, F., Zhu, W., Guo, Y., Zhang, Y., Ju, Y., Feng, R., Liu, Y., Chen, Z., and Zhou, J. (2019): Polyethylene glycol/halloysite@ Ag nanocomposite PCM for thermal energy storage: simultaneously high latent heat and enhanced thermal conductivity, Solar Energy Materials and Solar Cells, 193, 237–245. https://doi.org/https://doi.org/10.1016/j.solmat.2019.01.023
162. Souayfane, F., Fardoun, F., and Biwole, P. H. (2016): Phase change materials (PCM) for cooling applications in buildings: A review, Energy and Buildings, 129, 396–431. https://doi.org/10.1016/j.enbuild.2016.04.006
163. Soudian, S., and Berardi, U. (2019): Assessing the effect of night ventilation on PCM performance in high-rise residential buildings, Journal of Building Physics, 43(3), 229–249. https://doi.org/10.1177/1744259119848128
164. Sovetova, M., Memon, S. A., and Kim, J. (2019a): Energy savings of PCM-incorporated building in hot dry climate, Key Engineering Materials, 821 KEM, 518–524. https://doi.org/10.4028/www.scientific.net/KEM.821.518
165. Sovetova, M., Memon, S. A., and Kim, J. (2019b): Thermal performance and energy efficiency of building integrated with PCMs in hot desert climate region, Solar Energy, 189, 357–371. https://doi.org/10.1016/j.solener.2019.07.067
166. Su, W., Darkwa, J., and Kokogiannakis, G. (2020): Numerical thermal evaluation of laminated binary microencapsulated phase change material drywall systems, Building Simulation, 13(1), 89–98. https://doi.org/10.1007/s12273-019-0563-z
167. Sun, X., Chu, Y., Medina, M. A., Mo, Y., Fan, S., and Liao, S. (2019): Experimental investigations on the thermal behavior of phase change material (PCM) in ventilated slabs, Applied Thermal Engineering, 148(December 2018), 1359–1369. https://doi.org/10.1016/j.applthermaleng.2018.12.032
168. Sun, X., Jovanovic, J., Zhang, Y., Fan, S., Chu, Y., Mo, Y., and Liao, S. (2019): Use of encapsulated phase change materials in lightweight building walls for annual thermal regulation, Energy, 180, 858–872. https://doi.org/10.1016/j.energy.2019.05.112
169. Sun, X., Medina, M. A., Lee, K. O., and Jin, X. (2018): Laboratory assessment of residential building walls containing pipe-encapsulated phase change materials for thermal management, Energy, 163, 383–391. https://doi.org/10.1016/j.energy.2018.08.159
170. Suresh, C., Kumar Hotta, T., and Saha, S. K. (2022): Phase change material incorporation techniques in building envelopes for enhancing the building thermal Comfort-A review, Energy and Buildings, 268, 112225. https://doi.org/https://doi.org/10.1016/j.enbuild.2022.112225
171. Syath Abuthakeer, S., Arunkumar, D., Ramu, M., and Sripriyan, K. (2023): Numerical Investigation on Phase Change Material (PCM) for Thermal Management Buildings Using Design-Builder Software BT - Advances in Forming, Machining and Automation, in Dixit, U. S., Kanthababu, M., Ramesh Babu, A., and Udhayakumar, S. (eds). Singapore: Springer Nature Singapore, 617–629
172. Thiele, A. M., Liggett, R. S., Sant, G., and Pilon, L. (2017): Simple thermal evaluation of building envelopes containing phase change materials using a modified admittance method, Energy and Buildings, 145, 238–250. https://doi.org/https://doi.org/10.1016/j.enbuild.2017.03.046
173. Thongtha, A., Khongthon, A., Boonsri, T., and Hoy-Yen, C. (2019): Thermal effectiveness enhancement of autoclaved aerated concrete wall with PCM-contained conical holes to reduce the cooling load, Materials, 12(13), 2170. https://doi.org/10.3390/ma12132170
174. Touma, A. Al, and Ouahrani, D. (2018): Improved human thermal comfort with indoor PCM-Enhanced tiles in living spaces in the arabian gulf, E3S Web of Conferences, 57, 04001. https://doi.org/10.1051/e3sconf/20185704001
175. Toure, P. M., Dieye, Y., Gueye, P. M., Sambou, V., Bodian, S., and Tiguampo, S. (2019): Experimental determination of time lag and decrement factor, Case Studies in Construction Materials, 11, e00298. https://doi.org/10.1016/j.cscm.2019.e00298

176. Tunçbilek, E., Arıcı, M., Bouadila, S., and Wonorahardjo, S. (2020): Seasonal and annual performance analysis of PCM-integrated building brick under the climatic conditions of Marmara region, Journal of Thermal Analysis and Calorimetry, 141(0123456789), 613–624. https://doi.org/10.1007/s10973-020-09320-8
177. Tyagi, V. V., Pandey, A. K., Buddhi, D., and Kothari, R. (2016): Thermal performance assessment of encapsulated PCM based thermal management system to reduce peak energy demand in buildings, Energy and Buildings, 117, 44–52. https://doi.org/10.1016/j.enbuild.2016.01.042
178. Uludaş, M. Ç., Tunçbilek, E., Yıldız, Ç., Arıcı, M., Li, D., and Krajčík, M. (2022): PCM-enhanced sunspace for energy efficiency and CO2 mitigation in a house in mediterranean climate, Journal of Building Engineering, 57, 104856. https://doi.org/https://doi.org/10.1016/j.jobe.2022.104856
179. Ürge-Vorsatz, D., Cabeza, L. F., Serrano, S., Barreneche, C., and Petrichenko, K. (2015): Heating and cooling energy trends and drivers in buildings, Renewable and Sustainable Energy Reviews, 41, 85–98. https://doi.org/10.1016/j.rser.2014.08.039
180. Vukadinović, A., Radosavljević, J., and Đorđević, A. (2020): Energy performance impact of using phase-change materials in thermal storage walls of detached residential buildings with a sunspace, Solar Energy, 206, 228–244. https://doi.org/https://doi.org/10.1016/j.solener.2020.06.008
181. Wahid, M. A., Hosseini, S. E., Hussen, H. M., Akeiber, H. J., Saud, S. N., and Mohammad, A. T. (2017): An overview of phase change materials for construction architecture thermal management in hot and dry climate region, Applied Thermal Engineering, 112, 1240–1259. https://doi.org/https://doi.org/10.1016/j.applthermaleng.2016.07.032
182. Wang, H., Lu, W., Wu, Z., and Zhang, G. (2020): Parametric analysis of applying PCM wallboards for energy saving in high-rise lightweight buildings in Shanghai, Renewable Energy, 145, 52–64. https://doi.org/https://doi.org/10.1016/j.renene.2019.05.124
183. Wi, S., Yang, S., Park, J. H., Chang, S. J., and Kim, S. (2020): Climatic cycling assessment of red clay/perlite and vermiculite composite PCM for improving thermal inertia in buildings, Building and Environment, 167, 106464. https://doi.org/https://doi.org/10.1016/j.buildenv.2019.106464
184. Wu, Q., Wang, J., and Meng, X. (2021): Influence of wall thermal performance on the contribution efficiency of the Phase-Change Material (PCM) layer, Case Studies in Thermal Engineering, 28, 101398. https://doi.org/https://doi.org/10.1016/j.csite.2021.101398
185. Yan, T., Sun, Z., Gao, J., Xu, X., Yu, J., and Gang, W. (2020): Simulation study of a pipe-encapsulated PCM wall system with self-activated heat removal by nocturnal sky radiation, Renewable Energy, 146, 1451–1464. https://doi.org/10.1016/j.renene.2019.07.060
186. Ye, R., Huang, R., Fang, X., and Zhang, Z. (2020): Simulative optimization on energy saving performance of phase change panels with different phase transition temperatures, Sustainable Cities and Society, 52, 101833. https://doi.org/https://doi.org/10.1016/j.scs.2019.101833
187. Yoon, S. G., Yang, Y. K., Kim, T. W., Chung, M. H., and Park, J. C. (2018): Thermal Performance Test of a Phase-Change-Material Cool Roof System by a Scaled Model, Advances in Civil Engineering, 2018, 2646103. https://doi.org/10.1155/2018/2646103
188. Younsi, Z., and Naji, H. (2020): Numerical simulation and thermal performance of hybrid brick walls embedding a phase change material for passive building applications, Journal of Thermal Analysis and Calorimetry, 140(3), 965–978. https://doi.org/10.1007/s10973-019-08950-x
189. Yu, J., Leng, K., Ye, H., Xu, X., Luo, Y., Wang, J., Yang, X., Yang, Q., and Gang, W. (2020): Study on thermal insulation characteristics and optimized design of pipe-embedded ventilation roof with outer-layer shape-stabilized PCM in different climate

zones, Renewable Energy, 147, 1609–1622. https://doi.org/10.1016/j.renene.2019.09.115
190. Yu, J., Yang, Q., Ye, H., Huang, J., Liu, Y., and Tao, J. (2019): The optimum phase transition temperature for building roof with outer layer PCM in different climate regions of China, Energy Procedia, 158, 3045–3051. https://doi.org/10.1016/j.egypro.2019.01.989
191. Yun, H. Do, Ahn, K. L., Jang, S. J., Khil, B. S., Park, W. S., and Kim, S. W. (2019): Thermal and Mechanical Behaviors of Concrete with Incorporation of Strontium-Based Phase Change Material (PCM), International Journal of Concrete Structures and Materials, 13(1). https://doi.org/10.1186/s40069-018-0326-8
192. Zhang, Y., Huang, J., Fang, X., Ling, Z., and Zhang, Z. (2020): Optimal roof structure with multilayer cooling function materials for building energy saving, International Journal of Energy Research, 44(3), 1594–1606. https://doi.org/10.1002/er.4969
193. Zhang, Y., Zhuang, S., Wang, Q., and He, J. (2016): Experimental Research on the Thermal Performance of Composite PCM Hollow Block Walls and Validation of Phase Transition Heat Transfer Models, Advances in Materials Science and Engineering. Edited by F. Lusquiños, 2016, 6359414. https://doi.org/10.1155/2016/6359414
194. Zhu, N., Li, S., Hu, P., Lei, F., and Deng, R. (2019): Numerical investigations on performance of phase change material Trombe wall in building, Energy, 187, 116057. https://doi.org/10.1016/j.energy.2019.116057

A2: Publications related to the dissertation

Refereed papers in foreign languages:

1. **Al-Yasiri, Q.**, Szabó, M. (2021): Incorporation of phase change materials into building envelope for thermal comfort and energy saving: A comprehensive analysis, Journal of Building Engineering, Vol. 36, pp. 102122. ISSN 2352-7102. https://doi.org/10.1016/j.jobe.2020.102122 (Scopus: Q1/D1, IF: 7.144).
2. **Al-Yasiri, Q.**, Szabó, M. (2021): Influential aspects on melting and solidification of PCM energy storage containers in building envelope applications, International Journal of Green Energy, Vol. 18, No. 9, ISSN 1543-5083. https://doi.org/10.1080/15435075.2021.1890082 (Scopus: Q2, IF: 2.642).
3. **Al-Yasiri, Q.**, Szabó, M. (2021): Experimental investigation of phase change material incorporated composite flat roof for energy-saving under Iraq hot climatic conditions, AIP Conference Proceedings, Vol. 2404, pp. 080015, ISSN 1551-7616. https://doi.org/10.1063/5.0069010 (Scopus: Q4).
4. **Al-Yasiri, Q.**, Szabó, M. (2021): Experimental evaluation of the optimal position of a macroencapsulated phase change material incorporated composite roof under hot climate conditions, Sustainable Energy Technologies and Assessments, Vol. 45, pp. 101121. ISSN 2213-1388. https://doi.org/10.1016/j.seta.2021.101121 (Scopus: Q1, IF: 7,632).
5. **Al-Yasiri, Q.**, Szabó, M. (2021): Case study on the optimal thickness of phase change material incorporated composite roof under hot climate conditions, Case Studies in Construction Materials, Vol. 14, pp. e00522. ISSN 2214-5095. https://doi.org/10.1016/j.cscm.2021.e00522 (Scopus: Q1, IF: 4.934).
6. **Al-Yasiri, Q.**, Szabó, M. (2021): Performance assessment of phase change material integrated with building envelope for heating application on cold locations, European Journal of Energy Research, Vol. 1, pp. 7-14., ISSN 2736-5506. https://doi.org/10.24018/ejenergy.2021.1.1.5.
7. **Al-Yasiri, Q.**, Szabó, M. (2021): PCMs in building envelope: Characteristics, applications, key parameters and energy contribution, R&D in Mechanical Engineering Letters, Vol. 20, pp. 31-38., HU ISSN 2060-3789.
8. **Al-Yasiri, Q.**, Szabó, M. (2021): Thermal performance of concrete bricks based phase change material encapsulated by various aluminium containers: An experimental study under Iraqi hot climate conditions, Journal of Energy Storage, Vol. 40, pp. 102710. ISSN 2214-5095. https://doi.org/10.1016/j.est.2021.102710 (Scopus: Q1, IF: 8.907).
9. **Al-Yasiri, Q.**, Szabó, M. (2021): Effect of encapsulation area on the thermal performance of PCM incorporated concrete bricks: a case study under Iraq summer conditions, Case Studies in Construction Materials, Vol. 15, pp. e00686. ISSN 2214-5095. https://doi.org/10.1016/j.cscm.2021.e00686 (Scopus: Q1, IF: 4.934).
10. **Al-Yasiri, Q.**, Szabó, M. (2021): Paraffin as a phase change material to improve building performance: an overview of applications and thermal conductivity enhancement techniques, Renewable Energy and Environmental Sustainability, Vol. 6, pp. 38. ISSN 2493-9439. https://doi.org/10.1051/rees/2021040.
11. **Al-Yasiri, Q.**, Szabó, M. (2021): Selection of phase change material suitable for building heating applications based on qualitative decision matrix, Energy Conversion and Management: X, Vol. 12, pp. 100150. ISSN 2590-1745. https://doi.org/10.1016/j.ecmx.2021.100150 (Scopus: Q1).
12. **Al-Yasiri, Q.**, Szabó, M. (2022): Energetic and thermal comfort assessment of phase change material passively incorporated building envelope in severe hot climate: An experimental study, Applied Energy, Vol. 314, pp. 118957. ISSN 0306-2619.

https://doi.org/10.1016/j.apenergy.2022.118957 (Scopus: Q1/D1, IF: 11.446).

13. **Al-Yasiri, Q.**, Szabó, M. (2022): Phase change material coupled building envelope for thermal comfort and energy-saving: Effect of natural night ventilation under hot climate, Journal of Cleaner Production, Vol. 365, pp. 132839. ISSN 0959-6526. https://doi.org/10.1016/j.jclepro.2022.132839 (Scopus: Q1/D1, IF: 11.072).
14. **Al-Yasiri, Q.**, Szabó, M. (2023): Experimental study of PCM-enhanced building envelope towards energy-saving and decarbonisation in a severe hot climate, Energy and Buildings, Vol. 279, pp. 112680. ISSN 0378-7788. https://doi.org/10.1016/j.enbuild.2022.112680 (Scopus: Q1/D1, IF: 7.201).
15. **Al-Yasiri, Q.**, Szabó, M. (2023): Numerical analysis of thin building envelope-integrated phase change material towards energy-efficient buildings in a severely hot location, Sustainable Cities and Society, Vol. 89, pp. 104365. ISSN 2210-6715. https://doi.org/10.1016/j.scs.2022.104365 (Scopus: Q1/D1, IF: 10.696).
16. **Al-Yasiri, Q.**, Szabó, M. (2023): Building envelope-combined phase change material and thermal insulation for energy-effective buildings during harsh summer: Simulation-based analysis, Energy for Sustainable Development, Vol. 72, pp. 326-339. ISSN 2352-4669. https://doi.org/10.1016/j.esd.2023.01.003 (Scopus: Q1, IF: 5.655).
17. **Al-Yasiri, Q.**, Szabó, M. (2023): Hourly analysis of temperature and heat gain reduction for building envelope-integrated phase change material under severe hot summer conditions, Journal of Energy Storage, Vol., pp. ISSN 2214-5095. (Scopus: Q1, IF: 8.907). (under review)
18. **Al-Yasiri, Q.**, Szabó, M. (2023): Building envelope-coupled phase change material and night ventilation: Effect of window orientation and window-to-wall ratio during summer months, Building and Environment, Vol., pp. ISSN 1873-684X. (Scopus: Q1, IF: 7.093). (under review)
19. **Al-Yasiri, Q.**, Szabó, M. (2023): Thermal analysis of concrete bricks-embedded phase change material as a layer and capsules: A case study under hot weather conditions, Case Studies in Construction Materials, Vol., pp.. ISSN 2214-5095. (Scopus: Q1, IF: 4.934). (under review)

International conference proceedings:

20. **Al-Yasiri, Q.**, Szabó, M. (2021): Experimental investigation of phase change material incorporated composite flat roof for energy-saving under Iraq hot climatic conditions, Proceedings, 2nd International Conference on Engineering and Science 2021, The Technical Institute of Al-Samawah- Al- Samawah, Iraq, April 7-8, 2021.
21. **Al-Yasiri, Q.**, Szabó, M. (2021): Paraffin as a phase change material to improve building performance: Application and thermal conductivity enhancement techniques, Proceedings, World Renewable Energy Congress 2020, Instituto Superior Téchnico- Lisboa, Portugal, July 26-30, 2021.
22. **Al-Yasiri, Q.**, Szabó, M. (2022): Building envelope integrated phase change material under hot climate towards efficient energy and CO_2 emission saving, 7th International Conference on Smart and Sustainable Technologies, Split and Bol, Croatia, July 05-08 2022, ISBN: 978-1-6654-8828-0. Published by IEEE Xplore https://doi.org/10.23919/SpliTech55088.2022.9854246 (Scopus: Q1).

International conference abstracts:

23. **Al-Yasiri, Q.**, Szabó, M. (2021): Thermal comfort assessment of a PCM layer integrated composite roof at different positions under hot outdoor conditions, Book of Abstracts, Efficiency, solar and thermal energy for the human comfort, Gödöllő, Hungary: Hungarian University of Agriculture and Life Science, July 9, 2021, 47 p. ISBN 978-963-269-958-5.

24. **Al-Yasiri, Q.**, Szabó, M. (2021): Phase Change Material Application for Building Envelope Temperature Reduction: Experimental Study under Hot Climate Conditions, Book of Abstracts, 17th Miklós Iványi International PhD & DLA Symposium: Architectural, Engineering and Information Sciences, Pécs, Magyarország: Pollack Press (2021), p.187. ISBN: 9789634298113.

25. **Al-Yasiri, Q.**, Szabó, M.(2021): Thermal performance of building envelope integrated with phase change material in a hot region, Book of Abstracts, 27th Workshop on Energy and Environment, Gödöllő, Hungary, December 9-10, 2021, p. 20. ISBN 978-963-269-972-1.

A3: Commonly used terms in building engineering and thermodynamics

Term	Definition/description
Building envelope	The physical separation between the interior built environment and the external atmosphere includes the roof, walls, doors, windows and floors.
Thermal comfort	Human thermal comfort refers to a mental condition expressing satisfaction with its surroundings. The temperature and relative humidity are the main parameters for evaluating human thermal comfort.
Energy saving	The reduction in building energy consumption (heating, cooling, lighting, electricity, etc.) without reducing thermal comfort.
Temperature	The measure of hotness or coldness of a substance. It is usually expressed in several scales, including Fahrenheit and Celsius.
Heat	The transfer of kinetic energy from one medium or object to another or from an energy source to a medium or object. Such energy transfer can occur in three ways: radiation, conduction, and convection.
Melting temperature	The change of a material state from a solid into a liquid when heat is applied.
Enthalpy	The measurement of energy in a thermodynamic system. The quantity of enthalpy equals the total heat content of a system, equivalent to the system's internal energy plus the product of volume and pressure.
Specific heat	The amount of heat needed to raise the temperature of 1 gram of a substance by 1 degree Celsius.
Density	The total mass of a substance divided by the total volume occupied by that substance (mass per unit volume).

A4: Structure and setting of EnergyPlus software

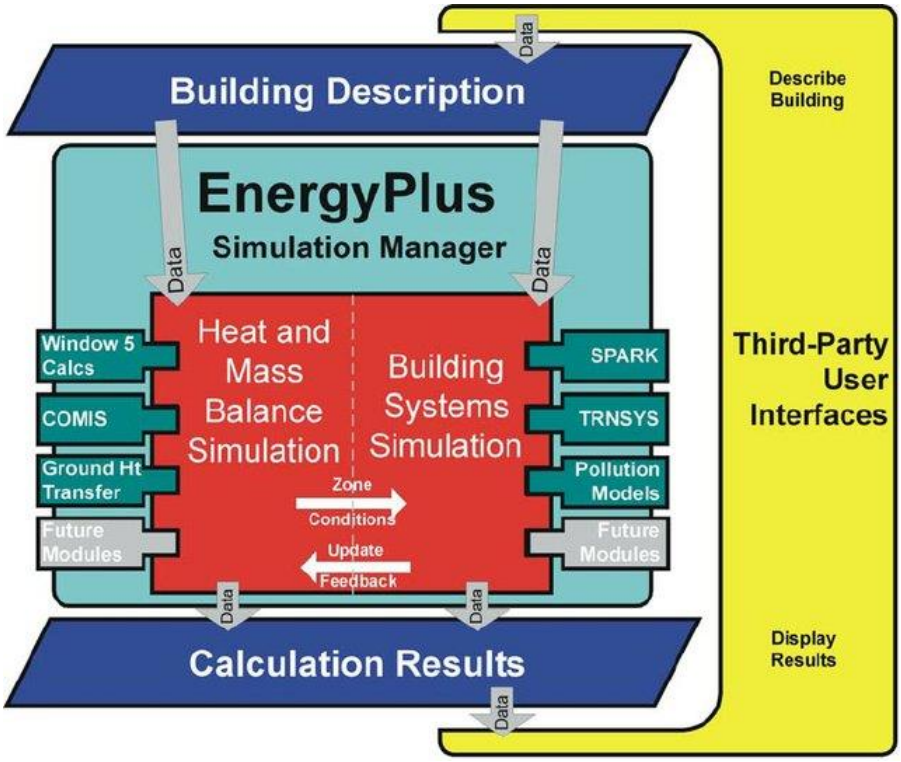

Fig. 8.1. Structure of EnergyPlus software

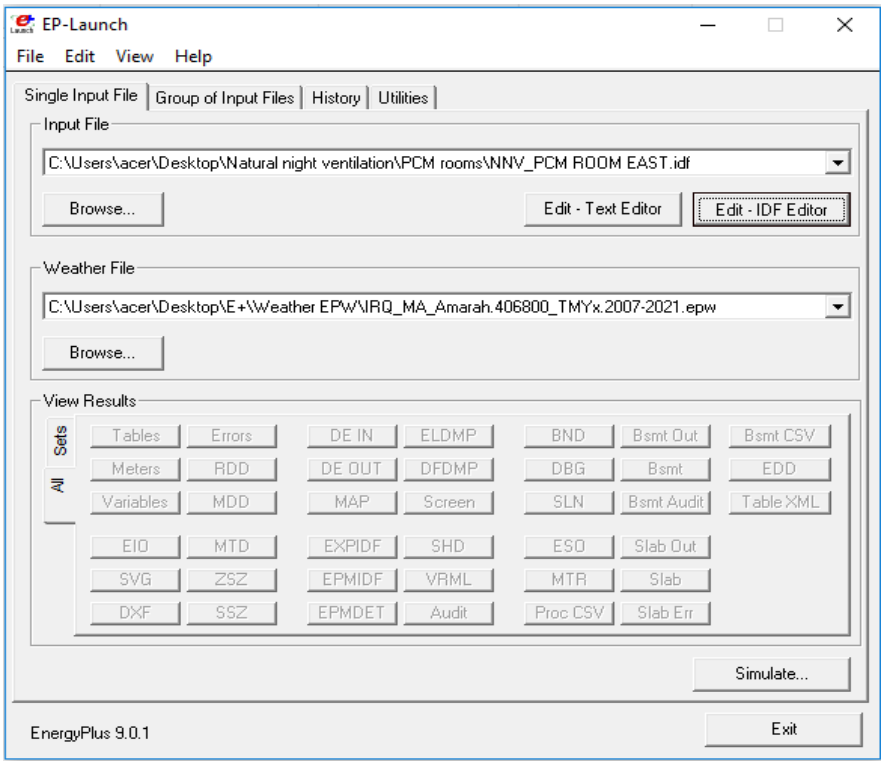

Fig. 8.2. User interface of EnergyPlus software

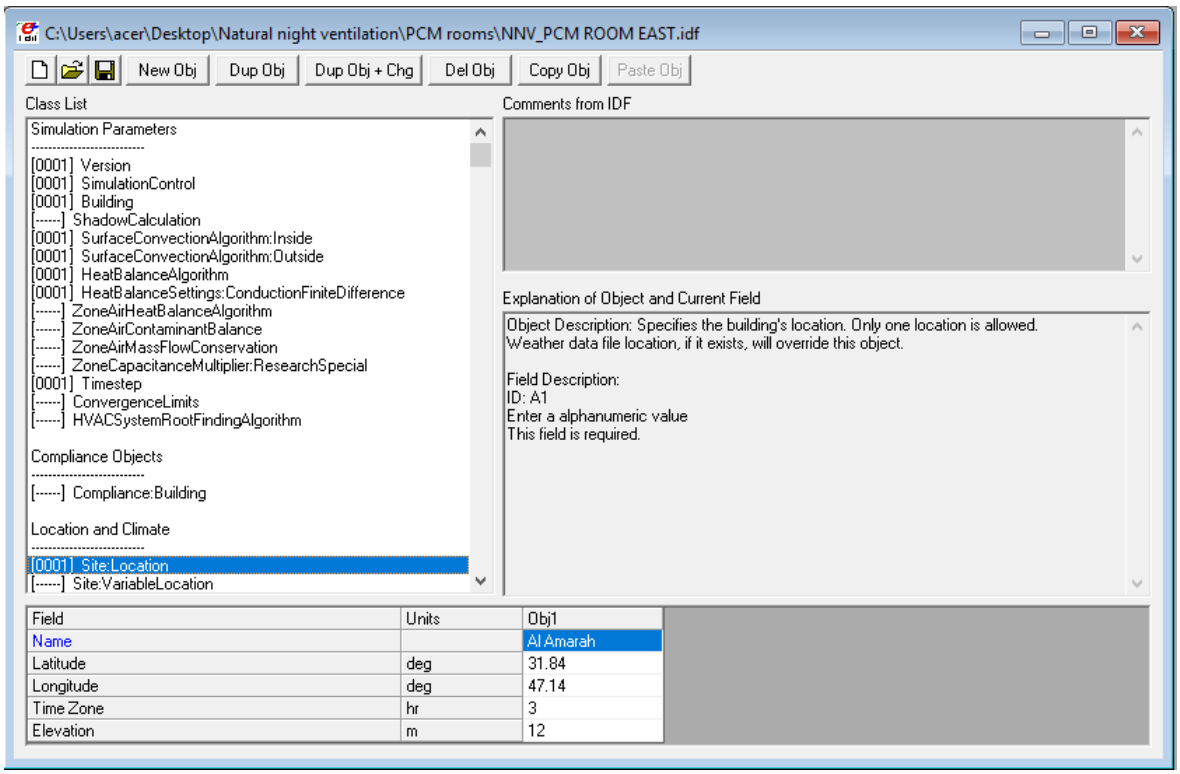

Fig. 8.3. Setting of location under study EnergyPlus software

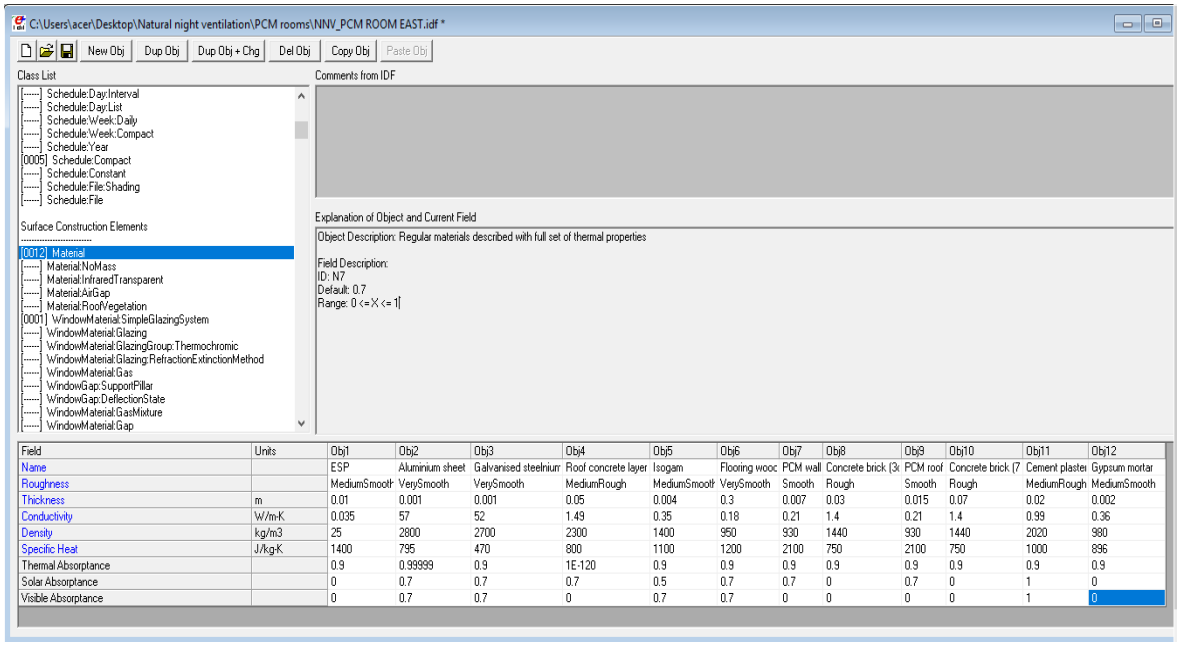

Fig. 8.4. Detailed information of input materials

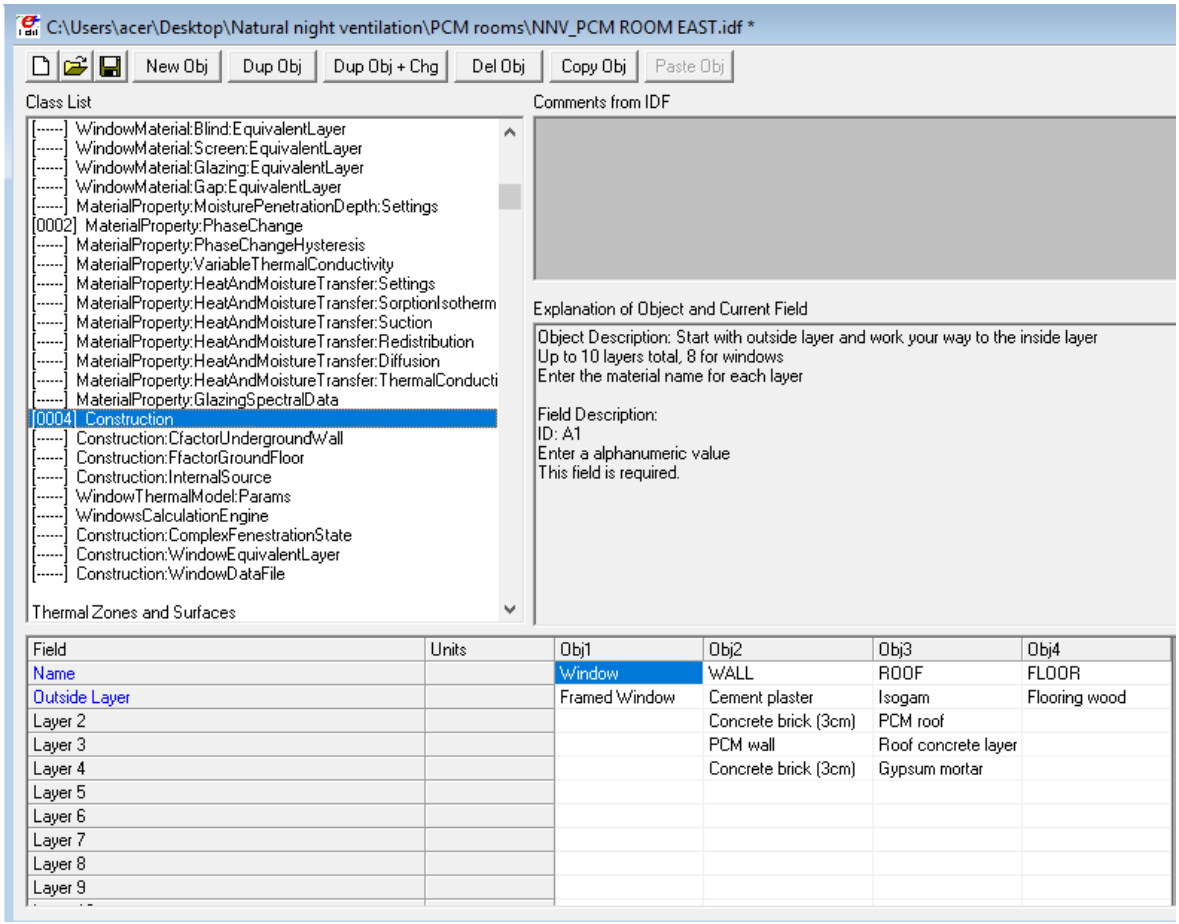

Fig. 8.5. Detailed information of room elements

9. ACKNOWLEDGEMENT

This work has been supported financially by the Stipendium Hungaricum Scholarship Programme and accomplished under the direction of the Doctoral School of Mechanical Engineering at MATE (Szent István University formerly), Gödöllő, Hungary.

In this long journey for my PhD, which started in September 2019 and ended by the middle of 2023, many people (including professors and staff members, classmates, senior and junior fellows, technical and support staff at the university, friends from local Hungarians and the internationals, and family members and relatives) have helped and supported me to attain this endeavour.

First and foremost, I am incredibly grateful to my supervisor, **Associate Prof Dr Márta Szabó,** for her valuable advice, consistent encouragement, uninterrupted support, and patience during my PhD studies. Her vast knowledge and experience have inspired me throughout my academic research. This dissertation would not have been feasible without her supervision and significant guidance.

I am very grateful to my beloved wife **Marwa**, my children **Layan** and **Yousuf**, family members and friends for their immeasurable love and sacrifices, which have made this feat possible.

I would like to express my gratitude and appreciation to **Prof Dr Gábor Kalácska**, the current head of the Doctoral School of Mechanical Engineering, and **Prof Dr István Farkas**, the former head of the Doctoral School, for their managerial support throughout the study period till the fulfilment of all requirements for obtaining this PhD.

I am so thankful to **Prof Dr Müslüm Arıcı** from Kocaeli University, Turkey, **Prof Dr Ahmed Alshara** and **Dr Hayder Alkhazraji** from the University of Misan, Iraq and **Dr Aakash Rai** from Birla Institute of Technology and Science, India for their endless encouragement, support and advice in many research, experimental and numerical matters.

I would like to give a special thanks to the Doctoral School of Mechanical Engineering staff and the University administration staff for their kindness and cooperation with me from the beginning of my study till the end. Among others, I would like to give special thanks to Ms **Csilla Kánai**, the coordinator of the Stipendium Scholarship Program at the university, Ms **Zsuzsanna Tassy**, the coordinator for international relations and administrative PhD studies, and Ms **Kárpáti Beáta Éva**, the international student coordinator in MATE dormitory, for their unconditional support during my PhD journey and staying in Hungary.

Finally, I wish to acknowledge the Ministry of Higher Education of Iraq and my home university, the University of Misan- Faculty of Engineering, for nominating and supporting me during this achievement.

Qudama Al-Yasiri

Gödöllő, February 2023